Dissecting the contribution of dipeptide repeats to the toxicity in C9orf72 iPSC-derived neurons from ALS/FTD patients



Paola Barbagallo

St Hilda's College

Nuffield Department of Clinical Neuroscience

University of Oxford

Supervised by Professor Kevin Talbot and Dr Ruxandra Dafinca

Submitted for the degree of *Doctor of Philosophy*

Hilary Term 2021

To Mamma e Papà,

Thomas,

PIF

Abstract

A large (GGGGCC) repeat expansion in *C9ORF72* gene is the commonest genetic cause of amyotrophic lateral sclerosis (ALS). It causes both loss- and gain-of-function, but the relative contribution of the different mechanisms to the development of ALS remains uncertain. One of the pathomechanisms is the production of dipeptide repeat proteins (PR, PA, GR, GP and GA) via repeat-associated non-ATG translation (DPRs). Animal and cellular models have suggested that the arginine-rich DPRs are toxic, but staining in fixed brains of C9orf72 patients show that the same DPRs are not very abundant compared to GA, GP and PA. Moreover, the DPR-related phenotypes exhibited in *in vitro* models are not always verified in C9orf72 patients. For these reasons I developed a doxycycline-inducible lentiviral system to regulate DPR expression in induced pluripotent stem cell (iPSC)-derived motor neuron (MN) cultures. The effects of GA and PR expression in CRISPR/Cas9 corrected C9orf72 iPSC-derived MNs were compared to the phenotypes of C9orf72 mutant lines. Both DPRs were partially accountable for altered ER and mitochondrial calcium homeostasis, and stress granule formation. Moreover, PR expression may reduce maximal mitochondrial respiration, while GA induced lysosomal activation. The activation of chaperone-mediated autophagy cleared CRISPR/Cas9 corrected iPSC-derived MNs from GA and PR, but it did not rescue C9orf72 mutant lines. Moreover, I studied the effects of a peptide designed to reduce RNA foci, and I showed that it may improve mitochondrial respiration in C9orf72 mutant iPSC-derived MNs.

Summary of planned work before Covid-19 closure

Due to Covid-19 pandemic the replicates for SeaHorse experiments (chapter 4-5), TDP43 staining (chapter 4), MCU and ATF4 immunoblots (chapter 5), LysoTracker® analysis (chapter 5) could not be completed. Samples for quality control data were collected but not processed, such as co-immunoprecipitation of tagged DPRs to test their direct interaction with targets described in this thesis, qPCR of tagged DPRs and further immunoblot and immunofluorescence to detect DPR expression in all the lines transduced with DPR-expressing virus. Please refer to Appendix for a guideline of the lines used in each experiment.

Declaration

Unless otherwise stated, all the work presented in this thesis is the work of the author and conducted at the Nuffield Department of Clinical Neuroscience, University of Oxford. This work has not been submitted for any other degrees at any other University or educational institute.

Acknowledgments

I would like to thank my mentors, Prof Kevin Talbot and Dr Ruxandra Dafinca, for their great supervision. I will be forever grateful to them, as they always believed in my potential and inspired me to work hard, improve my skills and be more confident. They gave me the freedom to lead my project, but were always there to advise and guide. Thank you to all of my team members. I will miss Martin's cultural references which, I usually did not understand, preferring Latin literature to English. Not to mention Matt's English humour: he really tried to be funny (which I appreciate, mate). And the Aussie accents of Jayden and Dave when talking to each other (so exotic). Speaking of accents, I need to apologise to Alex as during my first year (and maybe longer) it was very hard for me to understand him. Liz, Ruxandra and Lynn, the first three ladies I met when I landed at NDCN; you were there during the tough times and helped me a lot. Thank you Thanuja, Jakub and Lucy; you confirmed my theory about medical doctors. Joking, of course. I will miss 4 pm chats with Thanuja, thanks to you I was not the only one speaking (so much). Lucy, you are a great researcher: trust your gut. Jakub, you improved my stats, as well as my critical thinking and self-confidence. I truly hope our paths will cross again, also because your fashion sense has been better since you have known me. Luckily, you'll be there to support Bjorn. That guy enjoys life too much, he needs to focus more on his work. I will also miss fighting with Sukrat, who's a tough cookie but with a warm heart. Ana, Chaitra and Emily, we have been more than colleagues. Thanks to you girls my Oxfordian experience gained a different taste: our friendship will last many moons.

I need to thank Oxford, where I met Thomas, with whom I shared the huge ups and downs of a DPhil. His love, patience and kindness made my life easier. His passion for details and graphics made my presentations outstanding (ti amo). This thesis is also dedicated to Irene and Fede, who showed me that true life-long friendships are stronger than any distance. And last but not least, thank you mum and dad.

Publications arising from this work

Barbagallo Paola, Dafinca Ruxandra, Talbot Kevin. "Poly(PR) causes deficits to calcium homeostasis and induces stress granule formation" (In preparation).

Ababneh, Nidaa A, Jakub Scaber, Rowan Flynn, Andrew Douglas, **Paola Barbagallo**, Ana Candalija, Martin R Turner, et al. 2020. "Correction of Amyotrophic Lateral Sclerosis Related Phenotypes in Induced Pluripotent Stem Cell-Derived Motor Neurons Carrying a Hexanucleotide Expansion Mutation in C9orf72 by CRISPR/Cas9 Genome Editing Using Homology-Directed Repair." *Human Molecular Genetics*, June. https://doi.org/10.1093/hmg/ddaa106.

Dafinca, Ruxandra, **Paola Barbagallo**, Lucy Farrimond, Ana Candalija, Jakub Scaber, Nida'a A. Ababneh, Chaitra Sathyaprakash, Jane Vowles, Sally A. Cowley, and Kevin Talbot. 2020. "Impairment of Mitochondrial Calcium Buffering Links Mutations in C9ORF72 and TARDBP in IPS-Derived Motor Neurons from Patients with ALS/FTD." *Stem Cell Reports* 14 (5): 892–908. https://doi.org/10.1016/J.STEMCR.2020.03.023.

Table of contents

Abstract ... iii

Summary of planned work before Covid-19 closure ... iv

Declaration ... v

Acknowledgments ... vi

Publications arising from this work ... viii

List of tables ... xvi

List of Abbreviations ... xvii

Chapter 1 – Introduction ... 20

1.1. Amyotrophic Lateral Sclerosis ... 20

1.1.1. ALS and FTD in opposition of a disease continuum ... 21

1.1.2. Treatments for ALS ... 22

1.2. Genetic heterogeneity in ALS ... 24

1.2.1. Trans-activator response (TAR) DNA-binding protein 43 ... 24

1.2.2. Fused-in-sarcoma ... 26

1.2.3. C9ORF72 ... 27

1.2.4. Superoxide dismutase 1 ... 29

1.2.5. Other causative genes ... 31

1.3. C9ORF72 function ... 33

1.3.1. C9ORF72 is involved in vesicular transport ... 33

1.3.2. Hexanucleotide expansion causes C9ORF72 haploinsufficiency in ALS/FTD patients ... 35

1.3.3. C9ORF72 loss-of-function in animal and cellular models ... 37

1.3.4. C9ORF72 HRE mouse models ... 38

1.3.5. Microsatellite expansions in other diseases ... 40

1.4. RNA-mediated toxicity caused by HRE in *C9ORF72* ... 41

1.5. Repeat-associated non-ATG (RAN) initiated translation of the HRE *C9ORF72* transcripts generates poly-dipeptides ... 43

1.5.1. RAN-translated dipeptide repeat proteins are the pathological hallmark of C9ORF72 HRE ... 43

1.5.2. Regulation of DPR expression 45
1.5.3. DPR-mediated toxicity in animal and cellular models 47
1.6. Cellular mechanisms affected by DPR expression 50
1.6.1. Poly(PR) and poly(GR) cause nucleolar stress, reduce protein translation, and impair nucleocytoplasmic transport 51
1.6.2. Poly(GA) causes proteasomal dysfunction and axonal deficits 54
1.6.3. DPRs cause endoplasmic reticulum stress 55
1.7. ALS-related phenotypes induced by DPR expression 56
1.7.1. The relationship between DPR, RNA foci and TDP-43 proteinopathy 56
1.7.2. Oxidative stress and mitochondrial dysfunction 57
1.8. Cell-to-cell propagation of DPRs 59
1.9. Aims 60
Chapter 2 – Methods 63
2.1. Molecular cloning 63
2.1.1. List of plasmids 64
2.1.2. DPR sequences optimisation 64
2.1.3. Sanger sequencing 65
2.2. Lentivirus production, titration and transduction 66
2.3. Lipotransfection 67
2.4. iPSC-motor neurons differentiation and experiments 67
2.4.1. Induced pluripotent stem cell lines 67
2.4.2. Induced pluripotent stem cell culture 68
2.4.3. Motor neuron differentiation protocol 69
2.4.4. Doxycycline induction 73
2.4.5. TAT-BIND peptide treatment 73
2.4.6. Sodium arsenite treatment 74
2.4.7. Autophagy 74
2.5. Assessing phenotypes 74
2.5.1. Immunoblotting 74
2.5.2. Immunohistochemistry 75
2.5.3. Fluorescence In Situ Hybridisation (FISH-IF) 76
2.5.4. Confocal imaging analysis 79

2.5.5. Calcium imaging 79
2.5.6. Statistical analysis 80

Chapter 3 – Molecular cloning of the doxycycline inducible system in a lentiviral backbone 81

3.1. Introduction 81

3.2. Design and cloning strategy 82

3.2.1. Sub-cloning of the trans-activator rtTA3 85
3.2.2. Sub-cloning of the TRE operon 89
3.2.3. Insertion of the DPR sequences 93
3.3.1. Transfection of DPR vectors in HEK293T cells 96
3.3.2. Titration of lentivirus toxicity in mature iPSC-derived motor neurons 99
3.3.3. (PR)50–HA and (GA)50–c-myc detection in iPSC-derived motor neurons 101

3.4. Conclusion 106

Chapter 4 – Differential effects of poly(GA) and poly(PR) on calcium homeostasis, UPR, TDP-43 localisation and stress granule formation 107

4.1. Introduction 107

4.1.1. Mitochondria as a calcium store and energy supplier 107
4.1.2. Altered excitability in C9ORF72 models 108
4.1.3. ER-mitochondria cross-talk 109
4.1.4. Aims of the chapter 111

4.2. Effects of poly(GA) and poly(PR) on mitochondrial function and protein levels 111

4.2.1. Poly(GA) and poly(PR) cause reduction of calcium intake after glutamate stimulation and only poly(PR) limits mitochondrial calcium uptake 111
4.2.2. (GA)50 and (PR)50 upregulate COXIV, but only (GA)50 increases mitochondrial maximal respiration 116
4.2.3. Poly(GA) expression increases the mitochondrial mass 120

4.3. Effect of poly(GA) and poly(PR) on ER-calcium physiology and the Unfolded Protein Response 123

4.3.1. Low ER calcium release in C9orf72 mutant iPSC-MNs is caused by poly(PR) 123
4.3.2. UPR deficiency in C9orf72 mutant iPSC-derived MNs is not caused by poly(GA) and poly(PR) 126

4.4. Focus on ALS-related phenotypes: TDP-43 mislocalisation and and stress granule formation 129

4.4.1. TDP-43 nuclear retention in C9orf72 mutant iPSC-derived MNs is not caused by poly(GA) or poly(PR) 129

4.4.2. (PR)50 induces stress granule formation 133

4.5 Conclusions 135

Chapter 5: Activation of Chaperone-Mediated Autophagy and clearance of RNA foci as possible mechanisms to reduce DPR toxicity 138

5.1. Introduction 138

5.1.1. Chaperone-Mediated Autophagy 138

5.1.2. Targeting RNA foci as ALS therapy 140

5.1.3. Targeting DPRs for ALS therapy 141

5.1.4. Aims of the chapter 142

5.2. Induction of Chaperone Mediated Autophagy clears iPSC-MNs from (GA)50 and (PR)50 142

5.2.1. Poly(GA) and poly(PR) cause autophagic and proteasomal dysfunction 142

5.2.2. Poly(GA) induces lysosome activation 145

5.2.3. Activation of CMA clears MNs of (GA)50 and (PR)50 148

5.2.4. Activation of CMA in C9orf72 mutant iPSC-derived MNs does not rescue the phenotypes 150

5.3. Clearance of RNA foci as a potential therapy in C9orf72 mutant iPSC-derived MNs 152

5.3.1. TAT-BIND peptide clears sense RNA foci in only one C9orf72 mutant iPSC line .153

5.3.2. TAT- peptide activates UPR and autophagy in C9orf72 mutant iPSC-derived MNs 157

5.3.3. TAT-BIND peptide rescues COXIV function in C9orf72 mutant iPSC-MNs 159

5.4. Conclusions 162

Chapter 6 – Discussion 164

6.1. The doxycycline inducible system is efficient and sensitive 164

6.2. Expression of poly(GA) and poly(PR) in the context of C9ORF72 cellular phenotypes 166

6.2.1. Poly(GA) and poly(PR) may partially cause calcium homeostasis and mitochondrial deficits recorded in C9orf72 mutant iPSC-derived MNs 166
6.2.2. DPR expression increases sensitivity to oxidative stress 169
6.2.3. Poly(GA) and poly(PR) reduce total ER calcium and poly(PR) inhibits IP3Rs 170
6.2.4. Poly(GA) activates lysosomes while poly(PR) reduces autophagy 171
6.3. DPRs do not cause TDP-43 pathology 172
6.4. Autophagy and RNA foci degradation as therapeutic approaches 172
6.5. Conclusions and future directions 175
Appendix 176
References 183

List of Figures

Figure 1.1: Diagram of C9ORF72 gene, RNA transcripts and protein isoforms. *36*

Figure 2.1 Differentiation of Induced Pluripotent Stem Cells in motor neurons. *71*

Figure 3.1: Scheme of the cloning strategy. *84*

Figure 3.2: Cloning of a human ubiquitin promoter into pUltradox. *86*

Figure 3.3. Cloning of the trans-activator element rtTA3 in pUltradox. *88*

Figure 3.4. Cloning of eGFP in pTRE3G. *90*

Figure 3.5. Cloning of the fragment carrying the operon TRE3G and eGFP in pUltradox_rtTA3. ..... *92*

Figure 3.6: Design of dipeptide repeat sequences. *94*

Figure 3.7: Insertion of DPR sequences in pUltradox_rtTA3_TRE3G. *95*

Figure 3.8: Efficiency of the doxycycline inducible system with the operon TRE3G in HEK293T cells. *98*

Figure 3.9: Titration of the lentivirus and doxycycline toxicity in mature iPSC-MNs. *100*

Figure 3.10: Schematic timeline for immunoblot detection of (GA)50–c-myc and (PR)50–HA in MNs. *101*

Figure 3.11: Detection of (GA)50–c-myc in MNs. *103*

Figure 3.12: Detection of (PR)50–HA in MNs. *104*

Figure 3.13: Doxycycline induction protocol used in following experiments. *105*

Figure 4.1: (GA)50 and (PR)50 lower calcium intake after glutamate and (PR)50 reduces mitochondrial calcium intake in edited C9orf72 iPSC-derived MNs. *113*

Figure 4.2: MCU downregulation in C9orf72 mutant lines is not caused by poly(PR) or poly(GA). *115*

Figure 4.3: C9orf72 mutant iPSC-derived MNs show deficits in mitochondrial respiration not caused by DPRs. *117*

Figure 4.4: (GA)50–c-myc and (PR)50–HA upregulate COXIV. *119*

Figure 4.5: (GA)50–c-myc upregulates TOMM20. ..... *121*

Figure 4.6: (GA)50–c-myc does not localise to mitochondria. *122*

Figure 4.7: (PR)50 lowers the amount of calcium released from the ER. *124*

Figure 4.8: (GA)50 and (PR)50 reduce total ER calcium level. *125*

Figure 4.9: The UPR pathway is downregulated in C9orf72 mutant MNs. *127*

Figure 4.10: (GA)50 and (PR)50 do not affect the expression of proteins belonging to the UPR pathway. *128*

Figure 4.11: C9orf72 mutant iPSC-derived MNs show TDP-43 nuclear retention that delocalises to the cytosol after sodium arsenite treatment. *131*

Figure 4.12: (GA)50 and (PR)50 expression does not cause TDP-43 mislocalisation or nuclear retention. *132*

Figure 4.13: (PR)50 induces stress granule formation in genome edited MNs treated with sodium arsenite. *134*

Figure 4.14: Conclusions. *137*

Figure 5.1: (GA)50 and (PR)50 expression causes autophagic and proteasomal dysfunction. *144*

Figure 5.2: C9orf72 mutant iPSC-MNs have more active lysosomes. *146*

Figure 5.3: (GA)50 induces lysosome activation. *147*

Figure 5.4: (GA)50 and (PR)50 are degraded by CMA. *149*

Figure 5.5: Activation of CMA in C9orf72 mutant iPSC-derived MNs does not rescue the phenotypes. *151*

Figure 5.6: TAT-peptide shows different cell survival when used on C9orf72 mutant iPSCs. *155*

Figure 5.7: Sense foci are cleared from C901-iPSCs by TAT-peptide. *156*

Figure 5.8: TAT-peptide effects on ER and lysosomal markers in C9orf72 mutant iPSC-derived MNs. *158*

Figure 5.9: TAT-peptide upregulates mitochondrial markers in C9orf72 mutant MNs. *160*

Figure 5.10: TAT-BIND treatment increases maximal mitochondrial respiration. *161*

Figure S1: Plasmid maps. *176*

Figure S2: Differentiation Gann charts. *177*

Figure S3: Immunoblot quantification of tagged DPRs in edited and wild-type iPSC-derived MNs. *178*

Figure S4: Calcium imaging analysis of each line used. *179*

Figure S5: Immunoblot quantifications of mitochondrial markers in each line. *180*

Figure S6: Immunoblot quantifications of UPR markers in each line. *181*

Figure S7: Immunoblot quantifications of autophagy markers in each line. *182*

List of tables

Table 2.1: List of primers used in cloning and Sanger sequencing. *65*

Table 2.2: iPSC lines and demographic characteristics. *68*

Table 2.3: Plating concentrations. *70*

Table 2.4: Media used during neuronal differentiation *70*

Table 2.5: List of reagents used for iPSC culture and motor neuron differentiation protocol. *72*

Table 2.6: List of antibodies used for immunoblotting (WB) and immunohistochemistry (IF) *77*

List of Abbreviations

α-amino-3-hydroxyl-5-methyl-4-isoxazolepropionic acid (AMPA)
Adeno-associated virus (AAV)
Adenosine triphosphate (ATP)
ADP-ribosylation factor-6 (Arf6)
Amyotrophic Lateral Sclerosis (ALS)
Antisense oligonucleotide (ASO)
Bacterial Artificial chromosome (BAC)
Beta actin (β-ACT)
Beta-tubulin (β-tub)
Blood brain barrier (BBB)
C/EBP homologues protein (CHOP)
Carbonyl cyanide-4 phenylhydrazone (FCCP)
Carbonyl cyanide m-chlorophenyl hydrazine (CCCP)
Central nervous system (CNS)
Cerebral spinal fluid (CSF)
Choline acetyl transferase (ChAT)
Clustered regularly interspaced short palindromic repeats (CRISPR)
Cyclic AMP-dependent transcription factor (ATF)
Cytochrome c oxidase subunit 4 (COXIV)
Deoxyribonucleic acid (DNA)
Differentially expressed in normal and neoplasia (DENN)
Dipeptide repeat protein (DPR)
Doxycycline (dox)
Endoplasmic reticulum (ER)
Enhanced green fluorescent protein (eGFP)
ER-associated degradation (ERAD)
Eukaryotic initiation factor-2 (eIF2)
Fluorescence in situ hybridization (FISH)
Frontotemporal lateral dementia (FTLD)
Fused-in-sarcoma (FUS)
Genome-wide association study (GWAS)
Glyceraldehyde-3-Phosphate Dehydrogenase (GAPDH)

Guanine Exchange Factor (GEF)
Green fluorescent protein (GFP)
Hexanucleotide repeat expansion (HRE)
Islet 1 (ISL1)
Induced pluripotent stem cell (iPSC)
Inositol triphosphate receptors (IP3R)
Integrated stress response (ISR)
Liquid-liquid phase separation (LLPS)
Long terminal repeats (LTR)
Lysosome-associated membrane glycoprotein 2 (LAMP2A)
Matrin-3 (MATR3)
Messenger RNA (mRNA)
Micro RNA (miRNA)
Mitochondrial calcium uniporter (MCU)
Mitochondrial calcium uptake protein 1/2 (MICU1/2)
Motor neuron disease (MND)
Multiplicity of infection (MOI)
N-methyl-D-aspartate (NMDA)
Neurofilament heavy (NEFH)
Neuromuscular junction (NMJ)
Nonsense-mediated mRNA decay (NMD)
Nuclear export signal (NES)
Nuclear localisation signal (NLS)
Open reading frames (ORF)
Optineurin (OPTN)
Oxygen consumption rate (OCR)
Phosphate buffered saline (PBS)
Polymerase chain reaction (PCR)
Protein kinase RNA-like endoplasmic reticulum kinase (PERK)
Quantitative reverse transcription polymerase chain reaction (qRT-PCR)
Ran guanine nucleotide exchange factor (RanGEF)
Reactive oxygen species (ROS)
Red fluorescent protein (RFP)
Repeat-associated non-AUG (RAN)

Rho-associated, coiled-coil containing protein kinase inhibitor (ROCKi)
Ribonucleic acid (RNA)
Ribosomal RNA (rRNA)
RNA interference (RNAi)
RNA-recognition motifs (RRM)
Ryanodine receptors (RyR)
Sarco/endoplasmic reticulum Ca^{2+}-ATPase (SERCA)
Serine/threonine-protein kinase/endoribonuclease ire-1 (IRE1)
Short interfering RNA (siRNA)
Smith–Magenis syndrome chromosome region candidate 8 (SMCR8)
Smoothened agonist (SAG)
Stromal Interaction Molecule-1/2 (STIM1/2)
Store-Operated Calcium Entry (SOCE)
Stress granule (SG)
Superoxide dismutase 1 (SOD1)
TAR DNA binding protein (TARDBP)
TAR DNA binding protein 43 (TDP-43)
TRAF family member-associated NF-κB activator-binding kinase 1 (TBK1)
Transfer RNA (tRNA)
Translocase of outer mitochondrial membrane 20 (TOMM20)
Ubiquitin-proteasome system (UPS)
Unfolded protein response (UPR)
Untranslated Region (UTR)
Unc-51-like kinase 1 (ULK1)
Unfolded protein response (UPR)
Valosin-containing protein (VCP)

Chapter 1 – Introduction

1.1. Amyotrophic Lateral Sclerosis

Motor neuron diseases (MND) are progressive neurodegenerative disorders that lead to motor neuron loss resulting in paralysis (van Es et al., 2017). Neurons are post-mitotic cells with the unique characteristic of generating electrical waves, called action potentials, that trigger a signal in a connected neuron (Purves, 2018). Major components of neurons include the cell body (the soma), dendritic processes (which are the targets of synaptic input) and an axon, the lengths of which vary based on the functional class of neurons. Neurons in local circuits or interneurons have relatively short axons, while the axons of some projection neurons, like corticospinal neurons, synapse or innervate targets up to a metre from their soma. A subtype of spinal neurons are the motor neurons, which are also found in brain stem motor nuclei, and stimulate skeletal muscles to induce movements. The function of spinal and bulbar motor neurons is modulated by descending ('upper motor neuron') influences from the corticospinal tract and local innervation from interneurons. One muscle is innervated by pools of motor neurons that are connected to the muscle fibres at the neuromuscular junction.

The most common form of MND is amyotrophic lateral sclerosis (ALS), which was first formally defined in 1869 by Jean-Martin Charcot (Cleveland & Rothstein, 2001). Most epidemiological studies conducted on ALS patients of a European

origin describe a yearly disease incidence of 2 – 3 people per 100,000, and with men having a higher lifetime risk of developing the disease (1:350) than women (1:400) (Al-Chalabi & Hardiman, 2013; Chiò et al., 2013; Cronin et al., 2007; Logroscino et al., 2010; Wittie et al., 2013). ALS is a clinically and aetiologically heterogeneous disorder whose cause is largely unknown, and leads to death from respiratory failure with a median survival of 30 months from symptom onset (Kiernan et al., 2011). No clinically significant disease modifying therapy is available, and treatment is largely supportive in nature.

1.1.1. ALS and FTD in opposition of a disease continuum

ALS is diagnosed primarily by clinical examination and EMG, with other investigations largely restricted to ruling out mimic disorders, (Kiernan et al., 2011; Shefner et al., 2020; van Es et al., 2017). Any voluntary muscle can be affected, resulting in a variability of site of onset: either spinal, bulbar or respiratory (van Es et al., 2017). Two-thirds of ALS patients show spinal onset, characterised by asymmetric and painless weakness in a limb, muscular atrophy and fasciculation when there is lower motor neuron involvement, and hyper-reflexia and hypertonia indicating upper motor neuron involvement (Swinnen & Robberecht, 2014; van Es et al., 2017). About 30% of ALS patients are classified as bulbar onset, presenting with dysarthria, dysphagia and tongue fasciculation, while a minority of patients initially displays orthopnoea or dyspnoea, described as respiratory onset (Swinnen & Robberecht, 2014; van Es et al., 2017). Even though the disease starts as a focal process, it spreads within the same region, and between neuro-anatomically linked regions (Ravits & La Spada, 2009; van Es et al., 2017). However there is debate as to what extent the disease exists as a system or cell type vulnerability (Nolan et al., 2020; Talbot, 2020).

Up to 50% of ALS patients show cognitive impairments and behavioural changes, and around 15% patients also meet clinical criteria for the additional diagnosis of frontotemporal dementia (FTD), a specific type of dementia characterised by loss of neurons in the frontal temporal lobes (Massman et al., 1996; Neary et al., 1990; Ringholz et al., 2005). For this reason pure ALS and FTD have been placed at ends of a disease continuum (Burrell et al., 2016). Neuropathological evidence of the ALS/FTD spectrum came with the finding that the major component of ubiquitinated cytoplasmic aggregates in both diseases was the RNA-binding protein TDP-43, not only in surviving spinal motor neurons, but also in cortical neurons (Leigh et al., 1991; Neumann et al., 2006; Sreedharan et al., 2008). Further confirmation of the link between the two diseases was the discovery of the intronic hexanucleotide (GGGGCC) repeat expansion in the gene *C9orf72* in ALS/FTD patients (Al-Sarraj et al., 2011; DeJesus-Hernandez et al., 2011; Hsiung et al., 2012; Troakes et al., 2012).

1.1.2. Treatments for ALS

Neurotransmitters are released from pre-synaptic terminals and activate postsynaptic receptors, and the major excitatory amino acid transmitter in the central nervous system (CNS) is glutamate (Heath & Shaw, 2002). Glutamate receptors can be linked to G-proteins (metabotropic), or form ion channels (ionotropic), as in *N*-methyl-D-aspartate (NMDA), α-amino-3-hydroxyl-5-methyl-4-isoxazole propionic acid (AMPA), and kainate receptors (Heath & Shaw, 2002). The excitatory signal ends only after glutamate is removed by transporters located on astrocytes, EAAT1 and EAAT2, and on neurons, EAAT3. Excessive pre-synaptic glutamate release or deficits in glutamate uptake cause abnormal activation of the receptors which promotes neuronal death.

The discovery of increased levels of glutamate in the cerebrospinal fluid of ALS patients was followed by clinical trials to test the effects of riluzole, a glutamate receptor inhibitor (Rothstein et al., 1990, 1992; Spreux-Varoquaux et al., 2002). In 1995, the drug was approved by the US Food and Drug Administration (FDA), with the mean increase in survival time of treated patients being 10% in clinical trials, equal to 2 – 3 months for most sALS, with possibly years for slow progressive cases (Bensimon et al., 1994; Fang et al., 2018). There is still speculation regarding the effect and mechanism of riluzole and its molecular targets, leading to further investigations into its therapeutic potential in newer models of the disease (Dharmadasa & Kiernan, 2018; Foster & Salajegheh, 2019).

Another proposed cause of neuronal death is oxidative stress, which leads to mitochondrial dysfunction and formation of reactive oxygen species (ROS) (Foster & Salajegheh, 2019). In 2017, edaravone, a treatment originally developed for use in ischaemic stroke, was approved as therapy for ALS (Abe et al., 2017; Ito et al., 2008; Yoshino & Kimura, 2006). Edaravone is believed to be a free radical scavenger which decreases oxidative stress and reduces the rate of disease progression in ALS patients (Abe et al., 2017; Ito et al., 2008; Yoshino & Kimura, 2006).

It is evident that these drugs have very limited effects on life expectancy of MND patients and do not amount to anything close to a cure for the disease. Clinicians therefore focus on the management of symptoms, while studies on known genetic mutations are looking into gene therapies and common disease pathomechanisms to find specific and more efficient disease modifying therapies for ALS (Foster & Salajegheh, 2019; van Es et al., 2017). An example is the use of antisense oligonucleotides (ASOs) downregulating *SOD1* to limit a toxic gain-of-function

mechanism caused by mutant SOD1, already tested in rats and a phase I clinical trial (Miller et al., 2013; Smith et al., 2006). A new generation of ASOs is now being tested in a phase I – II clinical trial led by Ionis Pharmaceuticals and Biogen (NCT02623699) (Miller et al., 2020).

1.2. Genetic heterogeneity in ALS

The majority of ALS cases are classified as sporadic (sALS), while the remaining 5 – 10% of cases are considered to be familial (fALS), a classification largely based on the presence or absence of a family history in first degree relatives. More than twenty candidate genes have been discovered in fALS thanks to the advances made in genome sequencing techniques, and some of those genes have now also been linked to sALS. It suggests that sALS is the result of the combinatorial effect of rare and common variants, and that rare variants can act as low penetrance dominant alleles (Talbot, 2011). However, the frequency of these mutations differs between populations, suggesting the presence of other genetic and environmental risk factors (Chia et al., 2018; Mathis et al., 2019; Zou et al., 2017).

1.2.1. Trans-activator response (TAR) DNA-binding protein 43

TAR DNA-binding protein 43 (TDP-43), the product of the gene *TARDBP*, is a nuclear RNA binding protein involved in RNA maturation – splicing, trafficking, stabilisation – as well as the biogenesis of membraneless organelles, such as stress granules (Buratti et al., 2001, 2005; Fuentealba et al., 2010; Ou et al., 1995). TDP-43 possesses several domains that determine its function and localisation, including an N-terminal nuclear localisation signal (NLS) and a C-terminal nuclear export signal (NES), allowing the protein to shuttle between its predominant nuclear

localisation and the cytosol. It has two highly conserved RNA-recognition motifs (RRM) at the N-terminal, while at the C-terminal there is a low complexity domain. The C-terminal domain is essential for self-regulatory activity by binding TDP-43 mRNA at the 3′ UTR and promoting its own degradation. Moreover, the low complexity domain takes part in the biogenesis of membraneless organelles by mediating liquid-liquid phase separation (Y. Ayala et al., 2011; Berning & Walker, 2019; Buratti et al., 2005).

The deposition of ubiquitinated aggregates containing TDP-43 is the pathological hallmark in around 97% of all ALS, and around 40% of all FTD patients (Arai et al., 2006; Leigh et al., 1991; Neumann et al., 2006; Sreedharan et al., 2008). TDP-43 can be cleaved into C-terminal fragments of varying exact length, which become hyper-phosphorylated and aggregated in the cytosol. However, the relative contribution of TDP-43 dysfunction as either a loss or toxic gain-of-function mechanism in disease pathogenesis is debated. Nuclear depletion of TDP-43 from mouse adult brain has been shown to alter RNA splicing, as TDP-43 binds to 30% of the genome, in particular gene with long intronic regions (Polymenidou et al., 2011). Recently it has been demonstrated that one of the targets of TDP-43 is *STMN2*, a regulator of neuronal growth, the transcript level of which decreases after nuclear depletion of TDP-43, indicating a possible pathway affected by TDP-43 loss of function (Klim et al., 2019). Evidence of a toxic gain-of-function mechanism comes from *post-mortem* studies that suggest phosphorylated TDP-43 seeds its aggregation in neighbouring and connected cells, implicating a prion-like behaviour that could explain how the disease begins with a focality of onset before progressing along neuroanatomical pathways (Braak et al., 2013, 2017; Brettschneider et al., 2013; Harrison & Shorter, 2017). Moreover, a recent study

demonstrated that primary motor cortex of sALS/TDP cases exhibits more phospho-TDP-43 aggregates and microgliosis when compared to fALS cases, indicating genome-specific vulnerability to proteinopathy (Nolan et al., 2020).

A small percentage of familial ALS cases (4 – 5%) exhibits missense mutations within *TARDBP*, with the majority being in the C-terminal glycine-rich domain, and are associated with TDP-43 aggregation and loss-of-function (Mutihac et al., 2015; Prasad et al., 2019; Sreedharan et al., 2008). Other mechanisms implicated in TDP-43 toxicity are deficits of TDP-43 turnover, leading to its toxic overexpression, and aberrant splicing of target mRNAs (Gao et al., 2018).

1.2.2. Fused-in-sarcoma

Another RNA/DNA binding-protein implicated in ALS is fused-in-sarcoma (FUS), encoded by *FUS*. FUS protein is composed of an N-terminal transcription activation domain, a RRM domain and a C-terminal NLS, and bioinformatic analysis identified two prion-like domains (Harrison & Shorter, 2017; Morohoshi et al., 1998). Like TDP-43, under normal conditions FUS is localised within nuclei, where it comprises one component of transcriptional complexes. FUS is also involved in RNA splicing, where it preferentially binds long introns, and in nuclear mRNA export. It can also bind to single and double stranded DNA, where it is involved in the DNA damage response (Guerrero et al., 2016). There is growing evidence of functional overlap between FUS and TDP-43, as they interact to regulate the expression of a common target (histone deacetylase 6), and FUS overexpression rescues TDP-43 knockdown in zebrafish (Kabashi et al., 2011; Kim et al., 2010).

Similar to *TARDBP* mutations, *FUS* mutations are also found in a small percentage of familial ALS cases (4%) (Kwiatkowski et al., 2009). *FUS* mutations are mainly located in the NLS, leading to its cytoplasmic sequestration and aggregation. A proposed pathomechanism in mutant FUS models is cytoplasmic FUS retention in stress granules, causing loss-of-nuclear function. A mouse model of R514G FUS showed that mutant FUS aggregates in axons, where it reduces axonal translation and synaptic functions (Guerrero et al., 2016; López-Erauskin et al., 2018; Vance et al., 2009; X. Zhang et al., 2020). A small minority of FTD cases are associated with FUS pathology, but there is no evidence that FTD is ever caused by FUS mutations (Nolan et al., 2016).

1.2.3. C9ORF72

The most common mutation in European sALS and fALS is a hexanucleotide (GGGGCC) repeat expansion (HRE) in intron-1a of *C9ORF72* (DeJesus-Hernandez et al., 2011; Renton et al., 2011). It accounts for 33.7% fALS cases and 7.4% sALS cases (Mathis et al., 2019; Zou et al., 2017), and it is the main genetic link between ALS and FTD, causing nearly 60% familial ALS/FTD, 15% sporadic ALS/FTD, and 25% FTD-only cases (van der Zee et al., 2013). After the locus was narrowed down to a common signal on the short arm of chromosome 9, in 2011 two independent groups discovered this HRE in a non-coding region of *C9ORF72* (DeJesus-Hernandez et al., 2011; Morita et al., 2006; Renton et al., 2011; van Es et al., 2009). While the precise number of repeats required to illicit disease is unclear, healthy subjects carry up to 30 hexanucleotide repeats, whereas symptomatic patients normally carry between hundreds and several thousand repeats (Beck et al., 2013; Chen et al., 2016; Van Mossevelde et al., 2017). The detection methods used to determine repeat lengths are repeat-primed PCR (RP-PCR) and Southern

blot hybridisation from samples such as blood, cerebrospinal fluid, brain and spinal cord. There is some evidence that different repeat lengths can be found in the same patient in different biofluids and tissues, with studies suggesting that CNS tissue has longer repeats compared to non-neuronal cells, which may contribute to an increased neuronal vulnerability (Akimoto et al., 2014; Floeter & Gendron, 2018; Suh et al., 2018; van Blitterswijk et al., 2013; Vu & Bowser, 2016).

There is no clear evidence of a link between HRE length, disease severity and age of onset. However, one meta-analysis study calculated that units between 24 and 30 repeats are a risk factor for developing ALS (Chen et al., 2016). Another risk factor in fALS may be the methylation level of CpG islands, even if there is still an open debate about the relationship between methylation and C9ORF72 pathology. One study observed a direct correlation between repeat size and methylation level of the CpG island, suggesting that increased methylation is coupled with HRE amplification (Hsiung et al., 2012). In contrast, a later study indicated that *C9ORF72* promoter hyper-methylation is associated with slower disease progression (Russ et al., 2015).

The first studies that identified the HRE in *C9ORF72* also reported a reduction in *C9ORF72* transcript levels, implicating a pathological loss-of-function mechanism (DeJesus-Hernandez et al., 2011; Renton et al., 2011). The product of *C9ORF72* is structurally homologous to guanine nucleotide exchange factor (GEF) proteins, belonging to the differentially expressed in normal and neoplasia (DENN)-like family. GEF proteins interact with Rab proteins, suggesting that C9ORF72 is a Rab-GEF (Levine et al., 2013). However, the finding of RNA and protein aggregates in *post-mortem* C9orf72-ALS/FTD patients suggested a toxic gain-of-function mechanism. RNA foci contain sense and antisense transcripts of the HRE,

and have been found to sequester nuclear proteins (DeJesus-Hernandez et al., 2011; Fratta et al., 2012; Gendron et al., 2013; Y. B. Lee et al., 2013; Mizielinska et al., 2013). Both sense and antisense HRE transcripts can be translated by non-canonical repeat-associated non-ATG initiated (RAN) translation, producing five different polypeptides: glycine-alanine (GA), glycine-proline (GP), glycine-arginine (GR), proline-arginine (PR), and proline-alanine (PA) (Mori, Arzberger, et al., 2013; Mori, Weng, et al., 2013; Zu et al., 2013). *Post-mortem* immunohistochemistry analysis of C9orf72 patients revealed aggregates of p62-positive, TDP-43 negative dipeptide-repeat proteins (DPR) (Mackenzie et al., 2013; Mann et al., 2013; Stewart et al., 2012). However, as these DPRs are rare in the spinal cord but abundant in cerebellar molecular layer, their role in the pathogenesis of ALS remains unclear (Al-Sarraj et al., 2011; Gomez-Deza et al., 2015). The size and biological effects of the DPRs are still under investigation, but they may cause nucleolar stress, translational deficits, nucleocytoplasmic dysfunction, oxidative stress, and autophagy (Freibaum & Taylor, 2017; Kramer et al., 2018).

1.2.4. Superoxide dismutase 1

The first genetic mutation discovered to be linked to fALS was a dominant missense mutation in the gene *superoxide dismutase 1* (*SOD1*), encoding a zinc/copper metalloenzyme that reduces superoxide to hydrogen peroxide (Azadmanesh & Borgstahl, 2018; Rosen et al., 1993). Mutations in SOD1 are the second most common genetic cause of fALS, accounting for 14 – 15% familial cases in Europe and more than 30% in Asia (Mathis et al., 2019). Since 1993, more than 180 mutations in *SOD1* have been discovered, but many have been identified only in single families or individuals and have not yet been functionally validated

(Abel et al., 2012). *SOD1* mutations cause a variety of different disease onsets and severities, even within individual lineages. The alanine 4 to valine (A4V) mutation, for example, is associated with a severe, fast-progressing disease, while the recessive mutation aspartic acid 90 to alanine (D90A) correlates with a slow-progressing disease (Turner & Talbot, 2008).

The discovery of the first *SOD1*-ALS mutation by Rosen et al., was followed by the measurement of a significant reduction in SOD1 activity and accumulation of ROS, suggesting a loss-of-function pathomechanism (Bowling et al., 1993; Rosen et al., 1993). Soon after, a transgenic SOD1 mouse model carrying the glycine to alanine mutation ($SOD1^{G93A}$) recapitulated many ALS-like phenotypes, including locomotor deficits, hyper reflexia, paralysis and premature death. However, SOD1 activity was upregulated, demonstrating a gain-of-function toxicity (Gurney et al., 1994). These results were corroborated by mouse and rat models overexpressing wild-type SOD1, that showed axonal degeneration, loss of spinal motor neurons, and mitochondrial SOD1 accumulation (Jaarsma et al., 2000). Additionally, SOD1 knock-out mice did not develop ALS-like behaviours and motor neuron degeneration, demonstrating that SOD1 loss-of-function is not sufficient to cause neurodegeneration (Ho et al., 1998; Kondo et al., 1997; Reaume et al., 1996; Turner & Talbot, 2008). The prevailing belief therefore is that the pathogenic effect of mutated SOD1 is predominantly via a toxic gain-of-function mechanism.

Many mutant SOD1 models, however, exhibit ALS-like downstream phenotypes, including oxidative stress, excitotoxicity, neuroinflammation, axonal transport deficits, and mitochondrial dysfunction. The difference from other ALS cases is the nature of the cytosolic protein aggregates. Mutant SOD1 models and *SOD1*-ALS *post-mortem* data demonstrated that the main component of the aggregates is

SOD1 itself, and not TDP-43 (Mackenzie et al., 2007). However, one study conducted in cells overexpressing mutant and wild-type SOD1 demonstrated direct interactions between mutant SOD1 and TDP-43, suggesting that SOD1 neurotoxicity might be linked to TDP-43 (Higashi et al., 2010).

1.2.5. Other causative genes

Causative mutations in other genes occur in < 1% of all ALS cases. These genes include ***optineurin* (*OPTN*)**, a multi-functional protein involved in cargo-trafficking, organelle maintenance, and autophagic adaptation (Ryan & Tumbarello, 2018). OPTN function is driven by interactions with many proteins and post-translational modifications. One of its main regulators is TRAF family member-associated NF-κB activator-binding kinase 1 (**TBK1**), mutations in which are also associated with ALS/FTD (Ahmad et al., 2016). There are cases with both OPTN and TBK1 mutations, suggesting an oligogenic component to the disease (Pottier et al., 2015). *OPTN*-ALS cases carry mutations on its ubiquitin-binding site, suggesting autophagic dysfunction. Neuropathological studies in *OPTN*-ALS cases describe occasional wild-type OPTN inclusions, and the few *post-mortem* mutant OPTN cases showed multiple proteinopathies, such as phosphorylated TDP-43, α-synuclein, tau, or mutations in other ALS/FTD genes, supporting the evidence of ALS as a complex neurodegenerative disease (Maruyama et al., 2010).

Another gene implicated in ALS is ***ubiquilin-2***, encoding for a protein involved in protein homeostasis, autophagy and stress granule formation (K. Y. Zhang et al., 2014). The mutations in *ubiquilin*-2 causing ALS/FTD are in the domains that allow interactions between the protein, the proteasome and the ubiquitin chain of the cargo, suggesting that mutations in ubiquilin-2 would cause proteasomal

deficits (Deng et al., 2011; K. Y. Zhang et al., 2014). However, recent proteomic studies investigating possible interactors of ubiquilin-2 showed enrichment in stress granule components. In particular, it interacts with FUS to supress its recruitment to the stress granules (Alexander et al., 2018).

One of the first genes associated with ALS discovered by whole-exome sequencing was ***vasolin-containing protein* (*VCP*)** (J. Johnson et al., 2010). Mutations in VCP affect 1 – 2% fALS cases, and were already known to cause FTD (J. Johnson et al., 2010). VCP is a multifunctional protein involved in protein homeostasis, mitochondrial quality control and apoptosis. Mutations in VCP are associated with TDP-43 mislocalisation, mitochondrial dysfunction and oxidative stress (Evans & Holzbaur, 2019; Hall et al., 2017).

Another RNA/DNA binding protein linked to ALS/FTD is ***matrin-3* (*MATR3*)** (J. Johnson et al., 2014; Salton et al., 2011). *MATR3* mutations do not cause re-localisation of the protein, but it has been shown to create strong interactions with TDP-43 and FUS, suggesting it has a regulatory or compensatory action (Gallego-Iradi et al., 2015; Yamaguchi & Takanashi, 2016). Moreover, MATR3 interacts with the nuclear export complex, and mutant matrin-3 cells showed altered mRNA nuclear export, indicating a loss-of-function mechanism (Boehringer et al., 2017).

Together, the involvement of all the genes described here suggests that the pathogenesis of ALS converges on several established pathways including RNA homeostasis, cellular stress induced by protein aggregation, nucleocytoplasmic trafficking, autophagic deficits and oxidative stress. However, it is still unclear how the products of different genes which are involved in diverse pathways could lead to the same disease. Moreover, the HRE in *C9ORF72* increases the variables to consider – haploinsufficiency, RNA toxicity, and proteinopathy.

1.3. C9ORF72 function

1.3.1. C9ORF72 is involved in vesicular transport

Bioinformatic analysis placed C9ORF72 as a member of the Rab-GEF family, a group of proteins that regulate intracellular membrane dynamics via vesicle formation, movement and fusion (Levine et al., 2013). For this reason, many groups have focused on the role of C9ORF72 in macroautophagy, a catabolic process that requires the formation of double-membranous organelles, called autophagosomes, and their fusion with lysosomes (Oku & Sakai, 2018). Moreover, autophagy dysfunction is a common pathomechanism in several neurodegenerative diseases including Parkinson's, Alzheimer's, and Huntington's diseases, as well as in ALS cases associated with mutations in *p62* and *VCP* (Nixon, 2013).

Overexpression of human C9ORF72 in neuronal N2a mouse cells identified the formation of a complex between C9ORF72, WDR41 and Smith–Magenis syndrome chromosome region candidate 8 (SMCR8) (Sellier et al., 2016). SMCR8 contains a DENN domain like C9ORF72, and it is regulated by the kinase TBK1, already shown to be involved in autophagy regulation (Jung & Behrends, 2020). Moreover, C9ORF72 was found to interact with Rab8 and Rab39, which are GTPases involved in autophagy and vesicular trafficking (Sellier et al., 2016). Further studies have corroborated these findings, indicating that C9ORF72 might regulate vesicular trafficking and play a role in autophagy (Amick et al., 2016; Leskelä et al., 2019; Sullivan et al., 2016; M. Yang et al., 2016). Other studies have also demonstrated increased autophagic flux and lower extracellular vesicle secretion in *C9ORF72* knockout models and C9orf72 mutant induced pluripotent stem cell

(iPSC)-derived MNs, caused by reduced interaction between C9ORF72 and Rab7L1 (Aoki et al., 2017; Dafinca et al., 2016; Ugolino et al., 2016).

Mass spectrometry analysis identified another potential function of C9ORF72. Overexpressed C9ORF72 interacted with cofilin, a regulator of actin dynamics, inducing axonal growth, while C9ORF72 downregulation reduced axonal length (Sivadasan et al., 2016). The study showed that C9ORF72 downregulation activated ADP-ribosylation factor-6 (Arf6), a GTPase involved in vesicle trafficking and actin dynamics. GTP-bound Arf6 activated a second small GTPase, Rac1, which led to the phosphorylation and activation of the kinases LIMK-1/2 that inactivated cofilin. The phosphorylation of cofilin lowered actin dynamics and reduced axonal growth.

More recent studies with optimised C9ORF72 antibodies have demonstrated that C9ORF72 localises in the pre-synaptic region, in particular with synaptic vesicular proteins, lysosomes, Rabs and SMCR8 (Frick et al., 2018). Furthermore, SMCR8 loss-of-function mutant mice developed similar phenotypes reported in *C9ORF72* knockout mice, such as autoimmunity and lysosomal activation, indicating that C9ORF72 and SMCR8 are factors in the same molecular pathway (Y. Zhang et al., 2018). The role of C9ORF72 in vesicular trafficking was also supported by transcriptomic profiles of cerebellum and frontal cortex of C9orf72 patients, which exhibited differential expression of genes involved in vesicles and intracellular transport, lysosome organisation, and synaptic transmission (Prudencio et al., 2015). Deficits in vesicle transport at the pre-synaptic level could lead to the decreased regulation of glutamate receptors, causing glutamate excitotoxity described in C9orf72 mutant iPSC-derived MNs and *C9ORF72* knockdown models (Dafinca et al., 2020; Fomin et al., 2018; Selvaraj et al., 2018).

1.3.2. Hexanucleotide expansion causes C9ORF72 haploinsufficiency in ALS/FTD patients

Alternative splicing leads to the transcription of three variants of *C9ORF72*, which include a short isoform (NM_145005), expressing a 222 amino acid protein encoded by exons 2 – 5, and two long variants expressing the same 481 amino acid-long protein encoded by exons 2 – 11 (NM_018325 and NM_001256054). The HRE lies in a non-coding region between exon-1a and exon-1b, meaning that it is located in the promoter of the short isoform or in intron-1a of the long isoforms (Figure 1.1). The first two publications describing the (GGGGCC) expansion in ALS/FTD patients reported reduced expression of all the transcript variants and downregulation of C9ORF72 protein (DeJesus-Hernandez et al., 2011; Renton et al., 2011). Since then, many other studies measured the total C9ORF72 protein level in *post-mortem* tissue, and tried to determine its subcellular localisation. However, difficulties in generating reliable antibodies and small sample sizes have produced inconsistent results.

One study developed isoform-specific antibodies to localise and quantify both isoforms (Xiao et al., 2015). The short C9ORF72 isoform localised to the nuclear membrane in healthy brain patients, while in C9orf72 patients it shifted to the plasma membrane, and it was upregulated in the temporal and frontal cortex. The same study also showed a significant downregulation of the long isoform in C9ORF72 patients, describing a cytosolic localisation and speckle-organisation in Purkinje cells (Xiao et al., 2015). Other studies described the long isoform of C9ORF72 to be a cytosolic protein, downregulated in the brains of C9ORF72 patients, and not in the spinal cord (Frick et al., 2018; Saberi et al., 2017; Viodé et al., 2018; Waite et al., 2014). Few studies detected significant reduction of *C9ORF72*

transcripts, but this did not correlate with protein downregulation (DeJesus-Hernandez et al., 2011; Stewart et al., 2012). However, increasing data from *post-mortem* tissue confirmed C9ORF72 mRNA downregulation throughout the whole brain of C9ORF72 patients (TargetALS.org). One report of a single unaffected HRE-carrier (70 repeats) showed C9ORF72 upregulation, RNA foci, DPRs, and absent TDP-43 pathology (McGoldrick et al., 2018).

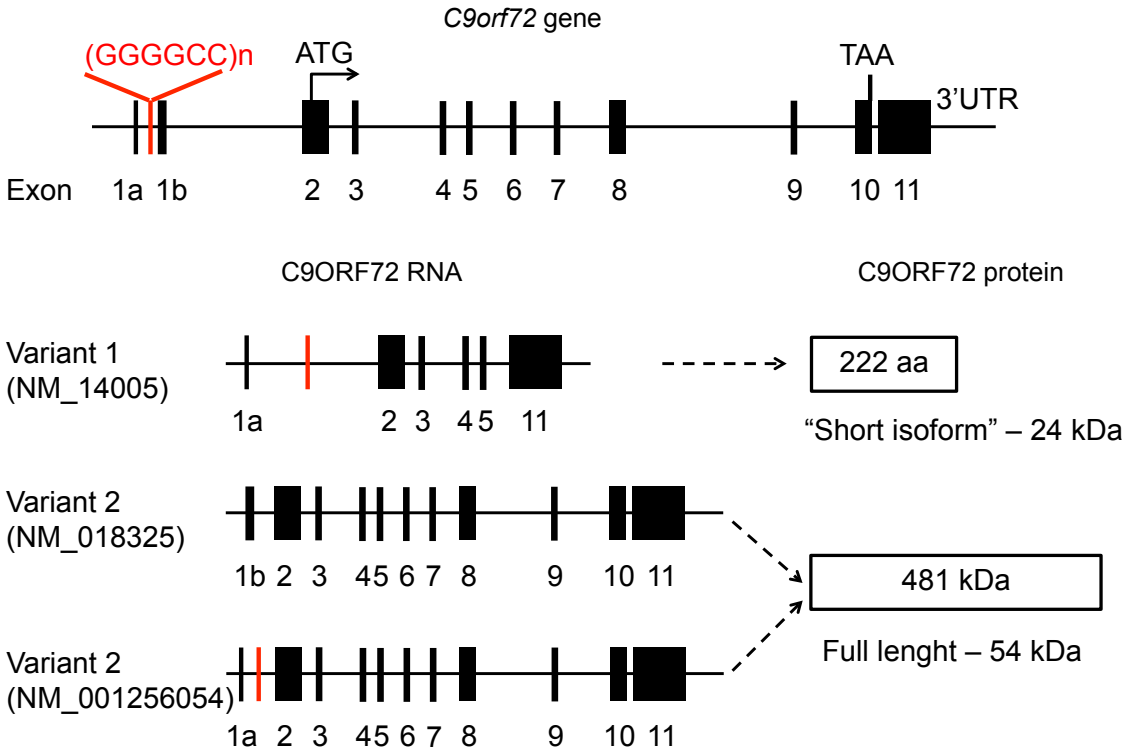


Figure 1.1: Diagram of *C9ORF72* gene, RNA transcripts and protein isoforms.

1.3.3. C9ORF72 loss-of-function in animal and cellular models

C9ORF72 haploinsufficiency has been studied in animal and cellular models with knockdown and knockout of the gene. Knockdown of the *C9ORF72* orthologue in zebrafish led to short motor neuron processes and locomotor deficits, behaviours previously described in zebrafish models of TDP-43 and FUS (Ciura et al., 2013; Kabashi et al., 2010, 2011). The same year a null mutation of the *C9ORF72* orthologue in *C. elegans* led to motility defects followed by paralysis, and degeneration of motor neurons (Therrien et al., 2013). In contrast, conditional *C9ORF72* knockout mice did not exhibit motor neuron degeneration or motor function deficits, suggesting that C9ORF72 loss-of-function is not sufficient to cause ALS (Koppers et al., 2015). Furthermore, other *C9ORF72* knockout mice did not display ALS-like phenotypes, but they showed that C9ORF72 might be implicated in lysosomal function and autophagy, as the mice showed accumulation of lysosomes in macrophages and microglia, age-related inflammation, and immune system dysregulation (Amick et al., 2016; Atanasio et al., 2016; Burberry et al., 2016; O'Rourke et al., 2016; Sullivan et al., 2016; Ugolino et al., 2016). However, each of these C9orf72 KO models displayed different survival curves. The cause of this discrepancy is unclear, but recent evidence suggests that the microbiological environment where each is raised may be important (Burberry et al., 2020)

The evidence that ALS and FTD are complex diseases with oligogenic influences, and the differences seen between animal models, highlight the importance of using human cell lines. The use of iPSC technologies in particular allows for the study of genetic diseases in their native genetic background and in different cell types. Additionally, CRISPR/Cas9 genome editing is a powerful tool with the

ability to correct *in vitro* mutations with a high degree of precision, permitting the study of downstream phenotypes in an identical genetic context to that of the patient. There are mixed reports of *C9ORF72* transcript levels in iPSC-derived MNs and cortical neurons (CNs) from HRE carriers, with only some studies detecting significant reduction of *C9ORF72* mRNA, that suggest transcriptional downregulation (Ababneh et al., 2020; Donnelly et al., 2013; Y. Shi et al., 2018). Functional experiments in iPSC-derived MNs and CNs described common phenotypes, such as increased susceptibility to autophagic treatments and increased apoptosis, disruption of lysosomal trafficking, glutamate excitotoxicity caused by increased calcium permeable subunits in AMPA receptors, and mitochondrial calcium buffering deficits (Almeida et al., 2013; Bursch et al., 2019; Dafinca et al., 2016, 2020; Donnelly et al., 2013; Sareen et al., 2013; Selvaraj et al., 2018; Y. Shi et al., 2018). Correction of the HRE with CRISPR/Cas9 technology rescued the normal *C9ORF72* transcript level and reduced glutamate excitotoxicity, indicating that C9ORF72 downregulation may affect the turnover of glutamate receptors (Ababneh et al., 2020; Dafinca et al., 2020; Selvaraj et al., 2018).

1.3.4. C9ORF72 HRE mouse models

Three independent mouse models carrying a bacterial artificial chromosome (BAC) containing the human *C9ORF72* gene with (GGGGCC) repeats have been established (Baloh et al., 2016; Y. Liu et al., 2016; Peters et al., 2015). Two of these models, one using 500 repeats and the other up to 1000 repeats, did not develop cognitive or motor deficits or decreased survival, despite neuropathological analysis showing RNA foci formation and DPR expression (Baloh et al., 2016; Peters et al., 2015). In contrast, another BAC mouse carrying 500 repeats inserted in the full *C9ORF72* gene exhibited anxiety, motor deficits and decreased survival,

coupled with denervation, axonal degeneration, neuronal loss, RNA foci formation and DPR expression (Y. Liu et al., 2016). The discrepancy between models is probably due to the insert chosen. Peters cloned the first six exons and the upstream sequence, while Liu used the full gene with flanking regions to replicate the human genomic environment, probably leading to C9ORF72 loss of function. If this were true, it would be a clear evidence that the formation of RNA foci and DPR translation are not sufficient for triggering the disease. However, mice infected with an adeno-associated viral (AAV) vectors expressing $(GGGGCC)_{66}$ repeats under an actin promoter developed behavioural deficits including anxiety, hyperactivity and motor impairments (Chew et al., 2015; Herranz-Martin et al., 2017). These also showed RNA foci formation, poly(GP), poly(GA) and poly(GR) aggregates, TDP-43 pathology, as well as neuronal loss and denervation. Additionally, a different AAV-mouse model expressing 149 repeats exhibited co-localisation of poly(GR) with stress granules and phospho-TDP-43, suggesting that poly(GR) might be responsible for promoting stress responses and TDP-43 pathology in C9ORF72 cases (Chew et al., 2019).

One study treated HRE-C9ORF72 BAC mice with antisense oligonucleotides (ASOs) targeting the 450 repeat expansion (Jiang et al., 2016). The treatment reduced RNA foci formation, DPR expression and improved behavioural deficits, suggesting that C9ORF72 pathology is dependent on the gain-of-function of the expansion. When these mice were crossed with C9ORF72 loss-of-function mice, the resulting animals showed exacerbated phenotypes, including premature death, DPR accumulation and increased apoptosis (Zhu et al., 2020). This recent study provided evidence that C9ORF72 pathology may be caused by the combination of gain- and loss-of-function.

1.3.5. Microsatellite expansions in other diseases

Microsatellite expansion mutations were already known to be involved in other diseases, such as myotonic dystrophies, Fragile X Syndrome, Spinocerebellar Ataxia and Huntington's Disease. Fragile X Syndrome (FXS) is characterised by a (CGG) expansion in *fragile X mental retardation 1 (FMR1)* gene, leading to epigenetic silencing and loss-of-function of FMR1 caused by DNA aberrant methylation and histone deacetylation (Coffee et al., 1999; Sutcliffe et al., 1992). Shorter (CGG) expansion in *FMR1* was found in patients with the related disorder fragile X-associated tremor/ataxia syndrome (FXTAS) (Goodwin & Swanson, 2014). Current evidence suggest that FXTAS is caused by RNA gain-of-function mechanism, as patients present nuclear RNA foci containing (CGG) repeats, without FMR1 loss-of-function. Several RNPs have been proposed to interact with the repeats, including hnRNP A2/B1, hnRNP G, Purα and CELF1. Misregulation of CELF1 caused by a microsatellite expansion is also implicated in myotonic dystrophies (DM). There are two types of DMs: type 1 (DM1) is characterised by a (CTG) expansion in 3'UTR of *dystrophia myotonica protein kinase (DMPK)*, while type 2 (DM2) presents a (CCTG) expansion in the first intron of *cellular nucleic acid binding protein (CNBP)* (Brook et al., 1992; Liquori et al., 2001). Although they are two independent and distinct genes, the transcription of the expansions produces nuclear RNA foci that sequester RBPs involved in diverse RNA processing steps, resulting in their misregulation (Goodwin & Swanson, 2014). Moreover, myoblasts, skeletal muscles and blood of DM1 patients showed protein aggregates containing the product of (GTC) translation (Zu et al., 2011). The study demonstrated that RAN translation is responsible for the expression of poly-glutamine chain (polyQ) in DM1, and also in Spinocerebellar Ataxia type 8

(SCA8), characterised by (CTG/CAG) expansion in *ataxia 8* (*ATX8*). There are several types of SCAs resulting from mutations in 37 genes, and several of these mutations are (CTG/CAG) expansions (Klockgether et al., 2019). The polyQ SCAs present accumulation and aggregation of polyQ within the nuclei of neurons, but their toxicity is still under debate. As for DPRs in C9orf72 cases, protein aggregates are found in surviving neurons of SCA patients, questioning the toxic function showed in different animal and cellular models. Another polyQ disease is Huntington's Disease (HD), characterised by (GAC) expansion in a coding region of *Huntingtin* (*HTT*), resulting in HTT expression with a long polyQ tract (Bates et al., 2015). The length of the expansion determines whether an individual will develop the disease and the eventual time of onset. The expansion causes HTT fragmentation, leading to neuronal dysfunction and death. HTT fragments containing polyQ tract aggregate in nuclei and cytosol, causing UPS dysfunction and mitochondrial deficits, as reduced ATP production, mitochondrial depolarisation, and decreased calcium buffering ability (Johri et al., 2013).

1.4. RNA-mediated toxicity caused by HRE in *C9ORF72*

A second pathomechanism implicated in C9ORF72 pathology is RNA-mediated toxicity. RNA foci are found in the human spinal cord, motor and frontal cortex, but also in areas not clinically involved in C9orf72-ALS (DeJesus-Hernandez et al., 2011; Fratta et al., 2012; Gendron et al., 2013; Y. B. Lee et al., 2013; Mizielinska et al., 2013). The central nervous system of C9orf72 patients contains more sense than anti-sense RNA foci, but specific cell types, as cerebellar Purkinje cells and spinal lower motor neurons, have more antisense RNA foci. Moreover, RNA foci are present in lower concentrations in astrocytes, microglia and oligodendrocytes. RNA aggregates are predominantly nuclear and perinuclear. Several studies

analysed the correlation between RNA foci and TDP-43 aggregates in C9orf72 cases and cellular systems, and found no evidence of an association (Aladesuyi Arogundade et al., 2019; Cooper-Knock et al., 2015; DeJesus-Hernandez et al., 2011, 2017; Gendron et al., 2013; Lagier-Tourenne et al., 2013; Mizielinska et al., 2013; Zu et al., 2013).

Bioinformatic analysis predicted HRE to form G-quadruplexes, due to the presence of G-rich sequences, which has been confirmed using NMR and circular dichroism spectroscopy on *in vitro* synthesized $(GGGGCC)_4$ RNA (Fratta et al., 2012; Haeusler et al., 2014). G-quadruplexes were already known to sequester RNA-binding proteins in other diseases, such as myotonic dystrophy and Huntington's disease, therefore causing downstream effects to RNA splicing and transport (Cooper et al., 2009). Immunofluorescence and mass spectrometry analysis of *post-mortem* C9ORF72 cases, C9orf72 mutant iPSC-derived MNs, and pulldown of exogenous expressed HRE, demonstrated that RNA foci aggregated with RNA-binding proteins involved in splicing, mRNA transport and translation (Cooper-Knock et al., 2014, 2015; Haeusler et al., 2014; Y. B. Lee et al., 2013; Mori, Lammich, et al., 2013; Sareen et al., 2013). Moreover, C9orf72 mutant iPSC-derived MNs showed that (GGGGCC) transcripts are incorporated in granules to be transported to the synapse, and disrupt local translational events, reinforcing the hypothesis of RNA-mediated toxicity as mechanism leading to C9ORF72 pathology (Burguete et al., 2015).

The first animal model developed to study RNA foci-related toxicity used *Drosophila* expressing 30 sense repeats in the eyes or in the motor neurons (Z. Xu et al., 2013). The ocular expression of the repeats resulted in rapid disruption of eye morphology, and motor neuronal expression led to locomotor deficits.

Interactome analysis of the RNA foci-binding partners detected the same RNA-binding proteins identified in C9orf72 patients and mutant iPSC-derived MNs. The overexpression of RNA-binding proteins rescued the neurodegeneration induced by the repeats, indicating toxic gain-of-function of RNA foci. However, subsequent RNA-only *Drosophila* models did not show the same RNA-mediated toxicity, as the expression of up to 288 repeats did not cause eye degeneration and did not reduce the lifespan of the flies (Mizielinska et al., 2014; Moens et al., 2018; Tran et al., 2015).

1.5. Repeat-associated non-ATG (RAN) initiated translation of the HRE *C9ORF72* transcripts generates poly-dipeptides

1.5.1. RAN-translated dipeptide repeat proteins are the pathological hallmark of C9ORF72 HRE

Immunohistochemical analysis of *post-mortem* tissue revealed p62- and ubiquilin-2-positive, TDP-43-negative aggregates in brains of ALS patients (Al-Sarraj et al., 2011; Boxer et al., 2011; Stewart et al., 2012; Troakes et al., 2012). After the identification of the HRE in *C9ORF72*, other *post-mortem* studies characterised those aggregates as the products of repeat-associated non-ATG (RAN) initiated translation of the HRE transcripts. RAN-translation generates five dipeptide repeat (DPRs) from three open reading frames of both sense and antisense transcripts: the sense DPRs poly(GA), poly(GP) and poly(GR), and the antisense DPRs poly(GP), poly(PR) and poly(PA) (Ash et al., 2013; Gendron et al., 2013; Mann et al., 2013; Mori, Arzberger, et al., 2013; Mori, Weng, et al., 2013; Zu et al., 2013). One more component of cytoplasmic DPR aggregates is Drosha, a RNase involved in miRNA biogenesis (Porta et al., 2015).

Neuropathological studies of C9orf72 patients showed that poly(GP), poly(GA) and poly(GR) are more frequent than poly(PR) and poly(AP), and they are found throughout the whole brain of C9orf72 patients (Mackenzie et al., 2015; Schludi et al., 2015). DPR inclusions are most abundant in hippocampus, cerebellum, frontal and primary motor cortex, while they are rare in spinal cord (Davidson et al., 2014; Gomez-Deza et al., 2015; Mackenzie et al., 2015; Mann et al., 2013; Schludi et al., 2015). The only DPR that has been successfully related to neurodegeneration is poly(GR), which aggregation differs between ALS and FTD (Gittings et al., 2020; Saberi et al., 2017; Sakae et al., 2018). DPRs can be observed in different morphologies, believed to relate to their solubility. Most commonly the inclusions are star-shaped or amorphous. The arginine-rich DPRs are perinuclear or nuclear, while the other DPRs aggregate in the cytosol. The sense DPRs can also form aggregates in dendrites, and only poly(GP) and poly(GA) have rare cytoplasmic diffuse signals, suggesting they transit between soluble and insoluble states (Saberi et al., 2017). Moreover, poly(GP) was also found in cerebrospinal fluid and blood of asymptomatic HRE carriers, indicating poly(GP) as a potential biomarker for the pre-symptomatic phase of C9orf72-ALS/FTD (Gendron et al., 2017; Lehmer et al., 2017). This evidence and further pathological studies on HRE carriers who died prematurely suggest that DPR aggregates appear early in the disease, preceding TDP-43 pathology (Baborie et al., 2015; Vatsavayai et al., 2016).

The study of DPR pathology in *post-mortem* tissue poses considerable challenges. All the antibodies commercially available recognise short dipeptide repeat sequences, leaving unanswered questions about the actual DPR length and the possible relationship between their length and disease severity. Furthermore, if DPR toxicity were causing neuronal death, the most toxic DPRs might not be

detected by *post-mortem* immunohistochemistry, as the DPRs would be degraded along with the dying neurons. However, it is also possible that aggregates persist after the cell has been destroyed, as demonstrated with "ghost" Tau tangles in Alzheimer's Disease (Gendreau & Hall, 2013). Moreover, each DPR has different physico-chemical properties that determine solubility and interactions. Primary cortical neurons treated with *in vitro* synthesized DPRs helped the characterisation of their physico-chemical properties. Treatments with poly(GR) or long poly(GA) reduced neuronal survival, compared to poly(GP), poly(PA) and short poly(GA) (Flores et al., 2016). Poly(GP), poly(PA) and short poly(GA) were mostly soluble, while poly(GR) organised in spherical aggregates and long poly(GA) formed β-sheet fibrils, without an amyloid structure (Brasseur et al., 2020; Chang et al., 2016; Flores et al., 2016). A recent study examined the differences in DPR expression and DPR solubility between HRE of *C9ORF72* and the expansion in *NOP56*, causing spinocerebellar ataxia type 36 (SCA36) (McEachin et al., 2020). Translation across both expansions results in poly(GP) and poly(PR) expression. Notably, poly(GP) in SCA36 human tissue is soluble, while poly(GP) in C9ORF72 cases is also found in aggregates. They demonstrated that the different solubility is caused by the co-aggregation of poly(GP) and poly(GA) in C9orf72 mutant cells. The use of animal models and cellular systems solved the abovementioned problems and allowed the study of single DPRs. The current main issue is to link DPR-mediated toxicity to neurodegeneration in C9ORF72 disease.

1.5.2. Regulation of DPR expression

Right before the discovery of the (GGGGCC) expansion in *C9ORF72*, one study demonstrated that RAN translation was responsible for the expression of repeat expansions in spinocerebellar ataxia 8 and myotonic dystrophy type 1, leading to

the idea this may also be the case in C9orf72-ALS/FTD. Since then, considerable effort has been directed to studying the specific factors involved in HRE transcription, RAN translation, and their potential for therapeutic downregulation (Zu et al., 2011). Previous study established that ATG-independent translation was possible in the presence and formation of hairpin structures which slow down the scanning process of the ribosomal subunit 40S, allowing the formation of strong interactions between tRNA and the mRNA (Kochetov et al., 2007; Kozak, 1989; Peabody, 1989).

An elegant *in vitro* study described the translation of sense DPRs (Tabet et al., 2018). DPR translation is dependent on 5' cap insertion, initiates with a methionine and requires the same initiator factors as canonical translation. The translation of the three open reading frames starts from a specific CUG codon located upstream of the repeats and embedded in a Kozak sequence. Interestingly, in the event of a mutated start codon, poly(GA) expression starts downstream with a different start codon, while poly(GP) and poly(GR) translation is reduced. Further studies found more evidence that eukaryotic initiation factors 4B/H are necessary for RAN translation, and that the HRE transcription is mediated by the CDC73/PAF1 complex (PAF1C), a transcriptional regulator of RNA polymerase II (Goodman, Prudencio, Kramer, et al., 2019; Goodman, Prudencio, Srinivasan, et al., 2019). A genetic screen identified the small ribosomal protein subunit 25 (RPS25) as a factor required for efficient RAN translation, even if a recent did not corroborate this finding (A. G. Johnson et al., 2020; Yamada et al., 2019).

Even though RAN translation of the HRE requires the same factors as canonical translation, there is evidence of DPR upregulation during the integrated stress response (ISR) (Cheng et al., 2018). The core event of ISR is the phosphorylation of

the α subunit of eukaryotic initiation factor-2 (eIF2 α), which causes downregulation of canonical translation, upregulation of cap-independent RAN translation and expression of intronic repeats. Activation of glutamate receptors activated ISR in C9orf72 mutant iPSC-derived MNs causing DPR upregulation, further indicating that DPR translation is dependent on cellular environment and contributes to C9ORF72 pathology (Westergard et al., 2019).

Several studies have proposed downregulation of HRE transcription and RAN translation as therapy for C9orf72-ALS/FTD. Downregulation of the transcription factors SUPT4H1 and SUPT5H in human C9orf72 mutant fibroblasts and in iPSC-derived CNs reduced RNA repeat transcripts and poly(GP) expression (Kramer et al., 2016). Moreover, suggested repressors of repeat neurotoxicity in *Drosophila* were the zinc finger protein Zfp106, a specific GGGGCC RNA binding protein, and the RNA helicase DDX3X, as its upregulation remodelled sense transcripts and decreased RAN translation (Celona et al., 2017; Cheng et al., 2019). A different study showed that hairpin formation is required for efficient RAN translation, and indicated that upregulation of DDX3X could be a pharmacological strategy (Z. Wang et al., 2019).

1.5.3. DPR-mediated toxicity in animal and cellular models

Several animal models expressing the repeat expansion or optimised repeat sequences to avoid RNA foci formation have been established. The first *Drosophila* models were developed to dissect the differential contribution of RNA foci and DPRs to C9ORF72 pathology, and showed that DPR expression alone was sufficient to cause adult-onset neurodegeneration (Mizielinska et al., 2014; Z. Xu et al., 2013). The flies were cloned with up 103 (GGGGCC) repeats, or up to 288

repeats interrupted with stop codons to avoid DPR expression, or optimised codon repeats to avoid RNA foci formation. Only the flies expressing the DPRs showed motor neuronal deficits and decreased survival. Moreover, only poly(GR) and poly(PR) caused eye degeneration, compared to the other DPRs, indicating that arginine-rich DPRs are more toxic. Further evidence supporting the hypothesis of DPR-mediated toxicity was presented in different *Drosophila* models, which showed neurodegeneration and decreased survival in response to DPR expression in a dosage- and length-dependent mechanism (Freibaum et al., 2015; Goodman, Prudencio, Srinivasan, et al., 2019; Tran et al., 2015).

Animal and cellular models expressing optimised-codon repeats contributed to identifying the different toxicity of each DPR. Transfection of mouse motor neuron-like cells, such as NSC-34, and primary neurons, with tagged DPRs, demonstrated that arginine-rich DPRs induced cellular death, while the other DPRs and RNA repeats did not show such toxicity (Tao et al., 2015). The same study observed nuclear aggregates of poly(PR) and poly(GR), cytoplasmic aggregates of poly(GA) and poly(PA), and diffuse localisation of poly(GP). Expression of poly(PR) and poly(GR) in iPSC-derived MNs reduced cellular viability, further indicating their toxicity.

The arginine-rich DPRs have often been shown to exhibit the highest toxicity in various animal models. Flies expressing 80 FLAG-tagged optimised-codon repeats showed diffuse expression of poly(PR) and poly(GR), which decreased survival, and a different *Drosophila* study demonstrated that glutamatergic neurons were selectively vulnerable to the expression of arginine-rich DPRs (W. Xu & Xu, 2018; D. Yang et al., 2015). Moreover, poly(PR) and poly(GR) expression in mice decreased survival rate, caused motor and cognitive deficits, and induced synaptic

dysfunction, microgliosis and astrogliosis (Choi et al., 2019; Yamakawa et al., 2015; Y. J. Zhang et al., 2018, 2019). Poly(PR) accumulated in nucleoli, while poly(GR) co-localised with ribosomal subunits, translational factors, and mitochondrial proteins, indicating that the arginine-rich DPRs could cause transcriptional, translational and mitochondrial defects. In *C. elegans,* both $(PR)_{50}$ and $(GR)_{50}$ localised to the nuclei and caused motility defects, neuronal loss and decreased survival span (Rudich et al., 2017).

Other studies have instead demonstrated that poly(GA) expression is the main cause of DPR-mediated toxicity. Primary mouse neurons expressing only $(GA)_{50}$–GFP, showed poly(GA) nuclear aggregates positive for ubiquitin and p62, as in human *post-mortem* tissue, and exhibited cleaved-caspase 3 staining, demonstrating that poly(GA) is toxic for neurons (Y. J. Zhang et al., 2014). Similar results were found in primary rat hippocampal and cortical neurons transduced with lentivirus carrying $(GA)_{149}$, which also caused reduced branching, indicating that poly(GA) could affect axonal development (May et al., 2014). The expression of GFP tagged- and optimised-codon DPRs in cell culture confirmed that poly(GA) is more toxic compared to the other DPRs in this model, it induced TDP-43 cleavage, and it sequestered poly(GP) when co-transfected (Y. B. Lee et al., 2017). Furthermore, this study showed that poly(PA) reduced poly(GA)-mediated toxicity by lowering the number of poly(GA) aggregates and the cleavage of TDP-43, indicating that poly(PA) may act as a protective factor. Two different mouse models, one expressing poly(GA) via AAV vector and one transgenic mouse model, demonstrated that poly(GA) caused anxiety, hyperactivity, motor and cognitive deficits (Schludi et al., 2017; Y. J. Zhang et al., 2016). These mice exhibited p62-positive poly(GA) aggregates in neurons and interneurons,

neuronal loss and apoptosis activation. They also showed that poly(GA) co-aggregated with nucleocytoplasmic transport and proteasome proteins, previously identified in human samples. A zebrafish model showed that poly(GA) was the only DPR inducing degeneration, even though the following year a new zebrafish study argued against poly(GA) toxicity, bringing more evidence of motor neuronal deficits caused by poly(GR) (Ohki et al., 2017; Swaminathan et al., 2018).

In summary, the data from *in vivo* models is inconclusive because of the species differences (mouse, *Drosophila*, *C. elegans*, rat) and different cellular systems used (human iPSC-derived neurons, fibroblasts, mouse or rat primary neurons, neuronal like cells). Moreover, inconsistency in methods, such as different repeat lengths, optimised codons chosen and detection systems preferred, make any comparison between studies questionable. A further debatable element is that HRE or DPR sequences are overexpressed in *in vivo* systems, a condition not yet been proven in C9orf72 patients.

1.6. Cellular mechanisms affected by DPR expression

Transcriptomic profiles derived from C9orf72-ALS/FTD patient cerebellar tissue have demonstrated extensive alternative splicing events caused by the HRE, in particular intron retention and exon skipping affecting transcripts of proteins involved in calcium sensitivity, cell-cycle regulation and transcriptional factors, as well as ALS-related genes (Prudencio et al., 2015). Interestingly, genetic screens on *Drosophila* and *Saccharomyces cerevisiae* expressing DPRs, identified proteins of the abovementioned pathways as possible modifiers of HRE toxicity (Chai & Gitler, 2018; Freibaum et al., 2015; Goodman, Prudencio, Srinivasan, et al., 2019;

Jovičić et al., 2015; K. Zhang et al., 2015). Similar results have been found in CRISPR/Cas9 knockout screens in human cells and primary mouse neurons expressing arginine-rich proteins (Kramer et al., 2018). These screens identified proteins involved in nucleocytoplasmic transport, endoplasmic reticulum functions, proteasome, RNA processing, and chromatin modification, as possible modifiers of poly(PR)- and poly(GR)-mediated toxicity, suggesting that the characteristic transcriptomic profile of C9orf72 cases are highly dependent on arginine-rich DPR expression. Moreover, the exogenous expression of DPRs in iPSC-derived neurons allowed the comparison of transcriptional profiles induced by each DPR to C9orf72 mutant iPSC-derived MNs and *post mortem* tissue (Mordes et al., 2018). These analyses identified an overlap between poly(PR) and poly(GR) transcriptomes with C9orf72 cases, in particular upregulation of heat shock proteins, indicating that arginine-rich proteins cause cellular stress.

1.6.1. Poly(PR) and poly(GR) cause nucleolar stress, reduce protein translation, and impair nucleocytoplasmic transport

Nucleoli are membraneless organelles localised in the nuclei and composed of proteins, DNA and RNA. They are the site where ribosomal RNAs are transcribed and combined with proteins to form incomplete ribosomal subunits, which are transported to the cytosol for final maturation (Thomson et al., 2013). Neuropathological analysis of C9orf72 *post-mortem* tissue, primary mouse neurons and iPSC-MNs expressing poly(PR) or poly(GR), showed arginine-rich DPRs co-aggregating with heterochromatin regions and nucleolar proteins, suggesting that poly(PR) and poly(GR) can induce nucleolar stress and impair gene expression (Davidson et al., 2017; Haeusler et al., 2014; K. Lee et al., 2016; Schludi et al., 2015; Tao et al., 2015; Wen et al., 2014; Xiao et al., 2016; Y. J. Zhang et al., 2019).

Moreover, C9orf72 human brains, showed that neurons containing poly(GR) exhibited enlarged nucleoli, a sign of nucleolar stress (Mizielinska et al., 2017). Nucleolar stress can cause DNA damage, triggering the DNA damage response (DDR), and reduce ribosome biogenesis (Ogawa & Baserga, 2017). DDR markers were detected in lumbar MNs of C9orf72-ALS patients, and neuronal-like cells expressing arginine-rich DPRs showed upregulation of the same proteins, demonstrating that DDR activation in C9orf72 patients is mediated by poly(PR) and poly(GR) (Farg et al., 2017). Moreover, poly(GR) and poly(PR) transfected cells showed nuclear translocation of the nucleolar stress sensor B23, and decreased 18S and 28S rRNA levels, indicating that arginine-rich DPR cause nucleolar stress resulting in reduced ribosome biogenesis (Tao et al., 2015).

Mass spectrometry analysis revealed that poly(PR) and poly(GR) preferentially bind to proteins containing low complexity domains, as RNA binding proteins, nuclear pore components, nucleolar factors, ribosomal subunits, and translational factors (Kanekura et al., 2016; K. Lee et al., 2016; Lin et al., 2016). These findings suggest that arginine-rich DPRs could affect the formation or function of membraneless organelles, such as nucleoli and stress granules, but also translational events. Co-immunoprecipitation assays confirmed the proteomic findings, identifying also TDP-43 and FUS as poly(PR)-binding partners (Kanekura et al., 2016, 2018). Poly(PR) showed high affinity to mRNAs as well, and the DPR-RNA complexes were recognised by the chaperone HSP70, preventing the access of translational factors and causing reduction of the total translation. *In vitro* investigations found that arginine-rich DPRs preferentially bound nucleolar ribonucleoproteins, causing mis-splicing of the mRNA targets and cytoplasmic mislocalisation of spliceosomal factors (Kwon et al., 2014; M. R.

White et al., 2019; Yin et al., 2017). Immunofluorescence analysis on $(GR)_{100}$-mice and C9orf72 human brains showed co-localisation of poly(GR) with ribosomal proteins in the cytosol, resulting in impaired protein translation, further indicating that arginine-rich proteins affect ribosomal function (Y. J. Zhang et al., 2018).

Neuropathological analysis of C9orf72 human brains revealed punctae containing factors of the nuclear pore complex, and immunofluorescence analysis of C9orf72 mutant induced-neurons showed nuclear loss of RCC1, a Ran guanine nucleotide exchange factor (RanGEF) involved in nucleocytoplasmic transport (Jovičić et al., 2015). However, a later study did not detect nuclear abnormalities in C9orf72-ALS spinal cord and cerebellum (Saberi et al., 2017). Moreover, cells expressing (GGGGCC) repeats showed cytoplasmic mislocalisation of the component of the nuclear pore RanGAP1, nuclear envelope abnormalities, and RNA nuclear retention, indicating that the HRE in C9ORF72 may cause nucleocytoplasmic transport deficits (Freibaum et al., 2015; K. Zhang et al., 2015). Gain- and loss-of-function screens in yeast identified import proteins, nuclear import receptors, and a component of the nuclear pore complex as strong suppressors of poly(PR) toxicity, while deletion of translational factors and small ribosomal subunits suppressed poly(GR) toxicity (Chai & Gitler, 2018; Jovičić et al., 2015). The viability of primary cortical neurons expressing $(PR)_{50}$ improved with upregulation of karyopherins, a family of nuclear importins, indicating that poly(PR) may be responsible for the disruption of nucleocytoplasmic transport (Jovičić et al., 2015). Detailed analysis of poly(PR) expressing cells and PR-mice demonstrated that poly(PR) binds to the nuclear pore complex, causing disruption to the nuclear membrane and impeding both nuclear import and export of macromolecules (K. Y. Shi et al., 2017; Y. J. Zhang et al., 2019). On the other hand,

a poly(GA) fly model showed cytosolic sequestration of the nuclear pore complexes, and the expression of poly(GA) in human cells caused cytoplasmic TDP-43 mislocalisation, suggesting that poly(GA) also interferes with nucleocytoplasmic transport of TDP-43 (Khosravi et al., 2016; Y. J. Zhang et al., 2016).

1.6.2. Poly(GA) causes proteasomal dysfunction and axonal deficits

Quantitative proteomic studies of primary mouse cortical neurons expressing poly(GA) showed enrichment of p62, proteasomal subunits, and ubiquitin-related proteins (May et al., 2014). Further analysis with cryo-electron tomography revealed that poly(GA) recruits proteasomes, suggesting that poly(GA) might cause deficits to the ubiquitin-proteasome system (UPS) (Guo et al., 2018). This hypothesis was further refined by the demonstration that transient expression of each DPR showed that poly(GA), poly(GP) and poly(GR) reduced proteasomal activity (Yamakawa et al., 2015). Additionally, a poly(GA) mouse model exhibited delocalisation and aggregation of nuclear proteins HR23A/B with poly(GA). Similar aggregates of HR23A/B and poly(GA) were found in $(GGGGCC)_{66}$ mice and C9orf72 human brains (Y. J. Zhang et al., 2016). They showed that HR23A/B proteins regulate UPS, suggesting that poly(GA) interferes with HR23 functions, leading to UPS deficits. A recent study confirmed that poly(GA) co-localises with proteasomal subunits in *post-mortem* GA-mice and C9orf72 patients, resulting in impaired proteasomal degradation (Khosravi et al., 2020). One study demonstrated that poly(PR) also inhibits the proteasome, and lowers autophagy causing cell death (Gupta et al., 2017).

Moreover, the proteome of poly(GA) expressing cells was enriched with Unc119, a protein involved in axonal development and maintenance, and further analysis confirmed its downregulation and aggregation with poly(GA), indicating that poly(GA) caused Unc119 deficits that led to reduced branching and neuronal degeneration (May et al., 2014). Neuropathological analysis revealed co-aggregation of poly(GA) and Unc119 in C9orf72 patients, validating the previous *in vitro* study and suggesting that poly(GA) causes axonal deficits (Schludi et al., 2015).

1.6.3. DPRs cause endoplasmic reticulum stress

RNA sequencing of primary mouse neurons expressing poly(PR) identified upregulation of genes involved endoplasmic reticulum (ER) stress, in particular the factor ATF4, indicating that poly(PR) activates the integrated stress response or the unfolded protein response of the ER (Kramer et al., 2018). The downregulation of the ER transmembrane protein TMX2, located at the mitochondrial-associated membrane and identified as a possible poly(PR) modifier, also supressed DPR-mediated toxicity via upregulation of the Unfolded Protein Response (UPR) pathways and downregulation of calcium-binding and apoptotic proteins. Further experiments demonstrated that synthetic poly(PR) induced ER stress, and inhibition of the unfolded protein response increased cell survival (R. Wang et al., 2019). In contrast, HEK293T cells and primary mouse neurons expressing $(GA)_{50}$ showed upregulation of UPR, indicating that poly(GA) induced ER stress. The phenotype was rescued with the chemical chaperone TUDCA, an ER stress inhibitor (Y. J. Zhang et al., 2014).

1.7. ALS-related phenotypes induced by DPR expression

1.7.1. The relationship between DPR, RNA foci and TDP-43 proteinopathy

As previously described, C9orf72 human brains exhibit TDP-43 and DPR aggregates that are p62-positive (Mackenzie et al., 2013; Majounie et al., 2012; Mann et al., 2013; Stewart et al., 2012). DPRs have also been found in *post-mortem* brains of C9orf72 asymptomatic cases without TDP-43 pathology, suggesting that DPR pathology may precede TDP-43 mislocalisation (Baborie et al., 2015; Proudfoot et al., 2014). Several studies have analysed the co-occurrence of DPR and TDP-43 aggregates to unravel hidden mechanisms linking the two pathologies. Evidence is still mixed and whether there is a mechanistic relationship between DPR expression and TDP-43 pathology is still debated.

Immunohistochemical analysis of C9orf72 human tissue did not identify co-occurrence of the two pathologies, and a mouse model expressing poly(PR) did not show TDP-43 mislocalisation, indicating that DPRs do not lead to TDP-43 aggregation (Davidson et al., 2016; Gami et al., 2015; Gomez-Deza et al., 2015; Konno et al., 2014; Y. J. Zhang et al., 2019). Contrarily, a different study using in-house produced anti-DPR antibodies detected poly(GR) aggregates in dendrites and perinuclear regions of motor cortex neurons positive for phospho-TDP-43, suggesting that immunohistological studies on *post-mortem* human tissue are highly dependent on the specificity of antibodies used (Saberi et al., 2017). Two independent studies showed co-occurrence of antisense RNA foci and increased cytoplasmic TDP-43 in C9orf72 cases, indicating a possible association between the HRE and TDP-43 pathology (Aladesuyi Arogundade et al., 2019; Cooper-Knock et al., 2015). Mouse models showed that the HRE in *C9ORF72* causes both DPR and

TDP-43 aggregates, while C9ORF72 loss-of-function mice did not exhibit TDP-43 mislocalisation, indicating that the HRE is necessary for TDP-43 pathology in C9orf72 cases (Amick et al., 2016; Atanasio et al., 2016; Burberry et al., 2016; Chew et al., 2015, 2019; Koppers et al., 2015; Y. Liu et al., 2016; O'Rourke et al., 2016; Sullivan et al., 2016; Ugolino et al., 2016).

Further investigations of the effects of isolated DPR expression on TDP-43 pathology showed that poly(PR) and poly(GR) in Neuro2a cells recruited stress granule markers and RNA binding proteins, including TDP-43, and all DPRs caused upregulation of TDP-43, which is known to be toxic (Yamakawa et al., 2015). In addition, poly(GA) expression blocked the nuclear import of TDP-43, causing TDP-43 cytoplasmic mislocalisation and aggregation (Khosravi et al., 2016; Y. B. Lee et al., 2017). The following year two teams proposed a feedback loop between DPR expression and TDP-43 pathology. One group showed that poly(GA) aggregation was dependent on the number of repeats, and that DPR aggregates preceded the aggregation of phospho-TDP-43 (Nonaka et al., 2018). The second study used DPR-only *Drosophila* models, demonstrating that DPRs induce cytoplasmic TDP-43 aggregation, which enhances DPR expression, leading to decreased nucleocytoplasmic transport and subsequent neurodegeneration (Solomon et al., 2018). A recent study showed that vaccination targeting poly(GA) in mice prevented poly(GA) aggregation and TDP-43 mislocalisation, improving motor deficits and decreasing neuroinflammation (Zhou et al., 2020).

1.7.2. Oxidative stress and mitochondrial dysfunction

The comparison between C9orf72 mutant iPSC-derived MNs and iPSC-derived MNs expressing one or more DPRs, helps the understanding of C9ORF72

pathology mediated by DPR gain-of-function. C9orf72 mutant iPSC-derived MNs show upregulation of the p53 pathway and increased DNA damage after 4 weeks in culture, followed by production of reactive oxygen species (ROS) and increased mitochondrial membrane potential (Lopez-Gonzalez et al., 2016). The expression of $(GR)_{80}$ in wild-type iPSC-derived MNs induced similar phenotypes, which were partially rescued by antioxidant treatment. Moreover, the interactome of $(GR)_{80}$-HEK293T cells was enriched with mitochondrial ribosomal proteins, suggesting that poly(GR) in C9ORF72 pathology causes oxidative stress that leads to DNA damage and mitochondrial deficits. Further analysis of $(GR)_{80}$ mice showed compromised mitochondrial morphology, and that poly(GR) preferentially binds to a subunit of the mitochondrial ATP-synthase, inducing its ubiquitination and degradation (Choi et al., 2019).

Oxidative stress causes the formation of stress granules (SG), cytosolic membrane-less organelles composed of RNA and RNA-binding proteins containing low complexity domains. ALS-related proteins, such as TDP-43 and FUS, have been shown to assemble into protein aggregates via liquid-liquid phase separation, a process believed to precede formation of stress granules but not proved *in vivo* yet (Molliex et al., 2015). *In vitro* analysis of arginine-rich DPRs showed that they have high affinity for low complexity domains, and they aggregate via liquid-liquid phase separation in a dose- and length- dependent manner, inducing SG formation (Boeynaems et al., 2017). Moreover, poly(PR) and poly(GR) interactomes are enriched with stress granule components, suggesting that the two DPRs might affect stress granule dynamics. Expression of poly(GR) or poly(PR) in mice, primary mouse neurons, iPSC-derived MNs, and *Drosophila*, caused the spontaneous formation of stress granules, leading to reduced

translation and cellular survival (K. Lee et al., 2016; Wen et al., 2014; Y. J. Zhang et al., 2018). A recent study demonstrated that increased SG formation caused by poly(GR) is coupled with decreased processing bodies which aggregate the components of nonsense-mediated mRNA decay (NMD), a mechanism that regulates gene expression (W. Xu et al., 2019). Additionally, transcriptome profiles of C9orf72 patients showed that NMD genes are downregulated, and upregulation of the key components of NMD was sufficient to inhibit poly(GR)-mediated toxicity in cellular and fly models. This suggests that poly(GR) causes dysfunction of mRNA metabolism in C9orf72 patients as well. Only one team showed that poly(GA), poly(GP) and poly(PA) expression in HEK293T cells, induced stress granule formation (Tao et al., 2015).

1.8. Cell-to-cell propagation of DPRs

The presence of DPR pathology and poly(GP) secretion in CSF and blood of asymptomatic HRE carriers suggests active secretion and spread of DPRs (Baborie et al., 2015; Gendron et al., 2017; Lehmer et al., 2017; Proudfoot et al., 2014). However, their spread does not appear to be propagated along defined neuroanatomical pathways in the same way as TDP-43. *In vitro* analysis demonstrated a cell-to-cell transmission property of DPRs, as healthy neurons showed DPR aggregation when co-cultured with DPR expressing glia, and healthy glia showed DPR aggregation following co-culture with DPR expressing neurons (Westergard et al., 2016). Treatment with conditioned media of DPR expressing cultures induced DPR aggregation in recipient cells, indicating that DPRs are secreted and transmitted.

Molecules are secreted extracellularly via vesicles called exosomes, and exosomes of DPR expressing cells are enriched with (in descending order) poly(GA), poly(GR), poly(AP), and lower levels of poly(GP) and poly(PR) (Chang et al., 2016; Westergard et al., 2016). Further analysis confirmed that only the hydrophobic DPRs are transmitted between cells, and that poly(GA) aggregates could seed further aggregation of poly(GA) and RNA foci in recipient cells (Zhou et al., 2017). A recent study demonstrated that the cell-to-cell transmission of poly(GA) resulted in enhanced cytoplasmic expression of TDP-43, which was inhibited with anti-GA antibodies (Khosravi et al., 2020).

In vitro experiments used synthetic poly(PR) to study its toxicity in recipient cells, and have suggested that also poly(PR) can be internalised. CRISPR/Cas9 knockout screens in primary mouse neurons treated with synthetic poly(PR) showed that one of the strongest suppressors of poly(PR) toxicity was *Rab7a* (Kramer et al., 2018). RAB7A regulates the later steps of endo-lysosomal trafficking, implying that poly(PR) is absorbed via endocytosis. Further analysis demonstrated that synthetic poly(PR) is transferred into the cells by clathrin-dependent endocytosis, and inhibition of the pathway reduced cell death (R. Wang et al., 2019).

1.9. Aims

All the experiments used to study DPR-related phenotypes in cellular models utilise DPR overexpression, or genetic backgrounds dissimilar from human patients. The influence of DPRs within neurons at expression levels comparable to those seen in human C9orf72-ALS/FTD disease is therefore unknown. In this study, novel doxycycline-inducible constructs carrying poly(GA) or poly(PR) were

generated, which were designed to avoid the compounding issue of GC repeats and the subsequent formation of RNA foci, allowing the analysis of DPR effect in isolation. Inducible systems allow close control over the expression based on the concentration of the inducer. Using these constructs, the contribution of poly(GA) and poly(PR) to disease phenotypes in an *in vitro* iPSC-derived neuronal model from C9orf72 ALS patients was then assessed. iPSC-derived motor neurons were genome edited by CRISPR/Cas9 to remove the HRE while maintaining the genetic background of the patients (Ababneh et al., 2020). This study therefore represents the first attempt to analyse *C9ORF72*-HRE corrected isogenic lines expressing the most toxic (poly(PR)) or the most abundant DPR (poly(GA)), independent of repeat-size or RNA-foci formation.

Aim 1

Generation a doxycycline-inducible system to express optimised-codon repeats in iPSC-derived MNs. The system was cloned into a lentiviral backbone where each DPR had an ATG start codon and a different C-terminal tag.

Aim 2

We have previously shown that C9orf72 mutant iPSC-derived MNs exhibit reduced mitochondrial potential, glutamate excitotoxicity, hyperexcitability, ER stress and stress granules formation, that were rescued with HRE CRISPR/Cas9 correction (Ababneh et al., 2020; Dafinca et al., 2016, 2020). The aim was therefore to identify whether introducing poly(GA) and poly(PR) in isogenic lines recapitulates any of the previously identified phenotypes in C9orf72 mutant iPSC-derived MNs and to determine their contribution to pathology.

Aim 3

Lastly, whether clearance of the DPRs by autophagy and RNA foci degradation are valid therapies in C9orf72-ALS/FTD was assessed. Autophagic pathways were stimulated to induce DPR clearance and rescue DPR-related phenotypes. Additionally, C9orf72 mutant iPSC-derived MNs were treated with a peptide that targets HRE transcripts to analyse its effect on DPR expression and C9ORF72 pathology (Q. Zhang et al., 2019).

Chapter 2 – Methods

2.1. Molecular cloning

Polymerase chain reaction (PCR) kit (Q5 Hot Start High-Fidelity DNA Polymerase, New England Biolabs) was used to amplify the fragments of interest from their original location, using 50 – 100 ng of template DNA. The primers were designed with overlapping regions, one or two new and unique restriction site and at least 6 random bases. All primers were tested with a gradient PCR to determine the correct melting temperatures for the amplification of the insert. Cloned fragments were isolated by running at 100 V for 1 hour on a 1.5 – 2 % agarose gel (Sigma) and purified by gel extraction kit (Qiaquick Gel Extraction, QIAGEN). All DNA species for cloning had unique restriction sites at the 5′ and 3′ ends that produce sticky ends, to ensure correct orientation of the inserts into the plasmids. Phosphatase reactions (Antarctic Phosphatase, NEB) were setup for *pUltradox* after the restriction reactions to avoid the circularisation of the plasmid. Ligation reactions were set up at various ratios of insert and incubated with T4 DNA ligase (Promega) for 1 hour at room temperature, followed by inactivation for 10 minutes at 70 °C. Stbl3® OneShot competent *E. coli* (25 μL, Life Technologies) were transformed by 5 μL ligation products, spread onto Agar+LB and ampicillin (100 μg/mL) plates, and incubated over night at 30-37 °C. Colonies

were screened by colony PCR using 10 μL of diluted colony and MegaMix-Blue (Microzone). The positive colonies were then purified from 4 mL LB broth and 100 μg/mL ampicillin of overnight cultures at 37 °C or 30 °C (PureLink® Quick Plasmid DNA Miniprep Kits, Life Technologies). The plasmids were confirmed to produce bands of expected sizes by restriction enzymatic reactions (New England Biolabs). All the reactions were set with 1 μg of cDNA for 1 hour at 37 °C, with appropriate buffer and enzyme concentration. The digestion products were run on 1 – 1.5 % agarose gel. Larger amount of plasmids were purified from 300 – 500 mL LB overnight cultures (Endotoxin-free plasmid DNA purification Xtra Midi EF, Nucleobond®). All primers were synthetized by Life Technology.

2.1.1. List of plasmids

pUltradox is a 3rd generation lentiviral backbone containing the reporter gene *dTomato* (RFP) controlled by the TRE operon and a mini-CMV promoter (#58749, Addgene). *pUltra* is a 3rd generation lentiviral plasmid, containing a ubiquitin mammalian promoter (hUb), the enhanced green fluorescent protein (eGFP) and two bicistronic 'CHYSEL' sequences, P2A and T2A (#24129, Addgene). *pLentiCMVrtTA3Blast* is a 3rd generation lentiviral reverse tetracycline-controlled transactivator 3 (rtTA3) expression vector; it is controlled by a CMV promoter (#26429, Addgene). *pTRE3G* is a plasmid containing the 3rd generation *tet*-responsive promoter (TRE3G #631173, Clontech).

2.1.2. DPR sequences optimisation

Dipeptide sequences have been optimized to avoid [GGGGCC] and [CCCCGG] repeats, then corrected by Thermo Fisher Scientific software (GeneArt Synthetic

Gene). The three constructs produce 100 amino acid-long dipeptide repeat proteins linked to different tags, and they have start and stop codons.

2.1.3. Sanger sequencing

Before starting the cloning, the plasmids were sequenced by the Sanger Sequencing facility at the Weatherall Institute of Molecular Medicine, Oxford. The same facility sequenced the cloning products using sequencing primers designed to amplify the joint sequences between the new fragment and the host vector.

Table 2.1: List of primers used in cloning and Sanger sequencing.

USE	NAME	SEQUENCE (5′ – 3′)
Cloning hUb promoter	hUb_For(NheI)	gatttagctcgccccgtgtcggctccagatc
	hUb_Rev(EcoRI)	aaatatgaattcggatcggacctgcagccca
Checking hUb insertion	hUb_left	gtattaagcgggggagaat
	hUb_right	ctcctcctccaggtctgaa
Sequencing of *pUltradox* after hUb prom insertion	hUb_seq_left 01	aagggatctggagcaa
	hUb_seq_right 01	tgcagtctgcttcccgcgtc
	hUb_seq_left 02	gttggcgagtgtgtt
	hUb_seq_right 02	gatacacctatgcgac
Cloning rtTA3	rtTA3_For(EcoRI)	gatttagaattcggcaccatgtctagactgga
	rtTA3_Rev (SalI)	taaaatgtcgacttacccggggagcatgtcaa
Checking insertion of rtTA3 and sequencing of *pUltradox* after the insertion	rtTA3_seq_left 01	ctggccgtttttggct
	rtTA3_seq_right 01	tgttcctttgagcgag
	rtTA3_seq_left 02	gtgcgaaagcggcg
	rtTA3_seq_right 02	ccataagaattgatacaacgag
Cloning eGFP in *pTRE3G*	For_GFP (SalI-AgeI)	acagtcgacaccggtatggtgagcaagg
	Rev_GFP (BamHI)	aatcttctggatcccttgtacagctcgtccat
Cloning TRE3G-eGFP in *pUltradox_rtTA3*	For_pTRE3G (XhoI)	tgtatcttcaagaattcctcgagt
	Rev_pTRE3G (NheI)	actgctagctaagatcattgatgag
Sequencing *pUltradox_rtTA3_TRE3G_eGFP*	TRE3G_seq_left	agagaaatggcagtattcatccac

2.2. Lentivirus production, titration and transduction

To produce the 3rd lentivector generation system, HEK293T cells were transfected with three packaging plasmids (pRSV-Rev #12253, pMDLg/pRRE #12251 and envelope expressing plasmid #12259, Addgene) and the backbone vector carrying the gene of interest. The transfection mix was made using PEImax reagent (1 mg/mL, Polyplus-Transfection) and NaCl (150 mM). HEK293T cells were grown in DMEM/high glucose/pyruvate medium (Gibco) with 10% foetal bovine serum (Gibco) and 1% Penicillin – Streptomycin – Amphotericin B (Gibco). The medium was replaced 24 hours following transfection. After a further 48 hours, medium was filtered through a nitrocellulose-free 0.45 μm filter (Millipore) and concentrated with LentiX™ concentrator reagent (Clontech). The lentiviral pellet was isolated by centrifugation at 1500 g for 45 minutes at 4 °C. Pellet was resuspended in 1/100 PBS of total medium and 150 μL were used for the titration. The rest of the resuspended viral particles were aliquoted and and stored at – 80 °C.

Lentivirus titration was performed by qRT-PCR on viral isolated RNA (NucleoSpin® RNA Virus kit, MACHEREY – NAGEL). The concentration of lentiviral particles (copies/mL) was calculated by reference to a control standard curve plotted from known RNA samples (Lenti-XTM qRT-PCR Titration Kit, Clontech). The estimated concentrations of each lentivirus, expressed as copies/mL, were used to estimate Multiplicity Of Infection (MOI).

Cells to be transduced (iPSCs or iPSC-derived motor neurons) were seeded at specific densities (table 2.3) and transduced according to the experimental design. iPSCs were transduced after reaching a confluence of 50%, and iPSC-derived

motor neurons at day 24 of the differentiation protocol. The cells were then washed with PBS and transduced over night with lentiviruses diluted in mTeSR enriched with ROCKi (for iPSCs) or transduction medium (table 2.4). The following day the viral particles were washed away with PBS and the cells were normally fed.

2.3. Lipotransfection

HEK293T cells were transfected using LTX lipofectamine with Plus reagent (Invitrogen). 1.25 μg/mL of plasmid was transfected into HEK293T cells seeded $3*10^5$ cells/mL in 6-well plates 24 hours prior the transfection. The medium was changed after 4 hours with various doxycycline concentrations (Sigma-Aldrich).

2.4. iPSC-motor neurons differentiation and experiments

2.4.1. Induced pluripotent stem cell lines

Induced pluripotent stem cells (iPSCs) were reprogrammed from fibroblasts donated by age-matched, healthy control individuals and by C9orf72 patients (table 2.3). The skin biopsies and expansion of fibroblasts were performed at the Oxford Motor Neuron Disease Clinic, run by Prof Kevin Talbot, University of Oxford. Dr Sally Cowley's team (Stem Bank Facility, Dunn School of Pathology, University of Oxford) reprogrammed the fibroblasts in iPSCs via the Yamanaka method (Takahashi and Yamanaka, 2006), as described by Dr Dafinca (Dafinca et al., 2016).

One clone of one patient line (C902-2) has been edited with CRISPR/Cas9 technology by Dr Nidaa Ababneh during her DPhil project in our group. The HRE

had been corrected via the double nickase strategy leaving $[GGGGCC]_2$ in intron1a of the *C9ORF72* gene (Ababneh et al., 2020).

Table 2.2: iPSC lines and demographic characteristics.

LINE	CLONE	TYPE	HRE	GENDER	AGE	Correction
Ctrl180	01-1	Control 1 (CTRL-1)	–	Female	60	No
Ctrl840	03-3	Control 2 (CTRL-2)	–	Female	67	No
Ctrl841	01-1	Control 3 (CTRL-3)	–	Male	36	No
Ctrl856	03-4	Control 4 (CTRL-4)	–	Female	78	No
C9-01	06, 07	C9orf72	970	Female	72	No
C9-02	02, 03	C9orf72	1000	Female	58	Yes
C9-04	01, 12	C9orf72	?	Male	38	No
ED	01, 02, 03	CRISPR/Cas9 Isogenic control of C902	2			

2.4.2. Induced pluripotent stem cell culture

The iPSCs were expanded as monolayer cultures in mTeSR™1 growth medium, supplemented with 1% Antibiotic-Antimitotic and 10 μM Rho-associated, coiled-coil containing protein kinase inhibitor (ROCKi) on thawing.

All vials, stored at liquid nitrogen phase, were transferred to dry ice prior to rapid thawing (37 °C water bath for 1 minute). Thawed cells were moved to 10 mL PBS and centrifuged at 300 g, 5 minutes, 4 °C. Supernatant was discarded and the pellet was gently resuspended in mTeSR™1 medium, enriched with 10 μM ROCKi and 1% Antibiotic-Antimitotic. The cells were fed daily and ROCKi was removed after 24 hours post-thawing. The cultures were passaged at 80-90%

confluence by 0.5 mM EDTA. iPSCs were washed with PBS and incubated with EDTA for 5 minutes at 37 °C. EDTA was aspirated and cells were flushed with normal medium and plated onto fresh Geltrex™-coated wells. Before the splitting step, Geltrex™ was diluted in Knock-Out DMEM medium and added to the new wells.

2.4.3. Motor neuron differentiation protocol

Motor neuron differentiations from iPSC lines were performed following the protocol optimised by Dr Dafinca (Dafinca et al., 2016). The differentiation starts when the iPSCs present small gaps (70-80% confluence), and it lasts for approximately 30 days. The protocol involves a series of enriched growth media changes and passages (summary in Figure 2.1 and list of media in table 2.4) that emulate motor neuron developmental signalling. During the first two days glycogen synthase kinase 3 inhibitor CHIR-99021 activates the Wnt pathway and dorsomorphin (compound C) inhibits BMP signalling, simulating gastrulation and neurulation (Chambers et al., 2009; Gouti et al., 2014; Yu et al., 2008). On day 2 caudalisation and ventralisation of the neural ectoderm are promoted by retinoic acid and Smoothened Agonist (SAG), respectively (Ericson et al., 1996; J. Liu et al., 2001; Roelink et al., 1995). The cells proliferate, arranging in *rosettes*, and on day 9 of the differentiation they are split up to 1:3 into Geltrex™-coated wells, letting them grow to full confluence. After day 16 the cells are neuronal progenitors and they can be passaged for expansion, or split for the final step of the differentiation. The final induction medium is enriched with neurotrophic factors (BDNF, GDNF and laminin) and Notch response inhibitor DAPT, which accelerates the neuronal differentiation by promoting cell cycle exit and committing neurons to neurogenesis (Borghese et al., 2010; Crawford & Roelink, 2007). From day 9

onward Geltrex™ is diluted in DMEM/F12 medium and the medium used for splitting is enriched with ROCKi.

By the end of the differentiation protocol, the cells are positive for βIII-tubulin, Choline Acetyl Transferase, and neurofilament immunofluorescence staining, confirming successful motor neuron differentiation. All C9orf72 mutant iPSC-derived MNs express DPRs, as shown in the dot-blot staining, and produce RNA foci (Figure 2.1).

Table 2.3: Plating concentrations.

Plate	Seeding density	Coating
6 well-plate	250000 cell/mL	1 mL/well
24 well plate	100000 cell/mL	250 μL/well
96 well-plate	20000–50000 cell/mL	20 μL/well

Table 2.4: Media used during neuronal differentiation.

Media	Reagents
Day 0 – 1	DMEM/F12 Dulbecco, Neurobasal, N2 and B27 supplements, β-mercaptoethanol, Ascorbic acid, Chir99021, Compound C.
Day 2 – 3	DMEM/F12 Dulbecco, Neurobasal, N2 and B27 supplements, β-mercaptoethanol, Retinoic Acid, Ascorbic acid, SAG, Chir99021, Compound C.
Day 4 – 17	DMEM/F12 Dulbecco, Neurobasal, N2 and B27 supplements, β-mercaptoethanol, Retinoic Acid, Ascorbic acid, SAG.
Day 18 – 23	DMEM/F12 Dulbecco, Neurobasal, N2 and B27 supplements, β-mercaptoethanol, Retinoic Acid, Ascorbic acid, SAG, Laminin, BDNF, GDNF, DAPT.
Day 24+	DMEM/F12 Dulbecco, Neurobasal, N2 and B27 supplements, β-mercaptoethanol, Retinoic Acid, Ascorbic acid, SAG, Laminin, BDNF, GDNF.
Transduction medium	DMEM/F12 Dulbecco, Neurobasal, N2 and B27 supplements, ROCKi.

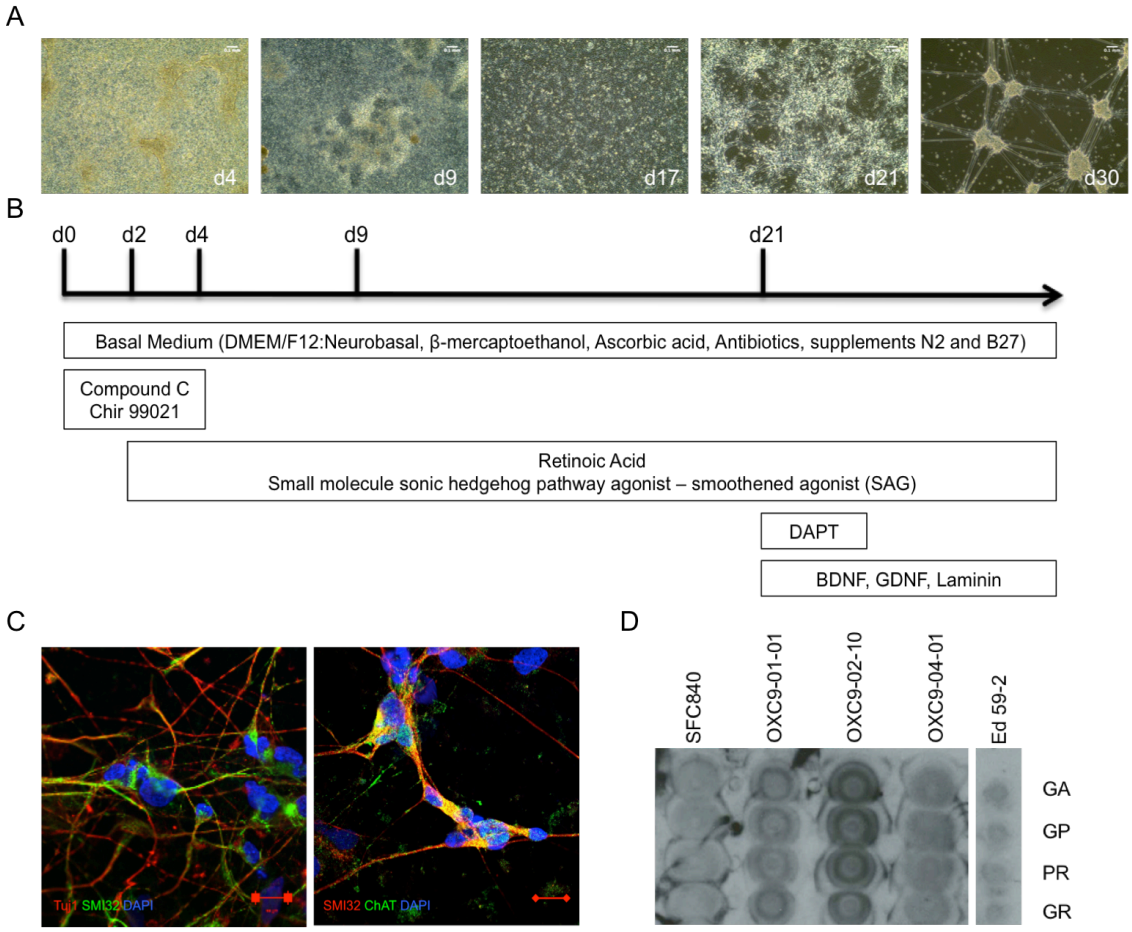


Figure 2.1 Differentiation of Induced Pluripotent Stem Cells in motor neurons.

A) Different stages of differentiation (scale bar 10 μm). **B)** Schematic representation of the motor neuron differentiation protocol. **C)** Immunostaining for neuronal marker βIII-tubulin (Tuj1), Choline Acetyl Transferase (ChAT) and neurofilament (SMI32) confirms successful differentiation of motor neurons (scale bar 100 μm). **D)** Dot blot analysis of GA, GP, PR, GR dipeptide repeat proteins in control Ctrl840, patient (C901, C902, and C904) and CRISPR/Cas9 edited (Ed-02) lines.

Table 2.5: List of reagents used for iPSC culture and motor neuron differentiation protocol.

Media or supplements	Catalogue number	Working dilution
mTeSR™1 Medium	05850, StemCell Tech	
KnockOut™ DMEM	10829018, Life Tech	
Fetal Bovine Serum	10439016, Life Tech	
Antibiotic-Antimitotic (100X)	15240096, Life Tech	1%
DMEM/F12 Dulbecco, HEPES	31330038, Life Tech	50%
Neurobasal™ medium, minus phenol red	12348017, Life Tech	50%
N2 Supplement (100X)	17502048, Life Tech	1%
B27 Supplement (50X)	12587010, Life Tech	2%
β-mercaptoethanol (50 mM)	31350010, ThermoFisher Scientific	0.1%
Ascorbic acid	95210, Sigma-Aldrich	0.5 μM
Chir99021	4423/50, Tocris Bioscience	3 μM
Compound C, InSolution™ AMPK inhibitor	171261, Sigma-Aldrich	1μM
Retinoic acid (100 mg)	R2625, Sigma-Aldrich	1μM
SAG	4366, Tocris Bioscience	0.5 μM
Laminin mouse protein, natural	23017015, Life Tech	0.5 μg/mL
BDNF	PHC7074, Life Tech	100 ng/mL
GDNF	PHC7041, Life Tech	100 ng/mL
DAPT	2634/10, Tocris Bioscience	10 μM
ROCKi (Y-27632 di-hydrochloride)	1254, Tocris Bioscience	10 μM
StemPro™ Accutase™ Cell dissociation reagent	A1110501, Life Tech	
EDTA	15575-038, Life Tech	0.5 mM
TrypLE™ Express Enzyme (1X), no phenol red	12604-013, LifeTech	
Geltrex™ LDEV-free	A1413302, ThermoFisher Scientific	0.15 ng/mL

2.4.4. Doxycycline induction

The doxycycline (Sigma-Aldrich, D3447-500MG) was dissolved in DMSO at 50 mg/mL, and freshly added to the media, followed by a filtration step. The doxycycline treatments and concentrations followed the feeding time and the experimental design.

For lipofected HEK293T cells, doxycycline was added after 4 hours in two different concentrations (100 ng/ml and 1000 ng/ml). The cells were harvested after one or two days of treatment to check the intensity of the signal. The doxycycline was washed out after 24 hours and the cells were harvested 24 hours later to test the sensitivity of the system.

The final protocol to induce higher DPR expression in iPSC-derived MNs, without doxycycline toxicity, is a three-day doxycycline treatment to express $(GA)_{50}$–*c*-myc, and five-day treatment to express $(PR)_{50}$–HA, both with 5 μg/ml doxycycline. The system can be switched off after three-day treatment to study whether the phenotypes are reversible (Figure 3.13).

2.4.5. TAT-BIND peptide treatment

The iPSCs were treated for three days with 3 μM TAT-BIND peptide or S-TAT-BIND scrambled peptide. iPSC-derived MNs were treated with the same concentration on day 25 for six days.

2.4.6. Sodium arsenite treatment

iPSC-derived MNs were treated with 0.5 mM sodium arsenite for 1 hour at 37 °C dissolved in basal medium (neurobasal, DMEM/F12 Dulbecco, N2 and B27 supplements). Cells were then collected and fixed for further analysis.

2.4.7. Autophagy

Autophagy in iPSC-derived motor neurons was induced with rapamycin (200 nM, Tocris) and inhibited with bafilomycin (10 nM, Tocris). The chaperone-mediated autophagy (CMA) was induced with 6-aminonicotinamide (5 μM, Sigma). All the compounds were dissolved in basal medium (neurobasal, DMEM/F12 Dulbecco, N2 and B27 supplements). Cells were treated for 24 hours.

2.5. Assessing phenotypes

2.5.1. Immunoblotting

Cells were harvested in 500 μL of PBS and pelleted at 4000 rpm for 3 minutes. The pellet was resuspended and sonicated in 100 – 150 μL of RIPA buffer (Sigma-Aldrich) with protein inhibitors and EDTA-phosphatase (Roche). The lysed mixture was kept on ice for 30 minutes and centrifuged at 5000 rpm for 10 minutes at 4 °C. The protein concentrations were measured by copper-based BCA protein assay (Sigma-Aldrich). 1 μg/μL of proteins were run on 4 – 12 % gel (Invitrogen) and transferred to a PVDF membrane using iBlot® system (Sigma-Aldrich). The membrane was blocked in 5 % skimmed milk, 1X TBS, 0.1% Tween (TBS-T) for 40 minutes at room temperature and blotted over night at 4 °C with primary antibodies diluted in 1 % skimmed milk, TBS-T. The primary antibodies used are

β-actin (Sigma-Aldrich) and GFP (A11122, Invitrogen). After three washes of 10 minutes each with 1X TBS-T, the membrane was incubated for 1 hour at room temperature with secondary antibodies anti-mouse or anti-rabbit HRP-linked (GE Healthcare), diluted 1:10000 in 1 % skimmed milk, TBS-T. For dot-blot analysis of DPRs in C9orf72 mutant iPSC-derived MNs, the primary and secondary antibodies were incubated in dot-blot apparatus. The membrane was washed three times in TBS-T and developed with ECL reagents (Amersham Pharmacia Bio-tech) to visualise the protein bands. Protein band quantification was done using Fiji ImageJ software.

2.5.2. Immunohistochemistry

Cells were fixed with 4% paraformaldehyde for 15 minutes at room temperature, followed by three washes with 1X PBS, 5 minutes each. Cells were permeabilised and blocked in 1X PBS, 0.2 % Triton X-100, 10% normal goat or donkey serum for one hour at room temperature. Primary antibodies were diluted in 1X PBS, 0.1 % Triton X-100, 1 % serum and incubated over night at 4 °C. Cells were then washed three times with 0.1% Triton X-100 PBS for 10 minutes each, at room temperature. The secondary antibodies (Alexa Fluor 488, 568 and 647 conjugated anti-mouse, anti-rabbit or anti-goat and diluted, Life Technologies) were diluted 1:500 in in 1X PBS, 0.1 % Triton X-100, 1 % serum and incubated at room temperature for one hour in the darkness. The cells were washed with 0.1% Triton X-100 PBS three times for 10 minutes each, and during the second wash the nuclei were stained with DAPI (1:2000). The coverslips were mounted on slides using VECTASHIELD Hardset Antifade Mounting Medium (Vector labs) and the fluorescence was visualised using confocal microscope Zeiss LSM.

2.5.3. Fluorescence In Situ Hybridisation (FISH-IF)

The protocol of RNA fluorescence *in situ* hybridisation (FISH) is based on previously published methods (Mizielinska et al., 2013). The protocol is carried out using RNA-clean techniques and on cells grown on 12 mm RNase-free coverslips. The cells were fixed with 4% paraformaldehyde for 20 minutes at room temperature, washed three times with PBS and permeabilised with 0.2 % Triton X-100 in PBS. After three washing steps, the cells were dehydrated in a graded diluted series of ethanol, air dried and rehydrated in PBS. Cells were quickly washed with 2X SSC (Life Technologies) and incubated for 30 minutes at 80 °C in pre-hybridisation solution – 50% formamide (Life Technologies), 2X SSC topped up with ddH_2O. This was followed by the hybridisation step, that was carried out for two in pre-heated solution prepared with 50% formamide, 2X SSC, 0.16% BSA (Sigma-Aldrich), 0.8 mg/mL salmon sperm (Life Technologies), 0.8 mg/mL tRNA (Sigma-Aldrich), 1.6 mM vanadyl ribonucleoside (New England Biolabs), 5 mM EDTA (ThermoFisher Scientific), 0.2 μg/mL probe and topped up with ddH_2O (300 μL/coverslip). After the hybridisation, coverslips where washed three times in 1 mL/coverslip high-stringency wash solution (50% formamide, 0.5X SSC, topped up with ddH_2O) for 30 minutes at 80 °C on rocking platform (highest setting). The cells where then washed other three times in 0.5X SCC for 10 minutes each wash at room temperature. This was followed by a brief PBS wash and immunofluorescence as previously described. 2'O-methyl RNA sense probes [$(CCCCGG)_4$] were conjugated with Cy3, whereas antisense probes [$(GGGGCC)_4$] were conjugated with Alexa Fluor 488 (Integrated DNA Technologies). RNase A treatment (0.1 mg/mL, Life Technologies) was used to evaluate the specificity of the probes (one hour at 37 °C following the permeabilisation).

Table 2.6: List of antibodies used for immunoblotting (WB) and immunohistochemistry (IF).

Antibody	Catalogue number	Source	Dilution	
			WB	IF
β-Actin	ab1978, Abcam	Mouse	1:5000	
HA	6908, Sigma	Rabbit	1:250 – 1:500	
	9658, Sigma	Mouse		1:250
***c*-Myc**	M4439, Sigma	Mouse	1:500	
	C3956, Sigma	Rabbit	1:500	
	ROAMYC, Roche	Mouse		1:100
GFP	A11122, Invitrogen	Rabbit	1:1000	1:500
RAN	610341, Biosciences	Mouse	1:1000	
KPNB1 (Importinβ)	ab2811, Abcam	Mouse	1:1000	
Transportin 1	ab10303, Abcam	Mouse	1:1000	
MCU	ab219827, Abcam	Mouse	1:500 - 1:2000	1:500
	ab121499, Abcam	Rabbit	1:500 - 1:1000	1:500
TOMM20	ab78547, Abcam	Rabbit	1:2000	1:500
COXIV	ab79393, Abcam	Rabbit	1:2000	
***p*-eIF2*α*(Ser51)**	119A11, Cell Signalling	Rabbit	1:1000	
eIF2*α*(Ser51)	9722, Cell Signalling	Rabbit	1:1000	
GRP78/BiP	ab21685, Abcam	Rabbit	1:1000	
p62	610833, BD Transd Lab	Mouse	1:2000	
Cyt*c*	ab133504, Abcam	Rabbit	1:1000	
LAMP2A	ab18528, Abcam	Rabbit	1:2000	1:250

CHOP	2895, Cell Signalling	Mouse	1:500	
ATF4	ab184909, Abcam	Rabbit	1:500	
PERK	5683, Cell Signalling	Rabbit	1:1000	
α -tubulin	ab4079, Abcam	Rabbit	1:10000	
GAPDH	AB2302, Sigma-Aldrich	Rabbit	1:10000	
ChAT	AB144P, Millipore	Goat		1:250
PABP	ab21060, Abcam	Rabbit		1:500
SMI32	801701, Biolegend	Mouse		1:1000
β -tubulin	Ab15568, Abcam	Rabbit		1:1000
	Ab107216, Abcam	Chicken		1:1000
TDP-43	60019-2-Ig, Proteintech	Mouse		1:1000
	10782-2-AP, Proteintech	Rabbit		1:1000
	H00023435-M01, Abnova	Mouse		1:1000
PR repeat antibody	23979-1-AP, Proteintech	Rabbit	1:500	
GA repeat antibody	24482-1-AP, Proteintech	Rabbit	1:500	
GR repeat antibody	23978-1-AP, Proteintech	Rabbit	1:500	
GP repeat antibody	24494-1-AP, Proteintech	Rabbit	1:500	
AP repeat antibody	24493-1-AP, Proteintech	Rabbit	1:500	

2.5.4. Confocal imaging analysis

All fluorescence pictures were processed and analysed with Fiji ImageJ software. A mask using ChAT or β-tubulin was created to analyse only mature motor neurons. The mask was placed on the other channels to study particles or intensity signal. Stress granules and lysosomes signals were processed to determine their threshold and analyse particles. The stress granules size range was 0.1 – 1.5 nm^2, while the circularity index for both stress granules and lysosomes was 0.6 – 1.

2.5.5. Calcium imaging

Cytosolic calcium was measured in iPSC-derived motor neurons loaded with Fluo 4-AM (20 μM, Life Technologies). Cells were first incubated with the dye dissolved in 0.2 % dimethyl sulfoxide (Sigma-Aldrich) with 0.04 % pluronic acid in Hank's balanced salts solution (HBSS) supplemented with HEPES, $CaCl_2$, and $MgCl_2$ for 30 minutes at 37 °C. After washing (HBSS+HEPES+$CaCl_2$+$MgCl_2$), the dye was excited at 488 nm and images were taken every 50 ms. The stimuli used were glutamate (1 mM, Sigma) for cellular calcium intake, carbonyl cyanide m-chlorophenyl hydrazine (CCCP, 4 μM, Tocris) for mitochondrial calcium release, carbachol (100 μM, Tocris) for ER calcium release from inositol 1,4,5-triphosphate receptor, and thapsigargin (10 μM, Life Technologies) to measure total ER calcium level.

All the protocols started with 30 s washing step (HBSS + HEPES + CaCl2 + $MgCl_2$), followed by 30 – 60 s stimulation (30 s glutamate, 60 s carbachol, 60 s CCCP). After each stimulus, cells were washed for 60 s with HBSS supplemented with HEPES, $CaCl_2$, and $MgCl_2$. Thapsigargin was added directly to the coverslip. The somas of neuronal looking cells were used to measure the fluorescence

intensity with FIJI. The fluorescence measurements are expressed as a ratio ($\Delta F/F_0$) of the mean change in fluorescence (ΔF) between the stimulation pick and resting fluorescence (F_0, intensity signal of the last picture taken before stimulation).

2.5.6. Statistical analysis

All statistical analysis were run using GraphPad Prism. For replicated experiments, data of each line from independent differentiations were pooled to compare means and standard deviations. In single experiments, multiple measurements were assessed. Clones from the same line were treated as replicates. Means of two groups were compared with paired Student's *t-test*, and means of three or more groups were analysed with ANOVA's followed by Tukey's *post-hoc* tests. For matched or repeated measures, but not normal distributed, nonparametric ANOVA with Friedman's test was preferred. Alpha was set at 0.05 for all ANOVA's and tests.

Chapter 3 – Molecular cloning of the doxycycline inducible system in a lentiviral backbone

3.1. Introduction

The dipeptide repeat proteins chosen for this project were poly(GA), for its abundance in C9orf72 patient *post-mortem* tissue, and the arginine–rich DPRs, poly(PR) and poly(GR), as these have shown the most prominent toxicity in cell culture systems. In order to study their effects in iPSC-derived motor neurons, I generated a lentivirus carrying the sequences of the DPRs under a doxycycline-inducible system.

The doxycycline-inducible system is based on tetracycline-dependent regulation of transcription and was developed by Manfred Gossen and Hermann Bujard (Gossen et al., 1995; Gossen & Bujard, 1992). The system involves a fused sequence of the VP16 transactivation domain and the *Escherichia coli* tetracycline repressor (TetR) protein to obtain an effector, which specifically binds both tetracycline and the 19-bp operator sequences (*tetO*) of the *tet* operon in the target transgene (TRE), resulting in its transcription. I chose a version of this system, called "reverse tTA" (rtTA3), in which the effector rtTA binds DNA only when the inducer is present (tet-on). The current inducer of choice is doxycycline (dox) because it efficiently

activates rtTA and inactivates tTA at doses that are well below cytotoxic levels (Gossen et al., 1995).

The dox-on system allowed a time-course study of the toxicity of the dipeptide repeat proteins in CRISPR-Cas9 corrected iPSC-derived motor neurons. Moreover, the ability to switch their expression off allowed to study whether the phenotypes induced by DPR expression are reversible.

3.2. Design and cloning strategy

I induced the expression of the DPRs in stem cell-derived motor neurons using a lentiviral vector for each dipeptide protein. The sequences generates DPRs long as 50 hexanucleotide repeats, and were optimised to avoid GC repeat sequences that would induce the formation of RNA foci (May et al., 2014; Mizielinska et al., 2014; Wen et al., 2014; Y. J. Zhang et al., 2014). Each dipeptide has a different tag added to the C-terminal (HA, FLAG, or *c*-myc). Although the pathological dipeptide repeat proteins are produced through an ATG-independent translation, I introduced start and stop codons in the constructs in order to control and modulate their expression.

The lentiviral backbone *pUltradox* has the reporter gene *dTomato* (RFP) controlled by the TRE operon and a mini-CMV promoter. The first step was cloning the *trans*-activator rtTA under the control of a human ubiqutin promoter (hUb-prom) into the backbone (Figure 3.1). The two elements were contained in two plasmids, *pLentiCMVrtTA3Blast* and *pUltra,* respectively. These were sub-cloned into the *pUltradox* using restriction digestions. The expression of *dTomato* was tested in HEK293T cells, which revealed that TRE operon is not sensitive enough to switch off RFP expression. To improve the quality of the system, the TRE operon was

replaced by the optimised operon TRE3G contained in *pTRE3G*. The difference resides in the spacers between the 7 operator sequences that allow more sensitivity. Before sub-cloning TRE3G in *pUltradox*, the gene for enhanced green fluorescent protein (eGFP) was inserted in *pTRE3G*. Subsequently, the eGFP sequence was replaced by sequences for $(GA)_{50}$–*c*-myc, $(PR)_{50}$–HA or $(GR)_{50}$–FLAG using restriction digestions (Figure 3.1).

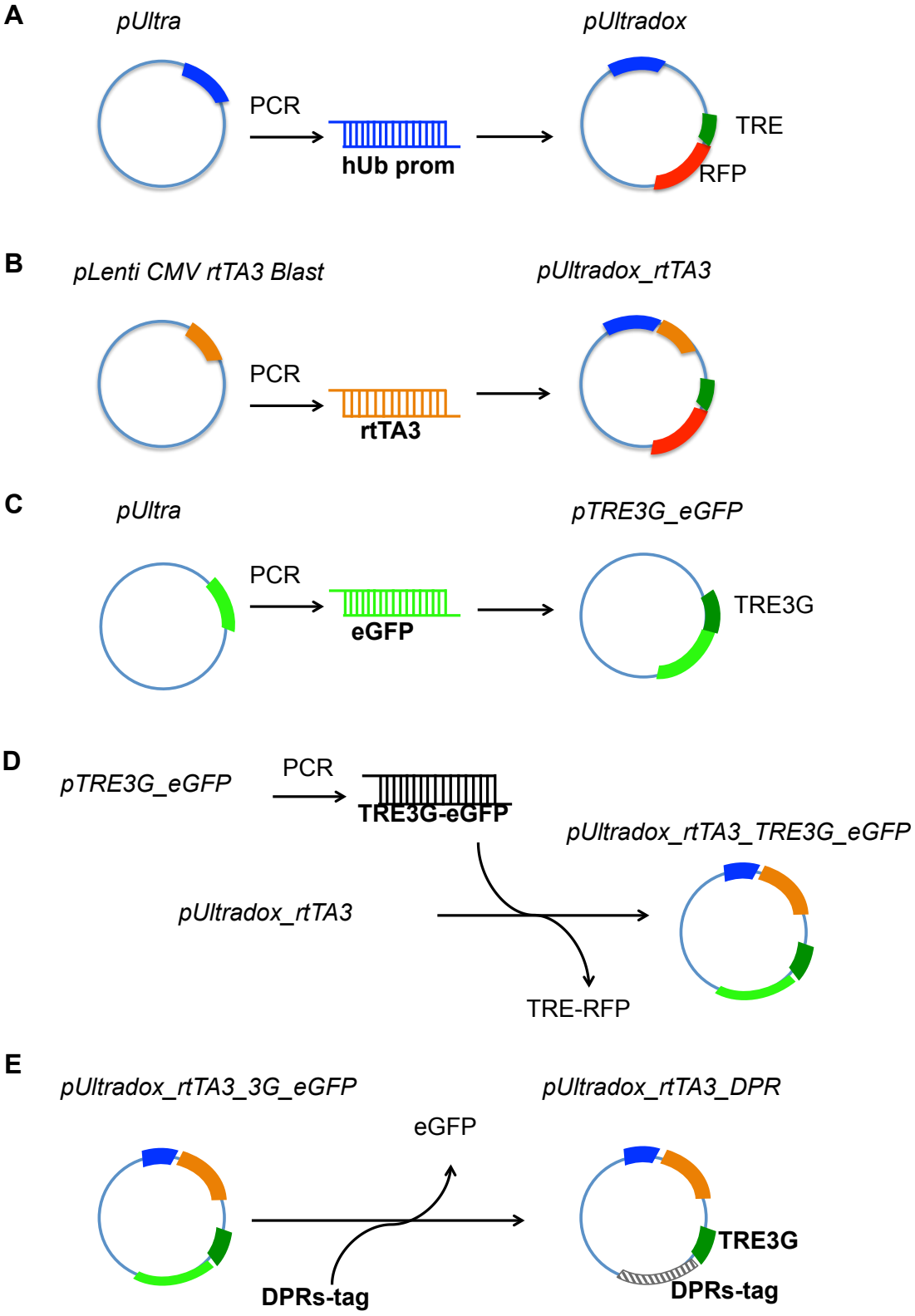


Figure 3.1: Scheme of the cloning strategy.

3.2.1. Sub-cloning of the trans-activator rtTA3

The primers used for cloning the human ubiquitin promoter were designed with a different restriction digestion site on each end: the site recognised by NheI on the 5′ end and the one recognised by EcoRI on the 3′ end. The combination of these two sites allowed the insertion of the promoter into the multiple cloning site of the plasmid *pUltradox*. The primers were tested by a temperature gradient PCR, and the expected product of 1257 bp was obtained with a melting temperature between 66 °C and 71 °C (Figure 3.2 A). The purified PCR product and the plasmid *pUltradox* were digested by the endonucleases NheI and EcoRI; the plasmid was then dephosphorylated to avoid the circularisation of the vector. Different ratios of fragment:plasmid were mixed for the ligation reaction and the competent cells Stbl3 were transformed with the ligation products. The colonies grown overnight were tested by colony PCR (Figure 3.2 B), and the DNA was extracted from the colonies showing the amplified fragment (1257 bp). The DNA was digested by different endonucleases to check the presence of hUb promoter in *pUltradox* (Figure 3.2 C – D): 1) NheI – EcoRI that excises the promoter from the plasmid (expected products 7.6 kb and 1257 bp), 2) NheI – SpeI, as the site recognised by SpeI is contained within hUb and not within the vector (expected products 7.7 kb and 1187 bp), 3) SmaI that cuts *pUltradox* twice, showing a higher digestion product if the promoter is inserted (7897 bp instead of 6649 bp).

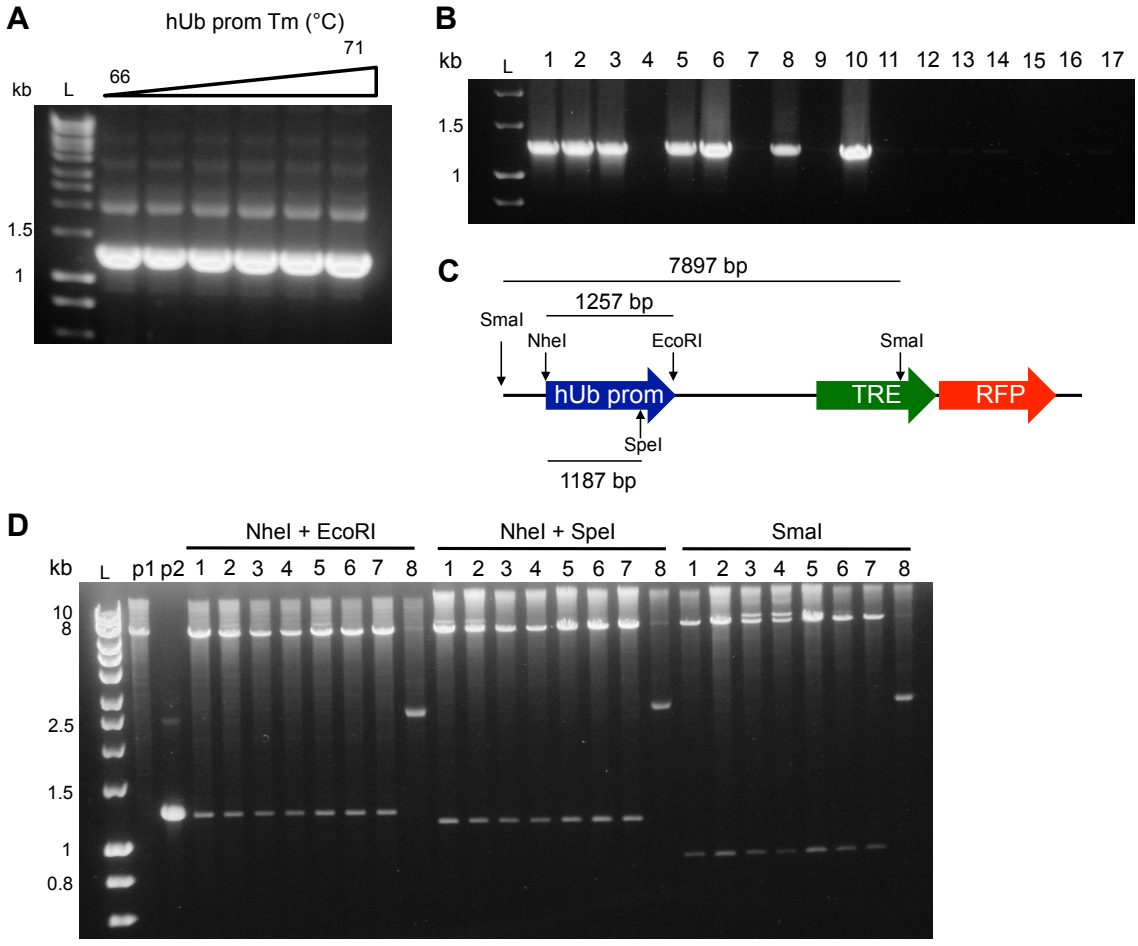


Figure 3.2: Cloning of a human ubiquitin promoter into *pUltradox*.

Agarose gel electrophoresis of PCR and restriction digest reactions confirming the insertion of the human ubiquitin promoter (hUb prom) into *pUltradox*. **A)** Temperature gradient PCR to determine the Tm for the amplification of hUb prom (1257 bp). **B)** Colony PCR, expected size is 1257 bp. **C)** Restriction digestion scheme to confirm the ligation between hUb prom and *pUltradox*. **D)** Agarose gel electrophoresis showing the digested fragments. p1 = *pUltradox* (7.6 kb); p2 = hUb prom (1257 bp); lines 1 – 7 = positive colonies of the colony PCR; line 8 = negative colony.

The primers for cloning the *trans*-activator rtTA3 were designed to allow the insertion of the element in *pUltradox* to be in frame with the human ubiquitin promoter: the site recognised by SpeI on the 5′ end and the one recognised by NdeI on the 3′ end. The primers were tested by temperature gradient PCR (Figure 3.3 A), and the PCR product was purified and digested by SpeI and NdeI. The same endonucleases digested *pUltradox* (containing the hUb promoter), then the plasmid was dephosphorylated and vector and fragment were mixed in different ratios. The competent cells Stbl3 were transformed with the ligation products and the colonies grown overnight were tested by colony PCR (Figure 3.3 B – C). I used three combinations of primers to check if the fragment containing rtTA3 was ligated into *pUltradox*, downstream of the hUb. The first pair of primers amplifies the whole fragment (expected product 725 bp), the other two pairs amplify joint sequences between the promoter and rtTA3 and between rtTA3 and the plasmid. The colonies showing positive bands in all three reactions were grown overnight in liquid culture and the DNA was extracted. The DNA was tested for the insertion of rtTA3 by endonuclease digestions. The plasmids were digested by SpeI and NdeI, cutting the ends of rtTA3 (expected products 666 bp and 8831 bp), and by SmaI, which has two restriction sites on *pUltradox,* but three sites in *pUltradox_rtTA3* (expected products: 6519 bp, 2058 bp, 920 bp (Figure 3.3 D). The DNA of the positive colony was then sequenced (Figure 3.3 E).

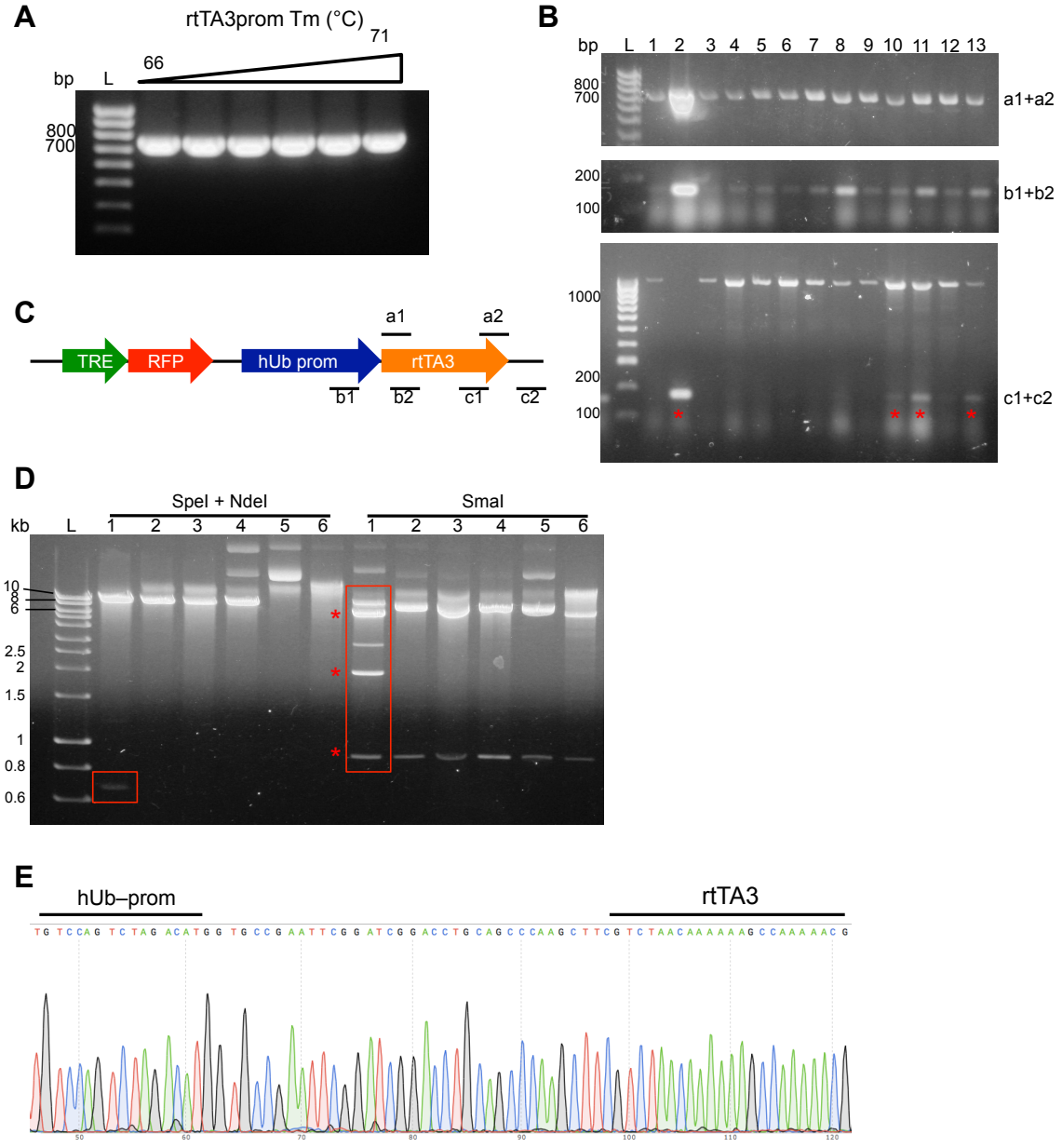


Figure 3.3. Cloning of the trans-activator element rtTA3 in *pUltradox*.

Agarose gel electrophoresis of PCR and restriction digest reactions confirming the insertion of rtTA3 in *pUltradox*. **A)** Temperature gradient PCR to determine the Tm for the amplification of rtTA3 (725 bp). **B)** Colony PCRs, expected sizes 725 bp (primers a1+a2), 157 bp (b1+b2), 175 bp (c1+c2). The asterisks indicate the positive colonies. **C)** Scheme showing the annealing sites of the primers used for the colony PCRs. **D)** Restriction endonuclease digestions to confirm the ligation between rtTA3 and *pUltradox*. SpeI+NdeI = 666 bp. SmaI = 6519 bp, 2058 bp, 920 bp (asterisks). Lines 1 – 4 = positive colonies of the colony PCRs; line 5 = *pUltradox* + hUb prom; line 6 = *pUltradox*. **E)** Sanger sequencing result of colony 1.

3.2.2. Sub-cloning of the TRE operon

The primers for cloning the reporter gene eGFP were designed to allow the insertion of the element into the multiple cloning site of *pTRE3G*, in frame with the operon TRE3G: the site recognised by AgeI on the 5′ end and that recognised by BamHI on the 3′ end. The primers were tested by temperature gradient PCR (Figure 3.4 A), and the amplified product was purified. The PCR product and the plasmid *pTRE3G* were digested by the endonucleases AgeI and BamHI and different ratios of fragment:plasmid were mixed for the ligation reaction. The competent cells Stbl3 were transformed and the colonies grown overnight were tested by a colony PCR, using two pairs of primers: one amplifies eGFP (746 bp), the other amplifies the fragment containing the operon TRE3G, eGFP and the termination signal (1630 bp) (Figure 3.4 B). The colonies showing positive bands in both reactions were grown overnight in liquid culture and the DNA was extracted. A double endonuclease digestion with AgeI and BamHI tested the DNA for the presence of eGFP (expected products 3.4 kb and 726 bp, Figure 3.4 C).

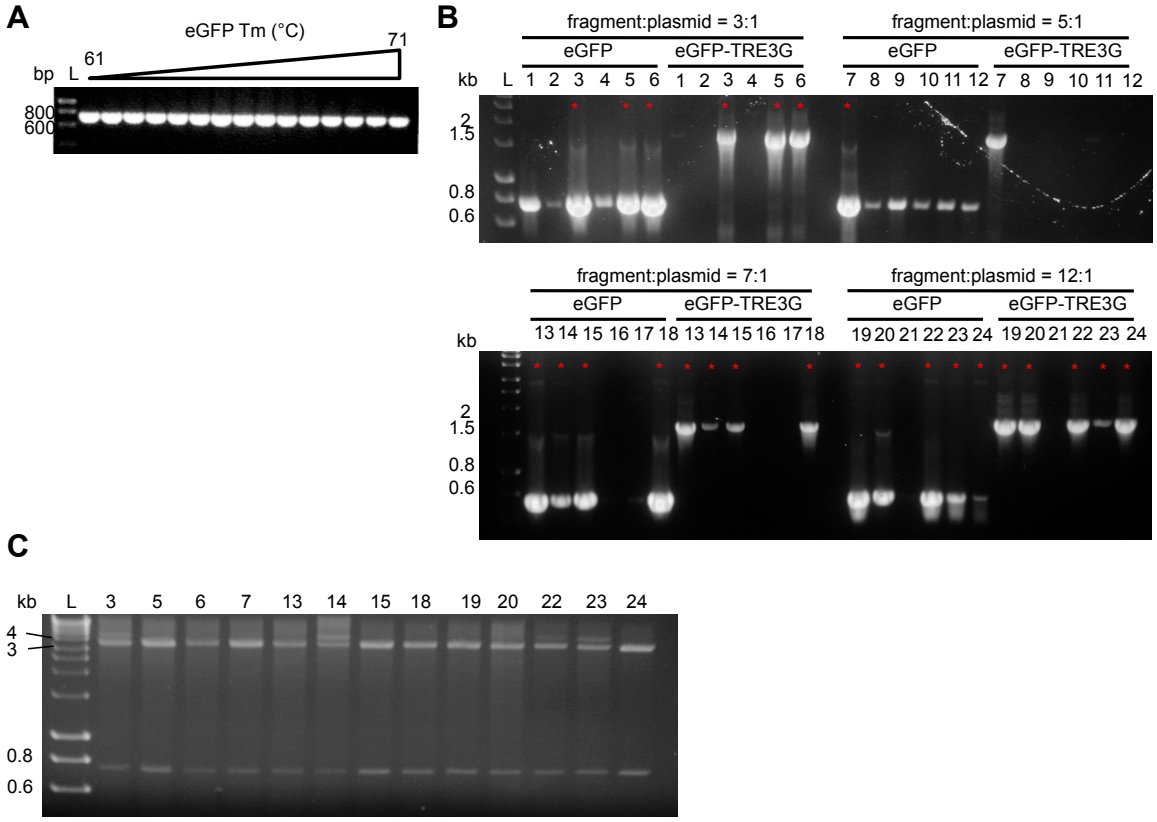


Figure 3.4. Cloning of eGFP in *pTRE3G*.

Agarose gel electrophoresis of PCR and restriction digest reactions confirming the insertion of eGFP in *pTRE3G*. **A)** Temperature gradient PCR to determine the Tm for the amplification of eGFP (746 bp). **B)** Colony PCRs on competent cells transformed with different ratios fragment:plasmid (3:1, 5:1, 7:1 and 12:1). Two couples of primers used: eGFP (expected size 746 bp), eGFP plus poly(A) site on *TRE3G* (expected size 1630 bp). Asterisks are the positive colonies. **C)** Double digestion with AgeI and BamHI (expected products 3.4 kb and 723 bp).

As the last step in cloning the backbone containing the reporter gene eGFP, the operon TRE3G and the *trans*-activator element, the fragment with TRE3G and eGFP, was cloned from *pTR3G_eGFP* to *pUltradox_rtTA3*. The primers were designed to introduce the restriction sites of XhoI on the 5′ end and NheI on the 3′ end of TRE3G-eGFP. The plasmid *pUltradox_rtTA3* cut by the same enzymes, loses the fragment containing the non-optimised operon TRE and its reporter gene RFP. The primers were tested by temperature gradient PCR, and the expected product 2050 bp was obtained with a melting temperature between 66 °C and 68 °C (Figure 3.5 A). The purified PCR product and *pUltradox_rtTA3* were digested by XhoI and NheI and mixed in different ratios of fragment:vector. The ligation products were used to transform the competent cells and the colonies were then tested by colony PCR for the detection of eGFP (expected product 746 bp, Figure 3.5 B). The DNA was extracted from the positive colonies and digested by two couples of restriction enzymes: XhoI and NheI produce a fragment 1311 bp long in *pUltradox_rtTA3* and 2003 bp in *pUltradox_rtTA3_TRE3G_eGFP*, BamHI and NheI cut out a fragment 69 bp long from *pUltradox_rtTA3* and 989 bp in *pUltradox_rtTA3_TRE3G_eGFP* (Figure 3.5 C – D). The DNA of the positive colonies was sequenced.

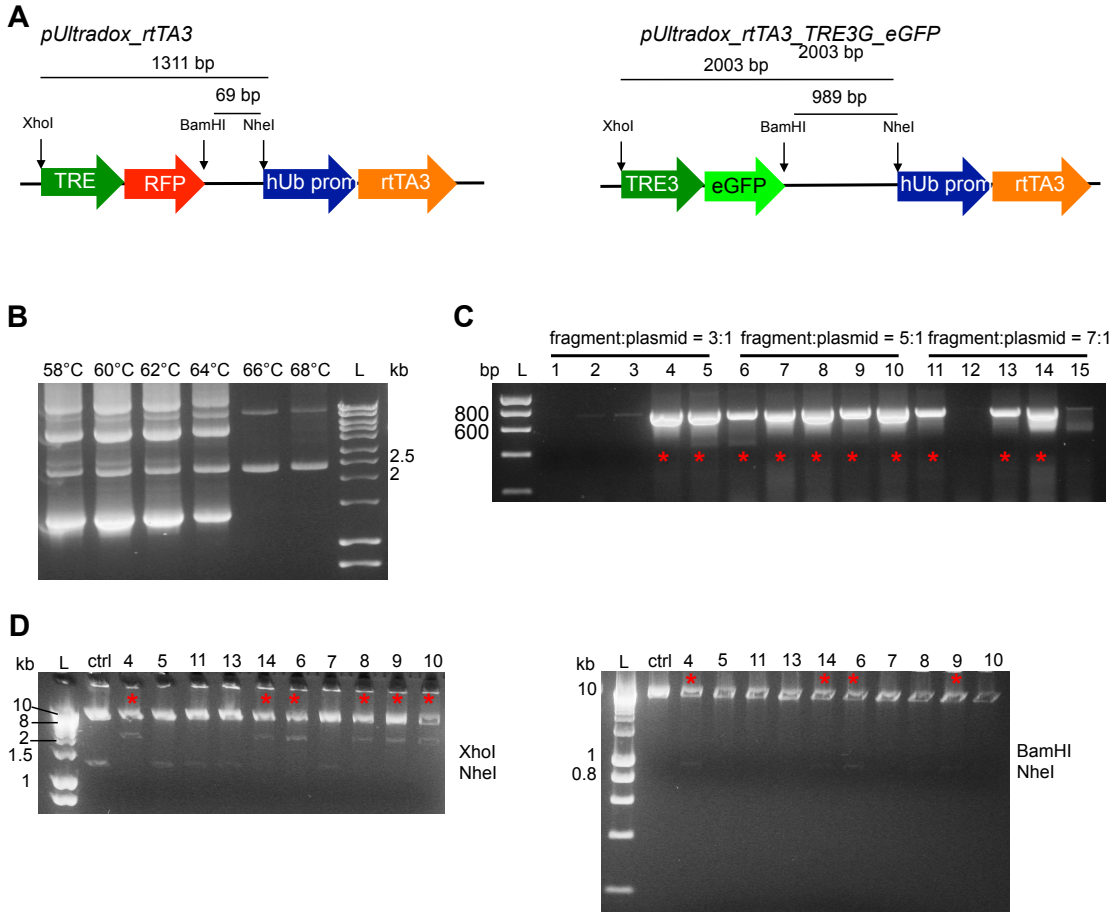


Figure 3.5. Cloning of the fragment carrying the operon TRE3G and eGFP in *pUltradox_rtTA3*.

Agarose gel electrophoresis of PCR and restriction digest reactions confirming the insertion of TRE3G-eGFP in *pUltradox_rtTA3*. **A)** Scheme of the strategy to replace TRE-RFP with TRE3G-eGFP in *pUltradox_rtTA3*, the restriction sites used for the digestions, and the expected bands. **B)** Temperature gradient PCR to determine the Tm for the amplification of the fragment containing TRE3G+eGFP (2050 bp). **C)** Colony PCRs on competent cells transformed with different ratios fragment:plasmid (3:1, 5:1 and 7: 1). Expected product 746 bp (asterisks). **D)** Restriction digestions of positive colonies with two sets of enzymes (scheme A, expected products 2003 bp for XhoI+NheI, 989 bp for BamHI+NheI). Ctrl = *pUltradox_rtTA3*.

3.2.3. Insertion of the DPR sequences

Dipeptide sequences were designed manually to avoid GGGGCC or CCCCGG repeats and corrected by Thermo Fisher Scientific software (GeneArt Synthetic Gene). All the sequences have start and stop codons enclosed between two different restriction sites (AgeI at 5′ end and BamHI at 3′ end, figure 3.6). Each fragment was amplified with specific primers annealing on restriction sites and part of the encoding sequence (Figure 3.7 A). The PCR products were purified from the agarose gel (2%) and digested by AgeI and BamHI. The plasmid *pUltradox_rtTA3_TRE3G_eGFP* was also digested to excise the eGFP sequence. Plasmid and PCR products were mixed in different ratios, together with T4 ligase, for 1 hour at 21 °C followed by a 10-minute-step at 70 °C to inactivate the enzyme. Competent cells were then transformed with the ligation products and grown overnight at 30 °C on agar plates. Colony PCR was used to verify the insertion of the fragments. The primers anneal on the TRE3G operon and the plasmid region downstream of the DPR sequences producing an expected size of 674 bp for PR, 671 bp for GR and 677 bp for GA (Figure 3.7 B). All the positive colonies were inoculated in 5 mL LB broth with ampicillin overnight at 30 °C, and DNA was extracted to have the plasmids sequenced. All the constructs carried the DPR sequences expected (Figure 3.7 C, S1).

PR50_HA

CGTAAAGTCGACCGGT**atg**CCTCGACCAAGGCCAAGGCCTCGGCCCCGTCCAAGACCCCGTCCGCGTCCTAGG
CCAAGGCCACGTCCTCGACCCCGGCCTAGACCCCGACCTCGCCCCAGACCTCGACCTAGACCACGGCCCCGCC
CTAGGCCGCGTCCCCGACCACGTCCAAGACCACGACCACGCCCTCGACCCAGACCTAGGCCACGACCTAGACC
GCGTCCTAGACCTCGACCCAGGCCTCGTCCGAGACCCAGGCCAAGGCCAAGACCGAGGCCGCGGCCAAGACCA
CGTCCTAGGCCTAGACCGCGACCCCGG*TACCCATACGATGTTCCAGATTACGCT***taa**GGATCCAATGTAACTG

MPRPRPRPRPRPRPRPRPRPRPRPRPRPRPRPRPRPRPRPRPRPRPRPRPRPRPRPRPRPRPRPRPRPRPRPR
PRPRPRPRPRPRPRPRPRPRPRPRPRPR*YPYDVPDYA**

GR50_FLAG

CGTAAAGTCGACCGGT**atg**GGGAGAGGTCGTGGGAGAGGCCGCGGTCGAGGGAGAGGCAGGGGACGCGGTAGA
GGGAGGGGCCGAGGCAGGGGTAGAGGACGGGGAAGGGGACGTGGCCGGGGGAGAGGAAGAGGAAGAGGGCGAG
GGAGAGGTAGAGGTCGTGGACGTGGGAGGGGACGAGGTCGTGGAAGAGGCAGAGGACGTGGTCGAGGTAGAGG
CCGAGGAAGAGGTCGGGGGCGTGGGCGTGGAAGGGGTAGGGGTCGTGGTCGCGGACGAGGTAGGGGGCGAGGC
CGCGGTAGGGGAAGAGGTAGGGGAAGA*GACTACAAAGACGATGACGACAAG***taa**GGATCCAATGTAACTG

MGRGRGRGRGRGRGRGRGRGRGRGRGRGRGRGRGRGRGRGRGRGRGRGRGRGRGRGRGRGRGRGRGRGRGR
GRGRGRGRGRGRGRGRGRGRGRGRGRGR*DYKDDDDK**

GA50_*c*-myc

CGTAAAGTCGACCGGT**atg**GGTGCTGGTGCAGGCGCTGGTGCCGGCGCAGGCGCAGGCGCTGGTGCTGGTGCC
GGTGCTGGCGCTGGTGCAGGCGCTGGCGCTGGCGCTGGTGCTGGCGCAGGCGCTGGTGCTGGTGCTGGTGCAG
GCGCAGGCGCAGGCGCTGGCGCAGGCGCAGGCGCAGGCGCTGGTGCTGGCGCTGGCGCAGGCGCAGGCGCTGG
TGCCGGTGCAGGCGCTGGTGCTGGTGCAGGCGCTGGCGCTGGTGCCGGCGCAGGCGCTGGCGCAGGCGCAGGC
GCTGGTGCAGGCGCTGGCGCTGGTGCA*GAACAAAAACTCATCTCAGAAGAGGATCTG***taa**GGATCCAATGTAA
CTG

MGAGAGAGAGAGAGAGAGAGAGAGAGAGAGAGAGAGAGAGAGAGAGAGAGAGAGAGAGAGAGAGAGAGAGA
GAGAGAGAGAGAGAGAGAGAGAGAGAGA*EQKLISEEDL**

Figure 3.6: Design of dipeptide repeat sequences.

Nucleotide and amino acid sequences of (PR)50–HA, (GR)50–FLAG and (GA)50–*c*-myc. They do not contain (GGGGCC)n or (CCCCGG)n and they are long as 50 hexanucleotide repeats. Start codon (atg) and stop codon (taa) were added. Each DPR has a tag on the 3′ end: HA, flag and *c*-myc (italic). Restriction sites for AgeI and BamHI were placed on the 3′ and 5′ ends, respectively (underscored).

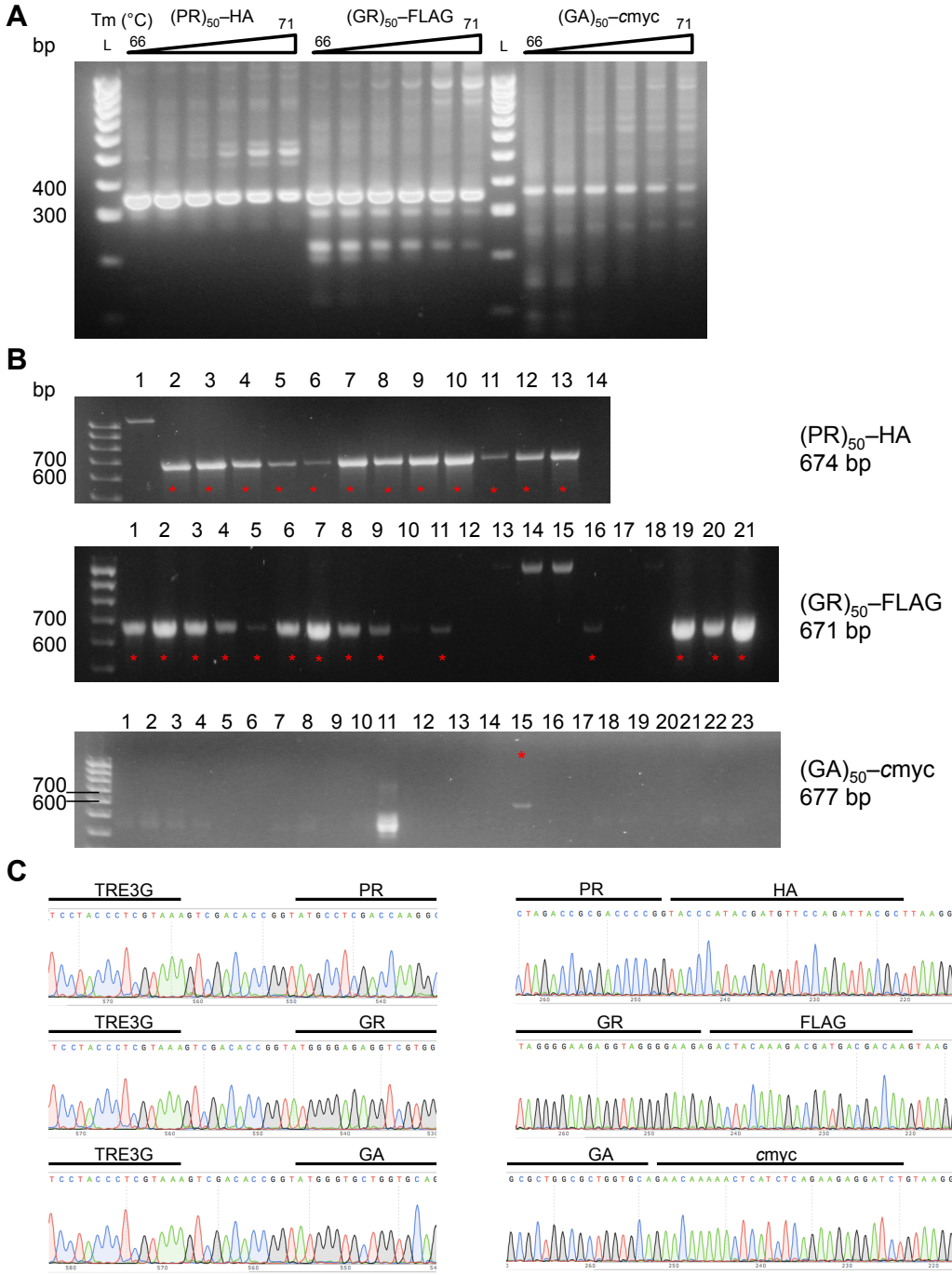


Figure 3.7: Insertion of DPR sequences in *pUltradox_rtTA3_TRE3G*.

Agarose gel electrophoresis of PCR reactions and Sanger sequencing used to check the insertion of the DPR sequences in *pUltradox_rtTA3_TRE3G*. **A)** Temperature gradient PCRs to determine the correct Tm for the amplification of (PR)50–HA (674 bp), (GR)50–FLAG (671 bp) and (GA)50–*c*-myc (677 bp). **B)** Colony PCRs showing the amplification of the inserts (asterisks = positive colonies). **C)** Sanger sequencing results of one colony per construct showing the correct insertion of the DPR+tags sequences in *pUltradox_rtTA3* (PR50-colony 1; GR50-colony 7; GA50-colony 15).

3.3. Test of the doxycycline inducible system and optimisation of the lentivirus transduction

3.3.1. Transfection of DPR vectors in HEK293T cells

Before producing the lentivirus, the new backbones were tested in HEK293T cells with a transient transfection (Figure 3.8). The expression of GFP or DPRs was induced by two concentrations of doxycycline (100 and 1000 ng/mL) and the cells were harvested after 24 and 48 hours. The western blot quantification of GFP, HA and *c*-myc showed that the system is highly sensitive, as the signal can be detected with a doxycycline concentration of 100 ng/mL (Figure 3.8 B, D, F). However, each construct showed a characteristic expressions. GFP did not show different expression levels depending on the doxycycline concentration used (Figure 3.8 B). GFP signal lowered during time and withdrawing the inducer after 24 hours, leaving the cells in normal media for another day (24 h + 24 h), reduced the expression of GFP. $(GA)_{50}$–*c*-myc followed a similar expression pattern when induced with the lower dose of doxycycline, while the higher concentration of the inducer increased *c*-myc signal over time, which could not be switched off after doxycycline withdrawal (Figure 3.8 D). $(PR)_{50}$–HA expression increased over time, but it lowered when the doxycycline was removed from the media (Figure 3.8 F).

Immunofluorescence analysis showed that the tags colocalise with the DPR antibodies, demonstrating that the tag detection will avoid the need to use DPR antibodies for future experiments (Figure 3.8 E, G). This first experiment also showed different intracellular localisations of $(PR)_{50}$–HA, localised in the nuclei, and $(GA)_{50}$–*c*-myc, mainly cytoplasmic, as previously shown in the published

literature. $(GR)_{50}$–FLAG could not be detected either by western blotting or by immunofluorescence.

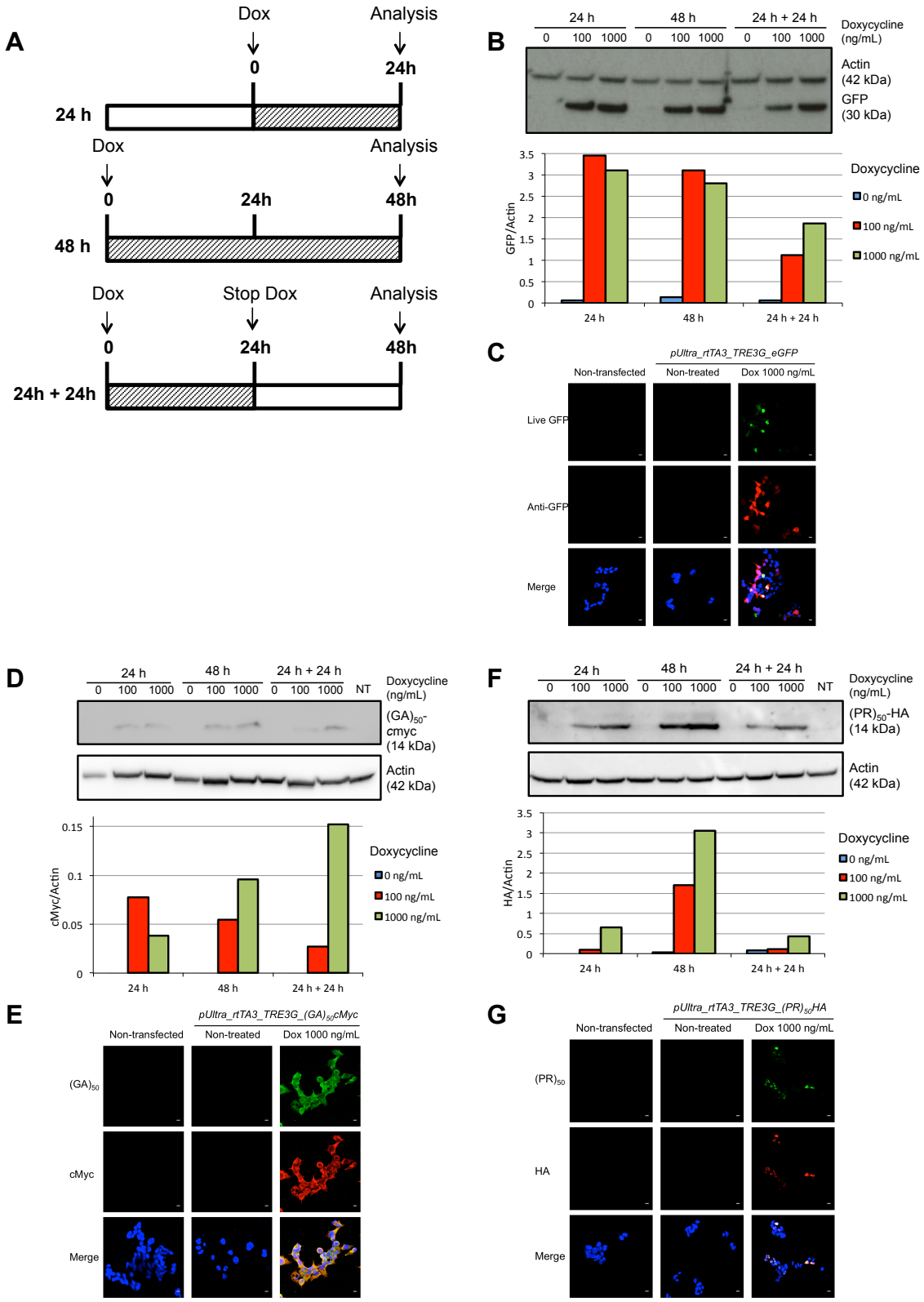


Figure 3.8: Efficiency of the doxycycline inducible system with the operon TRE3G in HEK293T cells.

Immunoblot and immunofluorescence analysis of HEK293T cells transfected with the lentiviral backbones. **A)** Schematic timeline of the treatments. **B-C)** Immunoblot quantification and immunofluorescence of *pUltradox_rtTA3_TRE3G_eGFP* transfected cells. **D-E)** Immunoblot quantification and immunofluorescence of *pUltradox_rtTA3_TRE3G_(PR)50HA.* **F-G)** Immunoblot quantification and immunofluorescence of *pUltradox_rtTA3_TRE3G_(GA)50c-myc.* Scale bar: 10 μm.

3.3.2. Titration of lentivirus toxicity in mature iPSC-derived motor neurons

The toxicity of doxycycline, lentivirus transduction and the combination of both was tested in iPSC-derived MNs with MTS assays (Promega). One age-matched control line (CTRL-1), one C9orf72 patient line (C9-02) and its CRISPR/Cas9 corrected control (ED-2) were differentiated. On day 18 of the differentiation protocol, the motor neuronal precursors were plated in 96-well plates at 10^4 cells/well. The cells were transduced overnight on day 24 in transduction medium at various multiplicities of infection (MOIs): 1, 10, 50, 100, 500, 1000, and 2000. The doxycycline was added the following day, diluted in day24+ medium in increasing concentrations (1 – 100 μg/mL). One plate per virus was left without doxycycline to test the viral toxicity (Figure 3.9 B). The MTS assay was run on day 31 showing that the optimal condition is transduction of the MNs with MOI=100 and induction of DPR expression with 5 μg/mL (Figure 3.9). The assay also showed that the GFP virus is highly toxic using the same conditions.

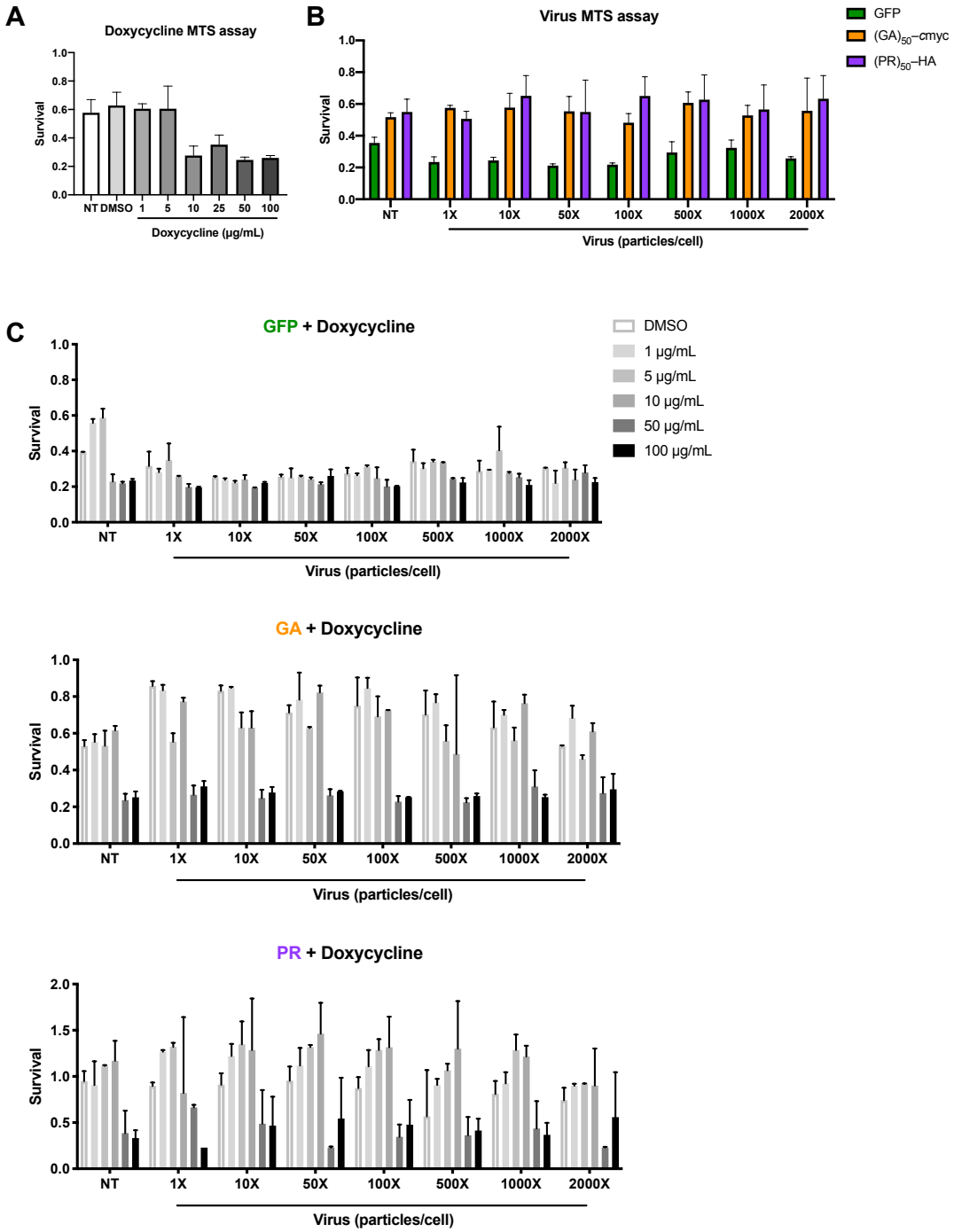


Figure 3.9: Titration of the lentivirus and doxycycline toxicity in mature iPSC-MNs.

Quantification of MTS assays of iPSC-MNs treated with doxycycline or lentivirus or the combination of both. **A)** MTS assay showing how different doxycycline concentrations affect MN survival. With more than 5 µg/mL, doxycycline toxicity increases. **B)** Increasing MOIs of lentivirus carrying DPR sequences do not affect cellular survival, while virus carrying GFP is more toxic. **C)** MTS assays showing how MN viability is affected by the combination of different MOIs and doxycycline concentrations.

3.3.3. (PR)50–HA and (GA)50–c-myc detection in iPSC-derived motor neurons

Wild-type controls and CRISPR/Cas9 corrected lines were differentiated to follow the time-line expression of (PR)50–HA and (GA)50–*c*-myc by immunoblotting. The iPSC-derived MNs were transduced overnight at day 24 in transduction medium with MOI=100. The following day the cells were washed and 5 μg/mL doxycycline was added to one well per day. All the MNs were harvested on day 31 (see figure 3.10 for scheme).

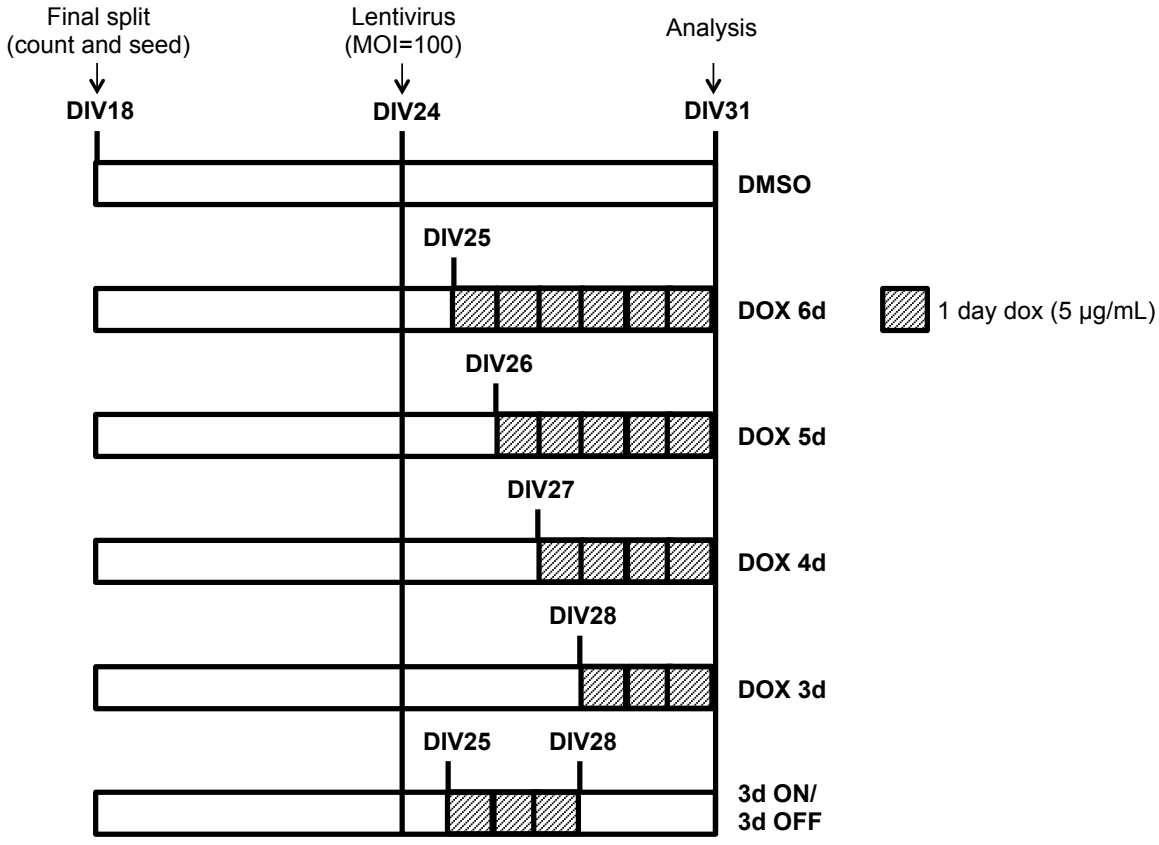


Figure 3.10: Schematic timeline for immunoblot detection of (GA)50–*c*-myc and (PR)50–HA in MNs.

The western blots showed that $(GA)_{50}$–*c*-myc expression required three days of doxycycline, after which the intensity of the *c*-myc signal was reduced (Figure 3.11 A). $(PR)_{50}$–HA was highly expressed after 5 days from doxycycline induction (Figure 3.12 A). The transduced MNs fed with media lacking doxycycline (DMSO-only) showed different basal expression of the tags, indicating leakiness of the constructs. However, the signal in DMSO-only cells was significantly lower compared to day3 ($(GA)_{50}$–*c*-myc) and day5 ($(PR)_{50}$–HA). For this reason, this condition was used in subsequent comparisons. To test the specificity of antibodies anti–*c*-myc and anti–GA, immunofluorescence analyses were performed on MNs transduced with $(GA)_{50}$–*c*-myc and treated with doxycycline for three days (Figure 3.11 B). Both signals significantly increased when doxycycline was added, compared to the MNs without the inducer and non-transduced cells. However, the anti-*c*myc antibody successfully detected the leaky signal of the construct, as shown in western blot analysis, demonstrating that the detection of the tag is more reliable then the poly(GA). Moreover, the anti-*c*myc antibody revealed occasional cytoplasmic punctae that anti–GA could not detect. This experiment showed that antibody anti-GA is less sensitive and specific than anti–*c*-myc.

The same immunofluorescence analysis was carried out on MNs transduced $(PR)_{50}$–HA and treated with doxycycline for five days (Figure 3.12 B). The transduced cells did not show HA or PR signals in the nuclei, as instead shown in lipofected HEK293T cells, but it was diffused in the cytosol. Both anti–HA and anti–PR antibodies showed higher signal when the DPR expression was switched on with doxycycline, demonstrating similar specificity and sensitivity.

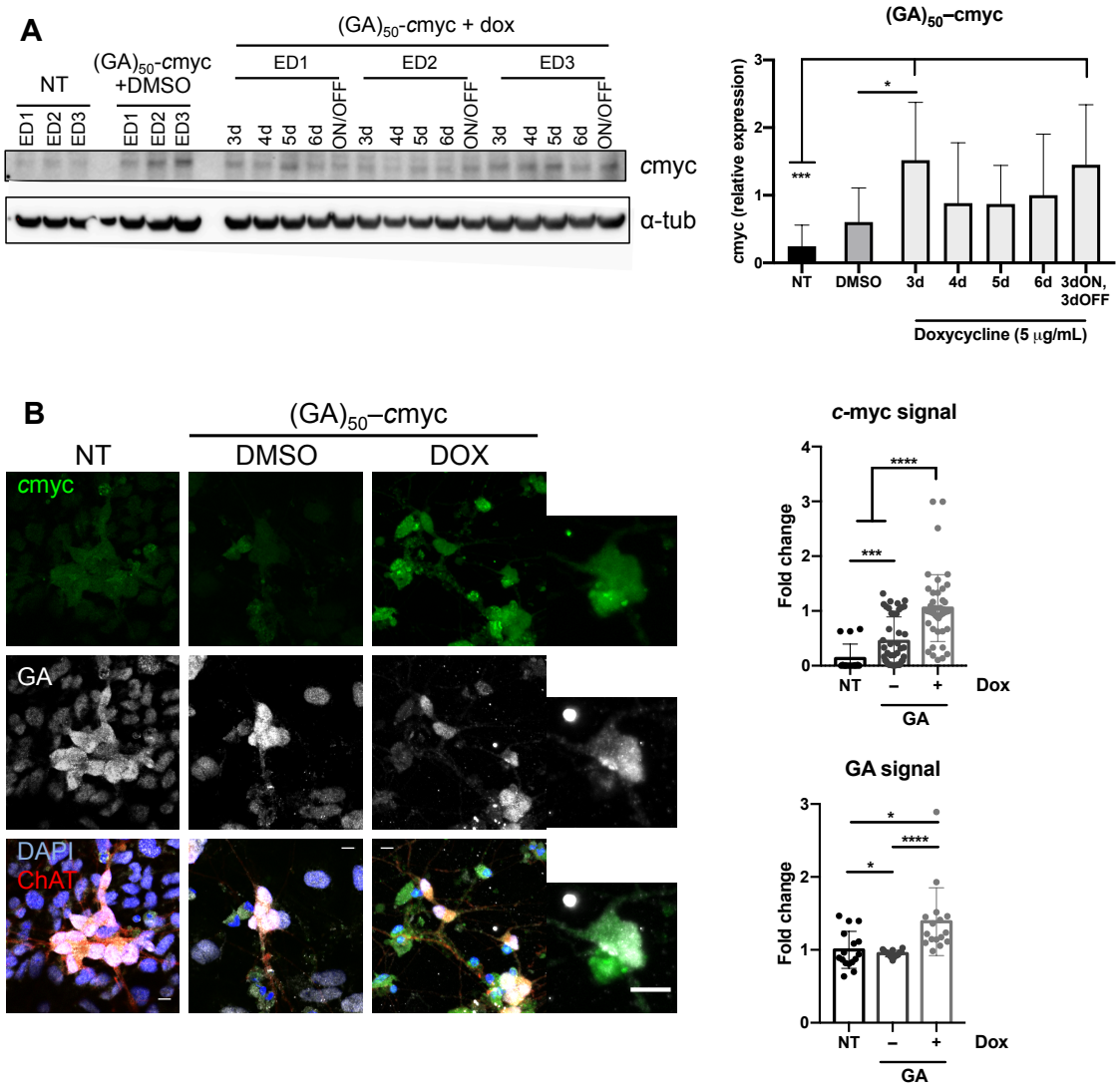


Figure 3.11: Detection of (GA)50–*c*-myc in MNs.

Immunoblot and immunofluorescence quantification of (GA)50–*c*-myc to determine its expression timeline and antibodies sensitivity and specificity. **A)** The higher expression of GA is reached with 3-day-treatment (vs NT $p = 0.0005$; vs DMSO $p = 0.047$), after which the DPR expression cannot be switched off (vs NT $p = 0.0006$). See Appendix for details (Figure S2-3). **B)** *c*-myc and GA intensities significantly increase with dox in the media, compared to the MNs without the inducer ($p<0.0001$). *c*-myc signal of the on-system is higher than non-transduced MNs ($p=0.012$). NT shows more GA intensity than the off-system ($p=0.0007$). *c*-myc green, GA white, Choline Acetyl Transferase (ChAT) red, dapi blue, scale bar 10 μm. NT=non-transduced; dox=doxycycline; –dox=off signal; +dox=on signal. Data analysed using two-way ANOVA or mixed-effect model using Tukey's *post-hoc* test (4 lines, n=2). The bars represent means and error bars are standard deviation.

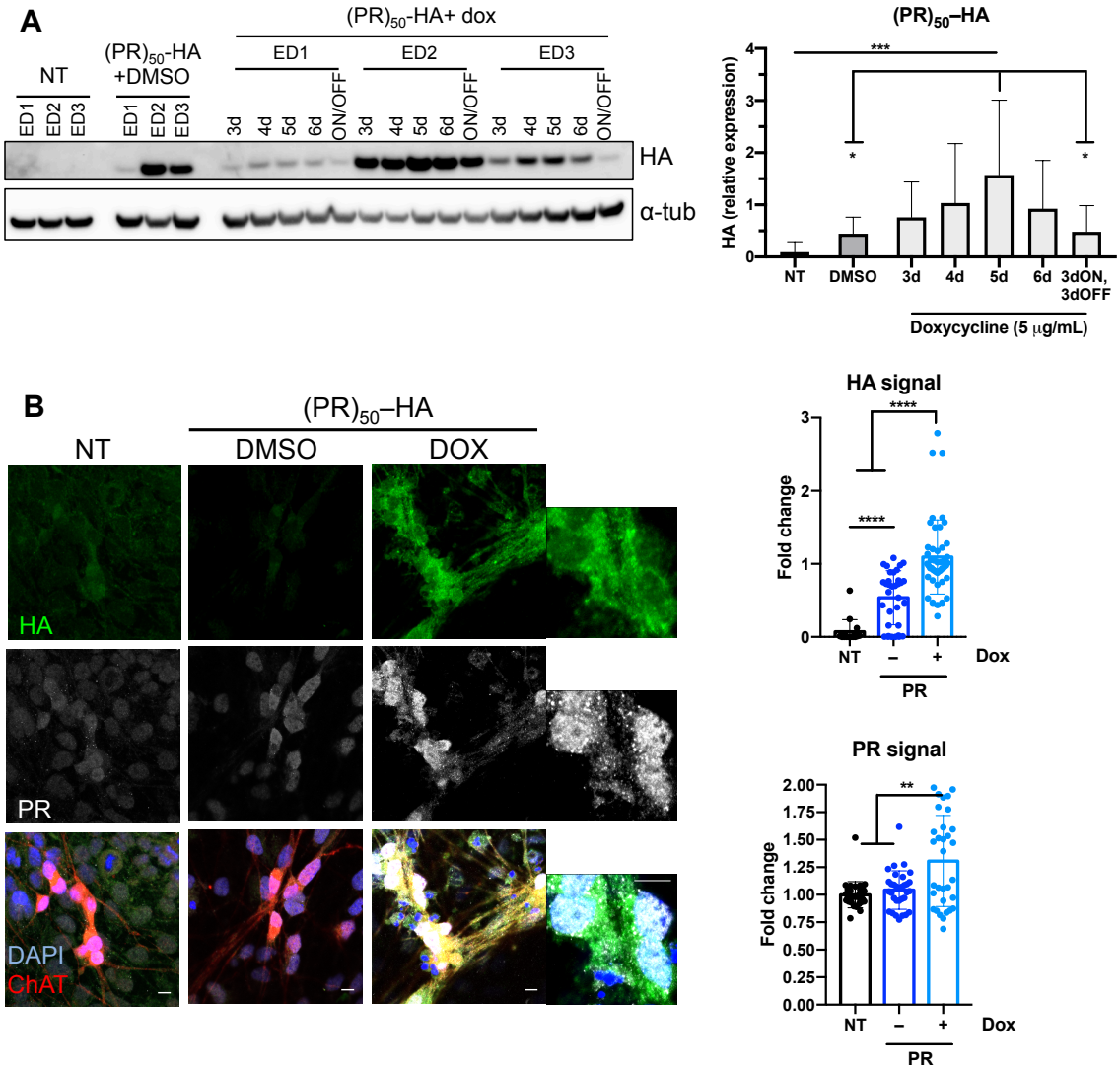


Figure 3.12: Detection of (PR)50–HA in MNs.

Immunoblot and immunofluorescence quantification of (PR)50–HA to determine its expression timeline and antibodies sensitivity and specificity. **A)** PR higher expression of is reached with 5-day-treatment (vs NT $p = 0.0002$; vs DMSO $p = 0.025$). See Appendix for details (Figure S2-3). **B)** HA and PR intensities significantly increase with dox in the media, compared to the NT MNs ($p < 0.0001$), and to the off-system (HA p=0.017; PR p=0.0002. HA green, PR white, Choline Acetyl Transferase (ChAT) red, dapi blue, scale bar 10 μm. NT=non-transduced; dox=doxycycline; –dox=off signal; +dox=on signal. Data analysed using two-way ANOVA or mixed-effect model using Tukey's *post-hoc* test (4 lines, n=2). The bars represent means and error bars are standard deviation.

The final induction protocol requires five days of doxycycline treatment for $(PR)_{50}$-HA expression, while three days treatment for $(GA)_{50}$-*c*-myc expression (Figure 3.13). The batches of cells analysed in this chapter were included in the analysis presented in the next chapters (Figure S1).

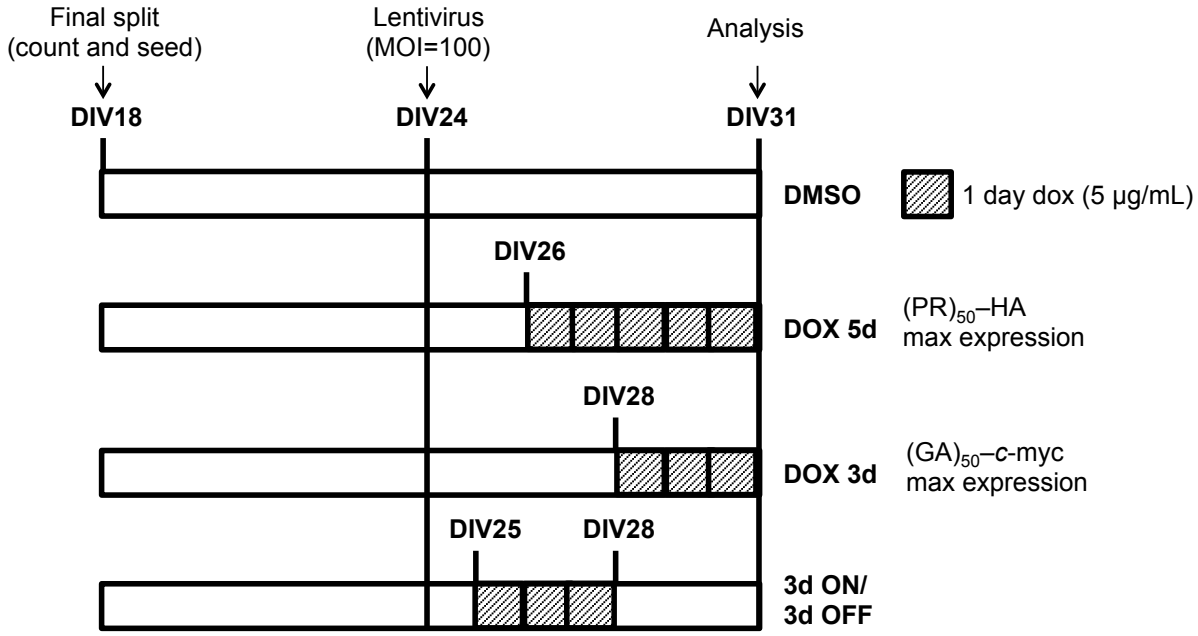


Figure 3.13: Doxycycline induction protocol used in following experiments.

Neurons were transduced over-night with lentivirus expressing the constructs on DIV24 (MOI=100). $(PR)_{50}$-HA expression was induced with doxycycline on DIV26, while $(GA)_{50}$-*c*-myc expression on DIV28. Neurons transduced but not treated with doxycycline were used as negative control (DMSO). Moreover, both constructs were induced for three days on DIV25 (3dON/3dOFF).

3.4. Conclusion

Expression of optimized sequences of $(PR)_{50}$–HA, $(GA)_{50}$–*c*-myc and $(GR)_{50}$-FLAG in cells allows the study of DPR related phenotypes. While it was not possible to detect $(GR)_{50}$–FLAG, lipofected HEK293T cells and transduced iPSC-derived MNs showed different intracellular localisations of the other two dipeptide repeat proteins, indicating cell-type specific intracellular distribution. $(GA)_{50}$–*c*-myc was diffuse in the cytosol of HEK293T cells, but it formed aggregate structures in MNs. $(PR)_{50}$–HA showed nuclear localisation, replicating previous findings. In contrast, transduced MNs did not have the same nuclear localisation and structure for poly(PR), exhibiting instead a diffuse cytoplasmic staining. These data demonstrate that the results presented in the literature so far are highly dependent on the system used to study DPR toxicity.

The doxycycline inducible system showed good sensitivity to the inducer in lipofected cells. The combination of lentivirus and drug was not toxic to the cells, allowing the study of poly(PR) and poly(GA) related phenotypes in iPSC-derived MNs. Transduced iPSC-derived MNs required higher concentrations of doxycycline to allow the detection of $(PR)_{50}$–HA and $(GA)_{50}$–*c*-myc, and both western blot and immunofluorescence analysis demonstrated that the constructs have a basal expression, which can be detected with antibodies against the tags. For this reason DMSO-only condition was used as comparison in all the following analysis. Future quality controlled is needed to quantify PR/GA transcripts.

Chapter 4 – Differential effects of poly(GA) and poly(PR) on calcium homeostasis, UPR, TDP-43 localisation and stress granule formation

4.1. Introduction

4.1.1. Mitochondria as a calcium store and energy supplier

Cytosolic calcium is buffered by mitochondria through the mitochondrial calcium uniporter (MCU), a transmembrane protein that sits on the inner mitochondrial membrane. Its activity is regulated by the EF-hand domain-containing proteins mitochondrial calcium uptake 1 (MICU1) and mitochondrial calcium uptake 2 (MICU2) (Perocchi et al., 2010; Plovanich et al., 2013). These regulators activate or inhibit MCU by sensing the calcium concentration in the intermembrane space (Patron et al., 2014). MICU2 inhibits MCU activity at resting cytoplasmic calcium levels, while MICU1 is both a positive and negative regulator, allowing calcium uptake with high calcium concentration and closing the channel in the resting state (Mallilankaraman et al., 2012; Matesanz-Isabel et al., 2016).

Mitochondrial calcium uptake is dependent on the electrochemical potential for calcium and on the mitochondrial membrane potential. Membrane potential is developed and maintained by mitochondrial respiration, which uses the electron

transport chain to reduce molecular oxygen and pump out protons. Four enzymatic complexes form the electron transport chain: NADH and succinate dehydrogenases (complex I and II), ubiquinone-cytochrome *c* reductase (complex III), and cytochrome *c* oxidase (complex IV). The proton electrochemical potential drives ATP synthase to produce energy (adenosine triphosphate, ATP).

It is now evident that mitochondrial calcium overload and deficits in the electron transport chain cause depolarisation of the mitochondrial membrane, decreased mitochondrial respiration, increased production of reactive oxygen species and release of cytochrome *c*, followed by apoptosis (Mallilankaraman et al., 2012; Pandya et al., 2013; Schinder et al., 1996).

4.1.2. Altered excitability in C9ORF72 models

We know that 40% of sporadic ALS cases show increased levels of glutamate in the cerebrospinal fluid (Rothstein et al., 1990; Spreux-Varoquaux et al., 2002). Abnormalities in extracellular glutamate concentration lead neurons to produce repetitive firing and release calcium, causing excitotoxicity. A recent study demonstrated that C9orf72 mutant iPSC-derived MNs express higher levels of GluA1, a calcium-permeable subunit of AMPA receptors, enhancing their vulnerability to glutamate-mediated excitotoxicity (Selvaraj et al., 2018). The same group also confirmed increased mRNA of GluA1 in C9 ALS spinal cord *post-mortem* tissue (Gregory et al., 2020). Another study showed that expression of the arginine-rich DPRs (PR_{36}/GR_{36}) in *Drosophila* caused increased glutamate release leading to the activation of NMDA receptors in glutamatergic neurons, and subsequent increased glutamate excitotoxicity (W. Xu & Xu, 2018). Work from our own group has demonstrated that C9orf72 mutant iPSC-derived MNs generate

lower calcium peaks when stimulated with glutamate, but they show longer recovery time, leading to glutamate-induced cell death. The longer recovery time is linked to mitochondrial deficits in calcium uptake caused by the downregulation of the mitochondrial calcium uniporter (Dafinca et al., 2020). A previous study in cortical neurons from a mouse model expressing $(GR)_{80}$, showed disruption of the mitochondrial organisation and morphology, and decreased activity of complexes I and V of the respiratory chain through interaction with ATP5A1 (Choi et al., 2019). In contrast, a different group observed high activity of the electron transport chain in C9orf72 mutant fibroblasts, paired with increased production of reactive oxygen species (Onesto et al., 2016).

4.1.3. ER-mitochondria cross-talk

The ER takes part in multiple cellular functions, like calcium homeostasis, lipid and protein biosynthesis, protein folding, post translational modifications and regulation of gene expression (Eden, 2016; Hetz & Saxena, 2017; Yoshida, 2007). Calcium is pumped into the endoplasmic reticulum (ER) by the sarco/endoplasmic reticulum Ca^{2+}-ATPase (SERCA) that actively transports calcium against its gradient. Inside the ER, calcium binding proteins sequester the ions to increase the ER storage capacity. The ER releases calcium through inositol triphosphate receptors (IP3R) and ryanodine receptors (RyR). In response to depletion of ER calcium stores, luminal calcium sensors Stromal Interaction Molecule-1/2 (STIM1/2) are free to oligomerise and facilitate the recruitment of Ora1 on the plasma membrane. The function of this complex is regulated by more proteins, and together they form the Store-Operated Calcium Entry (SOCE) (Avila-Medina et al., 2018; Krebs et al., 2015). The ER also creates membrane

contact sites with mitochondria via mitofusin 2 to mediate calcium exchange between compartments, playing an important role in calcium signalling (de Brito & Scorrano, 2008). Opening of IP3Rs raises the calcium concentration around MCU, allowing mitochondrial calcium uptake (Csordás et al., 2010). Calcium binding proteins present in the lumen participate in other ER functions, besides calcium buffering. In particular BiP/GRP78, a calcium binding protein, is a chaperone and regulator of the Unfolded Protein Response (UPR). It is involved in the folding, assembly and translocation of newly synthesised proteins, and its association with peptides is dependent on a high calcium concentration (Haas & Wabl, 1983; Suzuki et al., 1991; Vogel et al., 1990). It also binds and inhibits transmembrane proteins ATF6, IRE1 and PERK.

In the presence of misfolded proteins, due to a stress (temperature, reactive oxygen species), BiP frees ATF6, IRE1 and PERK activating the UPR, leading to attenuation of general translation, and enhanced expression of genes encoding chaperones, folding enzymes, and ER-associated degradation (ERAD) proteins. If the ER cannot restore its homeostasis, apoptotic pathways will be activated (Krebs et al., 2015; Malhotra & Kaufman, 2007). Cellular models expressing DPRs showed that poly(PR) and poly(GA) activate the UPR, indicating that the two DPRs cause ER stress (R. Wang et al., 2019; Y. J. Zhang et al., 2014). Previously we identified increased ER stress in C9orf72 mutant iPSC-derived MNs, followed by reduced mitochondrial membrane potential and altered mitochondrial morphology (Dafinca et al., 2016). The cells also presented evidence of oxidative stress, with stress granule formation and activation of apoptosis.

4.1.4. Aims of the chapter

The aim of the work described in this chapter is to systematically assess the effect on motor neurons of individual dipeptide repeat expression to identify the individual contribution of $(GA)_{50}$–*c*-myc and $(PR)_{50}$–HA to the following specific phenotypes seen in C9orf72 mutant iPSC-derived MNs:

1. Glutamate excitotoxicity
2. Calcium homeostasis
3. Mitochondrial respiration
4. Unfolded Protein Response
5. TDP-43 localisation
6. Stress granule formation

4.2. Effects of poly(GA) and poly(PR) on mitochondrial function and protein levels

4.2.1. Poly(GA) and poly(PR) cause reduction of calcium intake after glutamate stimulation and only poly(PR) limits mitochondrial calcium uptake

Glutamate excitotoxicity, caused by an excess of the neurotransmitter in the presynaptic space, can be analysed by measuring the amplitude of calcium waves in MNs expressing $(GA)_{50}$–*c*-myc or $(PR)_{50}$–HA compared to transduced cells not treated with doxycycline. Comparison between dox-on and dox-off status considered the possible leakiness of the constructs, as DPR expression could not be detected during line analysis, such as calcium imaging. CRISPR/Cas9 corrected

iPSC-derived MNs transduced with $(GA)_{50}$–*c*-myc or $(PR)_{50}$–HA were loaded with Fluo-4AM and exposed to 1 mM glutamate for 30 seconds. The expression of each DPR decreased the amplitude of calcium peaks compared to the dox-off state (Figure 4.1 B). While the expression of $(GA)_{50}$–*c*-myc did not affect the recovery after glutamate, MNs expressing $(PR)_{50}$–HA had an increased recovery rate back to baseline cytosolic calcium levels when compared to dox-off state (Figure 4.1 C).

Cytosolic calcium can be buffered by mitochondria, whose overload causes a reduction of the mitochondrial membrane potential, leading to decreased mitochondrial respiration and production of reactive oxygen species (Pandya et al., 2013). To study the mitochondrial calcium content, the cells can be treated with carbonyl cyanide m-chlorophenyl hydrazine (CCCP), a protonophore known to induce the depletion of total mitochondrial calcium and its release into the cytosol (Herrington et al., 1996; Werth & Thayer, 1994). To analyse the effects of the DPRs on mitochondrial calcium uptake, glutamate stimulation was followed by 4 μM CCCP coupled with 1 mM glutamate for 60 seconds. $(PR)_{50}$ expression reduced calcium release from the mitochondria of the edited MNs, indicating that mitochondrial calcium buffering during glutamate stimulation was significantly reduced in MNs expressing $(PR)_{50}$. $(GA)_{50}$ expression did not significantly affect mitochondrial calcium buffering in response to glutamate (Figure 4.1 D).

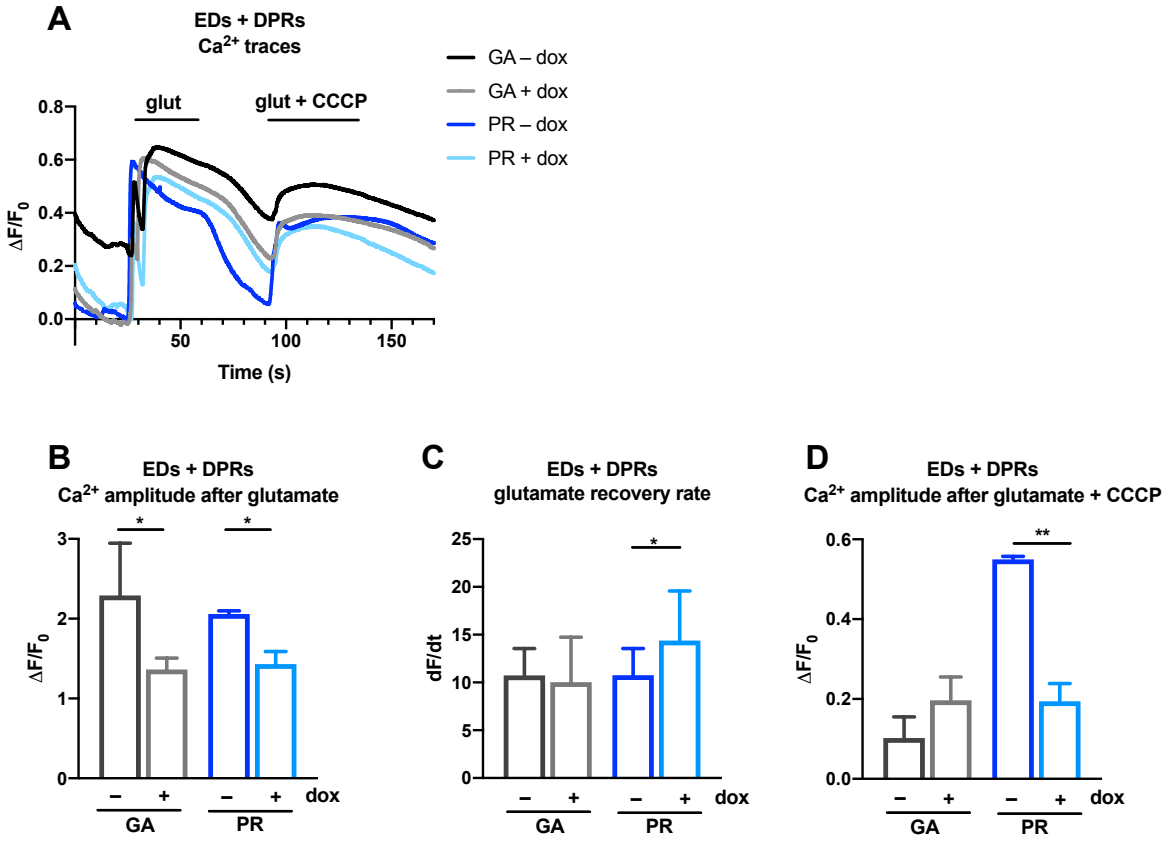


Figure 4.1: (GA)50 and (PR)50 lower calcium intake after glutamate and (PR)50 reduces mitochondrial calcium intake in edited C9orf72 iPSC-derived MNs.

Measurements and traces of cytosolic calcium, with reaction time and recovery rate, following glutamate stimulation and mitochondrial calcium release after CCCP treatment in Fluo-4AM loaded MNs. **A)** Calcium traces in Fluo-4AM loaded MNs. Lines tested: ED-1, ED-2 (n=1) collecting data from 10-25 MNs. **B)** CRISPR/Cas9 corrected MNs show reduced calcium intake following glutamate stimulation when expressing (GA)50 (p = 0.027) or (PR)50 (p = 0.044). **C)** Edited MNs expressing (PR)50 show faster recovery rate after glutamate (p = 0.042). **D)** CRISPR/Cas9 corrected MNs show reduced mitochondrial calcium release caused by (GA)50 expression (p = 0.004). Data analysed with one-way ANOVA using Tukey's *post-hoc* test. The bars represent means and error bars are standard deviation. See Appendix for details (Figure S2, S4A).

One key player in mitochondrial calcium buffering is the mitochondrial calcium uniporter (MCU) and its expression was shown to be downregulated in mature C9orf72 mutant iPSC-derived MNs (Figure 4.2 A) (Dafinca et al, 2020). However, the expression of $(GA)_{50}$–*c*-myc or $(PR)_{50}$–HA did not change MCU expression (Figure 4.2 B, C).

These experiments demonstrated that $(GA)_{50}$ and $(PR)_{50}$ reduced the cellular calcium intake of CRISPR/Cas9 corrected iPSC-derived MNs, as previously shown in C9orf72 MNs compared to wild-type and CRISPR/Cas9 corrected MNs (Dafinca et al, 2020). Moreover, $(PR)_{50}$ slowed down the reaction to glutamate and reduced mitochondrial buffering ability. However, mitochondrial calcium buffer deficits in $(PR)_{50}$ expressing MNs did not correlate with downregulation of MCU, suggesting that poly(PR) could indirectly interfere with calcium uptake through MCU by interacting with the gatekeepers of MCU.

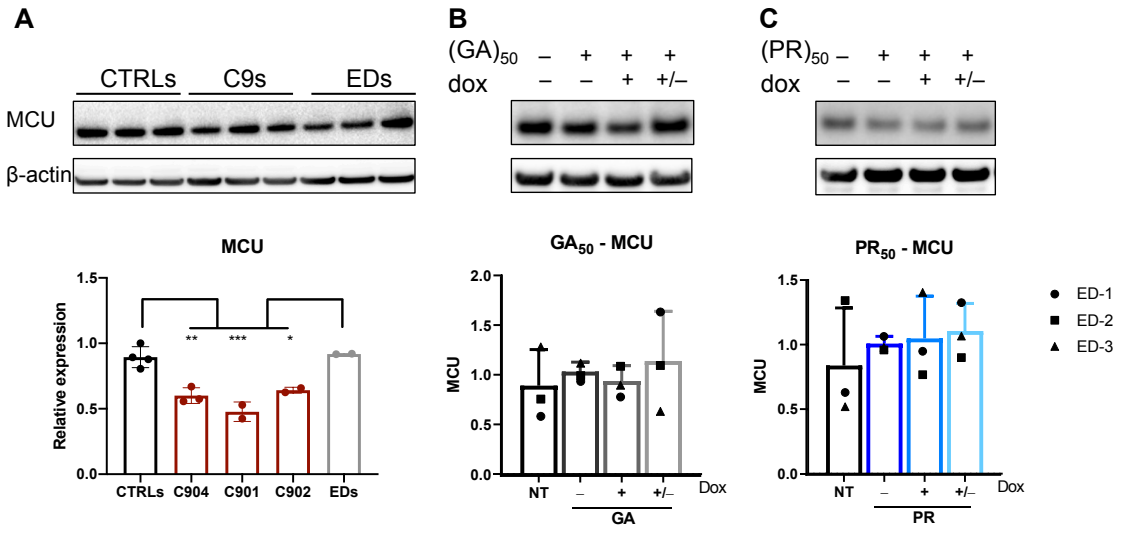


Figure 4.2: MCU downregulation in C9orf72 mutant lines is not caused by poly(PR) or poly(GA).

Immunoblots of MCU in non-treated lines and MNs expressing (GA)50–*c*-myc or (PR)50-HA. **A)** Baseline expression of MCU in controls (4 lines), C9-ALS/FTD (3 lines) and CRISPR/Cas9 corrected lines (3 lines). MCU protein level is significantly lower in all C9-ALS/FTD lines compared to healthy MNs (*p*-values 0.0021, 0.0005, 0.0115) and CRISPR/Cas9 lines (*p*-values 0.0039, 0.0008, 0.0154). One dot of the scatter plot indicates the mean of three independent differentiations per line/clone. Wild-type and CRISPR/Cas9 corrected lines formed two groups, while C9 clones were grouped per line (see table 2.2). **B-C)** Immunoblot quantifications of MCU in edited MNs non-transduced (NT) and transduced with (GA)50–*c*-myc or (PR)50–HA (see Figure S2 for details on batch of cells used). One dot of the scatter plot indicates the mean of three independent differentiations per line (for timeline expression refer to Figure 3.13). Data analysed with two-way ANOVA using Tukey's *post-hoc* test (n = 3). The bars represent means and error bars are standard deviation. See Appendix for details (Figure S5A).

4.2.2. $(GA)_{50}$ and $(PR)_{50}$ upregulate COXIV, but only $(GA)_{50}$ increases mitochondrial maximal respiration

I studied mitochondrial respiration using a Seahorse XFe96 assay, which measures the oxygen consumption rate (OCR) after the selective block of each complex of the respiratory chain. In particular, the first OCR indicates the basal respiration, after which oligomycin is added to block ATP synthase, and the following OCR indicates ATP production. The second compound used is the uncoupling agent carbonyl cyanide-4 phenylhydrazone (FCCP), which collapses the proton gradient and inhibits the electron transport chain. The subsequent OCR measures the maximal activity of complex IV (maximal respiration).

A single experiment in which three technical replicates per line were analysed showed decreased mitochondrial respiration in C9orf72 mutant iPSC-derived MNs (Figure 4.3 A), although only C9-01 and C9-04 showed significant reduction of basal respiration, ATP production and maximal respiration compared to healthy control lines (Figure 4.3 B-D). I then analysed if the expression of $(GA)_{50}$–*c*-myc or $(PR)_{50}$–HA could reduce the mitochondrial respiration in CRISPR/Cas9 corrected iPSC-derived MNs (Figure 4.3 E). Comparison between dox-on and dox-off status considered the possible leakiness of the constructs, as DPR expression could not be detected in such experiment. Contrarily to what was found in C9orf72 patient MNs, both DPRs boosted the mitochondrial respiration in edited MNs. In particular $(GA)_{50}$ significantly increased the maximal respiration (Figure 4.4 H), indicating a possible specific effect of poly(GA) on complex IV of the respiratory chain.

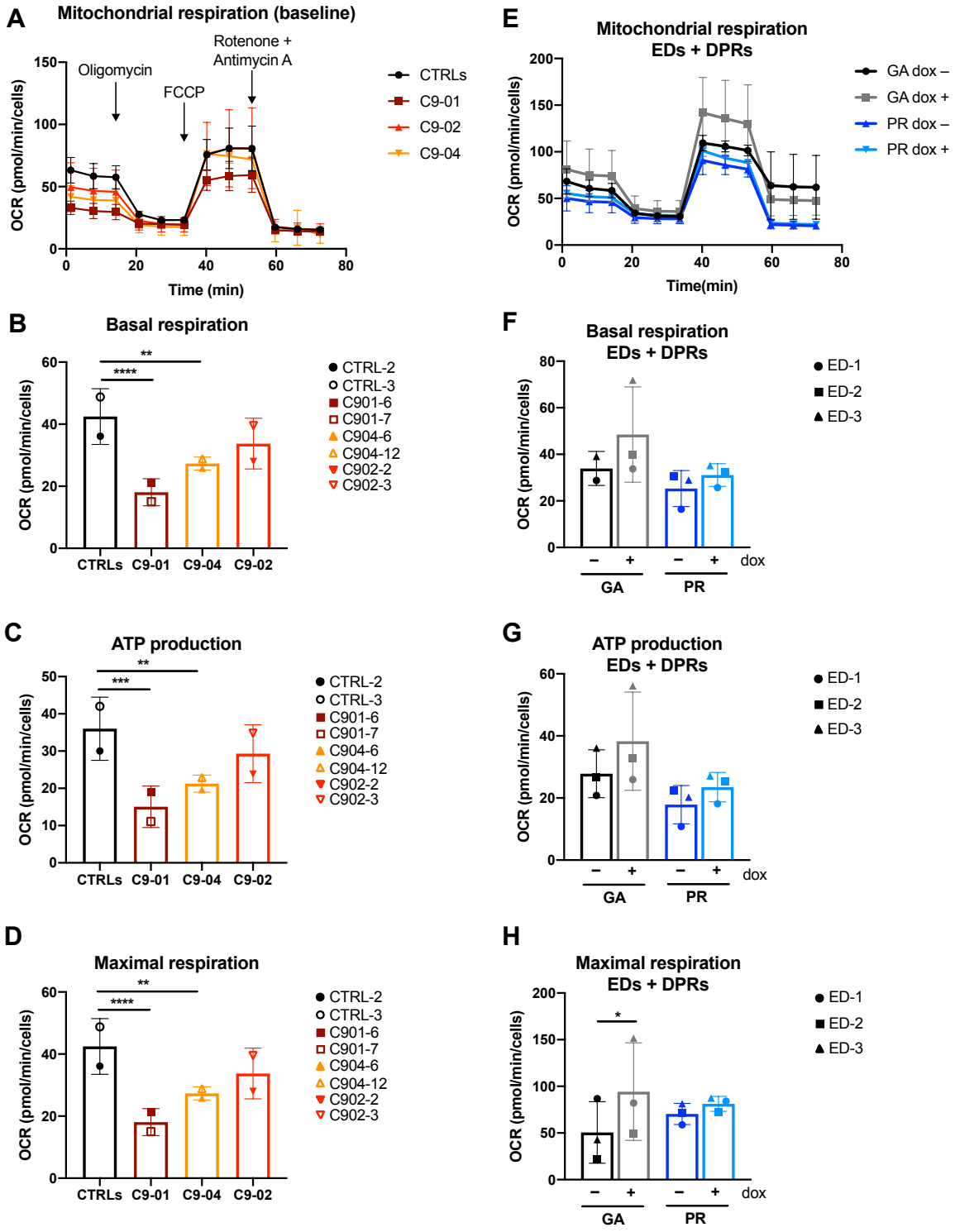


Figure 4.3: C9orf72 mutant iPSC-derived MNs show deficits in mitochondrial respiration not caused by DPRs.

Seahorse experiment to study mitochondrial respiration in healthy controls, C9orf72 mutant and edited lines expressing $(GA)_{50}$ or $(PR)_{50}$. **A)** Mitochondrial respiration profiles

of controls and C9orf72 mutant lines (see Figure S2 for details on batch of cells used). **B)** The basal respiration in WT iPSC-MNs is higher compared to C9-01 ($p < 0.0001$) and to C9-04 ($p = 0.004$). **C)** C9orf72 mutant iPSC-derived MNs produce less ATP compared to healthy controls (C9-01 $p = 0.0001$, C9-04 $p = 0.001$). **D)** C9orf72 mutant iPSC-derived MNs show low maximal respiration compared to healthy controls (C9-01 $p < 0.0001$, C9-04 $p = 0.004$). Data analysed with two-way ANOVA using Tukey's *post-hoc* test (n = 1 with three technical replicates per line). The bars represent means and error bars are standard deviations. **E)** Mitochondrial respiration profiles of CRISPR/Cas9 corrected iPSC-MNs transduced with $(GA)_{50}$ or $(PR)_{50}$. **F-H)** DPRs expression in edited lines do not significantly affect basal respiration and ATP production, but $(GA)_{50}$ increases maximal respiration ($p = 0.04$). Data analysed with two-way ANOVA using Tukey's *post-hoc* test (n = 1 with three technical replicates per line). The bars represent means and error bars are standard deviations.

For this reason I used immunoblotting to measure subunit 2 of complex IV (COXIV). C9orf72 mutant iPSC-derived MNs did not exhibit significantly low levels of COXIV protein (Figure 4.4 A), though transcriptional data, not yet validated by qPCR, from the same lines has shown that COXIV transcript is downregulated (Dr Ana Candalija, unpublished data). Reduced levels of COXIV in C9orf72 mutant lines corresponded to reduction of maximal respiration. As expected from the SeaHorse analysis, $(GA)_{50}$–*c*-myc and $(PR)_{50}$–HA expression in CRISPR/Cas9 corrected MNs upregulated COXIV expression (Figure 4.4 B, C).

The experiments demonstrate that reduced activity of the respiratory chain in C9orf72 mutant iPSC-derived MNs, corresponding to COXIV not significant downregulation, is not caused by DPR expression. In contrast, poly(GA) and poly(PR) increase energy demands and they could potentially damage the electron chain, leading to ROS production.

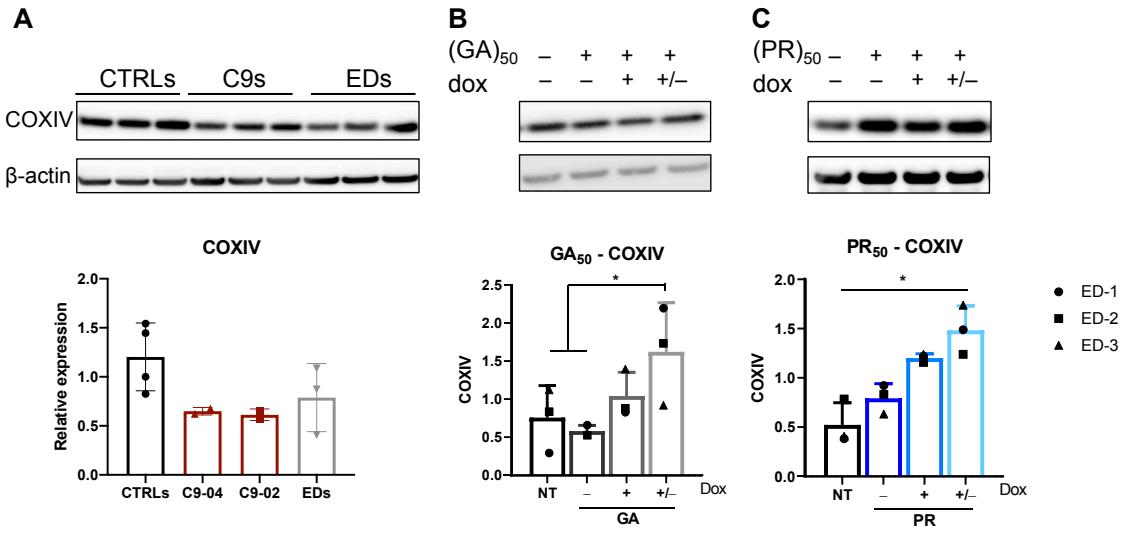


Figure 4.4: (GA)50–*c*-myc and (PR)50–HA upregulate COXIV.

Immunoblot of COXIV in non-treated lines and MNs expressing (GA)50–*c*-myc or (PR)50-HA. **A)** Baseline expression of COXIV in controls (4), C9-ALS/FTD (6) and CRISPR/Cas9 corrected lines (3). One dot of the scatter plot indicates the mean of three independent differentiations per line/clone. Wild-type and CRISPR/Cas9 corrected lines formed two groups, while C9 clones were grouped per line (see table 2.2). **B)** Poly(GA) upregulates COXIV expression after doxycycline withdraw compared to non-transduced (NT; $p = 0.046$) MNs and dox-off system (–; $p = 0.014$). **C)** Poly(PR) upregulates COXIV after doxycycline withdrawal compared to non-transduced (NT; $p = 0.029$) MNs. One dot of the scatter plot indicates the mean of three independent differentiations per line (for timeline expression refer to Figure 3.13). Data analysed with two-way ANOVA using Tukey's *post-hoc* test (n = 3). The bars represent means and error bars are standard deviation. See Appendix for details (Figure S5B) and S2 for details on batch of cells used.

4.2.3. Poly(GA) expression increases the mitochondrial mass

The total number of mitochondria influences the amount of mitochondrial proteins and their functions. I quantified the total Translocase of Outer Mitochondrial Membrane 20 (TOMM20) expression to investigate the possibility that decreased mitochondrial calcium buffering activity or increased mitochondrial respiration is due to a difference in the number of mitochondria. Immunoblot analysis of C9orf72 mutant iPSC-derived MNs did not show reduction of TOMM20 protein level (Figure 4.5 A), indicating that the mitochondrial phenotypes previously demonstrated are caused by deficits of mitochondrial function. $(GA)_{50}$–*c*-myc expression in CRISPR/Cas9 corrected MNs upregulated TOMM20 expression, showing that poly(GA) increases total mitochondrial mass (Figure 4.5 B). These data indicate that increased mitochondrial respiration in response to poly(GA) is caused by higher number of mitochondria. In contrast, $(PR)_{50}$–HA did not change expression of TOMM20 (Figure 4.5 C), suggesting that poly(PR) has a targeted effect on mitochondrial calcium buffering activity and COXIV upregulation.

I then investigated whether the DPRs bind specifically to mitochondria and alter the phenotypes by blocking channels. I analysed immunofluorescence images of transduced CRISPR/Cas9 corrected MNs, looking at co-localisation between DPRs and mitochondria. Using Pearson's correlation coefficients, I did not find co-localisation between $(GA)_{50}$–*c*-myc and TOMM20 (Figure 4.6). Unfortunately, I could not collect data of $(PR)_{50}$–HA due to the pandemic.

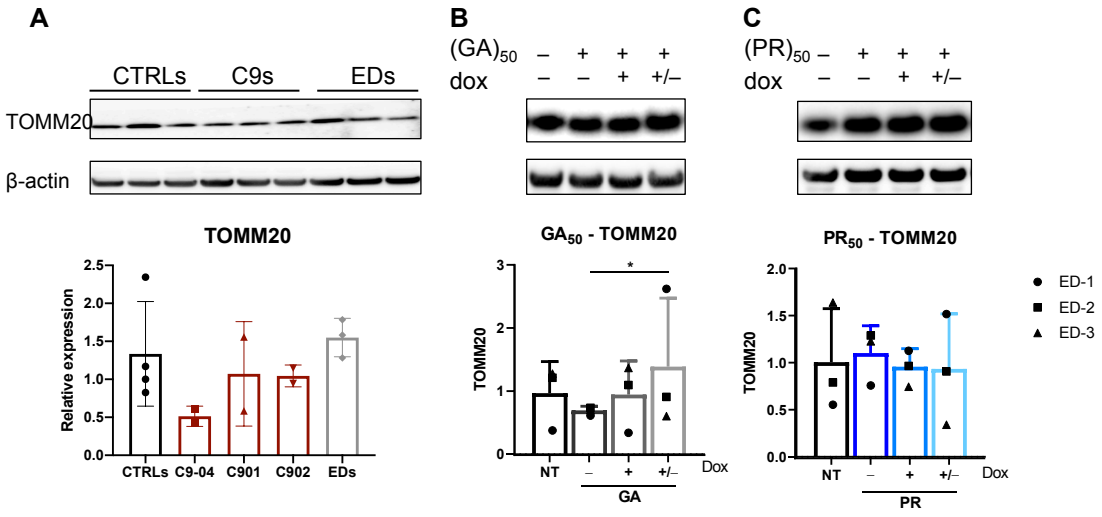


Figure 4.5: (GA)50–*c*-myc upregulates TOMM20.

Immunoblots of TOMM20 in non-treated lines and MNs expressing (GA)50–*c*-myc or (PR)50-HA. **A)** Baseline expression of TOMM20 in controls (4), C9-ALS/FTD (6) and CRISPR/Cas9 corrected lines (3). One dot of the scatter plot indicates the mean of three independent differentiations per line/clone. Wild-type and CRISPR/Cas9 corrected lines formed two groups, while C9 clones were grouped per line (see table 2.2). **B-C)** (GA)50 upregulates TOMM20 after doxycycline withdrawal compared to dox-off system (p = 0.045), while (PR)50 does not affect TOMM20 expression. One dot of the scatter plot indicates the mean of three independent differentiations per line (for timeline expression refer to Figure 3.13). Data analysed with two-way ANOVA using Tukey's *post-hoc* test (n = 3). The bars represent means and error bars are standard deviation. See Appendix for details (Figure S2, S5B).

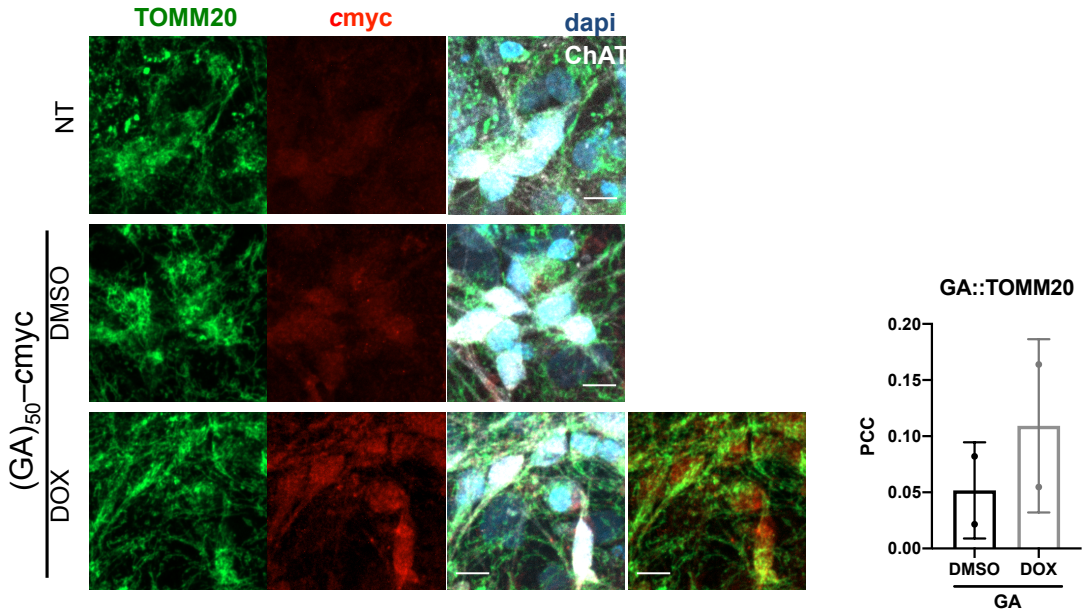


Figure 4.6: (GA)$_{50}$–*c*-myc does not localise to mitochondria.

Immunofluorescence of TOMM20 and (GA)$_{50}$-*c*-myc in ChAT-positive MNs (scale bar 10 μm). Pearson's correlation coefficient (PCC) of ED-1 and ED-3. Single MNs were analysed (13 – 25 cells, n = 2). The bars represent means and error bars are standard deviation.

4.3. Effect of poly(GA) and poly(PR) on ER-calcium physiology and the Unfolded Protein Response

4.3.1. Low ER calcium release in C9orf72 mutant iPSC-MNs is caused by poly(PR)

Calcium homeostasis in the ER is essential to many cellular functions and we and others have previously demonstrated it is deregulated in C9orf72 mutant iPSC-derived MNs. To investigate its levels in the presence of PR and GA in CRISPR/Cas9 edited MNs, I stimulated the cells with carbachol which induces the release of ER calcium through IP3R (C. White & McGeown, 2002). I first analysed the calcium amplitude generated by C9orf72 mutant iPSC-derived MNs and compared it to wild-type and CRISPR/Cas9 corrected lines (Figure 4.7 A). Two C9orf72 patient lines released significantly less calcium from their IP3Rs, compared to the isogenic line, while only one patient line showed a larger calcium amplitude (C9-01) compared to the wild-type lines. I then analysed the effects of DPR expression in CRISPR/Cas9 corrected MNs, showing that poly(PR) caused reduction of calcium released from IP3R, compared to transduced MNs not treated with doxycycline (Figure 4.7 B). Low ER calcium release in C9orf72 and PR-treated edited iPSC-MNs could indicate reduced IP3R activity or reduced ER calcium level.

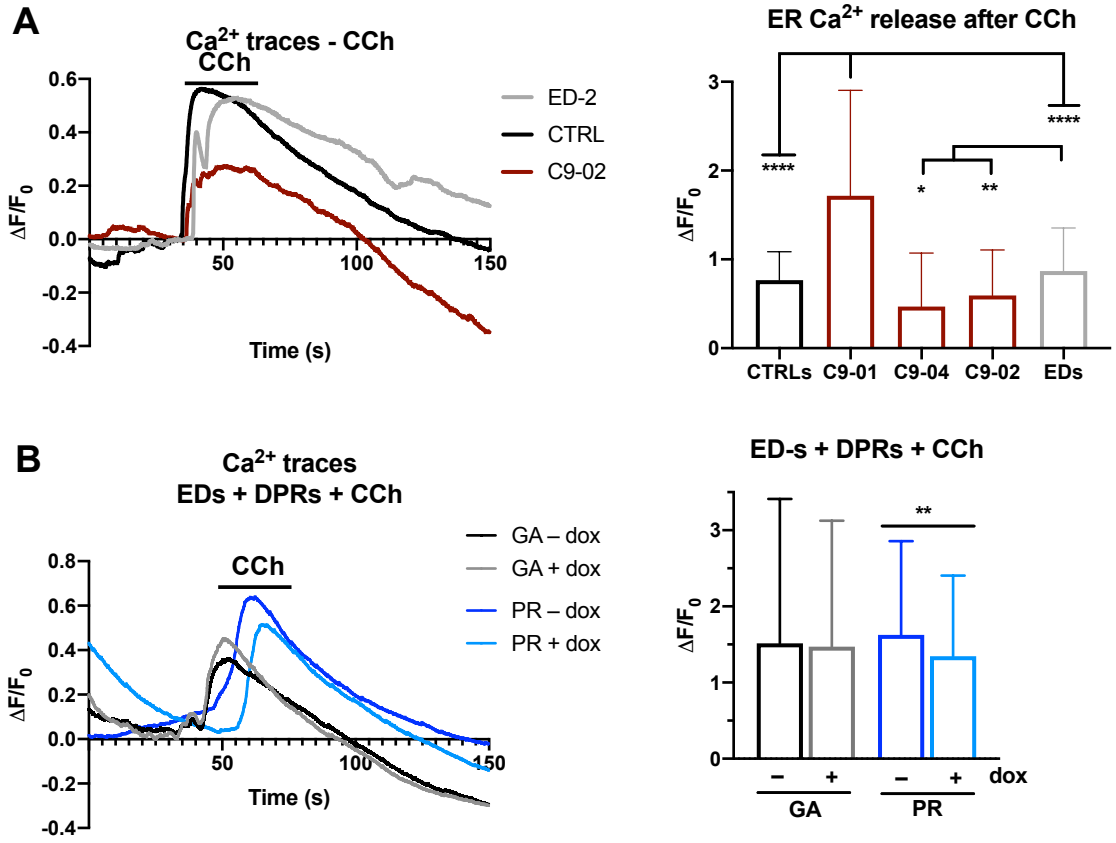


Figure 4.7: (PR)50 lowers the amount of calcium released from the ER.

Measurements of ER calcium released following carbachol in Fluo-4AM loaded cells and traces of single MN per group. **A)** C9-04 and C9-02 release less calcium from the ER compared to CRISPR/Cas9 corrected lines ($p = 0.0188$ and $p = 0.0064$). C9-01 releases more calcium from ER ($p < 0.0001$). Data analysed with one-way ANOVA using Tukey's *post-hoc* correction. **B)** (PR)50 decreases total ER calcium in genome edited MNs ($p = 0.0431$). Data analysed with paired *t*–test. The bars represent means and error bars are standard deviations. All lines and clones were tested, collecting data from 10 – 50 MNs (n = 3). See Appendix for details (Figure S2, S4B).

To measure the total ER calcium level, I treated the iPSC-derived MNs with thapsigargin an inhibitor of SERCA pumps which induces the release of total ER calcium (Lyttonsg et al., 1991). Following thapsigargin stimulation, the edited iPSC-MNs expressing $(GA)_{50}$–*c*-myc and $(PR)_{50}$–HA showed significantly reduced ER calcium levels, compared to transduced MNs not treated with doxycycline, similar to C9orf72 mutant iPSC-derived MNs (Figure 4.8).

These experiments demonstrate a deficiency in ER calcium release in C9orf72 mutant iPSC-derived MNs. This deficiency is partially explained by poly(PR) expression, which downregulates ER calcium release by reducing overall ER calcium levels in the edited lines.

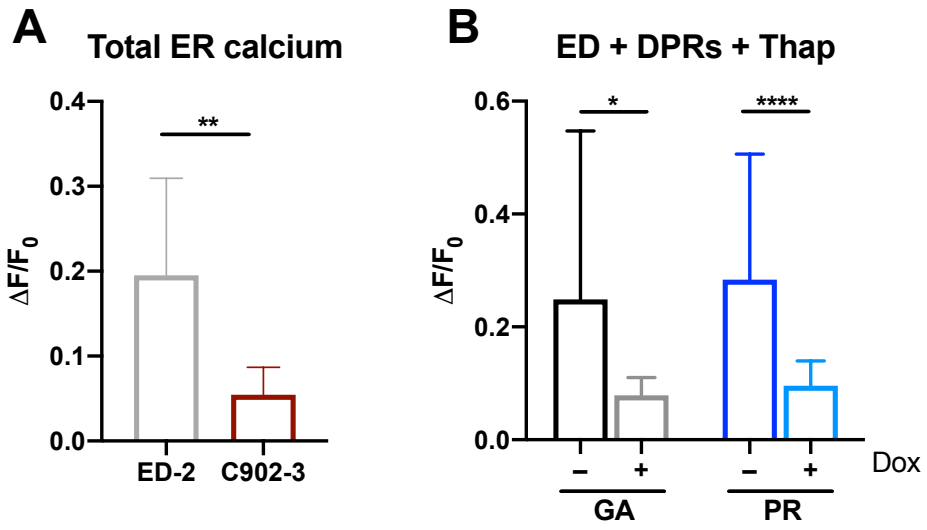


Figure 4.8: $(GA)_{50}$ and $(PR)_{50}$ reduce total ER calcium level.

Measurements of total ER calcium released from ER after thapsigargin stimulation. **A)** C9-02 MNs show reduced ER calcium level compared to ED-2 MNs ($p = 0.0013$). **B)** $(GA)_{50}$ and $(PR)_{50}$ reduce total ER calcium level in ED-1 and ED-2 MNs (GA $p = 0.05$; PR $p < 0.0001$). Data collected from 9-20 cells (n = 1). Data were analysed with paired *t*-test. The bars represent means and error bars are standard deviations. See Appendix for details (Figure S2, S4C).

4.3.2. UPR deficiency in C9orf72 mutant iPSC-derived MNs is not caused by poly(GA) and poly(PR)

Reduction in ER calcium can lead to stress responses, such as the activation of the Unfolded Protein Response (UPR). A common marker for ER stress is the upregulation of BiP/GRP78. In normal conditions, BiP associates with ATF6, PERK and IRE1. I focused on the PERK pathway, analysing its components by immunoblot. In the presence of stress, BiP disconnects from PERK, that phosphorylates itself and the translational factor eIF2α (Bertolotti et al., 2000). This leads to the translation of specific mRNAs, such as ATF4, a transcription factor that activates the expression of genes involved in the antioxidant response and ER-Golgi trafficking, but also ER chaperones, and C/EBP homologous protein (CHOP).

Immunoblots of BiP, PERK, ATF4, and CHOP showed general downregulation of the PERK pathway in C9orf72 mutant iPSC-derived MNs (Figure 4.9). In particular, the expression of BiP was moderately reduced in C9-02, followed by significant downregulation of PERK in C9-02 MNs, compared to CRISPR/Cas9 corrected MNs, and in C9-04, compared to wild-type MNs. Moreover, ATF4 was significantly downregulated in C9-04, lowering the expression of CHOP. CHOP was also downregulated in C9-02 MNs and CRISPR/Cas9 corrected lines.

The analysis of the PERK pathway in genome edited iPSC-derived MNs expressing $(GA)_{50}$ or $(PR)_{50}$ did not show downregulation or upregulation of the UPR (Figure 4.10), suggesting that the DPRs do not interact with these proteins or modulate their expression. However, phosphorylated forms of PERK and eIF2α would be more informative, but the antibodies did not work.

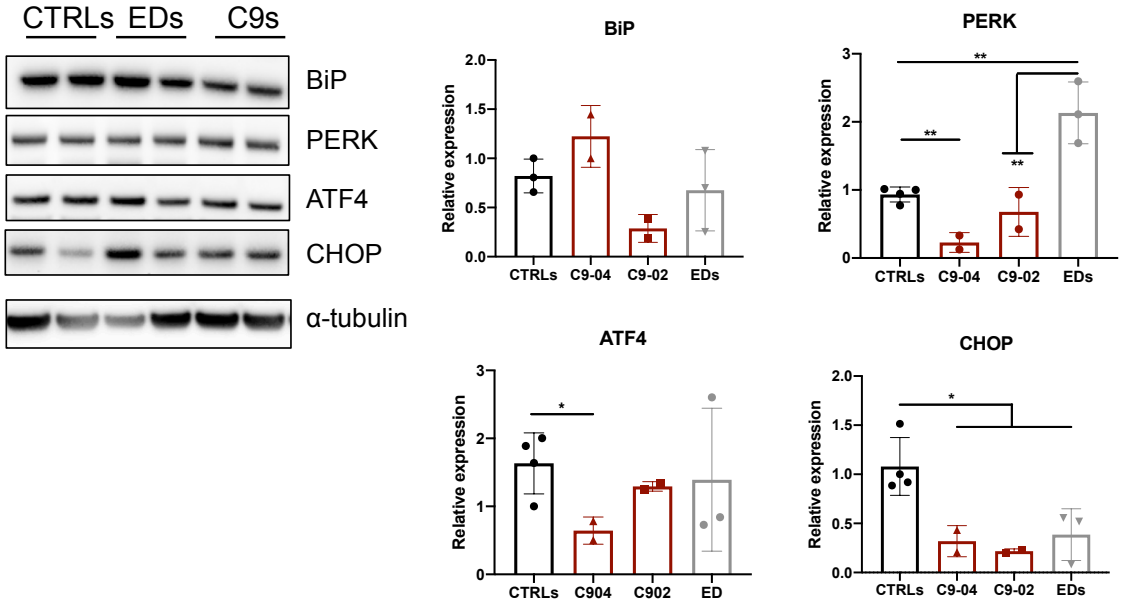


Figure 4.9: The UPR pathway is downregulated in C9orf72 mutant MNs.

Baseline expression of BiP, PERK, ATF4 and CHOP in healthy controls (3), C9-ALS/FTD (3) and CRISPR/Cas9 corrected lines (3). PERK is significantly downregulated in C9-04 compared to the control lines (p = 0.0025) and C9-02 compared to the edited lines (p = 0.0041). The edited line overexpress PERK compared to control MNs (p = 0.0044). ATF4 is downregulated in C9-04 compared to control lines (p = 0.0465) and all patient and edited lines show low expression of CHOP (p = 0.0358; 0.0197; 0.0306). One dot of the scatter plot indicates the mean of three independent differentiations per line/clone. Wild-type and CRISPR/Cas9 corrected lines formed two groups, while C9 clones were grouped per line (see table 2.2). Data analysed with one-way ANOVA using Tukey's *post-hoc* test (n = 4). The bars represent means and error bars are standard deviations. See Appendix for details (Figure S2, S6).

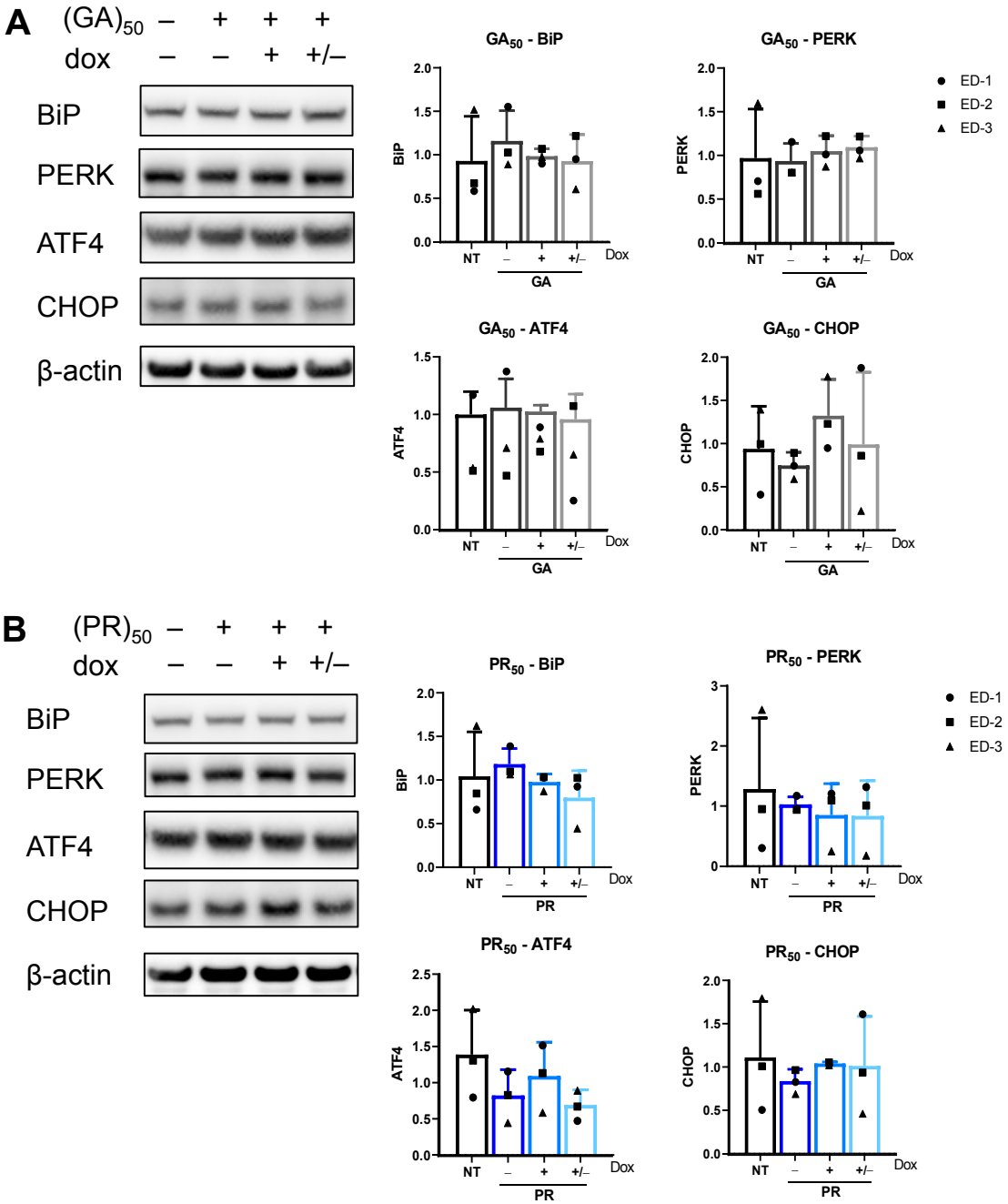


Figure 4.10: (GA)50 and (PR)50 do not affect the expression of proteins belonging to the UPR pathway.

Immunoblot quantifications of BiP, PERK, ATF4 and CHOP in CRISPR/Cas9 corrected MNs non-transduced (NT) and transduced with (GA)50–*c*-myc (**A**) or (PR)50–HA (**B**). One dot of the scatter plot indicates the mean of three independent differentiations per line (for timeline expression refer to Figure 3.13). Data analysed using two-way ANOVA using Tukey's *post-hoc* test (n = 3). The bars represent means and error bars are standard deviations. See Appendix for details (Figure S2, S6).

4.4. Focus on ALS-related phenotypes: TDP-43 mislocalisation and and stress granule formation

4.4.1. TDP-43 nuclear retention in C9orf72 mutant iPSC-derived MNs is not caused by poly(GA) or poly(PR)

Post-mortem case studies of C9orf72 patients who died prematurely (Baborie et al., 2015; Vatsavayai et al., 2016), and DPR overexpression studies (Khosravi et al., 2016, 2020; Nonaka et al., 2018) suggested that the accumulation of DPRs could cause TDP-43 mislocalisation. Moreover, the depletion of *C9ORF72* gene in mice does not cause TDP-43 mislocalisation, suggesting that DPRs or RNA foci might drive its cytosolic aggregation, not C9ORF72 haploinsufficiency (Koppers et al., 2015). Increased excitotoxicity, deficits in mitochondrial respiration and ER protein folding lead to the production of ROS, and their accumulation cause oxidative stress. It has been previously described that oxidative stress triggers TDP-43 cytoplasmic aggregation, demonstrating in principle how ALS cases, without known *TARDBP* mutations, might develop TDP-43 pathology (V. Ayala et al., 2011; Colombrita et al., 2009). However, the exact mechanism is still unclear.

A well established experimental paradigm to induce oxidative stress *in vitro* is treatment with sodium arsenite. I measured the TDP-43 fluorescent signal in untreated ChAT-positive cells or treated with sodium arsenite, and I normalised the nuclear signal over the cytosolic one. In normal conditions, our C9orf72 mutant iPSC-derived MNs showed higher expression of TDP-43 in the nuclei, but one-hour treatment with 0.5 mM sodium arsenite caused increased cytoplasmic TDP-43 (Figure 4.11). However, the treatment did not facilitate TDP-43 cytosolic mislocalisation in healthy controlled lines. Expression of $(GA)_{50}$ or $(PR)_{50}$ in

CRISPR/Cas9 corrected iPSC-derived MNs did not induce TDP-43 nuclear retention, as seen in C9orf72 mutant lines, or cytoplasmic mislocalisation, as showed in *post-mortem* C9orf72 human tissue. Moreover, the sodium arsenite treatment did not cause the above mentioned phenotype (Figure 4.12). This single experiment suggests that poly(GA) and poly(PR) do not directly and independently interfere with TDP-43 localisation, but further replicates and analysis on DPR-positive cells would be more informative.

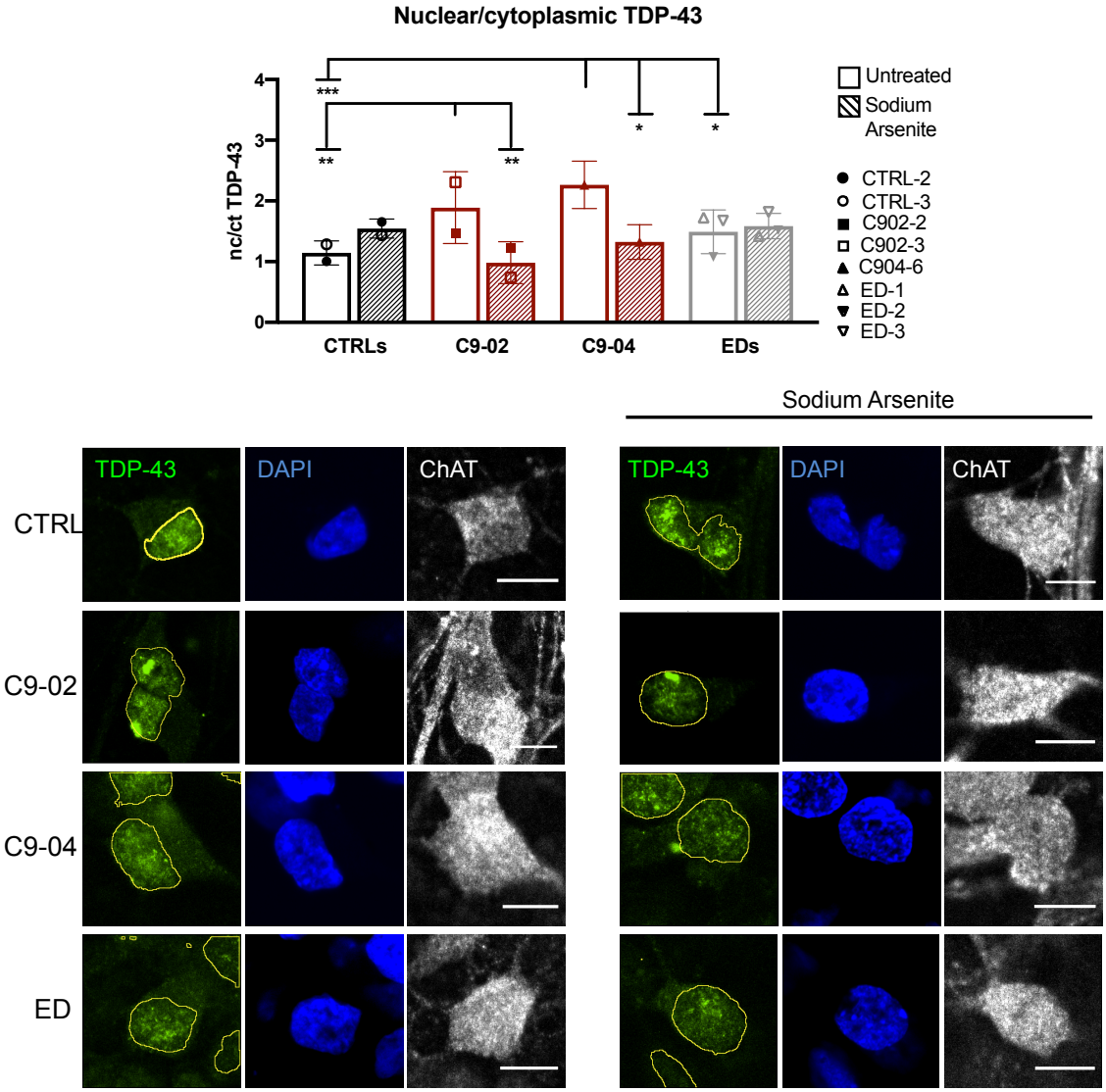


Figure 4.11: C9orf72 mutant iPSC-derived MNs show TDP-43 nuclear retention that delocalises to the cytosol after sodium arsenite treatment.

Immunofluorescence analysis of TDP-43 localisation in ChAT positive cells untreated or treated with sodium arsenite (TDP-43 green, dapi blue, ChAT white, scale bar 10 μm). C9-04 iPSC-MNs show significant cytosolic TDP-43 delocalisation after sodium arsenite treatment (p = 0.005). The mean of five pictures per sample was analysed with one-way ANOVA using Tukey's *post-hoc* test (n = 1). The bars represent means of five technical replicates and error bars are standard deviations. Wild-type and CRISPR/Cas9 corrected lines formed two groups, while C9 clones were grouped per line (see table 2.2).

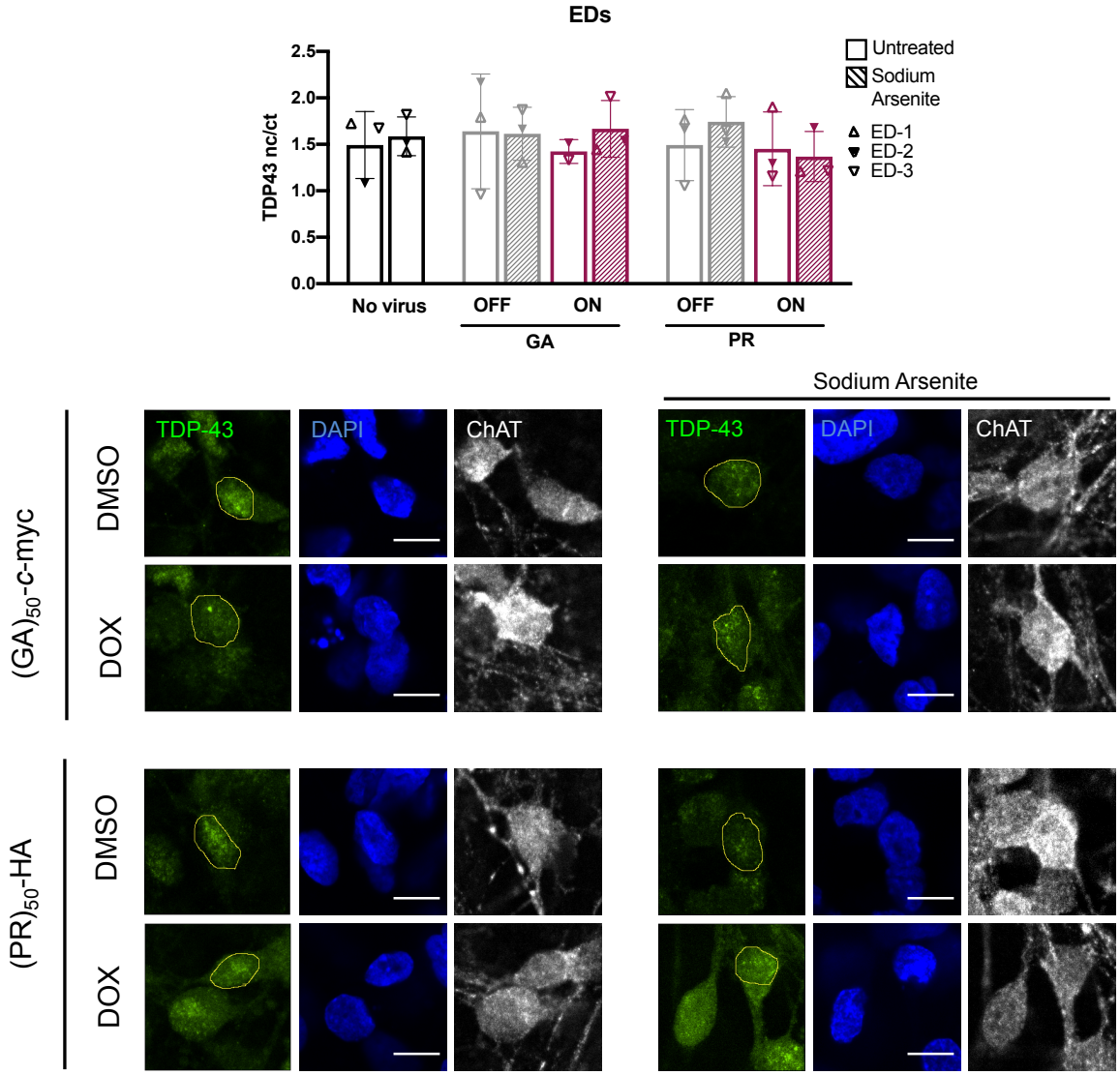


Figure 4.12: $(GA)_{50}$ and $(PR)_{50}$ expression does not cause TDP-43 mislocalisation or nuclear retention.

Immunofluorescence analysis of TDP-43 localisation in ChAT positive cells transduced with virus expressing $(GA)_{50}$–*c*-myc or $(PR)_{50}$–HA (TDP-43 green, dapi blue, ChAT white, scale bar 10 μm). The mean of five technical replicates per sample was analysed with one-way ANOVA using Tukey's *post-hoc* test (n = 1). The bars represent means of three CRISPR/Cas9 corrected lines and error bars are standard deviations (see Figure S2 for details on batch of cells used).

4.4.2. $(PR)_{50}$ induces stress granule formation

Oxidative stress caused by sodium arsenite treatment induces the formation of stress granules (SG) (Palangi et al., 2017). These ribonucleoprotein aggregates are necessary to silence mRNAs during stress conditions, inhibit apoptosis and activate the expression of stress-related mRNAs (Arimoto et al., 2008). Once the stress condition is over, the SGs disassemble (Nover et al., 1989). These aggregates are composed of RNAs and RNA binding proteins such as TIA1, G3BP and PABP.

I analysed the size of the PABP aggregates in sodium arsenite-treated iPSC-MNs (area 0.1 – 1.5 μm^2), and I counted the number of SGs per ChAT-positive cell. Even though the SG size did not change between lines, the C9orf72 mutant lines C9-01 and C9-02 showed more SGs per cell, but not significantly (Figure 4.13 A). I then studied the effects of DPR expression in CRISPR/Cas9 corrected iPSC-derived MNs treated with sodium arsenite. $(GA)_{50}$ expression did not change SG size, but viral transduction significantly increased the number of SGs per cell compared to non transduced MNs (Figure 4.13 B). When $(GA)_{50}$ expression was turned off after 3 days (dox +/–), MNs showed more SGs per cell compared to the other conditions, but not significantly. It suggests that GA expression makes the SGs irreversible through an as yet unknown mechanism, which could be clarified by further experiments. In contrast, continuous $(PR)_{50}$ expression enlarged the SGs and duplicated their number, whereas the dox+/– condition did not affect SG phenotype, suggesting a reversible mechanism (Figure 4.13 C).

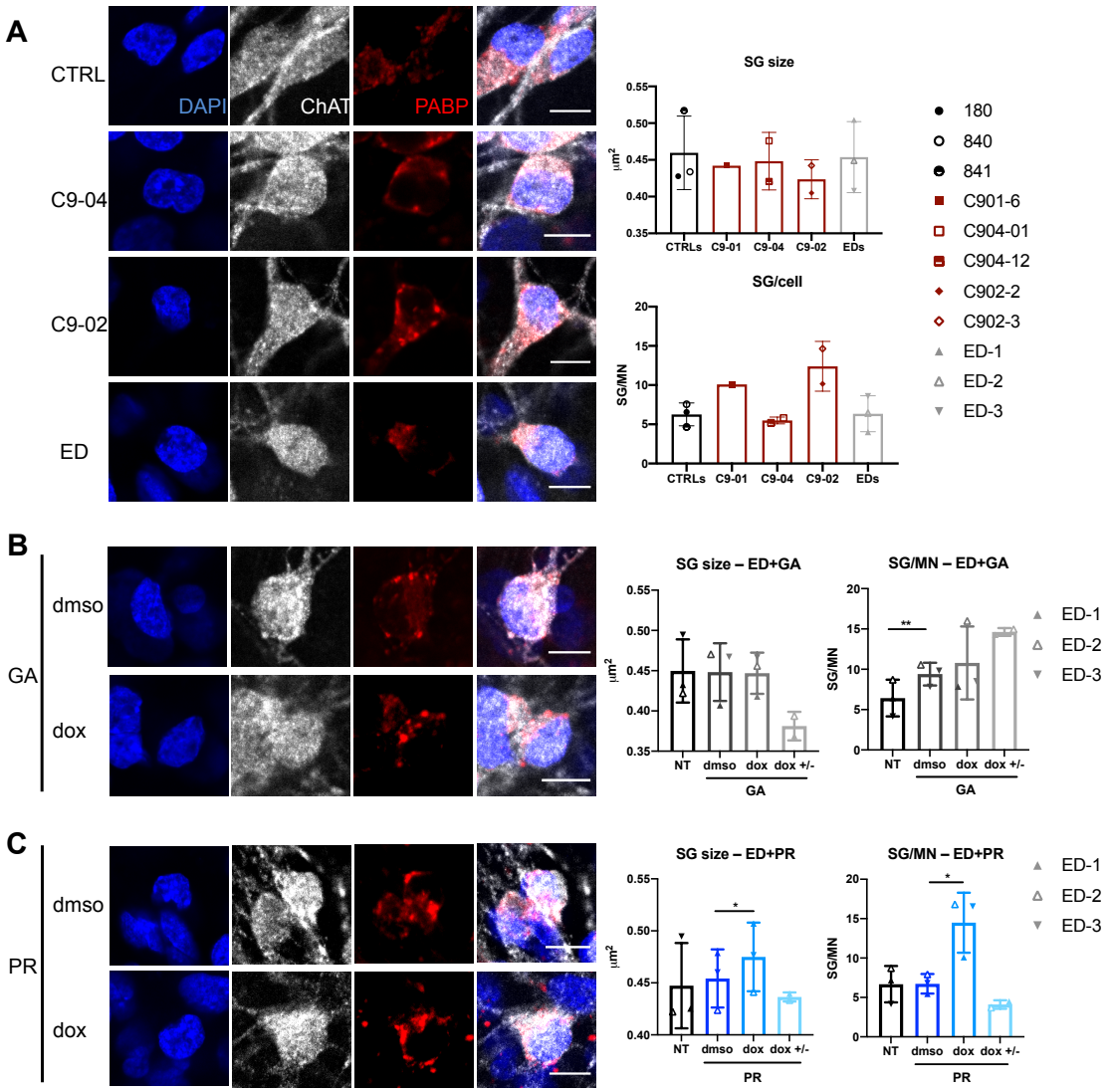


Figure 4.13: $(PR)_{50}$ induces stress granule formation in genome edited MNs treated with sodium arsenite.

Immunofluorescence analysis of SGs in sodium arsenite-treated ChAT-positive iPSC-MNs. **A)** The SG size does not change between WT, C9ORF72 mutant and CRISPR/Cas9 corrected iPSC-derived MNs. Patient C9-02 has more SGs per MN, but not significantly. Data analysed with one-way ANOVA using Tukey's *post-hoc* test (n=3). One dot of the scatter plot indicates the mean of three independent differentiations per line/clone. Wild-type and CRISPR/Cas9 corrected lines formed two groups, while C9 clones were grouped per line (see table 2.2). **B)** The viral transduction with $(GA)_{50}$ induces SG formation in edited lines ($p = 0.006$). **C)** $(PR)_{50}$ induces formation of larger SG ($p = 0.03$), and MNs contain more SGs when $(PR)_{50}$ is expressed compared to dox-off system ($p = 0.04$). Data analysed with two-way ANOVA using Tukey's *post-hoc* (n = 3). The bars represent means

and error bars are standard deviations (see Figure S2 for details on batch of cells used). Scale bar 10 μm.

4.5 Conclusions

C9orf72 mutant iPSC-derived MNs demonstrate deficits in calcium homeostasis, in particular reduced uptake of extracellular calcium following glutamate stimulation and low mitochondrial buffering capacity, caused by downregulation of MCU (Dafinca et al., 2020). Poly(GA) and Poly(PR) expression in genome edited lines lowered uptake of extracellular calcium after glutamate stimulation, but only poly(PR) caused deficits in mitochondrial buffering capacity, without affecting MCU expression (Figure 4.1 – 4.2). Moreover, poly(GA) and poly(PR) could cause the reduced total ER calcium, but only poly(PR) may specifically downregulate the IP3R function observed in C9orf72 lines (Figure 4.7 – 4.8). However, the UPR was not affected in MNs expressing poly(GA) or poly(PR), despite being downregulated in C9orf72 mutant lines (Figure 4.9 – 4.10). These experiments indicate that poly(GA) and poly(PR) may play a role in lowering calcium uptake of C9orf72 mutant iPSC-derived MNs, and further experiments could show if DPRs interfere with the function of glutamate receptors, or the vesicular trafficking involved in receptor regulation, or the components of SOCE. Moreover, analysis of MCU regulators could clarify the effects of poly(PR) on mitochondrial calcium buffering capacity and IP3R pull down experiments could show a direct connection with poly(PR).

This chapter presented divergent phenotypes in C9orf72 mutant iPSC-derived MNs and poly(GA)/poly(PR) expressing MNs, suggesting that the DPRs have distinct pathological effects. C9orf72 patient lines are characterised by reduced

mitochondrial respiration, corresponding with COXIV reduced expression. In contrast, the single SeaHorse analysis run on DPR expressing iPSC-derived MNs showed that poly(GA) expression boosted mitochondrial respiration in CRISPR/Cas9 corrected MNs, probably caused by COXIV overexpression and increased the total mitochondrial mass. However, poly(PR) upregulated COXIV expression without affecting mitochondrial respiration and the mitochondrial mass, indicating that the arginine-rich DPR could potentially interfere with the function of COXIV (Figure 4.3 – 4.5). Deficits of COXIV function could increase the sensitivity to oxidative stress, as shown in sodium arsenite-treated isogenic lines expressing poly(PR). The DPR boosted the production of stress granules, similar to what is seen in C9ORF72 MNs after sodium arsenite treatment (Figure 4.13). Moreover C9orf72 mutant iPSC-derived MNs showed nuclear TDP-43 retention (Figure 4.11), while the expression of poly(GA) or poly(PR) did not cause a similar phenotype in CRISPR/Cas9 corrected MNs, suggesting that the two DPRs do not affect TDP-43 localisation, but further replicates and analysis on DPR-positive cells would be more informative (Figure 4.12).

			CRISPR/Cas9	
Phenotype		**C9ORF72**	**GA**	**PR**
Mitochondria	$[Ca^{2+}]$ after glutamate	↓ Dafinca et al.2020	↓ $p = 0.027$	↓ $p = 0.044$
	Recovery rate after glutamate	↓ Dafinca et al. 2020		↑ $p = 0.042$
	$[Ca^{2+}]$ after glutamate + CCCP	↓ Dafinca et al. 2020		↓ $p = 0.004$
	MCU	↓ $p < 0.05$		
	COXIV	↓	↑ $p = 0.014$	↑ $p = 0.029$
	Mitochondrial max respiration	↓ $p < 0.001$	↑ $p = 0.04$	
ER	$[Ca^{2+}]$ after carbachol	↓ $p < 0.05$		↓ $p = 0.0431$
	Total ER $[Ca^{2+}]$	↓ $p < 0.01$	↓ $p = 0.05$	↓ $p < 0.0001$
Stress granule number		↑		↑ $p = 0.04$
Stress granule size				↑ $p = 0.03$
ncTDP-43		↑ $p < 0.01$		

Figure 4.14: Conclusions.

Chapter 5: Activation of Chaperone-Mediated Autophagy and clearance of RNA foci as possible mechanisms to reduce DPR toxicity

5.1. Introduction

5.1.1. Chaperone-Mediated Autophagy

In order to maintain the homeostasis of cellular proteins and sub-cellular organelles, cells use different types of autophagy. Macroautophagy encloses a cargo in a double membrane organelle (autophagosome) that will fuse to lysosomes. Macroautophagy targets proteins and damaged organelles, such as mitochondria, ER and peroxisomes (Fivenson et al., 2017; Iwata et al., 2006; Wilkinson, 2020). The second type of autophagy is called microautophagy, during which lysosomes directly engulf cytosolic targets (Oku & Sakai, 2018). Lysosomes can also actively translocate proteins in their lumen, a highly selective form of autophagy called Chaperone-Mediated Autophagy (CMA). The substrate containing a specific motif (KFERQ) is recognised by chaperones, and delivered to the lysosomal receptor, lysosome-associated membrane protein 2A (LAMP2A), to be translocated in lysosomes (Alfaro et al., 2019; Kaushik & Cuervo, 2018). The chaperone that recognises the motif is HSC70, a member of the heat-shock protein 70 family, and it interacts with LAMP2A through a multiprotein complex and

post translational modifications (Chiang et al., 1989; Fred Dice, 1990; Kaushik & Cuervo, 2016; Lv et al., 2011; Vasco Ferreira et al., 2015). The translocation is dependent on LAMP2A oligomerisation, and it can be used to determine CMA activity (Cuervo & Dice, 1996, 2000a). LAMP2A mRNA overexpression and immunofluorescence analysis of HSC70 and LAMP2A colocalization, or LAMP2A positive punctae, indicate increased activity of CMA (Arias, 2017).

Different cell types, including neurons, show basal activity of CMA (Koga et al., 2011). However, it has been shown that CMA activity peaks after macroautophagy gradually decreases during long starvation periods (Cuervo et al., 1995; Fuertes et al., 2003; Wing et al., 1991). In addition, CMA is activated during oxidative stress and in response to deficits in the ER stress response (Kiffin et al., 2004; Li et al., 2017). In specific cases, CMA upregulation has been described as protective, as in neurons during hypoxia (Dohi et al., 2012). CMA takes part in a negative feedback mechanism to lower macroautophagy, when LAMP2A is overexpressed and activates mTOR, which downregulates macroautophagy (Han et al., 2017).

There are studies suggesting that the induction of CMA is a potential therapy for neurodegenerative disorders, as proteins associated with Parkinson's Disease are substrates for CMA, and CMA activity shows a reduction with ageing (Cuervo & Dice, 2000b; Issa et al., 2018; Vogiatzi et al., 2008; B. Wang et al., 2016; Q. Yang et al., 2009; C. Zhang & Cuervo, 2008). Even though there is no evidence of CMA dysfunction, or CMA targets, linked to ALS, one study described the development of an antibody-based system that recognises cytosolic TDP-43 and induces its clearance via CMA (Tamaki et al., 2018). Moreover, in another study DPR degradation was induced by overexpressing HSPB8, a chaperone protein that removes TDP-43 aggregates in a complex with HSP70 to be degraded by CMA

(Crippa, Cicardi, et al., 2016; Crippa, D'Agostino, et al., 2016; Cristofani et al., 2018).

5.1.2. Targeting RNA foci as ALS therapy

Inducing the degradation of RNA transcripts generated from the HRE or transcriptionally silencing the expansion in the *C9ORF72* gene are all valid approaches to preventing the expression of DPRs and avoiding their toxicity. The techniques used to date include RNA-interference (RNAi), synthetic antisense oligonucleotides (ASOs) and synthetic compounds to prevent the transcription of the HRE or induce the degradation of RNA foci. The first approach studied was ASO treatment to specifically target the HRE, reducing RNA foci formation and improving cell viability (Donnelly et al., 2013; Lagier-Tourenne et al., 2013; Sareen et al., 2013). Engineered duplex RNAs and complementary single-stranded RNAs also successfully reduced sense and antisense RNA foci in C9orf72 mutant cells (Hu et al., 2015, 2016). Moreover, the downregulation of *C9ORF72* mRNA with microRNAs lowered RNA foci formation (Martier, Liefhebber, García-Osta, et al., 2019; Martier, Liefhebber, Miniarikova, et al., 2019).

A different approach is treating the cells with small molecules that bind the RNA hairpins containing the repeats, preventing their aggregation, even though there are no *in vitro* or *in vivo* experiments demonstrating a direct effect of RNA hairpins on pathology (Su et al., 2014; Z. Wang et al., 2019; Zamiri et al., 2014). The identification of factors associated with the transcription of repeat RNAs, SUPT4H and SUPT5H, promoted the possibility of modifying their expression as a therapeutic approach (Goodman, Prudencio, Kramer, et al., 2019; Kramer et al., 2016). However, further investigations highlighted the relevance of SUPT4H for

the global transcription, and its downregulation did not reduce HRE transcription (Naguib et al., 2019).

5.1.3. Targeting DPRs for ALS therapy

As mentioned above, reduction of *C9orf72* transcripts leads to downregulation of DPR expression. Another approach is inhibiting RAN translation via expression of factors involved in its activation during the integrated stress response (ISR). The ISR triggers phosphorylation of the regulatory initiation factor eIF2α, attenuating general translation and increasing the rate of RAN translation (Cheng et al., 2018; Green et al., 2017). More recent experiments have described the ribosomal subunit RPS25 and helicase DDX3X as factors promoting efficient RAN translation (Cheng et al., 2019; Yamada et al., 2019). These experiments suggest attenuation of the ISR and overexpression of DDX3X as possible therapeutic approaches to reduce DPR expression. However, downregulation of the ISR could be catastrophic for the whole organism, as it is a ubiquitous and necessary mechanism for cell survival. For this reason, different studies are evaluating the use of anti-DPR antibodies to clear cells of DPRs. Poly(GA), poly(GP) and poly(PA) in co-culture systems possess cell-to-cell transmission properties, triggering key features of ALS/FTLD in glial cells, which could be rescued with poly(GA) vaccination (Chang et al., 2016; Khosravi et al., 2020; Nguyen et al., 2020; Zhou et al., 2017, 2020). Other studies are targeting genes, whose deletion suppresses PR toxicity, or downstream events, such as modulation of stress granules biogenesis (Brown et al., 2020; Jovičić et al., 2015).

5.1.4. Aims of the chapter

In the work described in this chapter I have analysed the effects of $(GA)_{50}$ and $(PR)_{50}$ expression on autophagy and lysosomal activation. Moreover, I investigated the possibility of inducing degradation of DPRs via chaperone mediated autophagy, or the clearance of RNA foci using a specific peptide. The data presented here are not complete as the experiments could not be repeated due to Covid-19 pandemic.

5.2. Induction of Chaperone Mediated Autophagy clears iPSC-MNs from $(GA)_{50}$ and $(PR)_{50}$

5.2.1. Poly(GA) and poly(PR) cause autophagic and proteasomal dysfunction

It has been already demonstrated that poly(PR) and poly(GA) affect protein homeostasis by interacting with components of the ubiquitin-proteasome system (UPS) and cargo adaptor Unc119 inhibiting proteasomal functions, whereas proteasome induction protects cells from poly(PR) toxicity (Gupta et al., 2017; May et al., 2014). More generally, *post-mortem* studies using immunohistochemistry staining of nervous system tissue from C9orf72 patients describe p62/DPR positive aggregates, indicating that DPRs might be degraded not only by the proteasome, but also by autophagic pathways (Ash et al., 2013; Mann et al., 2013; Mori, Weng, et al., 2013; Schludi et al., 2015). In this study, immunoblot analysis of C9orf72 mutant iPSC-derived MNs did not show p62 overexpression, and the expression of the lysosomal marker LAMP2A was reduced in the two lines analysed, indicating that autophagy is not active (Figure 5.1 A). In contrast, $(GA)_{50}$

and $(PR)_{50}$ expression in CRISPR/Cas9 iPSC-derived MNs induced LAMP2A overexpression, which persisted after doxycycline withdrawal (Figure 5.1 B – C). Although increased expression of LAMP2A indicates active autophagy, p62 protein level was not affected by $(GA)_{50}$ (Figure 5.1 B) and $(PR)_{50}$ downregulated it (Figure 5.1 C). Because p62 is also a proteasomal marker, its downregulation suggests that poly(PR) reduces proteasomal activity, while both DPRs potentially induce lysosomal activation.

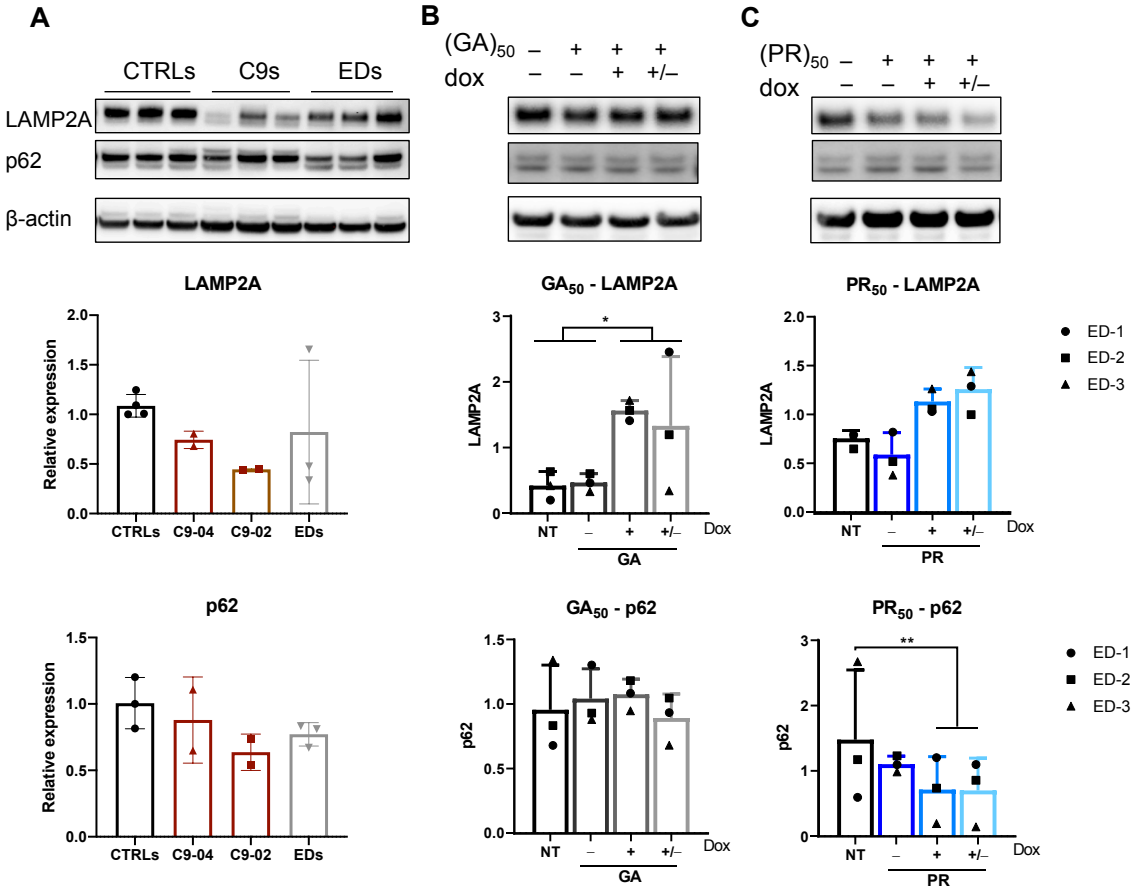


Figure 5.1: (GA)50 and (PR)50 expression causes autophagic and proteasomal dysfunction.

Immunoblots of LAMP2A and p62. **A)** Baseline expression of LAMP2A in controls (4), C9-ALS/FTD (6) and CRISPR/Cas9 corrected (3) iPSC-derived MNs. One dot of the scatter plot indicates the mean of three independent differentiations per line/clone. Wild-type and CRISPR/Cas9 corrected lines formed two groups, while C9 clones were grouped per line (see table 2.2). **B)** (GA)50–*c*-myc expression in genome edited MNs causes overexpression of LAMP2A (*p*-values: NT vs + = 0.015; NT vs +/– = 0.028; – vs + = 0.02; – vs +/– = 0.036). **C)** (PR)50–HA expression in genome edited MNs causes downregulation of p62 (*p*-values: NT vs + = 0.006; NT vs +/– = 0.005). Data analysed using two-way ANOVA using Tukey's *post-hoc* test (n = 3). The bars represent averages and error bars are standard deviations. See Appendix for details (Figure S2, S7).

5.2.2. Poly(GA) induces lysosome activation

I then analysed lysosomal activity using LysoTracker®, a deep red fluorophore which is highly selective for acidic organelles. I counted the total number of red punctae in the whole ChAT positive area, after cell fixation. I compared the results to the cells treated with bafilomycin A1 and the mTOR inhibitor rapamycin. Rapamycin activates autophagy, while bafilomycin A1 inhibits the V-ATPase on the lysosomes, resulting in lysosomal deactivation. Two C9orf72 patient lines (C9-02 and C9-04) showed an increased number of lysosomes compared to wild-type and CRISPR/Cas9 corrected iPSC-derived MNs, and the treatments demonstrated the staining specificity in all the lines (Figure 5.2). $(GA)_{50}$ expression in genome edited iPSC-derived MNs induced lysosomal acidification, while $(PR)_{50}$ expression did not increase lysosomal activity (Figure 5.3). The experiment has not been replicated yet, but, together with immunoblot results, it indicates that poly(GA) has a specific action on lysosomes, inducing their activation, and it is a potential cause of the higher lysosomal number in C9orf72 mutant lines.

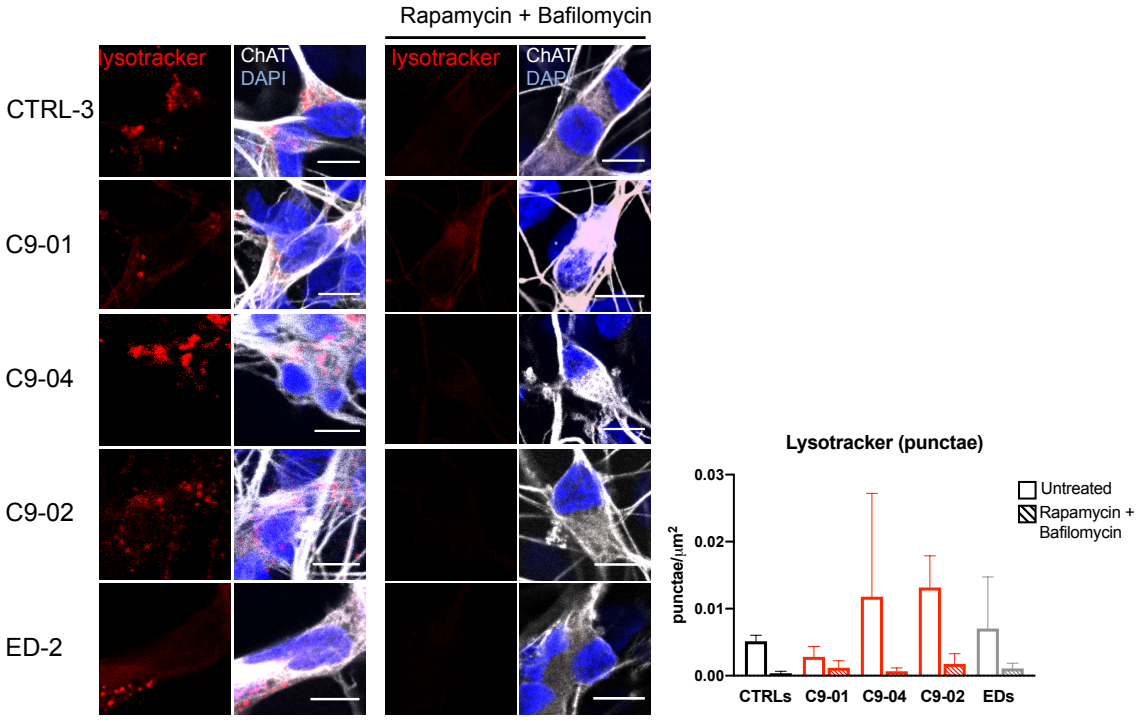


Figure 5.2: C9orf72 mutant iPSC-MNs have more active lysosomes.

Quantification of active lysosomes in immunofluorescence of fixed iPSC-derived MNs stained with lysotracker before and after inducing autophagy with rapamycin and blocking it with bafilomycin. All lines were tested once, and the mean of five technical replicates per sample was used to identify the number of lysosomes (lysotracker punctae) per μm^2 (see Figure S2 for details on batch of cells used). Wild-type and CRISPR/Cas9 corrected lines formed two groups, while C9 clones were grouped per line (see table 2.2). Scale bar 10 µm.

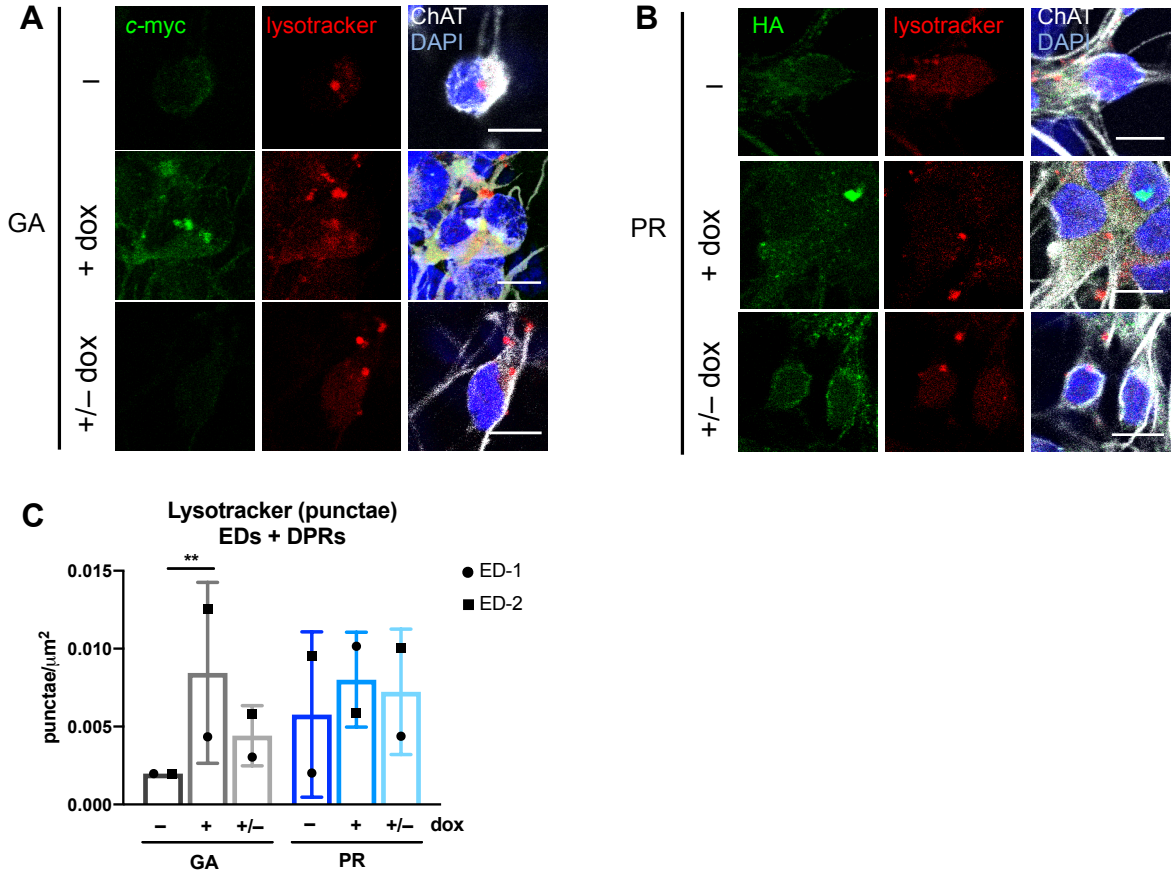


Figure 5.3: (GA)$_{50}$ induces lysosome activation.

Quantification of active lysosomes in immunofluorescence of fixed CRISPR/Cas9 corrected iPSC-derived MNs expressing DPRs. **A)** Immunofluorescence pictures of iPSC-MNs transduced with (GA)$_{50}$–*c*-myc (scale bar 10 µm). **B)** Immunofluorescence pictures of iPSC-MNs transduced with (PR)$_{50}$–HA (scale bar 10 µm). **C)** Quantification of lysotracker punctae shows that (GA)$_{50}$–*c*-myc induces lysosome activation (p = 0.008). All lines were tested once, and the average of five technical replicates per sample was used to identify the number of lysosomes (lysotracker punctae) per µm^2. Data analysed using two-way ANOVA using Tukey's *post-hoc* test. The bars represent means of two lines and error bars are standard deviations. One dot of the scatter plot indicates the mean of five technical replicates per line (see Figure S2 for details on batch of cells used).

5.2.3. Activation of CMA clears MNs of $(GA)_{50}$ and $(PR)_{50}$

The previous experiments showed that $(GA)_{50}$ induced lysosome activation, suggesting it might be degraded directly by lysosomes. To test this hypothesis, I measured the fluorescent signal of the tags linked to the DPRs after inducing CMA. I compared intensity levels of *c*-myc (GA) and HA (PR) in CRISPR/Cas9 corrected iPSC-derived MNs in four different conditions. The intensity of each dox-on system was compared to the background signals of transduced MNs untreated with doxycycline. The combination of rapamycin and bafilomycin caused poly(GA) and poly(PR) accumulation (Figure 5.4), indicating that $(GA)_{50}$ and $(PR)_{50}$ are soluble and actively degraded via autophagic pathways. In particular, rapamycin and bafilomycin treatments increased nuclear accumulation of $(PR)_{50}$, and in a few ChAT-positive cells poly(PR) occupied the whole nuclear area. The activation of CMA with 6-aminonicotinamide cleared the cells of aggregates, indicating that poly(GA) and poly(PR) can be degraded by lysosomes (Figure 5.4).

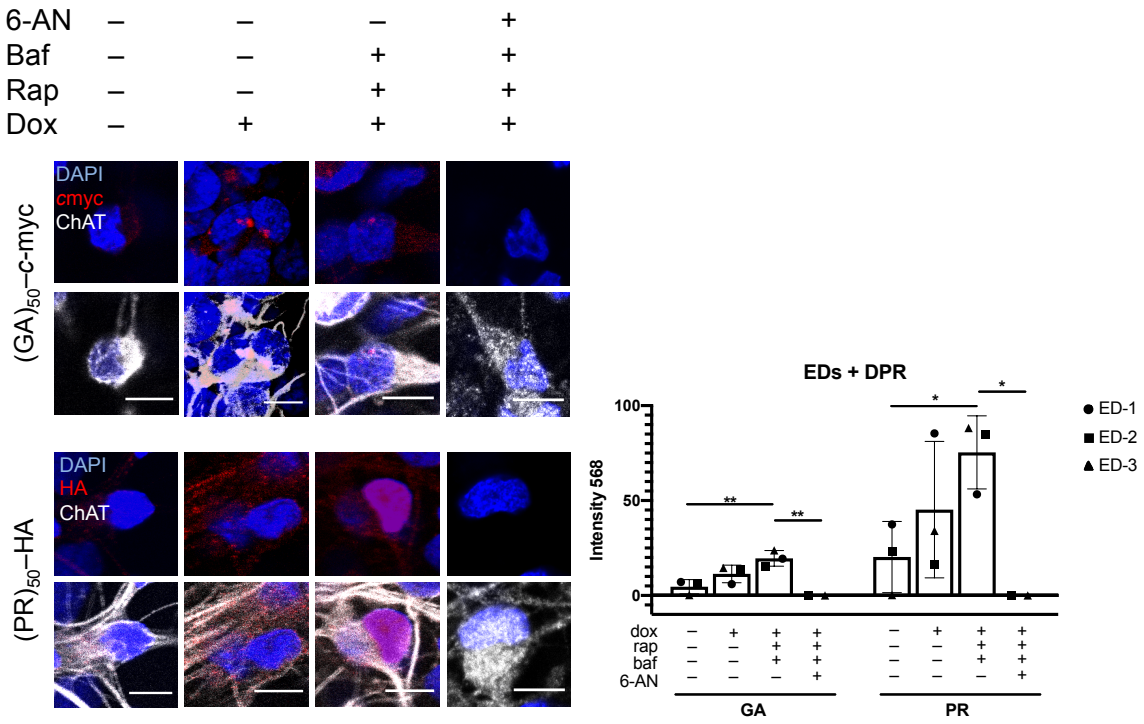


Figure 5.4: (GA)50 and (PR)50 are degraded by CMA.

Immunofluorescence quantification of (GA)50–*c*-myc and (PR)50–HA levels in CRISPR/Cas9 corrected iPSC-MNs after autophagic treatments. Intensity signal of (GA)50–*c*-myc increases with rap and baf (p = 0.005) and it decreases when 6-AN is added (p = 0.001). Intensity signal of (PR)50–HA increases with rap and baf in (p = 0.012) and it lowers when 6-AN is added (p = 0.012). Data analysed using one-way ANOVA using Tukey's *post-hoc* test (n = 1). The bars represent means of three lines and error bars are standard deviations. . One dot of the scatter plot indicates the mean of five technical replicates per line (see Figure S2 for details on batch of cells used). Scale bar 10 μm. Rap = rapamycin, Baf = bafilomycin, 6-AN = 6-aminonicotinamide.

5.2.4. Activation of CMA in C9orf72 mutant iPSC-derived MNs does not rescue the phenotypes

I analysed the effects of blocking autophagy with bafilomycin and inducing CMA with 6-aminonicotinamide on ER, mitochondria and lysosomes in C9orf72 mutant iPSC-derived MNs compared to control lines, to test if CMA activation could rescue abnormal phenotypes. I measured protein levels of UPR markers (BiP, ATF4, CHOP), mitochondrial protein MCU and lysosomal marker LAMP2A (Figure 5.5). The first evidence of 6-aminonicotinamide activity is the increased expression of LAMP2A in healthy lines. However it did not show the same effects on C9orf72 mutant and CRISPR/Cas9 corrected lines. Moreover, MCU expression worsens in all lines with all the treatment combinations, indicating that inducing or blocking autophagy is toxic and could lead to mitochondrial deficits. Only PERK expression slightly increased in C9orf72 mutant iPSC-MNs treated with the three compounds, but it could be due to non-specific stress caused by the treatments. Comparing the effects of the treatments between groups, it is evident that the UPR in C9orf72 mutant lines is compromised. In particular, autophagy induction with rapamycin and 6-aminonicotinamide upregulated ATF4 in healthy MNs, but it was downregulated in C9orf72 patient iPSC-derived MNs.

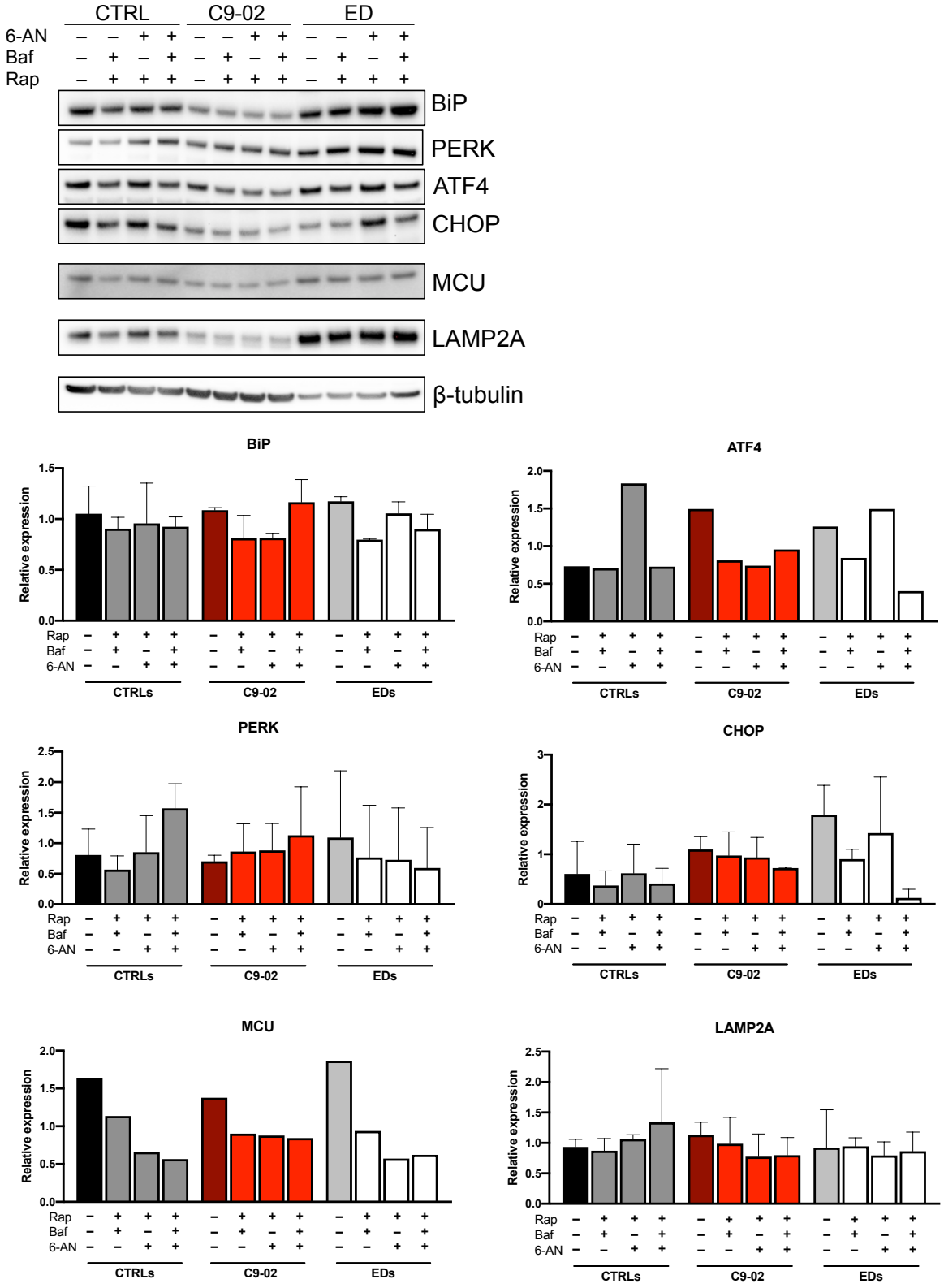


Figure 5.5: Activation of CMA in C9orf72 mutant iPSC-derived MNs does not rescue the phenotypes.

Immunoblot quantification of UPR markers (BiP, PERK, CHOP, ATF4), MCU and LAMP2A in WT, mutant and CRISPR/Cas9 corrected iPSC-MNs after autophagic treatments. Experiment run once on CTRL-1, CTRL-2, C9-02, ED-2, ED-3 . Data analysed with two-way ANOVA using Tukey's *post-hoc* test. The bars represent means of three technical replicates and error bars are standard deviations (replicates missing for MCU and ATF4). Rap = rapamycin, Baf = bafilomycin, 6-AN = 6-aminonicotinamide.

5.3. Clearance of RNA foci as a potential therapy in C9orf72 mutant iPSC-derived MNs

An alternative approach to reducing DPR expression is targeting RNA transcripts containing the *C9ORF72* HRE. Our collaborators (Dr Edwin Chan, Chinese University of Hong Kong) designed a small peptide (TAT-BIND) with the ability to reduce RNA foci and DPRs in cells overexpressing $(GGGGCC)_{66}$ and in *Drosophila* models carrying $(GGGGCC)_{36}$. The peptide was shown to improve cell viability and to suppress C9ORF72-related phenotypes in flies (Q. Zhang et al., 2019). The peptide carries a positively-charged sequence, derived from the transactivator of the transcription protein of HIV-1 (TAT), that allows membrane penetration (Koren et al., 2011), and has a high-affinity sequence for the G-quadruplex structures derived from the *C9ORF72* HRE. The second sequence is based on the RNA recognition motifs (RRMs) of nucleolin, one of the nucleolar proteins that is sequestered by RNA repeats causing nucleolar stress (Haeusler et al., 2014; Tsoi et al., 2012). Chan's team previously described a similar approach that successfully reduced RNA repeats toxicity in polyglutamine neurodegenerative disease, and they called the inhibitor 'beta-structured inhibitor for neurodegenerative diseases' (BIND) (Q. Zhang et al., 2018). I tested the effects

of TAT-BIND peptide on the C9ORF72-related phenotypes I observed in our iPSC-derived MNs.

5.3.1. TAT-BIND peptide clears sense RNA foci in only one C9orf72 mutant iPSC line

Before analysing the downstream phenotypes induced by TAT-BIND peptide in C9orf72 mutant iPSC-MNs, I titrated the optimal working concentration in C9orf72 patient iPSCs. I treated the cells for three days with increasing concentrations of TAT-BIND peptide, and I compared cell survival curves (MTS assay) to the data obtained with a scrambled control peptide (S-TAT-BIND). The scrambled peptide did not affect cell survival in any of the three C9orf72 mutant lines (Figure 5.6). In contrast, TAT-BIND peptide produced different survival curves in each of the lines, increasing cell viability in line C9-01 in the concentration range 0.5 – 5 μM, while decreasing the cell viability in the other two C9orf72 mutant lines, showing 50% reduction in the same range. This finding is in contrast to the previously reported working concentration (10 μM), probably due to the greater vulnerability of iPSC-MNs compared to the original publication, which used the human neuroblastoma cell line SK-N-MC transfected with a plasmid carrying 66 repeats.

For subsequent experiments I chose to treat iPSC and iPSC-MNs with 3 μM TAT-BIND or scrambled peptide, as this concentration did not affect cell viability in line C9-01, showed limited effects in line C9-02, while it caused 50% reduction cell survival in line C9-04. I assessed the ability of TAT-BIND peptide to decrease RNA foci formation in our C9orf72 mutant iPSCs by RNA-FISH (Figure 5.7 A, B), and I checked the probe specificity in RNase-treated cells (Figure 5.7 B). I treated

the cells for three days with 3 μM TAT-BIND or S-TAT-BIND peptide, and I manually counted the nuclear RNA foci. I analysed the percentage of nuclei with detectable RNA foci (Figure 5.7 C) and the number of RNA foci per nucleus (Figure 5.7 D). TAT-BIND peptide reduced the number of C9-01 cells with sense and antisense RNA foci by 50%, compared to non-treated and S-TAT-BIND treated cells (Figure 5.7 C), and it lowered the number of foci per cells (Figure 5.7 D). The opposite scenario was found in C9-04 iPSCs, in which TAT-BIND peptide induced RNA foci formation increasing the percentage of cells with detectable foci. The peptide did not affect the sense RNA foci in C9-02 iPSCs, but it increased the cells with antisense RNA foci and number of foci per nucleus.

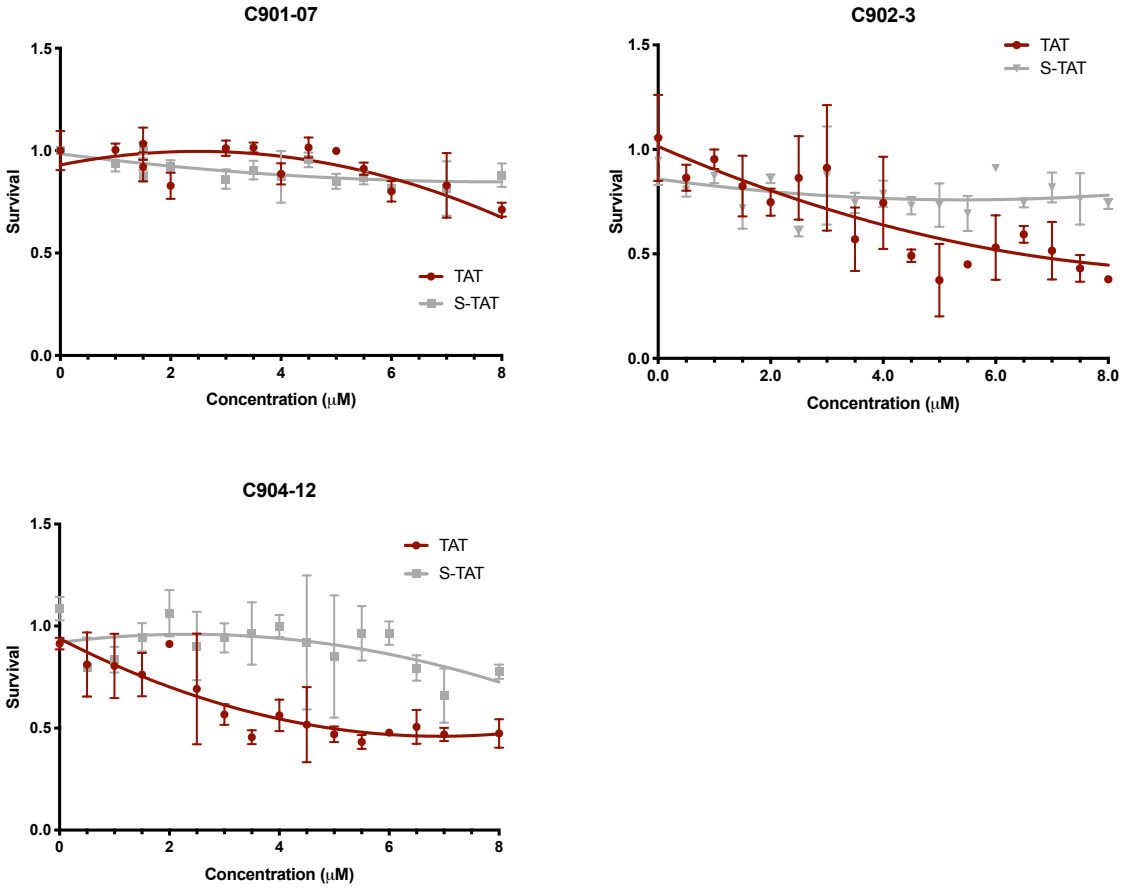


Figure 5.6: TAT-peptide shows different cell survival when used on C9orf72 mutant iPSCs.

MTS assays of C9orf72 patient iPSCs treated with TAT-BIND (TAT, red) or scrambled peptide (S-TAT, grey). Bars show standard deviations produced with technical replicates (n=3).

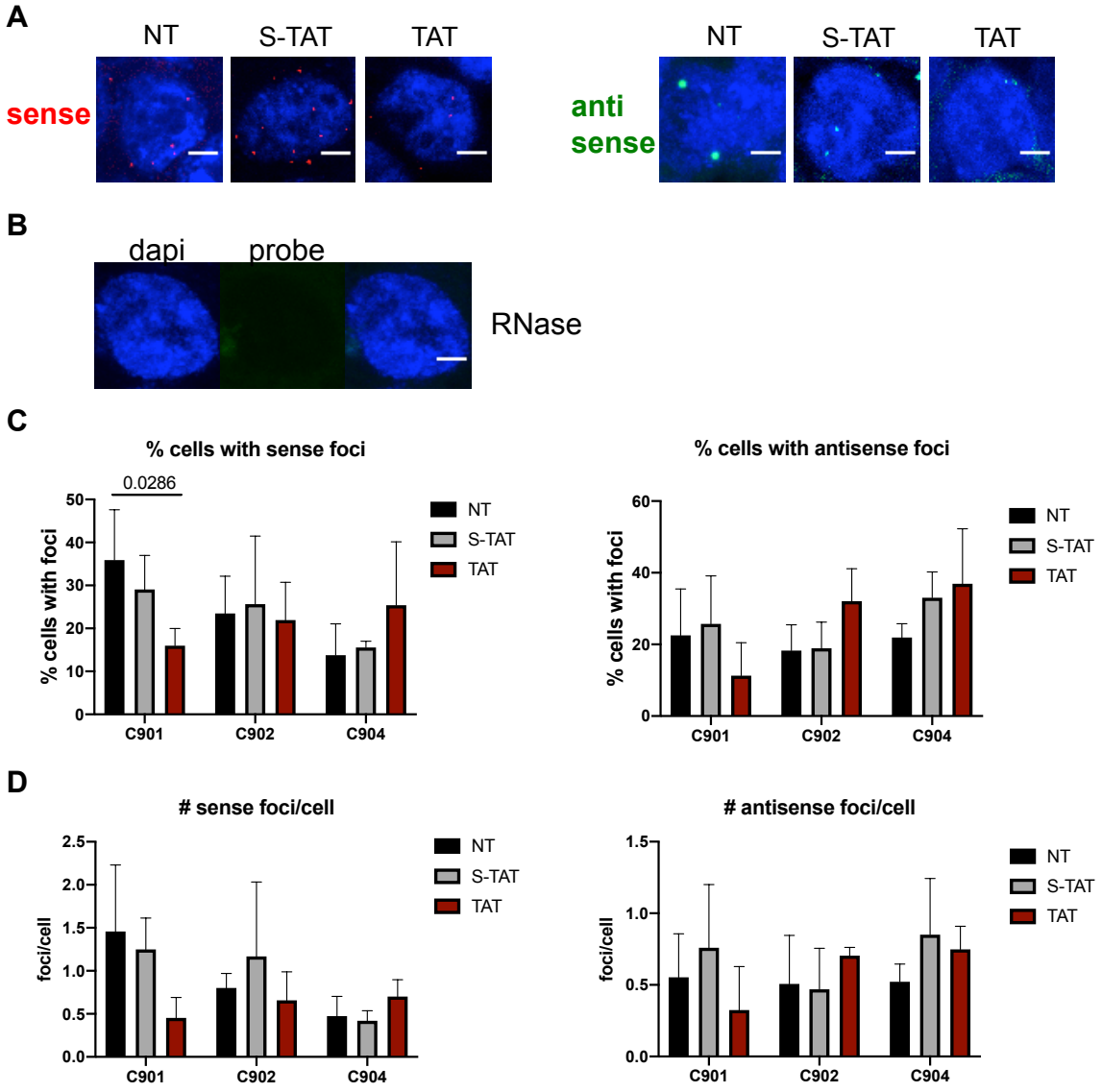


Figure 5.7: Sense foci are cleared from C901-iPSCs by TAT-peptide.

Immunofluorescence quantification of RNA foci in C9orf72 mutant iPSCs following TAT-BIND and S-TAT-BIND treatments. **A)** RNA-FISH showing sense (red) and antisense (green) RNA foci in non treated, scrambled treated, and TAT treated C9-01 iPSCs (scale bar 10 μm). **B)** RNA-FISH in RNase-treated iPSCs showing specificity of the probes (scale bar 10 μm). **C)** Percentage of iPSCs showing sense (left) and antisense RNA foci (right) in three patient lines. TAT-BIND peptide reduces the percentage of cells with sense RNA foci in C9-01 iPSCs. **D)** Quantification of number of RNA foci per nucleus with or without TAT treatment. Data analysed with Friedman's statistic using Dunn's *post-hoc* test (n=3). The bars represent means and error bars are standard deviations.

5.3.2. TAT- peptide activates UPR and autophagy in C9orf72 mutant iPSC-derived MNs

I investigated the downstream effects of the TAT-BIND peptide treatment in C9orf72 mutant iPSC-derived MNs by treating the MNs with 3 μM TAT-BIND for 6 days and I analysed the protein levels of the markers previously described (Figure 5.8 A). TAT-BIND peptide upregulated the UPR proteins PERK and ATF4, shown to be downregulated in both lines compared to control lines, whereas the expression of the downstream target CHOP was induced only in line C9-02 (Figure 5.8 B). Moreover, TAT-BIND peptide increased the protein level of LAMP2A in both lines, which was measured to be downregulated in C9ORF72 patient lines compared to wild-type and isogenic controls (Figure 5.8 C). These immunoblotting experiments suggest that TAT-BIND peptide activates the UPR and lysosomes probably due to its toxicity, as it did not clear the two lines of RNA foci. Unfortunately, I could not analyse TAT-BIND effects in C9-01 MNs due to the low differentiation efficiency.

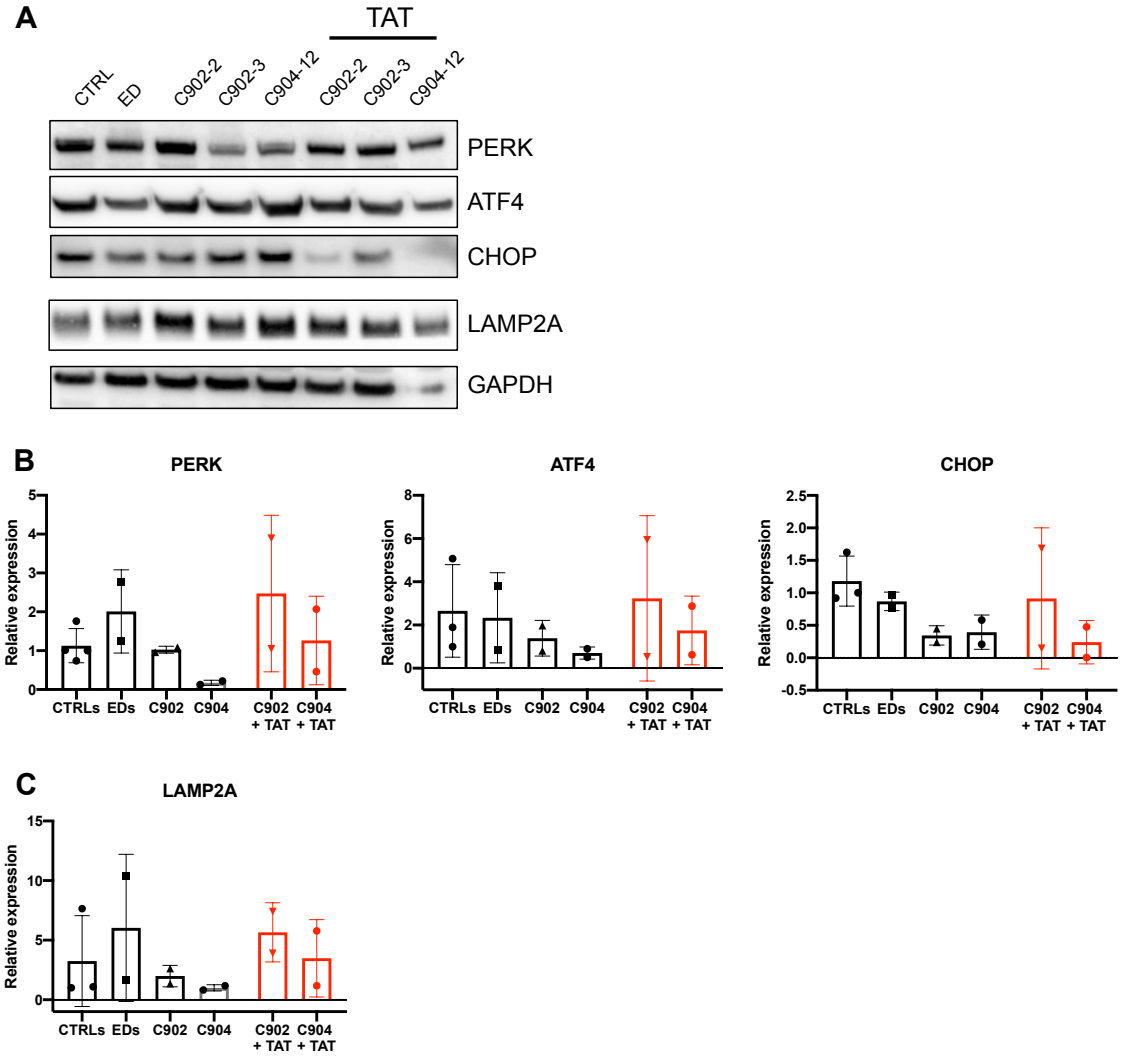


Figure 5.8: TAT-peptide effects on ER and lysosomal markers in C9orf72 mutant iPSC-derived MNs.

Immunoblot quantification of UPR markers and LAMP2A. **A)** Immunoblot staining of iPSC-MNs non treated or treated with 3 μM TAT-BIND peptide for 6 days. **B)** TAT-BIND treatment activates UPR. **C)** LAMP2A expression is upregulated by TAT-BIND. The bars represent means and error bars are standard deviations (n=2).

5.3.3. TAT-BIND peptide rescues COXIV function in C9orf72 mutant iPSC-MNs

Another organelle shown to be compromised in C9orf72 patient MNs was the mitochondrion. I analysed the effects of TAT-BIND peptide on mitochondrial markers and mitochondrial functions, in particular on mitochondrial respiration. The expression of MCU and COXIV, which were downregulated compared to wild-type and CRISPR/Cas9 corrected MNs, increased in C9-02 line, without affecting the total number of organelles. Also, COXIV in C9-04 MNs was upregulated by TAT-BIND peptide, while MCU expression was not affected (Figure 5.9).

The previous chapter showed that the mitochondrial respiration was lower in C9orf72 lines compared to healthy controls, probably due to COXIV downregulation. I repeated the SeaHorse experiment to analyse if the upregulation of COXIV induced by TAT-BIND peptide determined increased mitochondrial respiration as well. The mitochondrial respiration profiles of untreated C9orf72 mutant iPSC-derived MNs were different, as previously shown (Figure 5.10 A). In particular basal respiration and ATP production of C9-02 iPSC-MNs were higher compared to the other two lines, and TAT-BIND peptide lowered the parameters of C9-02 and C9-04 lines (Figure 5.10 B). On the other hand, the treatment raised the maximal respiration in all three C9orf72 mutant lines, indicating that COXIV function was upregulated. These results suggest that TAT-BIND peptide appears to rescue some of the mitochondrial phenotypes through a mechanism that requires further investigation, as its effect on RNA foci formation/clearance is not clear.

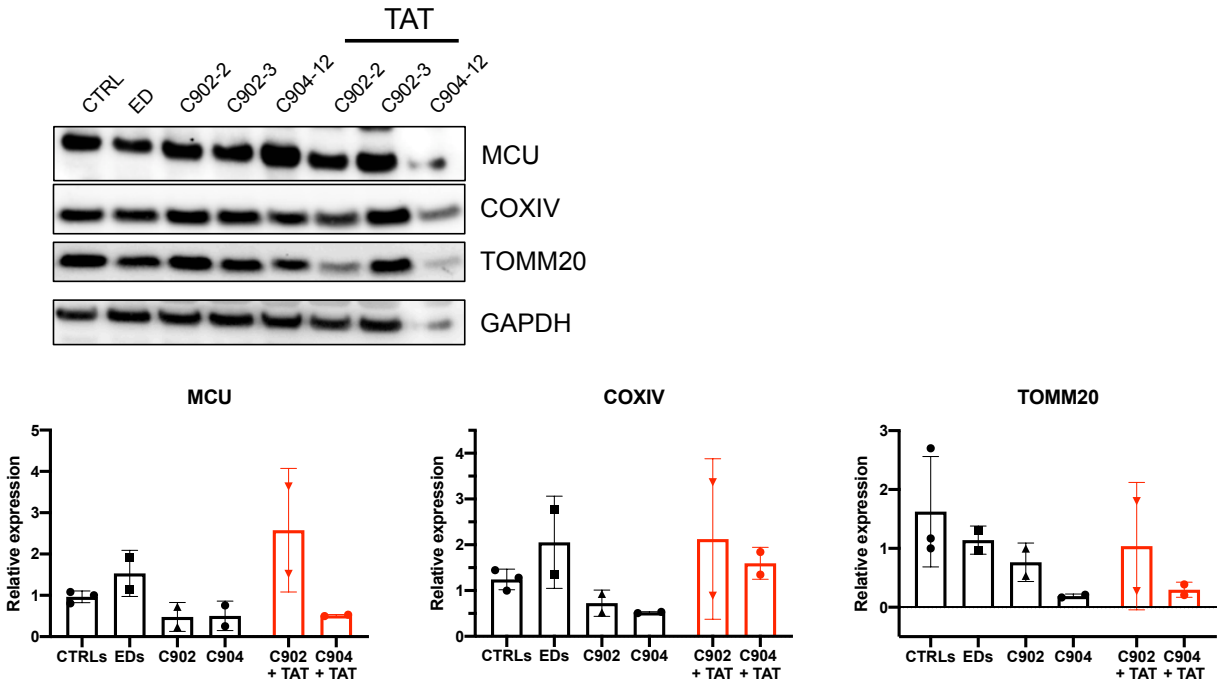


Figure 5.9: TAT-peptide upregulates mitochondrial markers in C9orf72 mutant MNs.

Immunoblot quantification of mitochondrial proteins MCU, COXIV and TOMM20 in iPSC-MNs non treated or treated with 3 μM TAT-BIND peptide for 6 days. The bars represent means and error bars are standard deviations (n=2).

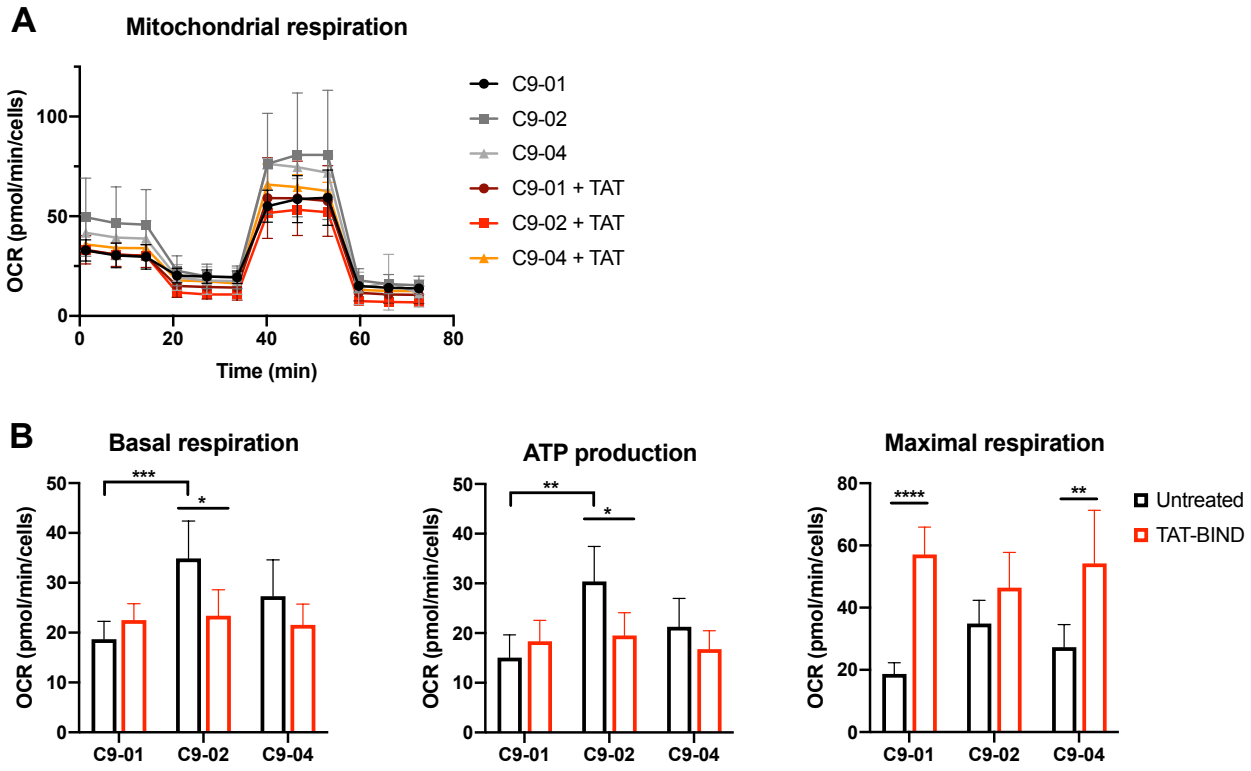


Figure 5.10: TAT-BIND treatment increases maximal mitochondrial respiration.

Seahorse experiment to study mitochondrial respiration in C9orf72 mutant iPSC-derived MNs. **A)** Mitochondrial respiration profiles of C9ORF72 patient lines untreated or treated with 3 μM TAT-BIND peptide for 6 days. **B)** C9-02 line shows high basal respiration (p = 0.0009) and ATP production (p = 0.0015) compared to C9-01 line, but they are reduced when C9-02 is treated with TAT-BIND peptide (basal respiration p = 0.019; ATP production p = 0.017). The maximal respiration increases in all lines when treated with TAT-BIND peptide (C9-01 p < 0.000.1; C9-04 p = 0.0016). Data analysed with two-way ANOVA using Tukey's *post-hoc* test (n = 2 with three technical replicates per line). The bars represent means and error bars are standard deviations.

5.4. Conclusions

In this chapter I analysed two different therapeutic approaches against DPR toxicity, starting with induction of autophagy to clear the cells of DPR. The immunoblot data did not show autophagy and proteasome activation in C9orf72 mutant iPSC-derived MNs, as p62 was stable between lines. However, functional experiments demonstrated lysosomal activation, showing high levels of LysoTracker®-positive lysosomes, but was not supported by immunoblot results exhibiting downregulation of the lysosomal marker LAMP2A. The results were not consistent probably because the LysoTracker® analysis was only run once, and further immunofluorescence experiments is required to identify the actual LAMP2A protein level in ChAT-positive iPSC-MNs. The lysosomes were activated in CRISPR/Cas9 corrected iPSC-MNs by $(GA)_{50}$, and limited activation was caused by $(PR)_{50}$, demonstrating that DPRs might be degraded via autophagy. Co-localisation assay between DPRs and LAMP2A/LysoTracker® would strongly support this theory, even though, blocking the autophagic pathway in iPSC-MNs expressing $(GA)_{50}$ or $(PR)_{50}$ caused DPR aggregation, and the activation of chaperone-mediated autophagy (CMA) induced DPR clearance, suggesting CMA activation could be explored as a potential therapy against DPR toxicity. However, the treatment did not rescue C9orf72 mutant iPSC-derived MNs as it did not cause upregulation of ER, mitochondrial and lysosomal markers. Only the protein level of the ER kinase PERK increased, but it could be a reflection of ER stress rather than a specific rescue. Further experiments in iPSC-MNs expressing $(GA)_{50}$ or $(PR)_{50}$ and inducing activation of CMA could confirm whether autophagy is a possible therapy against DPR toxicity in C9orf72 mutant cells.

The second therapeutic approach analysed was reducing RNA foci to decrease DPR content using a peptide previously described to target RNA repeats and improve cell survival. The treatment with the peptide in our C9orf72 mutant iPSCs caused mixed results, probably due to the variance in susceptibility to toxicity between different cell lines shown in the survival assays. When the peptide did not affect cell viability, the cells showed fewer sense RNA foci, indicating that TAT-BIND peptide clears cells from G-quadruplexes aggregates. On the other hand, the line with increased percentage of cells with RNA foci was the one whose survival was more adversely affected by the peptide, probably because TAT-BIND caused cellular stress, increasing the aggregation rate of RNA repeats. A further confirmation of cellular stress was the immunoblot results of two lines of C9orf72 mutant iPSC-derived MNs treated with TAT-BIND peptide. The treatment increased the expression of ER and lysosomal proteins, suggesting that the peptide causes ER stress and induces autophagy. The peptide recovered the expression of mitochondrial proteins as well. In particular, it rescued COXIV expression and increased its activity, previously shown to be reduced in C9orf72 mutant iPSC-derived MNs. In the previous chapter I demonstrated that poly(PR) downregulates COXIV, and together with the evidence that TAT-BIND peptide appears to rescue COXIV expression and function, I can speculate that TAT-BIND peptide induces RNA foci clearance, thus downregulating DPRs expression. I showed that TAT-BIND peptide clears the cells of one patient line from the RNA foci, and a dot-bot assay would have determined DPR expression, clarifying if the results were caused by decreased DPR levels. Unfortunately, I could not complete the analysis on DPR expression and RNA foci content on iPSC-MNs due to the Covid-19 restrictions.

Chapter 6 – Discussion

This thesis describes the development of an innovative model system that allows close control of protein expression to study the effects of DPRs in CRISPR/Cas9 corrected iPSC-derived MNs. By comparing their phenotypes to C9orf72 mutant lines and to the published literature, I was able to generate novel data providing an initial characterisation of the distinctive contribution of DPRs to C9orf72-related ALS pathogenesis.

6.1. The doxycycline inducible system is efficient and sensitive

Immunohistochemical analysis of human tissue carrying the HRE in *C9ORF72* demonstrated that the glycine-rich DPRs (GP, GA, and GR) are more frequent than poly(PR) and poly(AP) (Mackenzie et al., 2015; Schludi et al., 2015). The DPRs are p62- and ubiquitin-positive, star-shaped or amorphous aggregates spread throughout the brain, but rare in spinal cord (Davidson et al., 2014; Gomez-Deza et al., 2015; Mackenzie et al., 2015; Mann et al., 2013; Schludi et al., 2015). The arginine-rich DPRs are perinuclear or nuclear, while the other DPRs aggregate in the cytosol. Soon after the discovery of DPRs, many studies used exogenous expression of (GGGGCC) or optimised-codon repeats to analyse DPR-mediated pathology in cellular and animal models. Transfection of primary mouse neurons with tagged DPRs induced the formation of nuclear aggregates with poly(PR) and

poly(GR), cytoplasmic aggregates of poly(GA) and poly(PA), and diffuse localisation of poly(GP) (Tao et al., 2015). However, different studies of primary mouse neurons expressing different lengths of poly(GA) sequences (50 – 150 repeats) showed nuclear aggregates, coupled with cleaved-caspase 3 staining, TDP-43 cleavage and reduced branching, demonstrating that poly(GA) is toxic to neurons (Y. B. Lee et al., 2017; May et al., 2014; Y. J. Zhang et al., 2014). The variety of models, dipeptide lengths and tags does not allow a direct comparison to describe the actual function of each DPR. Moreover, the DPR sequences in these studies were overexpressed and, not co-expressed with the other DPRs, conditions not found in human C9orf72 cases.

In order to better control DPR expression, I chose to insert codon-optimised sequences, encoding $(GA)_{50}$, $(PR)_{50}$ and $(GR)_{50}$, in lentiviruses carrying a doxycycline-inducible system, which showed basal expression of the DPRs. The comparison between transfected HEK293T cells and transduced iPSC-derived MNs demonstrated that the previous studies are highly biased by the system used to study DPRs. The expression of poly(GA) and poly(PR) in HEK293T cells replicated previous findings, as $(GA)_{50}$ was diffusely distributed in the cytosol of HEK293T cells, and $(PR)_{50}$ aggregated in the nuclei. In contrast, transduced iPSC-derived MNs showed poly(GA) cytosolic aggregates and few poly(PR) nuclear clusters. Moreover, the withdrawal of the inducer doxycycline demonstrated that the GA-positive aggregates were not actively degraded, while $(PR)_{50}$ aggregates were cleared from HEK293T cells and iPSC-derived MNs. Interestingly, once autophagy was induced with rapamycin and the lysosomal degradation was blocked with bafilomycin, poly(PR) aggregated in the nuclei of iPSC-derived MNs, increasing the DPR concentration, indicating that PR-positive aggregates

found in *post-mortem* tissue could be the final result of autophagic or proteasomal dysfunction. Moreover, the MTS assays demonstrated that low expression of poly(PR) and poly(GA) in iPSCs did not affect neuronal viability. The doxycycline-inducible system will allow future experiments to titrate the dose-dependent toxicity of each DPR, and investigate the possible interactions or combinatorial effect of DPRs when co-expressed. The detection system could be also improved, by reducing the centrifugation speed, as the low signal on western blot membranes may indicate that the aggregates were lost in the pellet. Moreover, using ELISA platforms will increase the detection sensitivity of small DPR concentrations.

6.2. Expression of poly(GA) and poly(PR) in the context of C9ORF72 cellular phenotypes

6.2.1. Poly(GA) and poly(PR) may partially cause calcium homeostasis and mitochondrial deficits recorded in C9orf72 mutant iPSC-derived MNs

Glutamate excitotoxicity is a condition described in ALS patients and C9orf72 mutant iPSC-derived MNs (Dafinca et al., 2020; Rothstein et al., 1990; Selvaraj et al., 2018; Spreux-Varoquaux et al., 2002; W. Xu & Xu, 2018). Further studies in *Drosophila* expressing $(PR)_{36}$ or $(GR)_{36}$, and in iPSC-derived MNs suggest that DPR expression may cause glutamate excitotoxicity (Dafinca et al., 2020; Selvaraj et al., 2018; W. Xu & Xu, 2018). In particular, the latest study from my group showed the C9orf72 mutant iPSC-derived MNs exhibited reduced calcium uptake when stimulated with glutamate, but longer recovery time caused by reduced mitochondrial buffering ability and downregulation of calbindin (Dafinca et al., 2020). When depolarised, C9orf72 mutant iPSC-derived MNs exhibited elevated

calcium levels, indicating that the high free calcium concentration of patient cells leads the motor neurons to be more sensitive to minor calcium variations. These observations suggested that reduced calcium uptake of C9orf72 mutant iPSC-derived MNs after glutamate stimulation is enough to cause glutamate excitotoxicity. Moreover, C9orf72 mutant iPSC-derived MNs and patient samples showed increased calcium permeable subunits in AMPA receptors, a further piece of evidence supporting the glutamate excitotoxicity theory (Almeida et al., 2013; Bursch et al., 2019; Dafinca et al., 2016, 2020; Donnelly et al., 2013; Sareen et al., 2013; Selvaraj et al., 2018; Y. Shi et al., 2018). The main hypothesis has been that C9ORF72 protein is involved in receptor recycling, and C9ORF72 haploinsufficiency might affect the number of AMPA receptors in C9orf72 patients.

However, in the experiments presented in this thesis, CRISPR/Cas9 corrected iPSC-derived MNs expressing poly(GA) or poly(PR) showed lower calcium uptake compared to dox-off MNs, indicating that both DPRs may be responsible for the reduced AMPA receptor permeability. This condition could lead the neurons to express more calcium permeable subunits. Further RNA and protein quantifications of the subunits in CRISPR/Cas9 corrected MNs expressing the DPRs are necessary to fully describe the stoichiometry of these glutamate receptors. Moreover, the expression of poly(PR) in isogenic iPSC-derived MNs reduced the calcium buffered by mitochondria, as described in C9orf72 mutant iPSC-derived MNs, indicating that poly(PR) could increase free cytosolic calcium leading the MNs to be more sensitive to small calcium variations and to excitotoxicity. However, poly(PR) expression did not affect MCU expression, and further analysis of MCU regulators MICU1/2 is necessary to clarify the role of

poly(PR) in mitochondrial deficits of calcium uptake. In addition, poly(PR) reduces the recovery time of calcium levels after glutamate, suggesting that calbindin expression or function is not affected by poly(PR).

A mitochondrial complex affected by poly(PR) expression in CRISPR/Cas9 corrected iPSC-derived MNs was COXIV. Poly(PR) caused its overexpression, but it did not lead to increased mitochondrial maximal respiration, as instead detected in MNs expressing poly(GA). SeaHorse experiments showed mitochondrial respiration deficits in C9orf72 mutant iPSC-derived MNs, caused by COXIV downregulation. Moreover, poly(PR) expressing cells and C9orf72 lines did not show variation in TOMM20 expression, indicating that calcium buffering and COXIV deficits are not caused by a reduction of mitochondrial number. As poly(PR) induced COXIV overexpression but not its over activation, it could indicate that the arginine-rich DPR is responsible for COXIV deficits detected in C9orf72 lines. Reduced mitochondrial respiration would then lower the mitochondrial membrane potential, which is responsible for mitochondrial calcium uptake. We indeed previously recorded diminished mitochondrial membrane potential in C9orf72 mutant iPSC-derived MNs, that could be caused by reduced respiration due to COXIV deficits (Dafinca et al., 2016). In contrast, poly(GA) expression increased maximal respiration, indicating specific GA-mediated toxicity, not related to C9ORF72 pathology recorded in our patient lines. Poly(GA) would alter COXIV expression and induce mitochondrial genesis, as indicated by increased TOMM20 protein level, resulting in increased maximal respiration.

6.2.2. DPR expression increases sensitivity to oxidative stress

COXIV deficits or electron chain overload could lead to ROS production and oxidative stress, as previously shown in C9orf72 mutant fibroblasts (Onesto et al., 2016). I measured increased sensitivity to oxidative stress in C9orf72 mutant iPSC-derived MNs, which was associated with higher stress granule formation in one C9orf72 line (C9-02) compared to control lines, as well as isogenic iPSC-derived MNs expressing the DPRs. Poly(PR) triggered the transient formation of larger stress granules, which reduced when poly(PR) expression was switched off. These results were expected, as previous studies have demonstrated that arginine-rich DPRs preferentially bind stress granule proteins, suggesting that they could affect their biogenesis and transport (Boeynaems et al., 2017; Kanekura et al., 2016; K. Lee et al., 2016; Lin et al., 2016). In contrast, poly(GA) caused irreversible stress granule formation, as their number continued to increase after the doxycycline-inducible system was deactivated, as previously shown in HEK293T cells (Tao et al., 2015).

In summary, these data suggested a model in which poly(PR)-mediated toxicity causes COXIV reduced activity, that leads to mitochondrial calcium uptake and mitochondrial respiration deficits, resulting in the increased sensitivity to oxidative stress evidenced by increased SG formation in PR-expressing iPSC-derived MNs and C9orf72 lines. However, increased number of stress granules induced by poly(PR) expression is transient, probably caused by the solubility of the arginine-rich DPR. Moreover, the lack of colocalisation between $(PR)_{50}$ and PABP could indicate that poly(PR) is not actively involved in SG biogenesis, but it promotes the events that finally lead to SG formation. On the other hand, the insoluble nature of poly(GA), demonstrated by the stable presence of the DPR

after doxycycline withdrawal, could be the cause of the irreversible formation of stress granules. However, the increased number of SGs in GA-expressing iPSC-derived MNs can also be the result of electron transport chain overload caused by COXIV overexpression induced by poly(GA). Further experiments are necessary to show colocalisation or coimmunopresipitation of DPRs with SG proteins.

6.2.3. Poly(GA) and poly(PR) reduce total ER calcium and poly(PR) inhibits IP3Rs

Calcium is released from IP3Rs, passes through VDAC, and when the calcium concentration increases, it is buffered by MCU (Csordás et al., 2010). When stimulated with carbachol, C9orf72 mutant iPSC-derived MNs and poly(PR) expressing lines released less calcium, indicating that poly(PR) could be responsible for IP3R deficits. I also recorded reduced total ER calcium when stimulated with thapsigargin, which inhibits SERCA pumps. In contrast, poly(GA) expression did not affect IP3R function, but reduced the total ER calcium. Taken together these data explain that reduction in total ER calcium of C9orf72 mutant iPSC-derived MNs is caused by poly(GA) and poly(PR). Further experiments (co-immunoprecipitation assay or colocalisation analysis or electron microscopy imaging) are necessary to clarify where the DPRs affect the ER calcium content. They may interact with SERCA pumps, reducing the calcium pumped into the ER, but they may also affect the SOCE system, decreasing the total ER calcium and causing ER stress. However, western blot analysis did not show UPR activation in DPR-expressing iPSC-derived MNs, indicating that poly(GA) and poly(PR) do not cause ER stress, in contrast to previous studies showing UPR activation in response to DPR expression (R. Wang et al., 2019; Y. J. Zhang et al., 2014). Notably, C9orf72 mutant iPSC-MNs exhibited UPR downregulation, not related to

poly(GA) and poly(PR) expression, but probably linked to reduced total ER calcium.

6.2.4. Poly(GA) activates lysosomes while poly(PR) reduces autophagy

Cellular and mouse models have shown that C9ORF72 is a member of the Rab-GEF family, and it is involved in vesicular transport and autophagy regulation (Amick et al., 2016; Aoki et al., 2017; Dafinca et al., 2016; Leskelä et al., 2019; Levine et al., 2013; Prudencio et al., 2015; Sellier et al., 2016; Sullivan et al., 2016; Ugolino et al., 2016; M. Yang et al., 2016). C9orf72 lines used in this project displayed lysosomal activation, as in previous studies in C9orf72 knock-out mouse models that showed lysosome accumulation and autophagic dysfunction (Amick et al., 2016; Atanasio et al., 2016; Burberry et al., 2016; O'Rourke et al., 2016; Sullivan et al., 2016; Ugolino et al., 2016). However, expression of poly(GA) led to lysosomal activation together with LAMP2A overexpression, indicating that autophagic dysfunction is also caused by poly(GA) production, not only by C9ORF72 haploinsufficiency. Previous studies demonstrated that poly(GA) interacts with proteasomal subunits causing UPS deficits, that could be compensated for by lysosomal activation (Guo et al., 2018; Khosravi et al., 2020; Yamakawa et al., 2015; Y. J. Zhang et al., 2016). In contrast, poly(PR) did not activate lysosomes, and it downregulated p62, suggesting that poly(PR) could reduce autophagy and protein degradation, as previously shown in primary rat spinal neurons treated with synthetic PR (Gupta et al., 2017).

6.3. DPRs do not cause TDP-43 pathology

Analysis of TDP-43, known to aggregate in the cytosol of motor neurons from ALS patients, showed that it localises mainly in nuclei of C9orf72 mutant iPSC-derived MNs compared to control lines. Following oxidative stress, TDP-43 of neurons from ALS patients, showed that it localises mainly in nuclei of C9orf72 mutant lines moved to the cytosol, decreasing its nuclear/cytoplasmic ratio, but the reduction was not significant compared to stressed control MNs. Further analysis of the recovery of nuclear TDP-43 after oxidative stress would clarify the nuclear-cytoplasmic transport efficiency of C9orf72 cells, as previous studies of C9orf72 human brains and DPR-expressing models showed abnormalities in the nuclear-cytoplasmic transport system, which could lead to TDP-43 mislocalisation (Chai & Gitler, 2018; Freibaum et al., 2015; Jovičić et al., 2015; Khosravi et al., 2016; K. Y. Shi et al., 2017; K. Zhang et al., 2015; Y. J. Zhang et al., 2016, 2019). However, expression of poly(GA) or poly(PR) in CRISPR/Cas9 corrected iPSC-derived MNs did not cause TDP-43 mislocalisation, not even after oxidative stress. These observation are based on a single experiment (n=1) which does not support the theory that TDP-43 cytoplasmic mislocalisation is caused by DPRs, but future experiments co-expressing multiple DPRs could lead to TDP-43 aggregation or mislocalisation. All experiments come with the caveat that soluble, and potentially toxic, oligomeric species might not easily be detected using available TDP-43 antibodies.

6.4. Autophagy and RNA foci degradation as therapeutic approaches

A phase II clinical trial is currently investigating the use of the autophagic activator rapamycin for treating ALS, as it was previously shown to reduce TDP-

43 cytosolic mislocalisation (Mandrioli et al., 2018; I. Wang et al., 2012). Rapamycin induces autophagy via inactivating mTORC1, but now there are several other small molecules able to clear cells from TDP-43 cytosolic aggregates via mTOR1-independent pathways, which would increase the selectivity of the treatments (Brown et al., 2020). A different approach is to induce protein aggregate clearance by targeting them with specific signals that would be recognised by the cellular systems. An example is an antibody-based system that recognises TDP-43 aggregates and induces their clearance via CMA (Tamaki et al., 2018). DPRs can be degraded via CMA when the chaperone HSPB8 is overexpressed, removing the aggregates in a complex with HSP70 and delivering them to the lysosomes (Cristofani et al., 2018). The specific activation of CMA with 6-AN induced poly(GA) and poly(PR) degradation in CRISPR/Cas9 corrected iPSC-derived MNs, but the same treatment in C9orf2 lines did not rescue the phenotypes. DPR or CMA target quantification would clarify whether CMA was active. If DPRs were degraded, it would imply that clearing the C9orf72 mutant iPSC-derived MNs from the DPRs is not a sufficient therapeutic approach.

A different method other than inducing DPR degradation is downregulating their translation by reducing *C9ORF72* transcripts, RNA foci or inhibiting RAN translation. A small peptide (TAT-BIND) with high-affinity for the G-quadruplex of C9ORF72 HRE reduced sense RNA foci and sense DPRs in cellular and *Drosophila* models, rescuing their phenotypes (Q. Zhang et al., 2019). The same peptide cleared iPSCs of sense RNA foci in only one C9orf72 patient line, improving its survival. However, it showed toxicity in the other C9orf72 mutant lines, increasing the number of RNA foci and decreasing the cellular viability. TAT-BIND peptide treatment in C9orf72 mutant iPSC-derived MNs activated UPR

and autophagy, a further indication of toxicity. However, the treatment rescued MCU and COXIV expression and increased the mitochondrial maximal respiration. A further validation of DPR clearance could be a dot-blot assay in TAT-BIND peptide treated MNs.

6.5. Conclusions and future directions

In conclusion, the innovative approach in this thesis, expressing DPRs in CRISPR/Cas9 corrected iPSC-derived MNs at low levels, demonstrated that $(PR)_{50}$ and $(GA)_{50}$ do not affect cellular viability and do not induce TDP-43 pathology. Poly(GA) forms cytosolic insoluble aggregates, induces lysosomal activation and increases sensitivity to oxidative stress, causing irreversible formation of stress granules. Both poly(GA) and poly(PR) decrease total calcium in the ER, without causing ER stress, and they reduce calcium uptake after glutamate stimulation. Poly(PR) is soluble, and it moves to the nuclei only when the autophagy is inhibited. It may reduce mitochondrial respiration, lowering the mitochondrial membrane potential and causing reduced mitochondrial calcium uptake. This condition would potentially increase cytosolic free calcium, leading to glutamate excitotoxicity and sensitivity to oxidative stress. Future co-immunoprecipitation assays will validate the hypothesis that poly(GA) and poly(PR) interact directly with glutamate receptors, mitochondrial proteins, lysosomes, IP3R. Another future use of the doxycycline system will be to switch on the DPR expression during the early differentiation stage and follow neuronal maturation.

The two therapeutic approaches analysed showed that poly(GA) ad poly(PR) can be digested by CMA, but the method did not rescue the phenotype of C9orf2 lines, and RNA foci degradation with TAT-BIND peptide is toxic in C9orf72 mutant iPSC-derived MNs. CMA as therapeutic target could be further studied using live experiments to analyse calcium homeostasis and lysosomal degradation.

Appendix

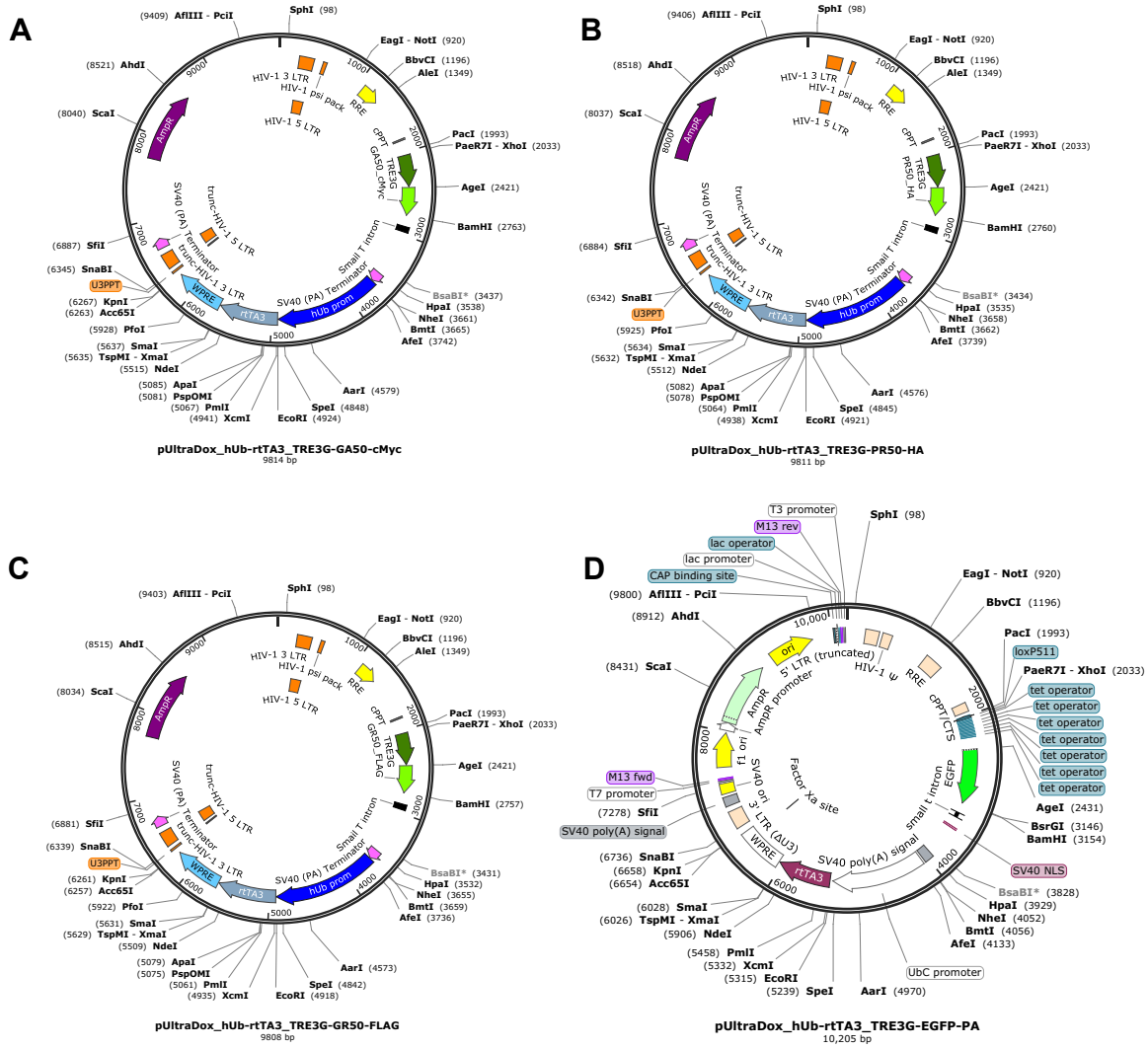


Figure S1: Plasmid maps.

A) pUltradox_hUb-rtTA3_TRE3G-GA50-*c*myc; **B)** pUltradox_hUb-rtTA3_TRE3G-PR50-HA; **C)** pUltradox_hUb-rtTA3_TRE3G-GR50-FLAG; **D)** pUltradox_hUb-rtTA3_TRE3G-eGFP.

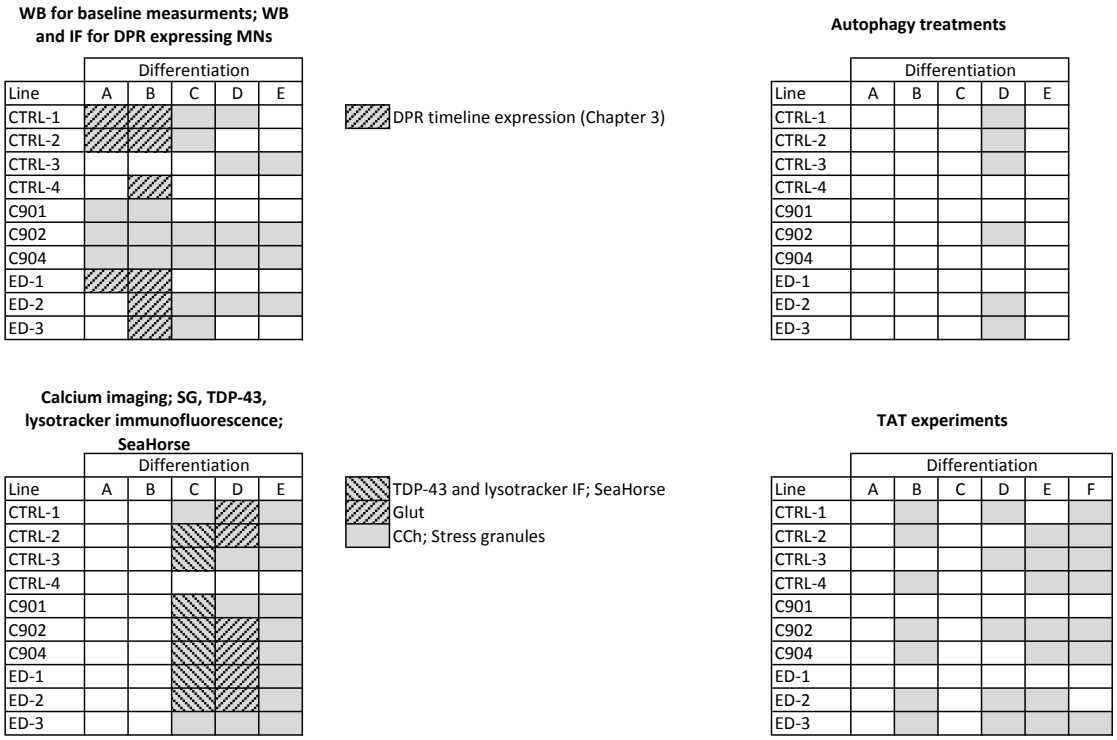


Figure S2: Differentiation Gann charts.

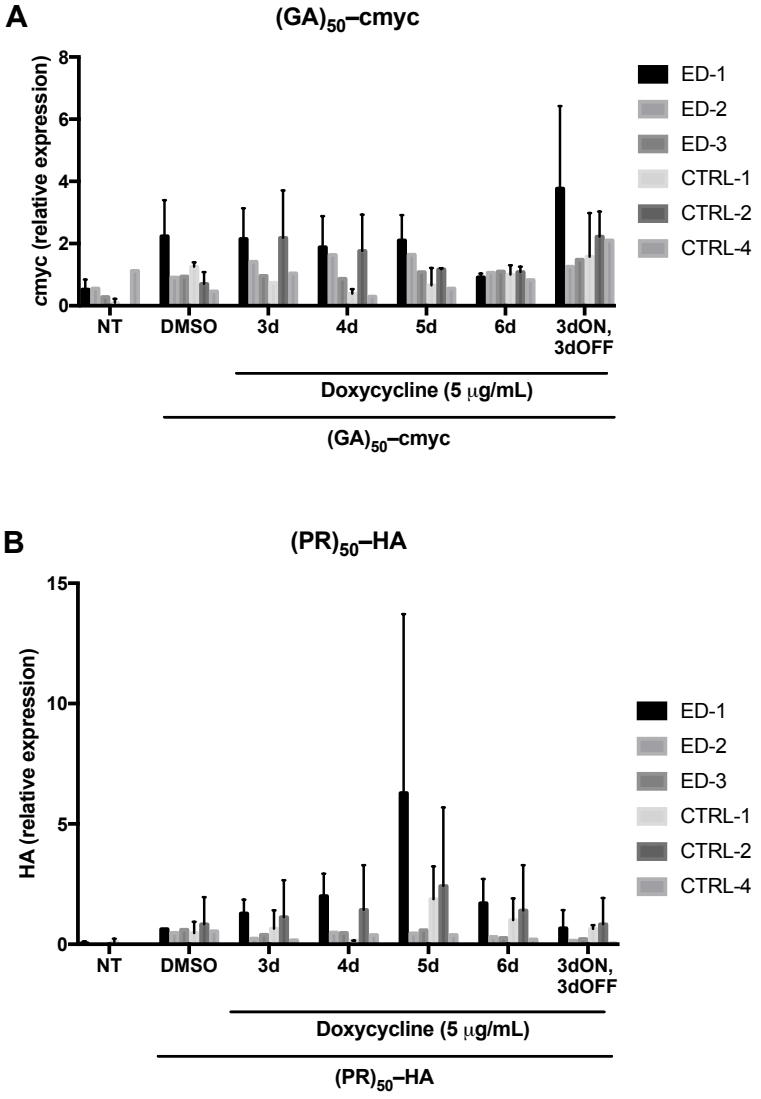


Figure S3: Immunoblot quantification of tagged DPRs in edited and wild-type iPSC-derived MNs.

Immunoblot quantification of tagged DPRs to determine their expression timeline in three CRISPR/Cas9 corrected lines (ED-1, ED-2, ED-3) and three wild-type iPSC-derived MNs (CTRL-1, CTRL-2, CTRL-3) from differentiations A and B. **A)** (GA)50-*c*-myc expression. **B)** (PR)50-HA expression. The bars represent means and error bars are standard deviation.

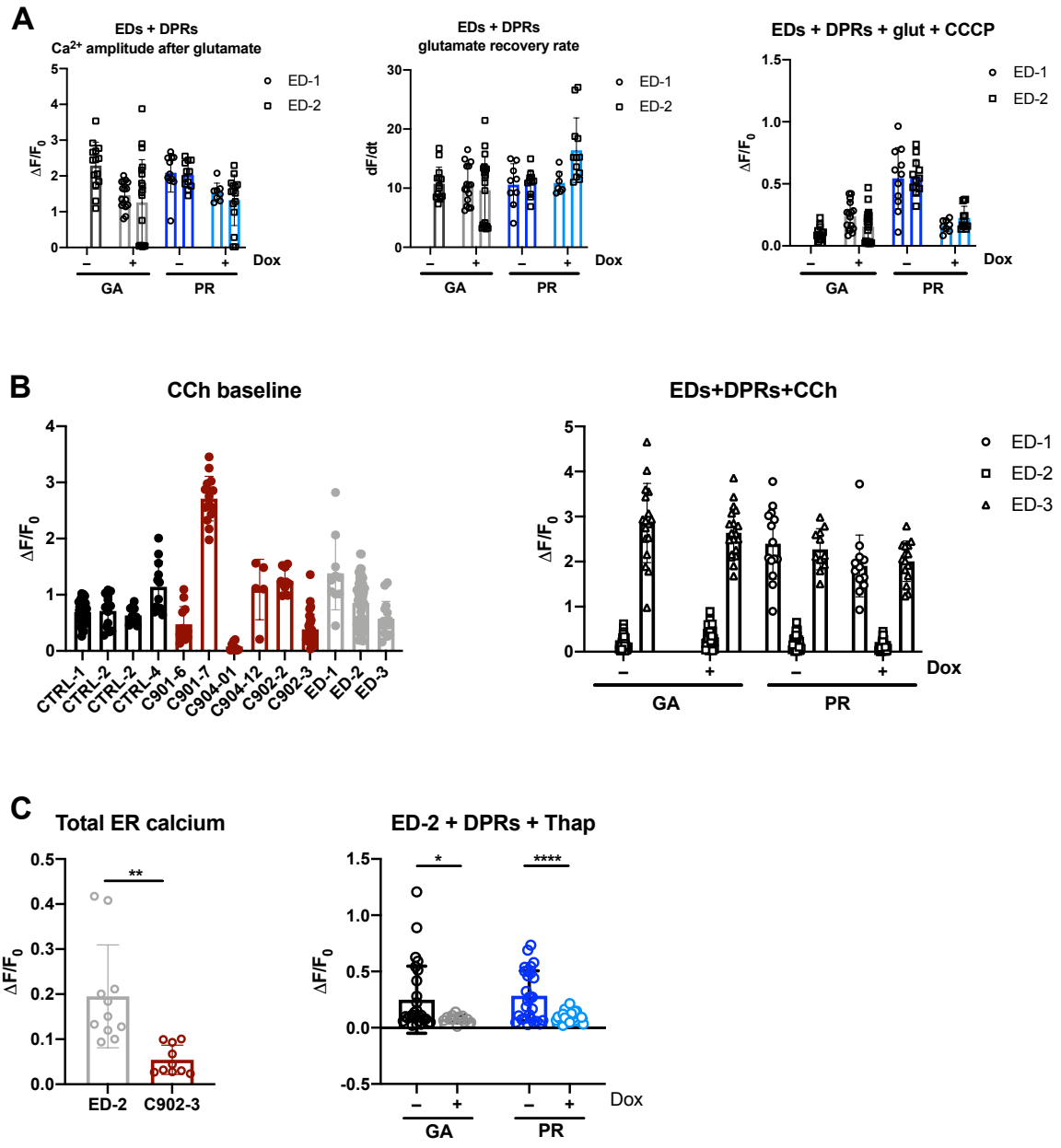


Figure S4: Calcium imaging analysis of each line used.

Measurements of cytosolic calcium, following different stimuli in Fluo-4AM loaded MNs. One dot of each scattered plot indicates one cell, the bars represent means and error bars are standard deviation. **A)** Measurements of cytosolic calcium and recovery rate following glutamate stimulation, and mitochondrial calcium release after CCCP treatment in CRISPR/Cas9 corrected iPSC-derived MNs transduced with tagged DPRs (ED-1, ED-2 replicated in two independent differentiations). **B)** Measurements of ER calcium released following carbachol in all lines (three independent differentiations). **C)** Measurements of total ER calcium released from ER after thapsigargin stimulation (one differentiation).

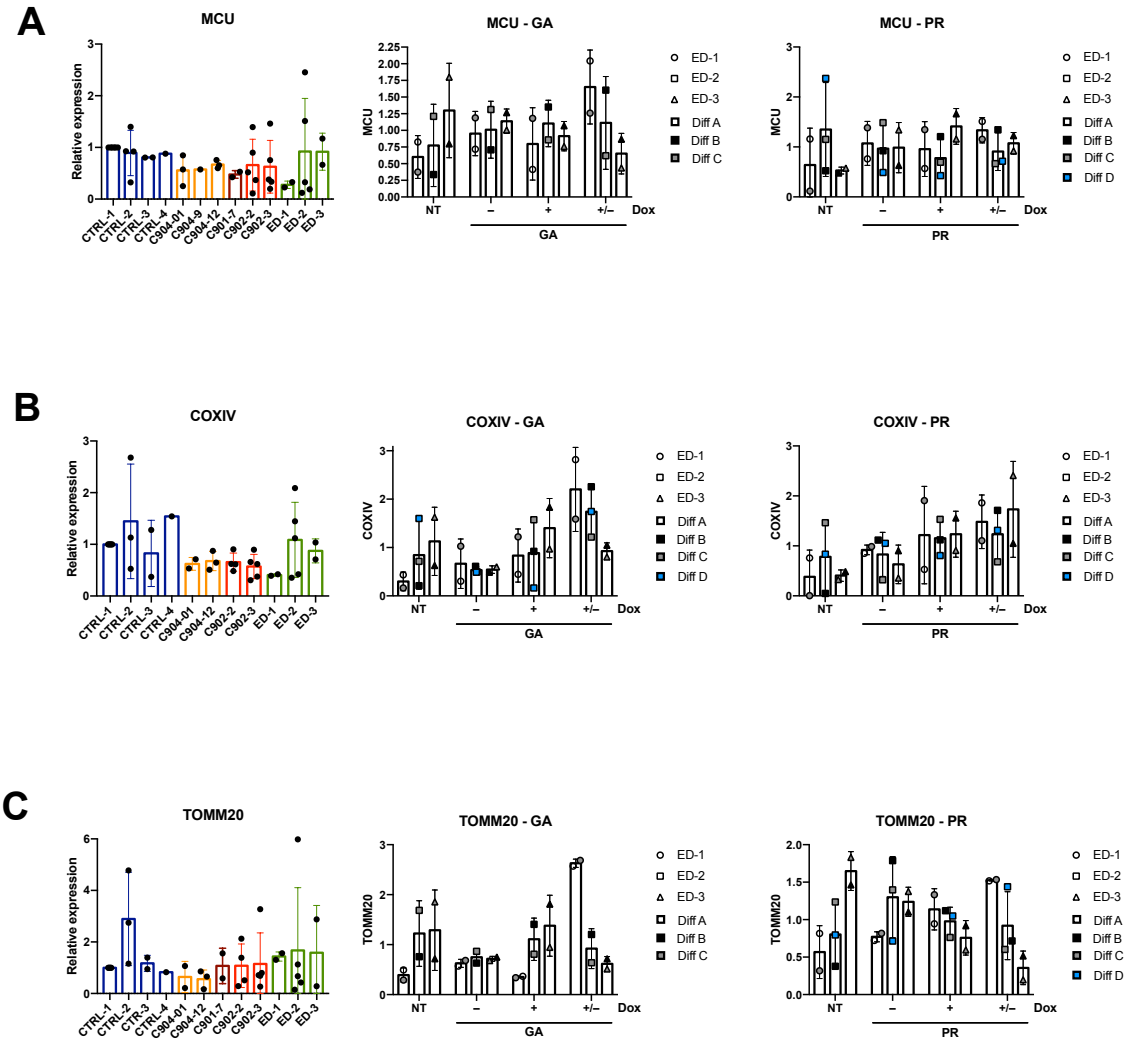


Figure S5: Immunoblot quantifications of mitochondrial markers in each line.

Immunoblots of mitochondrial markers MCU, COXIV and TOMM20 in non-treated lines (4 wild-type controls, 3 C9-ALS/FTD and 3 CRISPR/Cas9 corrected lines) and edited MNs expressing (GA)50–*c*-myc or (PR)50-HA. One dot of the scatter plot indicates a single differentiation. The bars represent means and error bars are standard deviation. **A)** Immunoblot quantification of MCU. **B)** Immunoblot quantifications of COXIV. **C)** Immunoblot quantification of TOMM20.

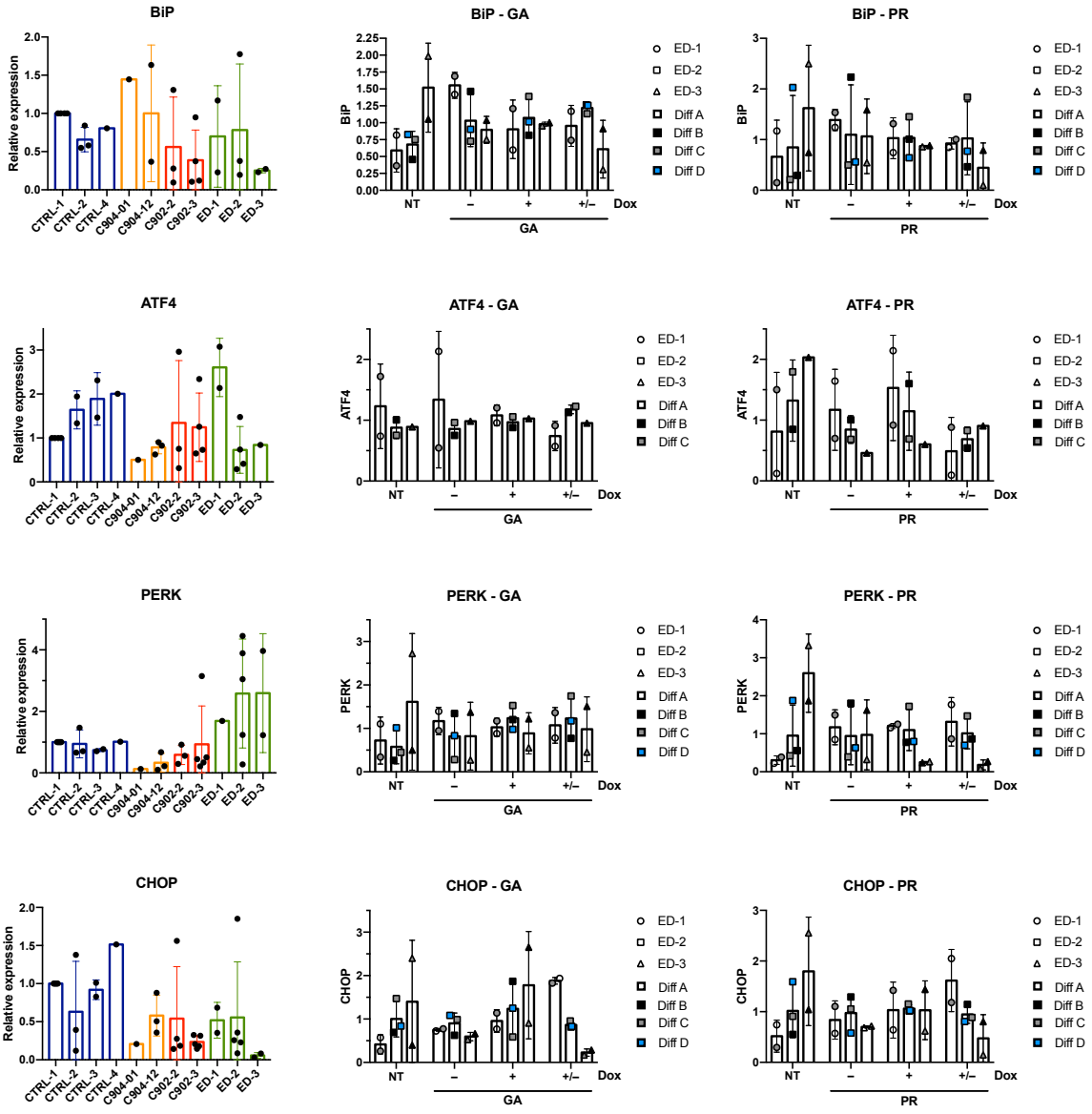


Figure S6: Immunoblot quantifications of UPR markers in each line.

Immunoblots of UPR markers in non-treated lines (4 wild-type controls, 2 C9-ALS/FTD and 3 CRISPR/Cas9 corrected lines) and edited MNs expressing $(GA)_{50}$–*c*-myc or $(PR)_{50}$-HA. One dot of the scatter plot indicates a single differentiation. The bars represent means and error bars are standard deviation.

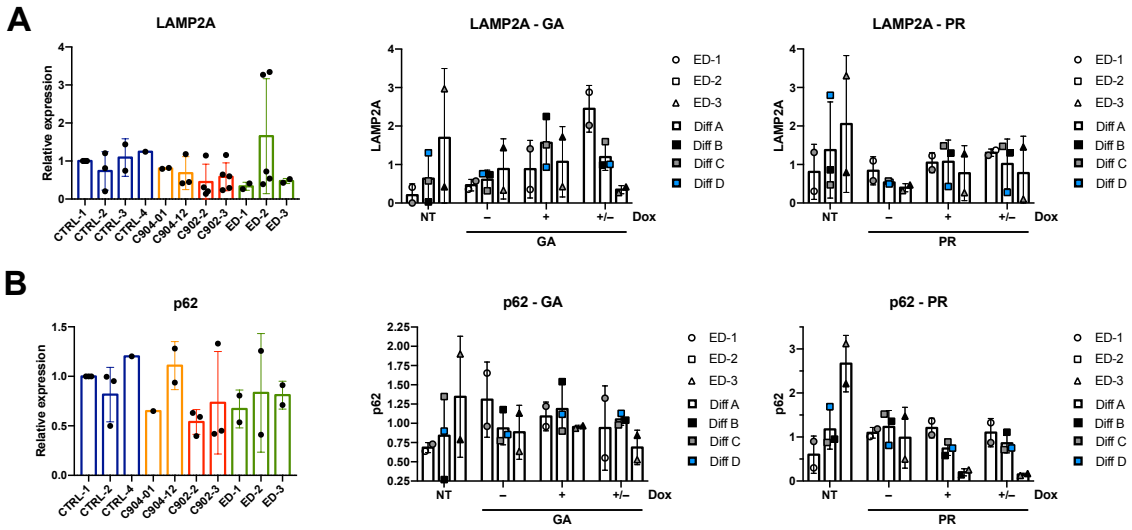


Figure S7: Immunoblot quantifications of autophagy markers in each line.

Immunoblots of LAMP2A and p62 in non-treated lines (4 wild-type controls, 2 C9-ALS/FTD and 3 CRISPR/Cas9 corrected lines) and edited MNs expressing $(GA)_{50}$–*c*-myc or $(PR)_{50}$-HA. One dot of the scatter plot indicates a single differentiation. The bars represent means and error bars are standard deviation. **A)** Immunoblot quantification of LAMP2A. **B)** Immunoblot quantifications of p62.

References

Ababneh, N., Scaber, J., Flynn, R., Douglas, A., Barbagallo, P., Candalija, A., Turner, M., Sims, D., Dafinca, R., Cowley, S., & Talbot, K. (2020). Correction of amyotrophic lateral sclerosis related phenotypes in induced pluripotent stem cell-derived motor neurons carrying a hexanucleotide expansion mutation in C9orf72 by CRISPR/Cas9 genome editing using homology-directed repair. *Human Molecular Genetics*. https://doi.org/10.1093/hmg/ddaa106

Abe, K., Aoki, M., Tsuji, S., Itoyama, Y., Sobue, G., Togo, M., Hamada, C., Tanaka, M., Akimoto, M., Nakamura, K., Takahashi, F., Kondo, K., & Yoshino, H. (2017). Safety and efficacy of edaravone in well defined patients with amyotrophic lateral sclerosis: a randomised, double-blind, placebo-controlled trial. *The Lancet Neurology*, *16*(7), 505–512. https://doi.org/10.1016/S1474-4422(17)30115-1

Abel, O., Powell, J., Andersen, P., & Al-Chalabi, A. (2012). ALSoD: A user-friendly online bioinformatics tool for amyotrophic lateral sclerosis genetics. *Human Mutation*, *33*(9), 1345–1351. https://doi.org/10.1002/humu.22157

Ahmad, L., Zhang, S., Casanova, J., & Sancho-Shimizu, V. (2016). Human TBK1: A Gatekeeper of Neuroinflammation. *Trends in Molecular Medicine*, *22*(6), 511–527. https://doi.org/10.1016/J.MOLMED.2016.04.006

Akimoto, C., Volk, A., Blitterswijk, M., Broeck, M., Leblond, C., Lumbroso, S., Camu, W., Neitzel, B., Onodera, O., Rheenen, W., Pinto, S., Weber, M., Smith, B., Proven, M., Talbot, K., Keagle, P., Chesi, A., Ratti, A., Zee, J., … Kubisch, C. (2014). A blinded international study on the reliability of genetic testing for GGGGCC-repeat expansions in C9orf72 reveals marked differences in results among 14 laboratories. *Journal of Medical Genetics*, *51*(6), 419–424. https://doi.org/10.1136/JMEDGENET-2014-102360

Al-Chalabi, A., & Hardiman, O. (2013). The epidemiology of ALS: a conspiracy of genes, environment and time. *Nature Reviews Neurology*, *9*(11), 617–628. https://doi.org/10.1038/nrneurol.2013.203

Al-Sarraj, S., King, A., Troakes, C., Smith, B., Maekawa, S., Bodi, I., Rogelj, B., Al-Chalabi, A., Hortobágyi, T., & Shaw, C. (2011). p62 positive, TDP-43 negative, neuronal cytoplasmic and intranuclear inclusions in the cerebellum and hippocampus define the pathology of C9orf72-linked FTLD and MND/ALS. *Acta Neuropathologica*, *122*(6), 691–702. https://doi.org/10.1007/s00401-011-0911-2

Aladesuyi Arogundade, O., Stauffer, J., Saberi, S., Diaz-Garcia, S., Malik, S., Basilim, H., Rodriguez, M., Ohkubo, T., & Ravits, J. (2019). Antisense RNA foci are associated with nucleoli and TDP-43 mislocalization in C9orf72-ALS/FTD: a quantitative study. In *Acta Neuropathologica* (Vol. 137, Issue 3, pp. 527–530). Springer. https://doi.org/10.1007/s00401-018-01955-0

Alexander, E., Ghanbari Niaki, A., Zhang, T., Sarkar, J., Liu, Y., Nirujogi, R., Pandey, A., Myong, S., & Wang, J. (2018). Ubiquilin 2 modulates ALS/FTD-linked FUS-RNA complex dynamics and stress granule formation. *Proceedings of the National Academy of Sciences of the United States of America*, *115*(49), E11485–E11494. https://doi.org/10.1073/pnas.1811997115

Alfaro, I., Albornoz, A., Molina, A., Moreno, J., Cordero, K., Criollo, A., & Budini, M. (2019). Chaperone Mediated Autophagy in the Crosstalk of Neurodegenerative Diseases and Metabolic Disorders. *Frontiers in Endocrinology*, *9*, 778. https://doi.org/10.3389/fendo.2018.00778

Almeida, S., Gascon, E., Tran, H., Chou, H., Gendron, T., Degroot, S., Tapper, A., Sellier, C., Charlet-Berguerand, N., Karydas, A., Seeley, W., Boxer, A., Petrucelli, L., Miller, B., & Gao, F. (2013). Modeling key pathological features of frontotemporal dementia with C9ORF72 repeat expansion in iPSC-derived human neurons. *Acta Neuropathologica*, *126*(3), 385–399. https://doi.org/10.1007/s00401-013-1149-y

Amick, J., Roczniak-Ferguson, A., & Ferguson, S. (2016). C9orf72 binds SMCR8, localizes to lysosomes, and regulates mTORC1 signaling. *Molecular Biology of the Cell*, *27*(20), 3040–3051. https://doi.org/10.1091/mbc.e16-01-0003

Aoki, Y., Manzano, R., Lee, Y., Dafinca, R., Aoki, M., Douglas, A., Varela, M., Sathyaprakash, C., Scaber, J., Barbagallo, P., Vader, P., Mäger, I., Ezzat, K., Turner, M., Ito, N., Gasco, S., Ohbayashi, N., El Andaloussi, S., Takeda, S., … Wood, M. (2017). C9orf72 and RAB7L1 regulate vesicle trafficking in amyotrophic lateral sclerosis and frontotemporal dementia. *Brain*, *140*(4), 887–897. https://doi.org/10.1093/brain/awx024

Arai, T., Hasegawa, M., Akiyama, H., Ikeda, K., Nonaka, T., Mori, H., Mann, D., Tsuchiya, K., Yoshida, M., Hashizume, Y., & Oda, T. (2006). TDP-43 is a component of ubiquitin-positive tau-negative inclusions in frontotemporal lobar degeneration and amyotrophic lateral sclerosis. *Biochemical and Biophysical Research Communications*, *351*(3), 602–611. https://doi.org/10.1016/J.BBRC.2006.10.093

Arias, E. (2017). Methods to Study Chaperone-Mediated Autophagy. *Methods in Enzymology*, *588*, 283–305. https://doi.org/10.1016/BS.MIE.2016.10.009

Arimoto, K., Fukuda, H., Imajoh-Ohmi, S., Saito, H., & Takekawa, M. (2008). Formation of stress granules inhibits apoptosis by suppressing stress-responsive MAPK pathways. *Nature Cell Biology*, *10*(11), 1324–1332. https://doi.org/10.1038/ncb1791

Ash, P., Bieniek, K., Gendron, T., Caulfield, T., Lin, W., Dejesus-Hernandez, M., van Blitterswijk, M., Jansen-West, K., Paul, J., Rademakers, R., Boylan, K., Dickson, D., & Petrucelli, L. (2013). Unconventional translation of C9ORF72 GGGGCC expansion generates insoluble polypeptides specific to c9FTD/ALS. *Neuron*, *77*(4), 639–646. https://doi.org/10.1016/j.neuron.2013.02.004

Atanasio, A., Decman, V., White, D., Ramos, M., Ikiz, B., Lee, H., Siao, C., Brydges, S., LaRosa, E., Bai, Y., Fury, W., Burfeind, P., Zamfirova, R., Warshaw, G., Orengo, J., Oyejide, A., Fralish, M., Auerbach, W., Poueymirou, W., … Lai, K. (2016). C9orf72 ablation causes immune dysregulation characterized by leukocyte expansion, autoantibody production and glomerulonephropathy in mice. *Scientific Reports*, *6*(1), 23204. https://doi.org/10.1038/srep23204

Avila-Medina, J., Mayoral-Gonzalez, I., Dominguez-Rodriguez, A., Gallardo-Castillo, I., Ribas, J., Ordoñez, A., Rosado, J., & Smani, T. (2018). The Complex Role of Store Operated Calcium Entry Pathways and Related Proteins in the Function of Cardiac, Skeletal and Vascular Smooth Muscle Cells. *Frontiers in Physiology*, *9*, 257. https://doi.org/10.3389/fphys.2018.00257

Ayala, V., Granado-Serrano, A., Cacabelos, D., Naudí, A., Ilieva, E., Boada, J., Caraballo-Miralles, V., Lladó, J., Ferrer, I., Pamplona, R., & Portero-Otin, M. (2011). Cell stress induces TDP-43 pathological changes associated with ERK1/2 dysfunction: implications in ALS. *Acta Neuropathologica*, *122*(3), 259–270. https://doi.org/10.1007/s00401-011-0850-y

Ayala, Y., De Conti, L., Avendaño-Vázquez, S., Dhir, A., Romano, M., D'Ambrogio, A., Tollervey, J., Ule, J., Baralle, M., Buratti, E., & Baralle, F. (2011). TDP-43 regulates its mRNA levels through a negative feedback loop. *The EMBO Journal*, *30*(2), 277–288.

https://doi.org/10.1038/emboj.2010.310

Azadmanesh, J., & Borgstahl, G. (2018). A Review of the Catalytic Mechanism of Human Manganese Superoxide Dismutase. *Antioxidants*, *7*(2), 25. https://doi.org/10.3390/antiox7020025

Baborie, A., Griffiths, T., Jaros, E., Perry, R., McKeith, I., Burn, D., Masuda-Suzukake, M., Hasegawa, M., Rollinson, S., Pickering-Brown, S., Robinson, A., Davidson, Y., & Mann, D. (2015). Accumulation of dipeptide repeat proteins predates that of TDP-43 in frontotemporal lobar degeneration associated with hexanucleotide repeat expansions in C9ORF72 gene. *Neuropathology and Applied Neurobiology*, *41*(5), 601–612. https://doi.org/10.1111/nan.12178

Baloh, R., O'Rourke, J., Bell, S., Bogdonik, L., Muhammad, A., Gendron, T., Kim, K., Austin, A., Cady, J., Liu, E., Zarrow, J., Grant, S., Ho, R., Carmona, S., Simpkinson, M., Wu, K., Daughrity, L., Dickson, D., Harms, M., … Lutz, C. (2016). C9orf72 BAC Transgenic Mice Display Typical Pathologic Features of ALS/FTD (P4.001). *Neurology*, *86*(16 Supplement).

Bates, G., Dorsey, R., Gusella, J., Hayden, M., Kay, C., Leavitt, B., Nance, M., Ross, C., Scahill, R., Wetzel, R., Wild, E., & Tabrizi, S. (2015). Huntington disease. *Nature Reviews Disease Primers*, *1*(1), 15005. https://doi.org/10.1038/nrdp.2015.5

Beck, J., Poulter, M., Hensman, D., Rohrer, J., Mahoney, C., Adamson, G., Campbell, T., Uphill, J., Borg, A., Fratta, P., Orrell, R., Malaspina, A., Rowe, J., Brown, J., Hodges, J., Sidle, K., Polke, J., Houlden, H., Schott, J., … Mead, S. (2013). Large C9orf72 Hexanucleotide Repeat Expansions Are Seen in Multiple Neurodegenerative Syndromes and Are More Frequent Than Expected in the UK Population. *The American Journal of Human Genetics*, *92*(3), 345–353. https://doi.org/10.1016/J.AJHG.2013.01.011

Bensimon, G., Lacomblez, L., Meininger, V., & Group, the A. S. (1994). A Controlled Trial of Riluzole in Amyotrophic Lateral Sclerosis. *New England Journal of Medicine*, *330*(9), 585–591. https://doi.org/10.1056/NEJM199403033300901

Berning, B., & Walker, A. (2019). The Pathobiology of TDP-43 C-Terminal Fragments in ALS and FTLD. *Frontiers in Neuroscience*, *13*, 335. https://doi.org/10.3389/fnins.2019.00335

Bertolotti, A., Zhang, Y., Hendershot, L., Harding, H., & Ron, D. (2000). Dynamic interaction of BiP and ER stress transducers in the unfolded-protein response. *Nature Cell Biology*, *2*(6), 326–332. https://doi.org/10.1038/35014014

Boehringer, A., Garcia-Mansfield, K., Singh, G., Bakkar, N., Pirrotte, P., & Bowser, R. (2017). ALS Associated Mutations in Matrin 3 Alter Protein-Protein Interactions and Impede mRNA Nuclear Export. *Scientific Reports*, *7*(1), 14529. https://doi.org/10.1038/s41598-017-14924-6

Boeynaems, S., Bogaert, E., Kovacs, D., Konijnenberg, A., Timmerman, E., Volkov, A., Guharoy, M., De Decker, M., Jaspers, T., Ryan, V., Janke, A., Baatsen, P., Vercruysse, T., Kolaitis, R., Daelemans, D., Taylor, J., Kedersha, N., Anderson, P., Impens, F., … Van Den Bosch, L. (2017). Phase Separation of C9orf72 Dipeptide Repeats Perturbs Stress Granule Dynamics. *Molecular Cell*, *65*(6), 1044-1055.e5. https://doi.org/10.1016/j.molcel.2017.02.013

Borghese, L., Dolezalova, D., Opitz, T., Haupt, S., Leinhaas, A., Steinfarz, B., Koch, P., Edenhofer, F., Hampl, A., & Brüstle, O. (2010). Inhibition of Notch Signaling in Human

Embryonic Stem Cell-Derived Neural Stem Cells Delays G1/S Phase Transition and Accelerates Neuronal Differentiation In Vitro and In Vivo. *STEM CELLS*, *28*(5), 955–964. https://doi.org/10.1002/stem.408

Bowling, A., Schulz, J., Brown, R., & Beal, M. (1993). Superoxide Dismutase Activity, Oxidative Damage, and Mitochondrial Energy Metabolism in Familial and Sporadic Amyotrophic Lateral Sclerosis. *Journal of Neurochemistry*, *61*(6), 2322–2325. https://doi.org/10.1111/j.1471-4159.1993.tb07478.x

Boxer, A., Mackenzie, I., Boeve, B., Baker, M., Seeley, W., Crook, R., Feldman, H., Hsiung, G., Rutherford, N., Laluz, V., Whitwell, J., Foti, D., McDade, E., Molano, J., Karydas, A., Wojtas, A., Goldman, J., Mirsky, J., Sengdy, P., … Rademakers, R. (2011). Clinical, neuroimaging and neuropathological features of a new chromosome 9p-linked FTD-ALS family. *Journal of Neurology, Neurosurgery, and Psychiatry*, *82*(2), 196–203. https://doi.org/10.1136/jnnp.2009.204081

Braak, H., Brettschneider, J., Ludolph, A. C., Lee, V. M., Trojanowski, J. Q., & Tredici, K. Del. (2013). Amyotrophic lateral sclerosis—a model of corticofugal axonal spread. *Nature Reviews Neurology*, *9*(12), 708–714. https://doi.org/10.1038/nrneurol.2013.221

Braak, H., Ludolph, A. C., Neumann, M., Ravits, J., & Del Tredici, K. (2017). Pathological TDP-43 changes in Betz cells differ from those in bulbar and spinal α-motoneurons in sporadic amyotrophic lateral sclerosis. *Acta Neuropathologica*, *133*(1), 79–90. https://doi.org/10.1007/s00401-016-1633-2

Brasseur, L., Coens, A., Waeytens, J., Melki, R., & Bousset, L. (2020). Dipeptide repeat derived from C9orf72 hexanucleotide expansions forms amyloids or natively unfolded structures in vitro. *Biochemical and Biophysical Research Communications*, *526*(2), 410–416. https://doi.org/10.1016/J.BBRC.2020.03.108

Brettschneider, J., Del Tredici, K., Toledo, J. B., Robinson, J. L., Irwin, D. J., Grossman, M., Suh, E., Van Deerlin, V. M., Wood, E. M., Baek, Y., Kwong, L., Lee, E. B., Elman, L., McCluskey, L., Fang, L., Feldengut, S., Ludolph, A. C., Lee, V. M.-Y., Braak, H., & Trojanowski, J. Q. (2013). Stages of pTDP-43 pathology in amyotrophic lateral sclerosis. *Annals of Neurology*, *74*(1), 20–38. https://doi.org/10.1002/ana.23937

Brook, J. D., McCurrach, M. E., Harley, H. G., Buckler, A. J., Church, D., Aburatani, H., Hunter, K., Stanton, V. P., Thirion, J.-P., Hudson, T., Sohn, R., Zemelman, B., Snell, R. G., Rundle, S. A., Crow, S., Davies, J., Shelbourne, P., Buxton, J., Jones, C., … Housman, D. E. (1992). Molecular basis of myotonic dystrophy: Expansion of a trinucleotide (CTG) repeat at the 3′ end of a transcript encoding a protein kinase family member. *Cell*, *68*(4), 799–808. https://doi.org/10.1016/0092-8674(92)90154-5

Brown, D. G., Shorter, J., & Wobst, H. J. (2020). Emerging small-molecule therapeutic approaches for amyotrophic lateral sclerosis and frontotemporal dementia. *Bioorganic & Medicinal Chemistry Letters*, *30*(4), 126942. https://doi.org/10.1016/J.BMCL.2019.126942

Buratti, E., Brindisi, A., Giombi, M., Tisminetzky, S., Ayala, Y. M., & Baralle, F. E. (2005). TDP-43 binds heterogeneous nuclear ribonucleoprotein A/B through its C-terminal tail: an important region for the inhibition of cystic fibrosis transmembrane conductance regulator exon 9 splicing. *The Journal of Biological Chemistry*, *280*(45), 37572–37584. https://doi.org/10.1074/jbc.M505557200

Buratti, E., Dörk, T., Zuccato, E., Pagani, F., Romano, M., & Baralle, F. E. (2001). Nuclear factor TDP-43 and SR proteins promote in vitro and in vivo CFTR exon 9 skipping. *The EMBO Journal*, *20*(7), 1774–1784. https://doi.org/10.1093/emboj/20.7.1774

Burberry, A., Suzuki, N., Wang, J.-Y., Moccia, R., Mordes, D. A., Stewart, M. H., Suzuki-Uematsu, S., Ghosh, S., Singh, A., Merkle, F. T., Koszka, K., Li, Q.-Z., Zon, L., Rossi, D. J., Trowbridge, J. J., Notarangelo, L. D., & Eggan, K. (2016). Loss-of-function mutations in the C9ORF72 mouse ortholog cause fatal autoimmune disease. *Science Translational Medicine*, *8*(347), 347ra93. https://doi.org/10.1126/scitranslmed.aaf6038

Burberry, A., Wells, M. F., Limone, F., Couto, A., Smith, K. S., Keaney, J., Gillet, G., van Gastel, N., Wang, J.-Y., Pietilainen, O., Qian, M., Eggan, P., Cantrell, C., Mok, J., Kadiu, I., Scadden, D. T., & Eggan, K. (2020). C9orf72 suppresses systemic and neural inflammation induced by gut bacteria. *Nature*, *582*(7810), 89–94. https://doi.org/10.1038/s41586-020-2288-7

Burguete, A. S., Almeida, S., Gao, F.-B., Kalb, R., Akins, M. R., & Bonini, N. M. (2015). GGGGCC microsatellite RNA is neuritically localized, induces branching defects, and perturbs transport granule function. *ELife*, *4*. https://doi.org/10.7554/eLife.08881

Burrell, J. R., Halliday, G. M., Kril, J. J., Ittner, L. M., Götz, J., Kiernan, M. C., & Hodges, J. R. (2016). The frontotemporal dementia-motor neuron disease continuum. *The Lancet*, *388*(10047), 919–931. https://doi.org/10.1016/S0140-6736(16)00737-6

Bursch, F., Kalmbach, N., Naujock, M., Staege, S., Eggenschwiler, R., Abo-Rady, M., Japtok, J., Guo, W., Hensel, N., Reinhardt, P., Boeckers, T. M., Cantz, T., Sterneckert, J., Van Den Bosch, L., Hermann, A., Petri, S., & Wegner, F. (2019). Altered calcium dynamics and glutamate receptor properties in iPSC-derived motor neurons from ALS patients with C9orf72, FUS, SOD1 or TDP43 mutations. *Human Molecular Genetics*, *28*(17), 2835–2850. https://doi.org/10.1093/hmg/ddz107

Celona, B., Dollen, J. von, Vatsavayai, S. C., Kashima, R., Johnson, J. R., Tang, A. A., Hata, A., Miller, B. L., Huang, E. J., Krogan, N. J., Seeley, W. W., & Black, B. L. (2017). Suppression of C9orf72 RNA repeat-induced neurotoxicity by the ALS-associated RNA-binding protein Zfp106. *ELife*, *6*. https://doi.org/10.7554/eLife.19032

Chai, N., & Gitler, A. D. (2018). Yeast screen for modifiers of C9orf72 poly(Glycine-Arginine) dipeptide repeat toxicity. *FEMS Yeast Research*. https://doi.org/10.1093/femsyr/foy024

Chambers, S. M., Fasano, C. A., Papapetrou, E. P., Tomishima, M., Sadelain, M., & Studer, L. (2009). Highly efficient neural conversion of human ES and iPS cells by dual inhibition of SMAD signaling. *Nature Biotechnology*, *27*(3), 275–280. https://doi.org/10.1038/nbt.1529

Chang, Y.-J., Jeng, U.-S., Chiang, Y.-L., Hwang, I.-S., & Chen, Y.-R. (2016). The Glycine-Alanine Dipeptide Repeat from C9orf72 Hexanucleotide Expansions Forms Toxic Amyloids Possessing Cell-to-Cell Transmission Properties. *The Journal of Biological Chemistry*, *291*(10), 4903–4911. https://doi.org/10.1074/jbc.M115.694273

Chen, Y., Lin, Z., Chen, X., Cao, B., Wei, Q., Ou, R., Zhao, B., Song, W., Wu, Y., & Shang, H.-F. (2016). Large C9orf72 repeat expansions are seen in Chinese patients with sporadic amyotrophic lateral sclerosis. *Neurobiology of Aging*, *38*, 217.e15-217.e22. https://doi.org/10.1016/J.NEUROBIOLAGING.2015.11.016

Cheng, W., Wang, S., Mestre, A. A., Fu, C., Makarem, A., Xian, F., Hayes, L. R., Lopez-Gonzalez, R., Drenner, K., Jiang, J., Cleveland, D. W., & Sun, S. (2018). C9ORF72 GGGGCC repeat-associated non-AUG translation is upregulated by stress through eIF2α phosphorylation. *Nature Communications*, *9*(1), 51. https://doi.org/10.1038/s41467-017-02495-z

Cheng, W., Wang, S., Zhang, Z., Morgens, D. W., Hayes, L. R., Lee, S., Portz, B., Xie, Y., Nguyen, B. V., Haney, M. S., Yan, S., Dong, D., Coyne, A. N., Yang, J., Xian, F., Cleveland, D. W., Qiu, Z., Rothstein, J. D., Shorter, J., … Sun, S. (2019). CRISPR-Cas9 Screens Identify the RNA Helicase DDX3X as a Repressor of C9ORF72 (GGGGCC)n Repeat-Associated Non-AUG Translation. *Neuron*, *104*(5), 885-898.e8. https://doi.org/10.1016/J.NEURON.2019.09.003

Chew, J., Cook, C., Gendron, T. F., Jansen-West, K., del Rosso, G., Daughrity, L. M., Castanedes-Casey, M., Kurti, A., Stankowski, J. N., Disney, M. D., Rothstein, J. D., Dickson, D. W., Fryer, J. D., Zhang, Y.-J., & Petrucelli, L. (2019). Aberrant deposition of stress granule-resident proteins linked to C9orf72-associated TDP-43 proteinopathy. *Molecular Neurodegeneration*, *14*(1), 9. https://doi.org/10.1186/s13024-019-0310-z

Chew, J., Gendron, T. F., Prudencio, M., Sasaguri, H., Zhang, Y.-J., Castanedes-Casey, M., Lee, C. W., Jansen-West, K., Kurti, A., Murray, M. E., Bieniek, K. F., Bauer, P. O., Whitelaw, E. C., Rousseau, L., Stankowski, J. N., Stetler, C., Daughrity, L. M., Perkerson, E. A., Desaro, P., … Petrucelli, L. (2015). C9ORF72 repeat expansions in mice cause TDP-43 pathology, neuronal loss, and behavioral deficits. *Science*, *348*(6239), 1151–1154. https://doi.org/10.1126/science.aaa9344

Chia, R., Chiò, A., & Traynor, B. J. (2018). Novel genes associated with amyotrophic lateral sclerosis: diagnostic and clinical implications. *The Lancet Neurology*, *17*(1), 94–102. https://doi.org/10.1016/S1474-4422(17)30401-5

Chiang, H., Terlecky, Plant, C., & Dice, J. (1989). A role for a 70-kilodalton heat shock protein in lysosomal degradation of intracellular proteins. *Science*, *246*(4928), 382–385. https://doi.org/10.1126/SCIENCE.2799391

Chiò, A., Logroscino, G., Traynor, B. J., Collins, J., Simeone, J. C., Goldstein, L. A., & White, L. A. (2013). Global Epidemiology of Amyotrophic Lateral Sclerosis: A Systematic Review of the Published Literature. *Neuroepidemiology*, *41*(2), 118–130. https://doi.org/10.1159/000351153

Choi, S. Y., Lopez-Gonzalez, R., Krishnan, G., Phillips, H. L., Li, A. N., Seeley, W. W., Yao, W.-D., Almeida, S., & Gao, F.-B. (2019). C9ORF72-ALS/FTD-associated poly(GR) binds Atp5a1 and compromises mitochondrial function in vivo. *Nature Neuroscience*, *22*(6), 851–862. https://doi.org/10.1038/s41593-019-0397-0

Ciura, S., Lattante, S., Le Ber, I., Latouche, M., Tostivint, H., Brice, A., & Kabashi, E. (2013). Loss of function of C9orf72 causes motor deficits in a zebrafish model of Amyotrophic Lateral Sclerosis. *Annals of Neurology*, *74*(2), n/a-n/a. https://doi.org/10.1002/ana.23946

Cleveland, D. W., & Rothstein, J. D. (2001). From Charcot to Lou Gehrig: deciphering selective motor neuron death in ALS. *Nature Reviews. Neuroscience*, *2*(11), 806–819. https://doi.org/10.1038/35097565

Coffee, B., Zhang, F., Warren, S. T., & Reines, D. (1999). Acetylated histones are associated with FMR1 in normal but not fragile X-syndrome cells. *Nature Genetics*, *22*(1), 98–101. https://doi.org/10.1038/8807

Colombrita, C., Zennaro, E., Fallini, C., Weber, M., Sommacal, A., Buratti, E., Silani, V., & Ratti, A. (2009). TDP-43 is recruited to stress granules in conditions of oxidative insult. *Journal of Neurochemistry*, *111*(4), 1051–1061. https://doi.org/10.1111/j.1471-4159.2009.06383.x

Cooper-Knock, J., Higginbottom, A., Stopford, M. J., Highley, J. R., Ince, P. G., Wharton, S.

B., Pickering-Brown, S., Kirby, J., Hautbergue, G. M., & Shaw, P. J. (2015). Antisense RNA foci in the motor neurons of C9ORF72-ALS patients are associated with TDP-43 proteinopathy. *Acta Neuropathologica*, *130*(1), 63–75. https://doi.org/10.1007/s00401-015-1429-9

Cooper-Knock, J., Walsh, M. J., Higginbottom, A., Robin Highley, J., Dickman, M. J., Edbauer, D., Ince, P. G., Wharton, S. B., Wilson, S. A., Kirby, J., Hautbergue, G. M., & Shaw, P. J. (2014). Sequestration of multiple RNA recognition motif-containing proteins by C9orf72 repeat expansions. *Brain*, *137*(7), 2040–2051. https://doi.org/10.1093/brain/awu120

Cooper, T. A., Wan, L., & Dreyfuss, G. (2009). RNA and Disease. *Cell*, *136*(4), 777–793. https://doi.org/10.1016/J.CELL.2009.02.011

Crawford, T. Q., & Roelink, H. (2007). The Notch response inhibitor DAPT enhances neuronal differentiation in embryonic stem cell-derived embryoid bodies independently of sonic hedgehog signaling. *Developmental Dynamics*, *236*(3), 886–892. https://doi.org/10.1002/dvdy.21083

Crippa, V., Cicardi, M. E., Ramesh, N., Seguin, S. J., Ganassi, M., Bigi, I., Diacci, C., Zelotti, E., Baratashvili, M., Gregory, J. M., Dobson, C. M., Cereda, C., Pandey, U. B., Poletti, A., & Carra, S. (2016). The chaperone HSPB8 reduces the accumulation of truncated TDP-43 species in cells and protects against TDP-43-mediated toxicity. *Human Molecular Genetics*, *25*(18), 3908–3924. https://doi.org/10.1093/hmg/ddw232

Crippa, V., D'Agostino, V. G., Cristofani, R., Rusmini, P., Cicardi, M. E., Messi, E., Loffredo, R., Pancher, M., Piccolella, M., Galbiati, M., Meroni, M., Cereda, C., Carra, S., Provenzani, A., & Poletti, A. (2016). Transcriptional induction of the heat shock protein B8 mediates the clearance of misfolded proteins responsible for motor neuron diseases. *Scientific Reports*, *6*(1), 22827. https://doi.org/10.1038/srep22827

Cristofani, R., Crippa, V., Vezzoli, G., Rusmini, P., Galbiati, M., Cicardi, M. E., Meroni, M., Ferrari, V., Tedesco, B., Piccolella, M., Messi, E., Carra, S., & Poletti, A. (2018). The small heat shock protein B8 (HSPB8) efficiently removes aggregating species of dipeptides produced in C9ORF72-related neurodegenerative diseases. *Cell Stress and Chaperones*, *23*(1), 1–12. https://doi.org/10.1007/s12192-017-0806-9

Cronin, S., Hardiman, O., & Traynor, B. J. (2007). Ethnic variation in the incidence of ALS: a systematic review. *Neurology*, *68*(13), 1002–1007. https://doi.org/10.1212/01.wnl.0000258551.96893.6f

Csordás, G., Várnai, P., Golenár, T., Roy, S., Purkins, G., Schneider, T. G., Balla, T., & Hajnóczky, G. (2010). Imaging Interorganelle Contacts and Local Calcium Dynamics at the ER-Mitochondrial Interface. *Molecular Cell*, *39*(1), 121–132. https://doi.org/10.1016/J.MOLCEL.2010.06.029

Cuervo, A. M., & Dice, J. F. (1996). A receptor for the selective uptake and degradation of proteins by lysosomes. *Science (New York, N.Y.)*, *273*(5274), 501–503. https://doi.org/10.1126/science.273.5274.501

Cuervo, A. M., & Dice, J. F. (2000a). Regulation of Lamp2a Levels in the Lysosomal Membrane. *Traffic*, *1*(7), 570–583. https://doi.org/10.1034/j.1600-0854.2000.010707.x

Cuervo, A. M., & Dice, J. F. (2000b). Age-related decline in chaperone-mediated autophagy. *The Journal of Biological Chemistry*, *275*(40), 31505–31513. https://doi.org/10.1074/jbc.M002102200

Cuervo, A. M., Knecht, E., Terlecky, S. R., & Dice, J. F. (1995). Activation of a selective pathway of lysosomal proteolysis in rat liver by prolonged starvation. *The American Journal of Physiology*, *269*(5 Pt 1), C1200-8. https://doi.org/10.1152/ajpcell.1995.269.5.C1200

Dafinca, R., Barbagallo, P., Farrimond, L., Candalija, A., Scaber, J., Ababneh, N. A., Sathyaprakash, C., Vowles, J., Cowley, S. A., & Talbot, K. (2020). Impairment of Mitochondrial Calcium Buffering Links Mutations in C9ORF72 and TARDBP in iPS-Derived Motor Neurons from Patients with ALS/FTD. *Stem Cell Reports*, *14*(5), 892–908. https://doi.org/10.1016/J.STEMCR.2020.03.023

Dafinca, R., Scaber, J., Ababneh, N., Lalic, T., Weir, G., Christian, H., Vowles, J., Douglas, A. G. L., Fletcher-Jones, A., Browne, C., Nakanishi, M., Turner, M. R., Wade-Martins, R., Cowley, S. A., & Talbot, K. (2016). C9orf72 Hexanucleotide Expansions are Associated with Altered ER Calcium Homeostasis and Stress Granule Formation in iPSC-Derived Neurons from Patients with Amyotrophic Lateral Sclerosis and Frontotemporal Dementia. *STEM CELLS*. https://doi.org/10.1002/stem.2388

Davidson, Y. S., Barker, H., Robinson, A. C., Thompson, J. C., Harris, J., Troakes, C., Smith, B., Al-Saraj, S., Shaw, C., Rollinson, S., Masuda-Suzukake, M., Hasegawa, M., Pickering-Brown, S., Snowden, J. S., & Mann, D. M. (2014). Brain distribution of dipeptide repeat proteins in frontotemporal lobar degeneration and motor neurone disease associated with expansions in C9ORF72. *Acta Neuropathologica Communications*, *2*(1), 70. https://doi.org/10.1186/2051-5960-2-70

Davidson, Y. S., Flood, L., Robinson, A. C., Nihei, Y., Mori, K., Rollinson, S., Richardson, A., Benson, B. C., Jones, M., Snowden, J. S., Pickering-Brown, S., Haass, C., Lashley, T., & Mann, D. M. A. (2017). Heterogeneous ribonuclear protein A3 (hnRNP A3) is present in dipeptide repeat protein containing inclusions in Frontotemporal Lobar Degeneration and Motor Neurone disease associated with expansions in C9orf72 gene. *Acta Neuropathologica Communications*, *5*(1), 31. https://doi.org/10.1186/s40478-017-0437-5

Davidson, Y. S., Robinson, A. C., Liu, X., Wu, D., Troakes, C., Rollinson, S., Masuda-Suzukake, M., Suzuki, G., Nonaka, T., Shi, J., Tian, J., Hamdalla, H., Ealing, J., Richardson, A., Jones, M., Pickering-Brown, S., Snowden, J. S., Hasegawa, M., & Mann, D. M. A. (2016). Neurodegeneration in frontotemporal lobar degeneration and motor neurone disease associated with expansions in C9orf72 is linked to TDP-43 pathology and not associated with aggregated forms of dipeptide repeat proteins. *Neuropathology and Applied Neurobiology*, *42*(3), 242–254. https://doi.org/10.1111/nan.12292

de Brito, O. M., & Scorrano, L. (2008). Mitofusin 2 tethers endoplasmic reticulum to mitochondria. *Nature*, *456*(7222), 605–610. https://doi.org/10.1038/nature07534

DeJesus-Hernandez, M., Finch, N. A., Wang, X., Gendron, T. F., Bieniek, K. F., Heckman, M. G., Vasilevich, A., Murray, M. E., Rousseau, L., Weesner, R., Lucido, A., Parsons, M., Chew, J., Josephs, K. A., Parisi, J. E., Knopman, D. S., Petersen, R. C., Boeve, B. F., Graff-Radford, N. R., … Rademakers, R. (2017). In-depth clinico-pathological examination of RNA foci in a large cohort of C9ORF72 expansion carriers. *Acta Neuropathologica*, *134*(2), 255–269. https://doi.org/10.1007/s00401-017-1725-7

DeJesus-Hernandez, M., Mackenzie, I. R., Boeve, B. F., Boxer, A. L., Baker, M., Rutherford, N. J., Nicholson, A. M., Finch, N. A., Flynn, H., Adamson, J., Kouri, N., Wojtas, A., Sengdy, P., Hsiung, G.-Y. R., Karydas, A., Seeley, W. W., Josephs, K. A., Coppola, G., Geschwind, D. H., … Rademakers, R. (2011). Expanded GGGGCC hexanucleotide repeat in noncoding region of C9ORF72 causes chromosome 9p-linked FTD and ALS. *Neuron*, *72*(2), 245–256. https://doi.org/10.1016/j.neuron.2011.09.011

Deng, H.-X., Chen, W., Hong, S.-T., Boycott, K. M., Gorrie, G. H., Siddique, N., Yang, Y., Fecto, F., Shi, Y., Zhai, H., Jiang, H., Hirano, M., Rampersaud, E., Jansen, G. H., Donkervoort, S., Bigio, E. H., Brooks, B. R., Ajroud, K., Sufit, R. L., … Siddique, T. (2011). Mutations in UBQLN2 cause dominant X-linked juvenile and adult-onset ALS and ALS/dementia. *Nature*, *477*(7363), 211–215. https://doi.org/10.1038/nature10353

Dharmadasa, T., & Kiernan, M. C. (2018). Riluzole, disease stage and survival in ALS. *The Lancet Neurology*, *17*(5), 385–386. https://doi.org/10.1016/S1474-4422(18)30091-7

Dohi, E., Tanaka, S., Seki, T., Miyagi, T., Hide, I., Takahashi, T., Matsumoto, M., & Sakai, N. (2012). Hypoxic stress activates chaperone-mediated autophagy and modulates neuronal cell survival. *Neurochemistry International*, *60*(4), 431–442. https://doi.org/10.1016/J.NEUINT.2012.01.020

Donnelly, C. J., Zhang, P.-W., Pham, J. T., Haeusler, A. R., Mistry, N. A., Vidensky, S., Daley, E. L., Poth, E. M., Hoover, B., Fines, D. M., Maragakis, N., Tienari, P. J., Petrucelli, L., Traynor, B. J., Wang, J., Rigo, F., Bennett, C. F., Blackshaw, S., Sattler, R., & Rothstein, J. D. (2013). RNA Toxicity from the ALS/FTD C9ORF72 Expansion Is Mitigated by Antisense Intervention. *Neuron*, *80*(2), 415–428. https://doi.org/10.1016/J.NEURON.2013.10.015

Eden, E. R. (2016). The formation and function of ER-endosome membrane contact sites. *Biochimica et Biophysica Acta (BBA) - Molecular and Cell Biology of Lipids*, *1861*(8), 874–879. https://doi.org/10.1016/J.BBALIP.2016.01.020

Ericson, J., Morton, S., Kawakami, A., Roelink, H., & Jessell, T. M. (1996). Two Critical Periods of Sonic Hedgehog Signaling Required for the Specification of Motor Neuron Identity. *Cell*, *87*(4), 661–673. https://doi.org/10.1016/S0092-8674(00)81386-0

Evans, C., & Holzbaur, E. (2019). Autophagy and mitophagy in ALS. *Neurobiology of Disease*, *122*, 35–40. https://doi.org/10.1016/J.NBD.2018.07.005

Fang, T., Al Khleifat, A., Meurgey, J.-H., Jones, A., Leigh, P. N., Bensimon, G., & Al-Chalabi, A. (2018). Stage at which riluzole treatment prolongs survival in patients with amyotrophic lateral sclerosis: a retrospective analysis of data from a dose-ranging study. *The Lancet Neurology*, *17*(5), 416–422. https://doi.org/10.1016/S1474-4422(18)30054-1

Farg, M. A., Konopka, A., Soo, K. Y., Ito, D., & Atkin, J. D. (2017). The DNA damage response (DDR) is induced by the C9orf72 repeat expansion in amyotrophic lateral sclerosis. *Human Molecular Genetics*, *26*(15), 2882–2896. https://doi.org/10.1093/hmg/ddx170

Fivenson, E. M., Lautrup, S., Sun, N., Scheibye-Knudsen, M., Stevnsner, T., Nilsen, H., Bohr, V. A., & Fang, E. F. (2017). Mitophagy in neurodegeneration and aging. *Neurochemistry International*, *109*, 202–209. https://doi.org/10.1016/J.NEUINT.2017.02.007

Floeter, M. K., & Gendron, T. F. (2018). Biomarkers for Amyotrophic Lateral Sclerosis and Frontotemporal Dementia Associated With Hexanucleotide Expansion Mutations in C9orf72. *Frontiers in Neurology*, *9*, 1063. https://doi.org/10.3389/fneur.2018.01063

Flores, B. N., Dulchavsky, M. E., Krans, A., Sawaya, M. R., Paulson, H. L., Todd, P. K., Barmada, S. J., & Ivanova, M. I. (2016). Distinct C9orf72-Associated Dipeptide Repeat Structures Correlate with Neuronal Toxicity. *PLOS ONE*, *11*(10), e0165084. https://doi.org/10.1371/journal.pone.0165084

Fomin, V., Richard, P., Hoque, M., Li, C., Gu, Z., Fissore-O'Leary, M., Tian, B., Prives, C.,

& Manley, J. L. (2018). The C9ORF72 Gene, Implicated in Amyotrophic Lateral Sclerosis and Frontotemporal Dementia, Encodes a Protein That Functions in Control of Endothelin and Glutamate Signaling. *Molecular and Cellular Biology*, *38*(22), e00155-18. https://doi.org/10.1128/MCB.00155-18

Foster, L. A., & Salajegheh, M. K. (2019). Motor Neuron Disease: Pathophysiology, Diagnosis, and Management. *The American Journal of Medicine*, *132*(1), 32–37. https://doi.org/10.1016/J.AMJMED.2018.07.012

Fratta, P., Mizielinska, S., Nicoll, A. J., Zloh, M., Fisher, E. M. C., Parkinson, G., & Isaacs, A. M. (2012). C9orf72 hexanucleotide repeat associated with amyotrophic lateral sclerosis and frontotemporal dementia forms RNA G-quadruplexes. *Scientific Reports*, *2*(1), 1016. https://doi.org/10.1038/srep01016

Fred Dice, J. (1990). Peptide sequences that target cytosolic proteins for lysosomal proteolysis. *Trends in Biochemical Sciences*, *15*(8), 305–309. https://doi.org/10.1016/0968-0004(90)90019-8

Freibaum, B. D., Lu, Y., Lopez-Gonzalez, R., Kim, N. C., Almeida, S., Lee, K.-H., Badders, N., Valentine, M., Miller, B. L., Wong, P. C., Petrucelli, L., Kim, H. J., Gao, F.-B., & Taylor, J. P. (2015). GGGGCC repeat expansion in C9orf72 compromises nucleocytoplasmic transport. *Nature*, *525*(7567), 129–133. https://doi.org/10.1038/nature14974

Freibaum, B. D., & Taylor, J. P. (2017). The Role of Dipeptide Repeats in C9ORF72-Related ALS-FTD. *Frontiers in Molecular Neuroscience*, *10*, 35. https://doi.org/10.3389/fnmol.2017.00035

Frick, P., Sellier, C., Mackenzie, I. R. A., Cheng, C.-Y., Tahraoui-Bories, J., Martinat, C., Pasterkamp, R. J., Prudlo, J., Edbauer, D., Oulad-Abdelghani, M., Feederle, R., Charlet-Berguerand, N., & Neumann, M. (2018). Novel antibodies reveal presynaptic localization of C9orf72 protein and reduced protein levels in C9orf72 mutation carriers. *Acta Neuropathologica Communications*, *6*(1), 72. https://doi.org/10.1186/s40478-018-0579-0

Fuentealba, R. A., Udan, M., Bell, S., Wegorzewska, I., Shao, J., Diamond, M. I., Weihl, C. C., & Baloh, R. H. (2010). Interaction with Polyglutamine Aggregates Reveals a Q/N-rich Domain in TDP-43. *Journal of Biological Chemistry*, *285*(34), 26304–26314. https://doi.org/10.1074/JBC.M110.125039

Fuertes, G., De Llano, J. J. M., Villarroya, A., Rivett, A. J., & Knechet, E. (2003). Changes in the proteolytic activities of proteasomes and lysosomes in human fibroblasts produced by serum withdrawal, amino-acid deprivation and confluent conditions. *Biochemical Journal*, *375*(1), 75–86. https://doi.org/10.1042/bj20030282

Gallego-Iradi, M. C., Clare, A. M., Brown, H. H., Janus, C., Lewis, J., & Borchelt, D. R. (2015). Subcellular Localization of Matrin 3 Containing Mutations Associated with ALS and Distal Myopathy. *PLOS ONE*, *10*(11), e0142144. https://doi.org/10.1371/journal.pone.0142144

Gami, P., Murray, C., Schottlaender, L., Bettencourt, C., De Pablo Fernandez, E., Mudanohwo, E., Mizielinska, S., Polke, J. M., Holton, J. L., Isaacs, A. M., Houlden, H., Revesz, T., & Lashley, T. (2015). A 30-unit hexanucleotide repeat expansion in C9orf72 induces pathological lesions with dipeptide-repeat proteins and RNA foci, but not TDP-43 inclusions and clinical disease. *Acta Neuropathologica*, *130*(4), 599–601. https://doi.org/10.1007/s00401-015-1473-5

Gao, J., Wang, L., Huntley, M. L., Perry, G., & Wang, X. (2018). Pathomechanisms of TDP-

43 in neurodegeneration. *Journal of Neurochemistry*, *146*(1), 7–20. https://doi.org/10.1111/jnc.14327

Gendreau, K. L., & Hall, G. F. (2013). Tangles, Toxicity, and Tau Secretion in AD – New Approaches to a Vexing Problem. *Frontiers in Neurology*, *4*, 160. https://doi.org/10.3389/fneur.2013.00160

Gendron, T. F., Bieniek, K. F., Zhang, Y. J., Jansen-West, K., Ash, P. E. A., Caulfield, T., Daughrity, L., Dunmore, J. H., Castanedes-Casey, M., Chew, J., Cosio, D. M., Van Blitterswijk, M., Lee, W. C., Rademakers, R., Boylan, K. B., Dickson, D. W., & Petrucelli, L. (2013). Antisense transcripts of the expanded C9ORF72 hexanucleotide repeat form nuclear RNA foci and undergo repeat-associated non-ATG translation in c9FTD/ALS. *Acta Neuropathologica*, *126*(6), 829–844. https://link.springer.com/article/10.1007/s00401-013-1192-8

Gendron, T. F., Chew, J., Stankowski, J. N., Hayes, L. R., Zhang, Y.-J., Prudencio, M., Carlomagno, Y., Daughrity, L. M., Jansen-West, K., Perkerson, E. A., O'Raw, A., Cook, C., Pregent, L., Belzil, V., van Blitterswijk, M., Tabassian, L. J., Lee, C. W., Yue, M., Tong, J., … Petrucelli, L. (2017). Poly(GP) proteins are a useful pharmacodynamic marker for C9ORF72-associated amyotrophic lateral sclerosis. *Science Translational Medicine*, *9*(383). http://stm.sciencemag.org/content/9/383/eaai7866.short

Gittings, L. M., Boeynaems, S., Lightwood, D., Clargo, A., Topia, S., Nakayama, L., Troakes, C., Mann, D. M. A., Gitler, A. D., Lashley, T., & Isaacs, A. M. (2020). Symmetric dimethylation of poly-GR correlates with disease duration in C9orf72 FTLD and ALS and reduces poly-GR phase separation and toxicity. *Acta Neuropathologica*, *139*(2), 407–410. https://doi.org/10.1007/s00401-019-02104-x

Gomez-Deza, J., Lee, Y., Troakes, C., Nolan, M., Al-Sarraj, S., Gallo, J.-M., & Shaw, C. E. (2015). Dipeptide repeat protein inclusions are rare in the spinal cord and almost absent from motor neurons in C9ORF72 mutant amyotrophic lateral sclerosis and are unlikely to cause their degeneration. *Acta Neuropathologica Communications*, *3*(1), 38. https://doi.org/10.1186/s40478-015-0218-y

Goodman, L. D., Prudencio, M., Kramer, N. J., Martinez-Ramirez, L. F., Srinivasan, A. R., Lan, M., Parisi, M. J., Zhu, Y., Chew, J., Cook, C. N., Berson, A., Gitler, A. D., Petrucelli, L., & Bonini, N. M. (2019). Toxic expanded GGGGCC repeat transcription is mediated by the PAF1 complex in C9orf72-associated FTD. *Nature Neuroscience*, *22*(6), 863–874. https://doi.org/10.1038/s41593-019-0396-1

Goodman, L. D., Prudencio, M., Srinivasan, A. R., Rifai, O. M., Lee, V. M.-Y., Petrucelli, L., & Bonini, N. M. (2019). eIF4B and eIF4H mediate GR production from expanded G4C2 in a Drosophila model for C9orf72-associated ALS. *Acta Neuropathologica Communications*, *7*(1), 62. https://doi.org/10.1186/s40478-019-0711-9

Goodwin, M., & Swanson, M. S. (2014). *RNA-Binding Protein Misregulation in Microsatellite Expansion Disorders* (pp. 353–388). Springer, New York, NY. https://doi.org/10.1007/978-1-4939-1221-6_10

Gossen, M., & Bujard, H. (1992). Tight control of gene expression in mammalian cells by tetracycline-responsive promoters. *Proceedings of the National Academy of Sciences*, *89*(12), 5547–5551. https://doi.org/10.1073/pnas.89.12.5547

Gossen, M., Freundlieb, S., Bender, G., Müller, G., Hillen, W., & Bujard, H. (1995). Transcriptional activation by tetracyclines in mammalian cells. *Science*, *268*(5218), 1766–1769.

Gouti, M., Tsakiridis, A., Wymeersch, F. J., Huang, Y., Kleinjung, J., Wilson, V., & Briscoe, J. (2014). In Vitro Generation of Neuromesodermal Progenitors Reveals Distinct Roles for Wnt Signalling in the Specification of Spinal Cord and Paraxial Mesoderm Identity. *PLoS Biology*, *12*(8), e1001937. https://doi.org/10.1371/journal.pbio.1001937

Green, K. M., Glineburg, M. R., Kearse, M. G., Flores, B. N., Linsalata, A. E., Fedak, S. J., Goldstrohm, A. C., Barmada, S. J., & Todd, P. K. (2017). RAN translation at C9orf72-associated repeat expansions is selectively enhanced by the integrated stress response. *Nature Communications*, *8*(1), 2005. https://doi.org/10.1038/s41467-017-02200-0

Gregory, J. M., Livesey, M. R., McDade, K., Selvaraj, B. T., Barton, S. K., Chandran, S., & Smith, C. (2020). Dysregulation of AMPA receptor subunit expression in sporadic ALS post-mortem brain. *The Journal of Pathology*, *250*(1), 67–78. https://doi.org/10.1002/path.5351

Guerrero, E. N., Wang, H., Mitra, J., Hegde, P. M., Stowell, S. E., Liachko, N. F., Kraemer, B. C., Garruto, R. M., Rao, K. S., & Hegde, M. L. (2016). TDP-43/FUS in motor neuron disease: Complexity and challenges. *Progress in Neurobiology*, *145–146*, 78–97. https://doi.org/10.1016/J.PNEUROBIO.2016.09.004

Guo, Q., Lehmer, C., Martínez-Sánchez, A., Rudack, T., Beck, F., Hartmann, H., Pérez-Berlanga, M., Frottin, F., Hipp, M. S., Hartl, F. U., Edbauer, D., Baumeister, W., & Fernández-Busnadiego, R. (2018). In Situ Structure of Neuronal C9orf72 Poly-GA Aggregates Reveals Proteasome Recruitment. *Cell*, *172*(4), 696-705.e12. https://doi.org/10.1016/j.cell.2017.12.030

Gupta, R., Lan, M., Mojsilovic-Petrovic, J., Choi, W. H., Safren, N., Barmada, S., Lee, M. J., & Kalb, R. (2017). The Proline/Arginine Dipeptide from Hexanucleotide Repeat Expanded C9ORF72 Inhibits the Proteasome. *ENeuro*, *4*(1). https://doi.org/10.1523/ENEURO.0249-16.2017

Gurney, M., Pu, H., Chiu, A., Canto, M. D., Polchow, C., Alexander, D., Caliendo, J., Hentati, A., Kwon, Y., Deng, H., & et, al. (1994). Motor neuron degeneration in mice that express a human Cu,Zn superoxide dismutase mutation. *Science*, *261*(5124), 1047–1051. https://doi.org/10.1126/science.8351519

Haas, I., & Wabl, M. (1983). Immunoglobulin Heavy Chain Binding Protein. *Nature*, *306*(5941). https://doi.org/10.1038/306387A0

Haeusler, A. R., Donnelly, C. J., Periz, G., Simko, E. A. J., Shaw, P. G., Kim, M.-S., Maragakis, N. J., Troncoso, J. C., Pandey, A., Sattler, R., Rothstein, J. D., & Wang, J. (2014). C9orf72 nucleotide repeat structures initiate molecular cascades of disease. *Nature*, *507*(7491), 195–200. https://doi.org/10.1038/nature13124

Hall, C. E., Yao, Z., Choi, M., Tyzack, G. E., Serio, A., Luisier, R., Harley, J., Preza, E., Arber, C., Crisp, S. J., Watson, P. M. D., Kullmann, D. M., Abramov, A. Y., Wray, S., Burley, R., Loh, S. H. Y., Martins, L. M., Stevens, M. M., Luscombe, N. M., … Patani, R. (2017). Progressive Motor Neuron Pathology and the Role of Astrocytes in a Human Stem Cell Model of VCP-Related ALS. *Cell Reports*, *19*(9), 1739–1749. https://doi.org/10.1016/J.CELREP.2017.05.024

Han, Q., Deng, Y., Chen, S., Chen, R., Yang, M., Zhang, Z., Sun, X., Wang, W., He, Y., Wang, F., Pan, X., Li, P., Lai, W., Luo, H., Huang, P., Guan, X., Deng, Y., Yan, J., Xu, X., … Li, S. (2017). Downregulation of ATG5-dependent macroautophagy by chaperone-mediated autophagy promotes breast cancer cell metastasis. *Scientific Reports*, *7*(1), 4759. https://doi.org/10.1038/s41598-017-04994-x

Harrison, A. F., & Shorter, J. (2017). RNA-binding proteins with prion-like domains in health and disease. *Biochemical Journal*, *474*(8), 1417–1438. https://doi.org/10.1042/BCJ20160499

Heath, P. R., & Shaw, P. J. (2002). Update on the glutamatergic neurotransmitter system and the role of excitotoxicity in amyotrophic lateral sclerosis. *Muscle & Nerve*, *26*(4), 438–458. https://doi.org/10.1002/mus.10186

Herranz-Martin, S., Chandran, J., Lewis, K., Mulcahy, P., Higginbottom, A., Walker, C., Valenzuela, I. M.-P. Y., Jones, R. A., Coldicott, I., Iannitti, T., Akaaboune, M., El-Khamisy, S. F., Gillingwater, T. H., Shaw, P. J., & Azzouz, M. (2017). Viral delivery of C9orf72 hexanucleotide repeat expansions in mice leads to repeat-length-dependent neuropathology and behavioural deficits. *Disease Models & Mechanisms*, *10*(7), 859–868. https://doi.org/10.1242/dmm.029892

Herrington, J., Park, Y. B., Babcock, D. F., & Hille, B. (1996). Dominant Role of Mitochondria in Clearance of Large Ca2+ Loads from Rat Adrenal Chromaffin Cells. *Neuron*, *16*(1), 219–228. https://doi.org/10.1016/S0896-6273(00)80038-0

Hetz, C., & Saxena, S. (2017). ER stress and the unfolded protein response in neurodegeneration. *Nature Reviews Neurology*, *13*(8), 477–491. https://doi.org/10.1038/nrneurol.2017.99

Higashi, S., Tsuchiya, Y., Araki, T., Wada, K., & Kabuta, T. (2010). TDP-43 physically interacts with amyotrophic lateral sclerosis-linked mutant CuZn superoxide dismutase. *Neurochemistry International*, *57*(8), 906–913. https://doi.org/10.1016/J.NEUINT.2010.09.010

Ho, Y. S., Gargano, M., Cao, J., Bronson, R. T., Heimler, I., & Hutz, R. J. (1998). Reduced fertility in female mice lacking copper-zinc superoxide dismutase. *The Journal of Biological Chemistry*, *273*(13), 7765–7769. https://doi.org/10.1074/jbc.273.13.7765

Hsiung, G.-Y. R., DeJesus-Hernandez, M., Feldman, H. H., Sengdy, P., Bouchard-Kerr, P., Dwosh, E., Butler, R., Leung, B., Fok, A., Rutherford, N. J., Baker, M., Rademakers, R., & Mackenzie, I. R. A. (2012). Clinical and pathological features of familial frontotemporal dementia caused by C9ORF72 mutation on chromosome 9p. *Brain*, *135*(3), 709–722. https://doi.org/10.1093/brain/awr354

Hu, J., Liu, J., Li, L., Gagnon, K. T., & Corey, D. R. (2015). Engineering Duplex RNAs for Challenging Targets: Recognition of GGGGCC/CCCCGG Repeats at the ALS/FTD C9orf72 Locus. *Chemistry & Biology*, *22*(11), 1505–1511. https://doi.org/10.1016/J.CHEMBIOL.2015.09.016

Hu, J., Rigo, F., Prakash, T. P., & Corey, D. R. (2016). Recognition of *c9orf72* Mutant RNA by Single-Stranded Silencing RNAs. *Nucleic Acid Therapeutics*, nat.2016.0655. https://doi.org/10.1089/nat.2016.0655

Issa, A.-R., Sun, J., Petitgas, C., Mesquita, A., Dulac, A., Robin, M., Mollereau, B., Jenny, A., Chérif-Zahar, B., & Birman, S. (2018). The lysosomal membrane protein LAMP2A promotes autophagic flux and prevents SNCA-induced Parkinson disease-like symptoms in the *Drosophila* brain. *Autophagy*, *14*(11), 1898–1910. https://doi.org/10.1080/15548627.2018.1491489

Ito, H., Wate, R., Zhang, J., Ohnishi, S., Kaneko, S., Ito, H., Nakano, S., & Kusaka, H. (2008). Treatment with edaravone, initiated at symptom onset, slows motor decline and decreases SOD1 deposition in ALS mice. *Experimental Neurology*, *213*(2), 448–455.

https://doi.org/10.1016/J.EXPNEUROL.2008.07.017

Iwata, J., Ezaki, J., Komatsu, M., Yokota, S., Ueno, T., Tanida, I., Chiba, T., Tanaka, K., & Kominami, E. (2006). Excess Peroxisomes Are Degraded by Autophagic Machinery in Mammals. *Journal of Biological Chemistry*, *281*(7), 4035–4041. https://doi.org/10.1074/JBC.M512283200

Jaarsma, D., Haasdijk, E. D., Grashorn, J. A. C., Hawkins, R., van Duijn, W., Verspaget, H. W., London, J., & Holstege, J. C. (2000). Human Cu/Zn Superoxide Dismutase (SOD1) Overexpression in Mice Causes Mitochondrial Vacuolization, Axonal Degeneration, and Premature Motoneuron Death and Accelerates Motoneuron Disease in Mice Expressing a Familial Amyotrophic Lateral Sclerosis Mutant SOD1. *Neurobiology of Disease*, *7*(6), 623–643. https://doi.org/10.1006/NBDI.2000.0299

Jiang, J., Zhu, Q., Gendron, T. F., Saberi, S., McAlonis-Downes, M., Seelman, A., Stauffer, J. E., Jafar-nejad, P., Drenner, K., Schulte, D., Chun, S., Sun, S., Ling, S.-C., Myers, B., Engelhardt, J., Katz, M., Baughn, M., Platoshyn, O., Marsala, M., … Lagier-Tourenne, C. (2016). Gain of Toxicity from ALS/FTD-Linked Repeat Expansions in C9ORF72 Is Alleviated by Antisense Oligonucleotides Targeting GGGGCC-Containing RNAs. *Neuron*, *90*(3), 535–550. https://doi.org/10.1016/J.NEURON.2016.04.006

Johnson, A. G., Flynn, R. A., Lapointe, C. P., Ooi, Y. S., Zhao, M. L., Richards, C. M., Qiao, W., Yamada, S. B., Couthouis, J., Gitler, A. D., Carette, J. E., & Puglisi, J. D. (2020). A memory of eS25 loss drives resistance phenotypes. *Nucleic Acids Research*, *48*(13), 7279–7297. https://doi.org/10.1093/nar/gkaa444

Johnson, J., Mandrioli, J., Benatar, M., Abramzon, Y., Van Deerlin, V., Trojanowski, J., Gibbs, J., Brunetti, M., Gronka, S., Wuu, J., Ding, J., McCluskey, L., Martinez-Lage, M., Falcone, D., Hernandez, D., Arepalli, S., Chong, S., Schymick, J., Rothstein, J., … Traynor, B. (2010). Exome Sequencing Reveals VCP Mutations as a Cause of Familial ALS. *Neuron*, *68*(5), 857–864. https://doi.org/10.1016/J.NEURON.2010.11.036

Johnson, J., Pioro, E., Boehringer, A., Chia, R., Feit, H., Renton, A., Pliner, H., Abramzon, Y., Marangi, G., Winborn, B., Gibbs, J., Nalls, M., Morgan, S., Shoai, M., Hardy, J., Pittman, A., Orrell, R., Malaspina, A., Sidle, K., … Traynor, B. (2014). Mutations in the Matrin 3 gene cause familial amyotrophic lateral sclerosis. *Nature Neuroscience*, *17*(5), 664–666. https://doi.org/10.1038/nn.3688

Johri, A., Chandra, A., & Flint Beal, M. (2013). PGC-1α, mitochondrial dysfunction, and Huntington's disease. *Free Radical Biology and Medicine*, *62*, 37–46. https://doi.org/10.1016/J.FREERADBIOMED.2013.04.016

Jovičić, A., Mertens, J., Boeynaems, S., Bogaert, E., Chai, N., Yamada, S. B., Paul, J. W., Sun, S., Herdy, J. R., Bieri, G., Kramer, N. J., Gage, F. H., Van Den Bosch, L., Robberecht, W., & Gitler, A. D. (2015). Modifiers of C9orf72 dipeptide repeat toxicity connect nucleocytoplasmic transport defects to FTD/ALS. *Nature Neuroscience*, *18*(9), 1226–1229. https://doi.org/10.1038/nn.4085

Jung, J., & Behrends, C. (2020). Multifaceted role of SMCR8 as autophagy regulator. *Small GTPases*, *11*(1), 53–61. https://doi.org/10.1080/21541248.2017.1346553

Kabashi, E., Bercier, V., Lissouba, A., Liao, M., Brustein, E., Rouleau, G. A., & Drapeau, P. (2011). FUS and TARDBP but Not SOD1 Interact in Genetic Models of Amyotrophic Lateral Sclerosis. *PLoS Genetics*, *7*(8). https://doi.org/10.1371/JOURNAL.PGEN.1002214

Kabashi, E., Lin, L., Tradewell, M. L., Dion, P. A., Bercier, V., Bourgouin, P., Rochefort, D.,

Bel Hadj, S., Durham, H. D., Velde, C. Vande, Rouleau, G. A., & Drapeau, P. (2010). Gain and loss of function of ALS-related mutations of TARDBP (TDP-43) cause motor deficits in vivo. *Human Molecular Genetics*, *19*(4), 671–683. https://doi.org/10.1093/hmg/ddp534

Kanekura, K., Harada, Y., Fujimoto, M., Yagi, T., Hayamizu, Y., Nagaoka, K., & Kuroda, M. (2018). Characterization of membrane penetration and cytotoxicity of C9orf72-encoding arginine-rich dipeptides. *Scientific Reports*, *8*(1), 12740. https://doi.org/10.1038/s41598-018-31096-z

Kanekura, K., Yagi, T., Cammack, A. J., Mahadevan, J., Kuroda, M., Harms, M. B., Miller, T. M., & Urano, F. (2016). Poly-dipeptides encoded by the C9ORF72 repeats block global protein translation. *Human Molecular Genetics*, *25*(9), 1803–1813. https://doi.org/10.1093/hmg/ddw052

Kaushik, S., & Cuervo, A. M. (2016). **AMPK-dependent phosphorylation of lipid droplet protein PLIN2 triggers its degradation by CMA**. *Autophagy*, *12*(2), 432–438. https://doi.org/10.1080/15548627.2015.1124226

Kaushik, S., & Cuervo, A. M. (2018). The coming of age of chaperone-mediated autophagy. *Nature Reviews Molecular Cell Biology*, *19*(6), 365–381. https://doi.org/10.1038/s41580-018-0001-6

Khosravi, B., Hartmann, H., May, S., Möhl, C., Ederle, H., Michaelsen, M., Schludi, M. H., Dormann, D., & Edbauer, D. (2016). Cytoplasmic poly-GA aggregates impair nuclear import of TDP-43 in C9orf72 ALS/FTLD. *Human Molecular Genetics*, *26*(4), 790–800. https://doi.org/10.1093/hmg/ddw432

Khosravi, B., LaClair, K. D., Riemenschneider, H., Zhou, Q., Frottin, F., Mareljic, N., Czuppa, M., Farny, D., Hartmann, H., Michaelsen, M., Arzberger, T., Hartl, F. U., Hipp, M. S., & Edbauer, D. (2020). Cell-to-cell transmission of C9orf72 poly-(Gly-Ala) triggers key features of ALS/FTD. *The EMBO Journal*, *39*(8), e102811. https://doi.org/10.15252/embj.2019102811

Kiernan, M. C., Vucic, S., Cheah, B. C., Turner, M. R., Eisen, A., Hardiman, O., Burrell, J. R., & Zoing, M. C. (2011). Amyotrophic lateral sclerosis. *The Lancet*, *377*(9769), 942–955. https://doi.org/10.1016/S0140-6736(10)61156-7

Kiffin, R., Christian, C., Knecht, E., & Cuervo, A. M. (2004). Activation of Chaperone-mediated Autophagy during Oxidative Stress. *Molecular Biology of the Cell*, *15*(11), 4829–4840. https://doi.org/10.1091/mbc.e04-06-0477

Kim, S. H., Shanware, N. P., Bowler, M. J., & Tibbetts, R. S. (2010). Amyotrophic Lateral Sclerosis-associated Proteins TDP-43 and FUS/TLS Function in a Common Biochemical Complex to Co-regulate HDAC6 mRNA. *Journal of Biological Chemistry*, *285*(44), 34097–34105. https://doi.org/10.1074/JBC.M110.154831

Klim, J. R., Williams, L. A., Limone, F., Guerra San Juan, I., Davis-Dusenbery, B. N., Mordes, D. A., Burberry, A., Steinbaugh, M. J., Gamage, K. K., Kirchner, R., Moccia, R., Cassel, S. H., Chen, K., Wainger, B. J., Woolf, C. J., & Eggan, K. (2019). ALS-implicated protein TDP-43 sustains levels of STMN2, a mediator of motor neuron growth and repair. *Nature Neuroscience*, *22*(2), 167–179. https://doi.org/10.1038/s41593-018-0300-4

Klockgether, T., Mariotti, C., & Paulson, H. L. (2019). Spinocerebellar ataxia. *Nature Reviews Disease Primers*, *5*(1), 24. https://doi.org/10.1038/s41572-019-0074-3

Kochetov, A. V, Palyanov, A., Titov, I. I., Grigorovich, D., Sarai, A., & Kolchanov, N. A.

(2007). AUG_hairpin: prediction of a downstream secondary structure influencing the recognition of a translation start site. *BMC Bioinformatics*, *8*(1), 318. https://doi.org/10.1186/1471-2105-8-318

Koga, H., Martinez-Vicente, M., Macian, F., Verkhusha, V. V., & Cuervo, A. M. (2011). A photoconvertible fluorescent reporter to track chaperone-mediated autophagy. *Nature Communications*, *2*(1), 386. https://doi.org/10.1038/ncomms1393

Kondo, T., Reaume, A. G., Huang, T. T., Carlson, E., Murakami, K., Chen, S. F., Hoffman, E. K., Scott, R. W., Epstein, C. J., & Chan, P. H. (1997). Reduction of CuZn-superoxide dismutase activity exacerbates neuronal cell injury and edema formation after transient focal cerebral ischemia. *The Journal of Neuroscience : The Official Journal of the Society for Neuroscience*, *17*(11), 4180–4189. https://doi.org/10.1523/JNEUROSCI.17-11-04180.1997

Konno, T., Tada, M., Shiga, A., Tsujino, A., Eguchi, H., Masuda-Suzukake, M., Hasegawa, M., Nishizawa, M., Onodera, O., Kakita, A., & Takahashi, H. (2014). *C9ORF72* repeat-associated non-ATG-translated polypeptides are distributed independently of TDP-43 in a Japanese patient with c9ALS. *Neuropathology and Applied Neurobiology*, *40*(6), 783–788. https://doi.org/10.1111/nan.12157

Koppers, M., Blokhuis, A. M., Westeneng, H.-J., Terpstra, M. L., Zundel, C. A. C., Vieira de Sá, R., Schellevis, R. D., Waite, A. J., Blake, D. J., Veldink, J. H., van den Berg, L. H., & Pasterkamp, R. J. (2015). C9orf72 ablation in mice does not cause motor neuron degeneration or motor deficits. *Annals of Neurology*, *78*(3), 426–438. https://doi.org/10.1002/ana.24453

Koren, E., Apte, A., Sawant, R. R., Grunwald, J., & Torchilin, V. P. (2011). Cell-penetrating TAT peptide in drug delivery systems: Proteolytic stability requirements. *Drug Delivery*, *18*(5), 377–384. https://doi.org/10.3109/10717544.2011.567310

Kozak, M. (1989). Context effects and inefficient initiation at non-AUG codons in eucaryotic cell-free translation systems. *Molecular and Cellular Biology*, *9*(11), 5073–5080. https://doi.org/10.1128/mcb.9.11.5073

Kramer, N. J., Carlomagno, Y., Zhang, Y.-J., Almeida, S., Cook, C. N., Gendron, T. F., Prudencio, M., Van Blitterswijk, M., Belzil, V., Couthouis, J., Paul, J. W., Goodman, L. D., Daughrity, L., Chew, J., Garrett, A., Pregent, L., Jansen-West, K., Tabassian, L. J., Rademakers, R., … Gitler, A. D. (2016). Spt4 selectively regulates the expression of C9orf72 sense and antisense mutant transcripts. *Science (New York, N.Y.)*, *353*(6300), 708–712. https://doi.org/10.1126/science.aaf7791

Kramer, N. J., Haney, M. S., Morgens, D. W., Jovičić, A., Couthouis, J., Li, A., Ousey, J., Ma, R., Bieri, G., Tsui, C. K., Shi, Y., Hertz, N. T., Tessier-Lavigne, M., Ichida, J. K., Bassik, M. C., & Gitler, A. D. (2018). CRISPR–Cas9 screens in human cells and primary neurons identify modifiers of C9ORF72 dipeptide-repeat-protein toxicity. *Nature Genetics*, *50*(4), 603–612. https://doi.org/10.1038/s41588-018-0070-7

Krebs, J., Agellon, L. B., & Michalak, M. (2015). Ca2+ homeostasis and endoplasmic reticulum (ER) stress: An integrated view of calcium signaling. *Biochemical and Biophysical Research Communications*, *460*(1), 114–121. https://doi.org/10.1016/J.BBRC.2015.02.004

Kwiatkowski, T. J., Bosco, D. A., Leclerc, A. L., Tamrazian, E., Vanderburg, C. R., Russ, C., Davis, A., Gilchrist, J., Kasarskis, E. J., Munsat, T., Valdmanis, P., Rouleau, G. A., Hosler, B. A., Cortelli, P., de Jong, P. J., Yoshinaga, Y., Haines, J. L., Pericak-Vance, M. A., Yan, J., … Brown, R. H. (2009). Mutations in the FUS/TLS gene on chromosome 16 cause familial amyotrophic lateral sclerosis. *Science (New York, N.Y.)*, *323*(5918), 1205–1208.

https://doi.org/10.1126/science.1166066

Kwon, I., Xiang, S., Kato, M., Wu, L., Theodoropoulos, P., Wang, T., Kim, J., Yun, J., Xie, Y., & McKnight, S. L. (2014). Poly-dipeptides encoded by the C9orf72 repeats bind nucleoli, impede RNA biogenesis, and kill cells. *Science*, *345*(6201).

Lagier-Tourenne, C., Baughn, M., Rigo, F., Sun, S., Liu, P., Li, H.-R., Jiang, J., Watt, A. T., Chun, S., Katz, M., Qiu, J., Sun, Y., Ling, S.-C., Zhu, Q., Polymenidou, M., Drenner, K., Artates, J. W., McAlonis-Downes, M., Markmiller, S., … Ravits, J. (2013). Targeted degradation of sense and antisense C9orf72 RNA foci as therapy for ALS and frontotemporal degeneration. *Proceedings of the National Academy of Sciences of the United States of America*, *110*(47), E4530-9. https://doi.org/10.1073/pnas.1318835110

Lee, K., Zhang, P., Kim, H., Mitrea, D. M., Sarkar, M., Freibaum, B. D., Cika, J., Coughlin, M., Messing, J., Molliex, A., Maxwell, B. A., Kim, N. C., Temirov, J., Moore, J., Kolaitis, R.-M., Shaw, T. I., Bai, B., Peng, J., Kriwacki, R. W., & Taylor, J. P. (2016). C9orf72 Dipeptide Repeats Impair the Assembly, Dynamics, and Function of Membrane-Less Organelles. *Cell*, *167*(3), 774-788.e17. https://doi.org/10.1016/j.cell.2016.10.002

Lee, Y. B., Baskaran, P., Gomez-Deza, J., Chen, H. J., Nishimura, A. L., Smith, B. N., Troakes, C., Adachi, Y., Stepto, A., Petrucelli, L., Gallo, J.-M., Hirth, F., Rogelj, B., Guthrie, S., & Shaw, C. E. (2017). C9orf72 poly GA RAN-translated protein plays a key role in amyotrophic lateral sclerosis via aggregation and toxicity. *Human Molecular Genetics*. https://doi.org/10.1093/hmg/ddx350

Lee, Y. B., Chen, H. J., Peres, J. N., Gomez-Deza, J., Attig, J., Štalekar, M., Troakes, C., Nishimura, A. L., Scotter, E. L., Vance, C., Adachi, Y., Sardone, V., Miller, J. W., Smith, B. N., Gallo, J.-M., Ule, J., Hirth, F., Rogelj, B., Houart, C., … Shaw, C. E. (2013). Hexanucleotide Repeats in ALS/FTD Form Length-Dependent RNA Foci, Sequester RNA Binding Proteins, and Are Neurotoxic. *Cell Reports*, *5*(5), 1178–1186. https://doi.org/10.1016/j.celrep.2013.10.049

Lehmer, C., Oeckl, P., Weishaupt, J. H., Volk, A. E., Diehl-Schmid, J., Schroeter, M. L., Lauer, M., Kornhuber, J., Levin, J., Fassbender, K., Landwehrmeyer, B., Schludi, M. H., Arzberger, T., Kremmer, E., Flatley, A., Feederle, R., Steinacker, P., Weydt, P., Ludolph, A. C., … Otto, M. (2017). Poly-GP in cerebrospinal fluid links C9orf72 -associated dipeptide repeat expression to the asymptomatic phase of ALS/FTD. *EMBO Molecular Medicine*, e201607486. https://doi.org/10.15252/emmm.201607486

Leigh, P. N., Whitwell, H., Garofalo, O., Buller, J., Swash, M., Martin, J. E., Gallo, J.-M., Weller, R. O., & Anderton, B. H. (1991). Ubiquitin-immunoreactive intraneuronal inclusions in Amyotrophic Laterlar Sclerosis. *Brain*, *114*(2), 775–788. https://doi.org/10.1093/brain/114.2.775

Leskelä, S., Huber, N., Rostalski, H., Natunen, T., Remes, A. M., Takalo, M., Hiltunen, M., & Haapasalo, A. (2019). C9orf72 Proteins Regulate Autophagy and Undergo Autophagosomal or Proteasomal Degradation in a Cell Type-Dependent Manner. *Cells*, *8*(10), 1233. https://doi.org/10.3390/cells8101233

Levine, T. P., Daniels, R. D., Gatta, A. T., Wong, L. H., & Hayes, M. J. (2013). The product of C9orf72, a gene strongly implicated in neurodegeneration, is structurally related to DENN Rab-GEFs. *Bioinformatics (Oxford, England)*, *29*(4), 499–503. https://doi.org/10.1093/bioinformatics/bts725

Li, W., Zhu, J., Dou, J., She, H., Tao, K., Xu, H., Yang, Q., & Mao, Z. (2017). Phosphorylation of LAMP2A by p38 MAPK couples ER stress to chaperone-mediated

autophagy. *Nature Communications*, *8*(1), 1763. https://doi.org/10.1038/s41467-017-01609-x

Lin, Y., Mori, E., Kato, M., Xiang, S., Wu, L., Kwon, I., & McKnight, S. L. (2016). Toxic PR Poly-Dipeptides Encoded by the C9orf72 Repeat Expansion Target LC Domain Polymers. *Cell*, *167*(3), 789-802.e12. https://doi.org/10.1016/j.cell.2016.10.003

Liquori, C. L., Ricker, K., Moseley, M. L., Jacobsen, J. F., Kress, W., Naylor, S. L., Day, J. W., & Ranum, L. P. (2001). Myotonic dystrophy type 2 caused by a CCTG expansion in intron 1 of ZNF9. *Science (New York, N.Y.)*, *293*(5531), 864–867. https://doi.org/10.1126/science.1062125

Liu, J., Laufer, E., & Jessell, T. M. (2001). Assigning the Positional Identity of Spinal Motor Neurons: Rostrocaudal Patterning of Hox-c Expression by FGFs, Gdf11, and Retinoids. *Neuron*, *32*(6), 997–1012. https://doi.org/10.1016/S0896-6273(01)00544-X

Liu, Y., Pattamatta, A., Zu, T., Reid, T., Bardhi, O., Borchelt, D. R., Yachnis, A. T., & Ranum, L. P. W. (2016). C9orf72 BAC Mouse Model with Motor Deficits and Neurodegenerative Features of ALS/FTD. *Neuron*, *90*(3), 521–534. https://doi.org/10.1016/J.NEURON.2016.04.005

Logroscino, G., Traynor, B. J., Hardiman, O., Chiò, A., Mitchell, D., Swingler, R. J., Millul, A., Benn, E., Beghi, E., & EURALS, for. (2010). Incidence of amyotrophic lateral sclerosis in Europe. *Journal of Neurology, Neurosurgery, and Psychiatry*, *81*(4), 385–390. https://doi.org/10.1136/jnnp.2009.183525

López-Erauskin, J., Tadokoro, T., Baughn, M. W., Myers, B., McAlonis-Downes, M., Chillon-Marinas, C., Asiaban, J. N., Artates, J., Bui, A. T., Vetto, A. P., Lee, S. K., Le, A. V., Sun, Y., Jambeau, M., Boubaker, J., Swing, D., Qiu, J., Hicks, G. G., Ouyang, Z., … Da Cruz, S. (2018). ALS/FTD-Linked Mutation in FUS Suppresses Intra-axonal Protein Synthesis and Drives Disease Without Nuclear Loss-of-Function of FUS. *Neuron*, *100*(4), 816-830.e7. https://doi.org/10.1016/J.NEURON.2018.09.044

Lopez-Gonzalez, R., Lu, Y., Gendron, T. F., Karydas, A., Tran, H., Yang, D., Petrucelli, L., Miller, B. L., Almeida, S., & Gao, F.-B. (2016). Poly(GR) in C9ORF72-Related ALS/FTD Compromises Mitochondrial Function and Increases Oxidative Stress and DNA Damage in iPSC-Derived Motor Neurons. In *Neuron* (Vol. 92, Issue 2). https://doi.org/10.1016/j.neuron.2016.09.015

Lv, L., Li, D., Zhao, D., Lin, R., Chu, Y., Zhang, H., Zha, Z., Liu, Y., Li, Z., Xu, Y., Wang, G., Huang, Y., Xiong, Y., Guan, K.-L., & Lei, Q.-Y. (2011). Acetylation Targets the M2 Isoform of Pyruvate Kinase for Degradation through Chaperone-Mediated Autophagy and Promotes Tumor Growth. *Molecular Cell*, *42*(6), 719–730. https://doi.org/10.1016/J.MOLCEL.2011.04.025

Lyttonsg, J., Westlins, M., & Hanleyll, M. R. (1991). *Thapsigargin Inhibits the Sarcoplasmic or Endoplasmic Reticulum Ca-ATPase Family of Calcium Pumps** (Vol. 266, Issue 26). https://www.jbc.org/content/266/26/17067.full.pdf

Mackenzie, I. R., Arzberger, T., Kremmer, E., Troost, D., Lorenzl, S., Mori, K., Weng, S.-M., Haass, C., Kretzschmar, H. A., Edbauer, D., & Neumann, M. (2013). Dipeptide repeat protein pathology in C9ORF72 mutation cases: clinico-pathological correlations. *Acta Neuropathologica*, *126*(6), 859–879. https://doi.org/10.1007/s00401-013-1181-y

Mackenzie, I. R., Bigio, E. H., Ince, P. G., Geser, F., Neumann, M., Cairns, N. J., Kwong, L. K., Forman, M. S., Ravits, J., Stewart, H., Eisen, A., McClusky, L., Kretzschmar, H. A.,

Monoranu, C. M., Highley, J. R., Kirby, J., Siddique, T., Shaw, P. J., Lee, V. M.-Y., & Trojanowski, J. Q. (2007). Pathological TDP-43 distinguishes sporadic amyotrophic lateral sclerosis from amyotrophic lateral sclerosis withSOD1 mutations. *Annals of Neurology*, *61*(5), 427–434. https://doi.org/10.1002/ana.21147

Mackenzie, I. R., Frick, P., Grässer, F. A., Gendron, T. F., Petrucelli, L., Cashman, N. R., Edbauer, D., Kremmer, E., Prudlo, J., Troost, D., & Neumann, M. (2015). Quantitative analysis and clinico-pathological correlations of different dipeptide repeat protein pathologies in C9ORF72 mutation carriers. *Acta Neuropathologica*, *130*(6), 845–861. https://doi.org/10.1007/s00401-015-1476-2

Majounie, E., Renton, A. E., Mok, K., Dopper, E. G., Waite, A., Rollinson, S., Chiò, A., Restagno, G., Nicolaou, N., Simon-Sanchez, J., van Swieten, J. C., Abramzon, Y., Johnson, J. O., Sendtner, M., Pamphlett, R., Orrell, R. W., Mead, S., Sidle, K. C., Houlden, H., … Al., E. (2012). Frequency of the C9orf72 hexanucleotide repeat expansion in patients with amyotrophic lateral sclerosis and frontotemporal dementia: a cross-sectional study. *The Lancet Neurology*, *11*(4), 323–330. https://doi.org/10.1016/S1474-4422(12)70043-1

Malhotra, J. D., & Kaufman, R. J. (2007). The endoplasmic reticulum and the unfolded protein response. *Seminars in Cell & Developmental Biology*, *18*(6), 716–731. https://doi.org/10.1016/J.SEMCDB.2007.09.003

Mallilankaraman, K., Doonan, P., Cárdenas, C., Chandramoorthy, H., Müller, M., Miller, R., Hoffman, N., Gandhirajan, R., Molgó, J., Birnbaum, M., Rothberg, B., Mak, D., Foskett, J., & Madesh, M. (2012). MICU1 Is an Essential Gatekeeper for MCU-mediated Mitochondrial Ca(2+) Uptake That Regulates Cell Survival. *Cell*, *151*(3). https://doi.org/10.1016/J.CELL.2012.10.011

Mandrioli, J., D'Amico, R., Zucchi, E., Gessani, A., Fini, N., Fasano, A., Caponnetto, C., Chiò, A., Dalla Bella, E., Lunetta, C., Mazzini, L., Marinou, K., Sorarù, G., de Biasi, S., Lo Tartaro, D., Pinti, M., & Cossarizza, A. (2018). Rapamycin treatment for amyotrophic lateral sclerosis. *Medicine*, *97*(24), e11119. https://doi.org/10.1097/MD.0000000000011119

Mann, D. M. A., Rollinson, S., Robinson, A., Bennion Callister, J., Thompson, J. C., Snowden, J. S., Gendron, T., Petrucelli, L., Masuda-Suzukake, M., Hasegawa, M., Davidson, Y., & Pickering-Brown, S. (2013). Dipeptide repeat proteins are present in the p62 positive inclusions in patients with frontotemporal lobar degeneration and motor neurone disease associated with expansions in C9ORF72. *Acta Neuropathologica Communications*, *1*(1), 68. https://doi.org/10.1186/2051-5960-1-68

Martier, R., Liefhebber, J. M., García-Osta, A., Miniarikova, J., Cuadrado-Tejedor, M., Espelosin, M., Ursua, S., Petry, H., van Deventer, S. J., Evers, M. M., & Konstantinova, P. (2019). Targeting RNA-Mediated Toxicity in C9orf72 ALS and/or FTD by RNAi-Based Gene Therapy. *Molecular Therapy - Nucleic Acids*, *16*, 26–37. https://doi.org/10.1016/J.OMTN.2019.02.001

Martier, R., Liefhebber, J. M., Miniarikova, J., van der Zon, T., Snapper, J., Kolder, I., Petry, H., van Deventer, S. J., Evers, M. M., & Konstantinova, P. (2019). Artificial MicroRNAs Targeting C9orf72 Can Reduce Accumulation of Intra-nuclear Transcripts in ALS and FTD Patients. *Molecular Therapy - Nucleic Acids*, *14*, 593–608. https://doi.org/10.1016/J.OMTN.2019.01.010

Maruyama, H., Morino, H., Ito, H., Izumi, Y., Kato, H., Watanabe, Y., Kinoshita, Y., Kamada, M., Nodera, H., Suzuki, H., Komure, O., Matsuura, S., Kobatake, K., Morimoto, N., Abe, K., Suzuki, N., Aoki, M., Kawata, A., Hirai, T., … Kawakami, H. (2010). Mutations of optineurin in amyotrophic lateral sclerosis. *Nature*, *465*(7295), 223–226.

https://doi.org/10.1038/nature08971

Massman, P. J., Sims, J., Cooke, N., Haverkamp, L. J., Appel, V., & Appel, S. H. (1996). Prevalence and correlates of neuropsychological deficits in amyotrophic lateral sclerosis. *Journal of Neurology, Neurosurgery, and Psychiatry*, *61*(5), 450–455. https://doi.org/10.1136/jnnp.61.5.450

Matesanz-Isabel, J., Arias-del-Val, J., Alvarez-Illera, P., Fonteriz, R. I., Montero, M., & Alvarez, J. (2016). Functional roles of MICU1 and MICU2 in mitochondrial Ca2 + uptake. *Biochimica et Biophysica Acta (BBA) - Biomembranes*, *1858*(6), 1110–1117. https://doi.org/10.1016/J.BBAMEM.2016.02.022

Mathis, S., Goizet, C., Soulages, A., Vallat, J.-M., & Masson, G. Le. (2019). Genetics of amyotrophic lateral sclerosis: A review. *Journal of the Neurological Sciences*, *399*, 217–226. https://doi.org/10.1016/J.JNS.2019.02.030

May, S., Hornburg, D., Schludi, M. H., Arzberger, T., Rentzsch, K., Schwenk, B. M., Grässer, F. A., Mori, K., Kremmer, E., Banzhaf-Strathmann, J., Mann, M., Meissner, F., & Edbauer, D. (2014). C9orf72 FTLD/ALS-associated Gly-Ala dipeptide repeat proteins cause neuronal toxicity and Unc119 sequestration. *Acta Neuropathologica*, *128*(4), 485–503. https://doi.org/10.1007/s00401-014-1329-4

McEachin, Z. T., Gendron, T. F., Raj, N., García-Murias, M., Banerjee, A., Purcell, R. H., Ward, P. J., Todd, T. W., Merritt-Garza, M. E., Jansen-West, K., Hales, C. M., García-Sobrino, T., Quintáns, B., Holler, C. J., Taylor, G., San Millán, B., Teijeira, S., Yamashita, T., Ohkubo, R., … Bassell, G. J. (2020). Chimeric Peptide Species Contribute to Divergent Dipeptide Repeat Pathology in c9ALS/FTD and SCA36. *Neuron*, *107*(2), 292-305.e6. https://doi.org/10.1016/J.NEURON.2020.04.011

McGoldrick, P., Zhang, M., van Blitterswijk, M., Sato, C., Moreno, D., Xiao, S., Zhang, A. B., McKeever, P. M., Weichert, A., Schneider, R., Keith, J., Petrucelli, L., Rademakers, R., Zinman, L., Robertson, J., & Rogaeva, E. (2018). Unaffected mosaic C9orf72 case: RNA foci, dipeptide proteins, but upregulated C9orf72 expression. *Neurology*, *90*(4), e323–e331. https://doi.org/10.1212/WNL.0000000000004865

Miller, T., Cudkowicz, M., Shaw, P. J., Andersen, P. M., Atassi, N., Bucelli, R. C., Genge, A., Glass, J., Ladha, S., Ludolph, A. L., Maragakis, N. J., McDermott, C. J., Pestronk, A., Ravits, J., Salachas, F., Trudell, R., Van Damme, P., Zinman, L., Bennett, C. F., … Ferguson, T. A. (2020). Phase 1–2 Trial of Antisense Oligonucleotide Tofersen for SOD1 ALS. *New England Journal of Medicine*, *383*(2), 109–119. https://doi.org/10.1056/NEJMoa2003715

Miller, T., Pestronk, A., David, W., Rothstein, J., Simpson, E., Appel, S. H., Andres, P. L., Mahoney, K., Allred, P., Alexander, K., Ostrow, L. W., Schoenfeld, D., Macklin, E. A., Norris, D. A., Manousakis, G., Crisp, M., Smith, R., Bennett, C. F., Bishop, K. M., & Cudkowicz, M. E. (2013). An antisense oligonucleotide against SOD1 delivered intrathecally for patients with SOD1 familial amyotrophic lateral sclerosis: a phase 1, randomised, first-in-man study. *The Lancet Neurology*, *12*(5), 435–442. https://doi.org/10.1016/S1474-4422(13)70061-9

Mizielinska, S., Grönke, S., Niccoli, T., Ridler, C. E., Clayton, E. L., Devoy, A., Moens, T., Norona, F. E., Woollacott, I. O. C., Pietrzyk, J., Cleverley, K., Nicoll, A. J., Pickering-Brown, S., Dols, J., Cabecinha, M., Hendrich, O., Fratta, P., Fisher, E. M. C., Partridge, L., & Isaacs, A. M. (2014). C9orf72 repeat expansions cause neurodegeneration in Drosophila through arginine-rich proteins. *Science (New York, N.Y.)*, *345*(6201), 1192–1194. https://doi.org/10.1126/science.1256800

Mizielinska, S., Lashley, T., Norona, F. E., Clayton, E. L., Ridler, C. E., Fratta, P., & Isaacs, A. M. (2013). C9orf72 frontotemporal lobar degeneration is characterised by frequent neuronal sense and antisense RNA foci. *Acta Neuropathologica*, *126*(6), 845–857. https://doi.org/10.1007/s00401-013-1200-z

Mizielinska, S., Ridler, C. E., Balendra, R., Thoeng, A., Woodling, N. S., Grässer, F. A., Plagnol, V., Lashley, T., Partridge, L., & Isaacs, A. M. (2017). Bidirectional nucleolar dysfunction in C9orf72 frontotemporal lobar degeneration. *Acta Neuropathologica Communications*, *5*(1), 29. https://doi.org/10.1186/s40478-017-0432-x

Moens, T. G., Mizielinska, S., Niccoli, T., Mitchell, J. S., Thoeng, A., Ridler, C. E., Grönke, S., Esser, J., Heslegrave, A., Zetterberg, H., Partridge, L., & Isaacs, A. M. (2018). Sense and antisense RNA are not toxic in Drosophila models of C9orf72-associated ALS/FTD. *Acta Neuropathologica*, *135*(3), 445–457. https://doi.org/10.1007/s00401-017-1798-3

Molliex, A., Temirov, J., Lee, J., Coughlin, M., Kanagaraj, A. P., Kim, H. J., Mittag, T., & Taylor, J. P. (2015). Phase Separation by Low Complexity Domains Promotes Stress Granule Assembly and Drives Pathological Fibrillization. *Cell*, *163*(1), 123–133. https://doi.org/10.1016/J.CELL.2015.09.015

Mordes, D. A., Prudencio, M., Goodman, L. D., Klim, J. R., Moccia, R., Limone, F., Pietilainen, O., Chowdhary, K., Dickson, D. W., Rademakers, R., Bonini, N. M., Petrucelli, L., & Eggan, K. (2018). Dipeptide repeat proteins activate a heat shock response found in C9ORF72-ALS/FTLD patients. *Acta Neuropathologica Communications*, *6*(1), 55. https://doi.org/10.1186/s40478-018-0555-8

Mori, K., Arzberger, T., Grässer, F. A., Gijselinck, I., May, S., Rentzsch, K., Weng, S.-M., Schludi, M. H., van der Zee, J., Cruts, M., Van Broeckhoven, C., Kremmer, E., Kretzschmar, H. A., Haass, C., & Edbauer, D. (2013). Bidirectional transcripts of the expanded C9orf72 hexanucleotide repeat are translated into aggregating dipeptide repeat proteins. *Acta Neuropathologica*, *126*(6), 881–893. https://doi.org/10.1007/s00401-013-1189-3

Mori, K., Lammich, S., Mackenzie, I. R. A., Forné, I., Zilow, S., Kretzschmar, H., Edbauer, D., Janssens, J., Kleinberger, G., Cruts, M., Herms, J., Neumann, M., Van Broeckhoven, C., Arzberger, T., & Haass, C. (2013). hnRNP A3 binds to GGGGCC repeats and is a constituent of p62-positive/TDP43-negative inclusions in the hippocampus of patients with C9orf72 mutations. *Acta Neuropathologica*, *125*(3), 413–423. https://doi.org/10.1007/s00401-013-1088-7

Mori, K., Weng, S., Arzberger, T., May, S., Rentzsch, K., Kremmer, E., Schmid, B., Kretzschmar, H. A., Cruts, M., Van Broeckhoven, C., Haass, C., Edbauer, D., Broeckhoven, C. Van, Haass, C., & Edbauer, D. (2013). The C9orf72 GGGGCC repeat is translated into aggregating dipeptide-repeat proteins in FTLD/ALS. *Science (New York, N.Y.)*, *339*(6125), 1335–1338. https://doi.org/10.1126/science.1232927

Morita, M., Al-Chalabi, A., Andersen, P. M., Hosler, B., Sapp, P., Englund, E., Mitchell, J. E., Habgood, J. J., de Belleroche, J., Xi, J., Jongjaroenprasert, W., Horvitz, H. R., Gunnarsson, L.-G., & Brown, R. H. (2006). A locus on chromosome 9p confers susceptibility to ALS and frontotemporal dementia. *Neurology*, *66*(6), 839–844. https://doi.org/10.1212/01.wnl.0000200048.53766.b4

Morohoshi, F., Ootsuka, Y., Arai, K., Ichikawa, H., Mitani, S., Munakata, N., & Ohki, M. (1998). Genomic structure of the human RBP56/hTAFII68 and FUS/TLS genes. *Gene*, *221*(2), 191–198. https://doi.org/10.1016/S0378-1119(98)00463-6

Mutihac, R., Alegre-Abarrategui, J., Gordon, D., Farrimond, L., Yamasaki-Mann, M., Talbot, K., & Wade-Martins, R. (2015). TARDBP pathogenic mutations increase cytoplasmic translocation of TDP-43 and cause reduction of endoplasmic reticulum Ca2 + signaling in motor neurons. *Neurobiology of Disease*, *75*, 64–77. https://doi.org/10.1016/J.NBD.2014.12.010

Naguib, A., Sandmann, T., Yi, F., Watts, R. J., Lewcock, J. W., & Dowdle, W. E. (2019). SUPT4H1 Depletion Leads to a Global Reduction in RNA. *Cell Reports*, *26*(1), 45-53.e4. https://doi.org/10.1016/J.CELREP.2018.12.004

Neary, D., Snowden, J. S., Mann, D. M., Northen, B., Goulding, P. J., & Macdermott, N. (1990). Frontal lobe dementia and motor neuron disease. *Journal of Neurology, Neurosurgery, and Psychiatry*, *53*(1), 23–32. https://doi.org/10.1136/jnnp.53.1.23

Neumann, M., Sampathu, D. M., Kwong, L. K., Truax, A. C., Micsenyi, M. C., Chou, T. T., Bruce, J., Schuck, T., Grossman, M., Clark, C. M., McCluskey, L. F., Miller, B. L., Masliah, E., Mackenzie, I. R., Feldman, H., Feiden, W., Kretzschmar, H. A., Trojanowski, J. Q., & Lee, V. M.-Y. (2006). Ubiquitinated TDP-43 in Frontotemporal Lobar Degeneration and Amyotrophic Lateral Sclerosis. *Science*, *314*(5796), 130–133. https://doi.org/10.1126/science.1134108

Nguyen, L., Montrasio, F., Pattamatta, A., Tusi, S. K., Bardhi, O., Meyer, K. D., Hayes, L., Nakamura, K., Banez-Coronel, M., Coyne, A., Guo, S., Laboissonniere, L. A., Gu, Y., Narayanan, S., Smith, B., Nitsch, R. M., Kankel, M. W., Rushe, M., Rothstein, J., … Ranum, L. P. W. (2020). Antibody Therapy Targeting RAN Proteins Rescues C9 ALS/FTD Phenotypes in C9orf72 Mouse Model. *Neuron*, *105*(4), 645-662.e11. https://doi.org/10.1016/J.NEURON.2019.11.007

Nixon, R. A. (2013). The role of autophagy in neurodegenerative disease. *Nature Medicine*, *19*(8), 983–997. https://doi.org/10.1038/nm.3232

Nolan, M., Scott, C., Gamarallage, M. P., Lunn, D., Carpenter, K., McDonough, E., Meyer, D., Kaanumalle, S., Santamaria-Pang, A., Turner, M. R., Talbot, K., & Ansorge, O. (2020). Quantitative patterns of motor cortex proteinopathy across ALS genotypes. *Acta Neuropathologica Communications*, *8*(1), 98. https://doi.org/10.1186/s40478-020-00961-2

Nolan, M., Talbot, K., & Ansorge, O. (2016). Pathogenesis of FUS-associated ALS and FTD: insights from rodent models. *Acta Neuropathologica Communications*, *4*(1), 99. https://doi.org/10.1186/s40478-016-0358-8

Nonaka, T., Masuda-Suzukake, M., Hosokawa, M., Shimozawa, A., Hirai, S., Okado, H., & Hasegawa, M. (2018). C9ORF72 dipeptide repeat poly-GA inclusions promote intracellular aggregation of phosphorylated TDP-43. *Human Molecular Genetics*, *27*(15), 2658–2670. https://doi.org/10.1093/hmg/ddy174

Nover, L., Scharf, K. D., & Neumann, D. (1989). Cytoplasmic heat shock granules are formed from precursor particles and are associated with a specific set of mRNAs. *Molecular and Cellular Biology*, *9*(3), 1298–1308. https://doi.org/10.1128/mcb.9.3.1298

O'Rourke, J. G., Bogdanik, L., Yáñez, A., Lall, D., Wolf, A. J., Muhammad, A. K. M. G., Ho, R., Carmona, S., Vit, J. P., Zarrow, J., Kim, K. J., Bell, S., Harms, M. B., Miller, T. M., Dangler, C. A., Underhill, D. M., Goodridge, H. S., Lutz, C. M., & Baloh, R. H. (2016). C9orf72 is required for proper macrophage and microglial function in mice. *Science (New York, N.Y.)*, *351*(6279), 1324–1329. https://doi.org/10.1126/science.aaf1064

Ogawa, L. M., & Baserga, S. J. (2017). Crosstalk between the nucleolus and the DNA

damage response. *Molecular BioSystems*, *13*(3), 443–455. https://doi.org/10.1039/C6MB00740F

Ohki, Y., Wenninger-Weinzierl, A., Hruscha, A., Asakawa, K., Kawakami, K., Haass, C., Edbauer, D., & Schmid, B. (2017). Glycine-alanine dipeptide repeat protein contributes to toxicity in a zebrafish model of C9orf72 associated neurodegeneration. *Molecular Neurodegeneration*, *12*(1), 6. https://doi.org/10.1186/s13024-016-0146-8

Oku, M., & Sakai, Y. (2018). Three Distinct Types of Microautophagy Based on Membrane Dynamics and Molecular Machineries. *BioEssays*, *40*(6), 1800008. https://doi.org/10.1002/bies.201800008

Onesto, E., Colombrita, C., Gumina, V., Borghi, M. O., Dusi, S., Doretti, A., Fagiolari, G., Invernizzi, F., Moggio, M., Tiranti, V., Silani, V., & Ratti, A. (2016). Gene-specific mitochondria dysfunctions in human TARDBP and C9ORF72 fibroblasts. *Acta Neuropathologica Communications*, *4*(1), 47. https://doi.org/10.1186/s40478-016-0316-5

Ou, S. H., Wu, F., Harrich, D., García-Martínez, L. F., & Gaynor, R. B. (1995). Cloning and characterization of a novel cellular protein, TDP-43, that binds to human immunodeficiency virus type 1 TAR DNA sequence motifs. *Journal of Virology*, *69*(6), 3584–3596. http://www.ncbi.nlm.nih.gov/pubmed/7745706

Palangi, F., Samuel, S. M., Thompson, I. R., Triggle, C. R., & Emara, M. M. (2017). Effects of oxidative and thermal stresses on stress granule formation in human induced pluripotent stem cells. *PLOS ONE*, *12*(7), e0182059. https://doi.org/10.1371/journal.pone.0182059

Pandya, J. D., Nukala, V. N., & Sullivan, P. G. (2013). Concentration dependent effect of calcium on brain mitochondrial bioenergetics and oxidative stress parameters. *Frontiers in Neuroenergetics*, *5*, 10. https://doi.org/10.3389/fnene.2013.00010

Patron, M., Checchetto, V., Raffaello, A., Teardo, E., Vecellio Reane, D., Mantoan, M., Granatiero, V., Szabò, I., De Stefani, D., & Rizzuto, R. (2014). MICU1 and MICU2 Finely Tune the Mitochondrial Ca2+ Uniporter by Exerting Opposite Effects on MCU Activity. *Molecular Cell*, *53*(5), 726–737. https://doi.org/10.1016/J.MOLCEL.2014.01.013

Peabody, D. S. (1989). *Translation Initiation at Non-AUG Triplets in Mammalian Cells** (Vol. 264, Issue 9). https://www.jbc.org/content/264/9/5031.full.pdf

Perocchi, F., Gohil, V. M., Girgis, H. S., Bao, X. R., McCombs, J. E., Palmer, A. E., & Mootha, V. K. (2010). MICU1 encodes a mitochondrial EF hand protein required for Ca2+ uptake. *Nature*, *467*(7313), 291–296. https://doi.org/10.1038/nature09358

Peters, O. M., Cabrera, G. T., Tran, H., Gendron, T. F., McKeon, J. E., Metterville, J., Weiss, A., Wightman, N., Salameh, J., Kim, J., Sun, H., Boylan, K. B., Dickson, D., Kennedy, Z., Lin, Z., Zhang, Y.-J., Daughrity, L., Jung, C., Gao, F.-B., … Brown, R. H. (2015). Human C9ORF72 Hexanucleotide Expansion Reproduces RNA Foci and Dipeptide Repeat Proteins but Not Neurodegeneration in BAC Transgenic Mice. *Neuron*, *88*(5), 902–909. https://doi.org/10.1016/J.NEURON.2015.11.018

Plovanich, M., Bogorad, R. L., Sancak, Y., Kamer, K. J., Strittmatter, L., Li, A. A., Girgis, H. S., Kuchimanchi, S., De Groot, J., Speciner, L., Taneja, N., OShea, J., Koteliansky, V., & Mootha, V. K. (2013). MICU2, a Paralog of MICU1, Resides within the Mitochondrial Uniporter Complex to Regulate Calcium Handling. *PLoS ONE*, *8*(2), e55785. https://doi.org/10.1371/journal.pone.0055785

Polymenidou, M., Lagier-Tourenne, C., Hutt, K. R., Huelga, S. C., Moran, J., Liang, T. Y., Ling, S.-C., Sun, E., Wancewicz, E., Mazur, C., Kordasiewicz, H., Sedaghat, Y., Donohue, J. P., Shiue, L., Bennett, C. F., Yeo, G. W., & Cleveland, D. W. (2011). Long pre-mRNA depletion and RNA missplicing contribute to neuronal vulnerability from loss of TDP-43. *Nature Neuroscience*, *14*(4), 459–468. https://doi.org/10.1038/nn.2779

Porta, S., Kwong, L. K., Trojanowski, J. Q., & Lee, V. M.-Y. (2015). Drosha Inclusions Are New Components of Dipeptide-Repeat Protein Aggregates in FTLD-TDP and ALS *C9orf72* Expansion Cases. *Journal of Neuropathology & Experimental Neurology*, *74*(4), 380–387. https://doi.org/10.1097/NEN.0000000000000182

Pottier, C., Bieniek, K. F., Finch, N., van de Vorst, M., Baker, M., Perkersen, R., Brown, P., Ravenscroft, T., van Blitterswijk, M., Nicholson, A. M., DeTure, M., Knopman, D. S., Josephs, K. A., Parisi, J. E., Petersen, R. C., Boylan, K. B., Boeve, B. F., Graff-Radford, N. R., Veltman, J. A., … Rademakers, R. (2015). Whole-genome sequencing reveals important role for TBK1 and OPTN mutations in frontotemporal lobar degeneration without motor neuron disease. *Acta Neuropathologica*, *130*(1), 77–92. https://doi.org/10.1007/s00401-015-1436-x

Prasad, A., Bharathi, V., Sivalingam, V., Girdhar, A., & Patel, B. K. (2019). Molecular Mechanisms of TDP-43 Misfolding and Pathology in Amyotrophic Lateral Sclerosis. *Frontiers in Molecular Neuroscience*, *12*, 25. https://doi.org/10.3389/fnmol.2019.00025

Proudfoot, M., Gutowski, N. J., Edbauer, D., Hilton, D. A., Stephens, M., Rankin, J., & Mackenzie, I. R. A. (2014). Early dipeptide repeat pathology in a frontotemporal dementia kindred with C9ORF72 mutation and intellectual disability. *Acta Neuropathologica*, *127*(3), 451–458. https://doi.org/10.1007/s00401-014-1245-7

Prudencio, M., Belzil, V. V, Batra, R., Ross, C. A., Gendron, T. F., Pregent, L. J., Murray, M. E., Overstreet, K. K., Piazza-Johnston, A. E., Desaro, P., Bieniek, K. F., DeTure, M., Lee, W. C., Biendarra, S. M., Davis, M. D., Baker, M. C., Perkerson, R. B., van Blitterswijk, M., Stetler, C. T., … Petrucelli, L. (2015). Distinct brain transcriptome profiles in C9orf72-associated and sporadic ALS. *Nature Neuroscience*, *18*(8), 1175–1182. https://doi.org/10.1038/nn.4065

Purves, D. (2018). *Neuroscience* (Sixth edition.).

Ravits, J. M., & La Spada, A. R. (2009). ALS motor phenotype heterogeneity, focality, and spread: deconstructing motor neuron degeneration. *Neurology*, *73*(10), 805–811. https://doi.org/10.1212/WNL.0b013e3181b6bbbd

Reaume, A. G., Elliott, J. L., Hoffman, E. K., Kowall, N. W., Ferrante, R. J., Siwek, D. R., Wilcox, H. M., Flood, D. G., Beal, M. F., Brown, R. H., Scott, R. W., & Snider, W. D. (1996). Motor neurons in Cu/Zn superoxide dismutase-deficient mice develop normally but exhibit enhanced cell death after axonal injury. *Nature Genetics*, *13*(1), 43–47. https://doi.org/10.1038/ng0596-43

Renton, A. E., Majounie, E., Waite, A., Simón-Sánchez, J., Rollinson, S., Gibbs, J. R., Schymick, J. C., Laaksovirta, H., van Swieten, J. C., Myllykangas, L., Kalimo, H., Paetau, A., Abramzon, Y., Remes, A. M., Kaganovich, A., Scholz, S. W., Duckworth, J., Ding, J., Harmer, D. W., … Traynor, B. J. (2011). A hexanucleotide repeat expansion in C9ORF72 is the cause of chromosome 9p21-linked ALS-FTD. *Neuron*, *72*(2), 257–268. https://doi.org/10.1016/j.neuron.2011.09.010

Ringholz, G. M., Appel, S. H., Bradshaw, M., Cooke, N. A., Mosnik, D. M., & Schulz, P. E. (2005). Prevalence and patterns of cognitive impairment in sporadic ALS. *Neurology*, *65*(4),

586–590. https://doi.org/10.1212/01.wnl.0000172911.39167.b6

Roelink, H., Porter, J. ., Chiang, C., Tanabe, Y., Chang, D. ., Beachy, P. ., & Jessell, T. . (1995). Floor plate and motor neuron induction by different concentrations of the amino-terminal cleavage product of sonic hedgehog autoproteolysis. *Cell*, *81*(3), 445–455. https://doi.org/10.1016/0092-8674(95)90397-6

Rosen, D. R., Siddique, T., Patterson, D., Figlewicz, D. A., Sapp, P., Hentati, A., Donaldson, D., Goto, J., O'Regan, J. P., Deng, H.-X., Rahmani, Z., Krizus, A., McKenna-Yasek, D., Cayabyab, A., Gaston, S. M., Berger, R., Tanzi, R. E., Halperin, J. J., Herzfeldt, B., … Brown, R. H. (1993). Mutations in Cu/Zn superoxide dismutase gene are associated with familial amyotrophic lateral sclerosis. *Nature*, *362*(6415), 59–62. https://doi.org/10.1038/362059a0

Rothstein, J. D., Martin, L. J., & Kuncl, R. W. (1992). Decreased Glutamate Transport by the Brain and Spinal Cord in Amyotrophic Lateral Sclerosis. *New England Journal of Medicine*, *326*(22), 1464–1468. https://doi.org/10.1056/NEJM199205283262204

Rothstein, J. D., Tsai, G., Kuncl, R. W., Clawson, L., Cornblath, D. R., Drachman, D. B., Pestronk, A., Stauch, B. L., & Coyle, J. T. (1990). Abnormal excitatory amino acid metabolism in amyotrophic lateral sclerosis. *Annals of Neurology*, *28*(1), 18–25. https://doi.org/10.1002/ana.410280106

Rudich, P., Snoznik, C., Watkins, S. C., Monaghan, J., Pandey, U. B., & Lamitina, S. T. (2017). Nuclear localized C9orf72-associated arginine-containing dipeptides exhibit age-dependent toxicity in C. elegans. *Human Molecular Genetics*. https://doi.org/10.1093/hmg/ddx372

Russ, J., Liu, E. Y., Wu, K., Neal, D., Suh, E., Irwin, D. J., McMillan, C. T., Harms, M. B., Cairns, N. J., Wood, E. M., Xie, S. X., Elman, L., McCluskey, L., Grossman, M., Van Deerlin, V. M., & Lee, E. B. (2015). Hypermethylation of repeat expanded C9orf72 is a clinical and molecular disease modifier. *Acta Neuropathologica*, *129*(1), 39–52. https://doi.org/10.1007/s00401-014-1365-0

Ryan, T. A., & Tumbarello, D. A. (2018). Optineurin: A Coordinator of Membrane-Associated Cargo Trafficking and Autophagy. *Frontiers in Immunology*, *9*, 1024. https://doi.org/10.3389/fimmu.2018.01024

Saberi, S., Stauffer, J. E., Jiang, J., Garcia, S. D., Taylor, A. E., Schulte, D., Ohkubo, T., Schloffman, C. L., Maldonado, M., Baughn, M., Rodriguez, M. J., Pizzo, D., Cleveland, D., & Ravits, J. (2017). Sense-encoded poly-GR dipeptide repeat proteins correlate to neurodegeneration and uniquely co-localize with TDP-43 in dendrites of repeat-expanded C9orf72 amyotrophic lateral sclerosis. *Acta Neuropathologica*, 1–16. https://doi.org/10.1007/s00401-017-1793-8

Sakae, N., Bieniek, K. F., Zhang, Y.-J., Ross, K., Gendron, T. F., Murray, M. E., Rademakers, R., Petrucelli, L., & Dickson, D. W. (2018). Poly-GR dipeptide repeat polymers correlate with neurodegeneration and Clinicopathological subtypes in C9ORF72-related brain disease. *Acta Neuropathologica Communications*, *6*(1), 63. https://doi.org/10.1186/s40478-018-0564-7

Salton, M., Elkon, R., Borodina, T., Davydov, A., Yaspo, M.-L., Halperin, E., & Shiloh, Y. (2011). Matrin 3 Binds and Stabilizes mRNA. *PLoS ONE*, *6*(8), e23882. https://doi.org/10.1371/journal.pone.0023882

Sareen, D., O'Rourke, J. G., Meera, P., Muhammad, A. K. M. G., Grant, S., Simpkinson, M.,

Bell, S., Carmona, S., Ornelas, L., Sahabian, A., Gendron, T., Petrucelli, L., Baughn, M., Ravits, J., Harms, M. B., Rigo, F., Bennett, C. F., Otis, T. S., Svendsen, C. N., & Baloh, R. H. (2013). Targeting RNA foci in iPSC-derived motor neurons from ALS patients with a C9ORF72 repeat expansion. *Science Translational Medicine*, *5*(208), 208ra149. https://doi.org/10.1126/scitranslmed.3007529

Schinder, A. F., Olson, E. C., Spitzer, N. C., & Montal, M. (1996). Mitochondrial Dysfunction Is a Primary Event in Glutamate Neurotoxicity. *Journal of Neuroscience*, *16*(19), 6125–6133. https://doi.org/10.1523/JNEUROSCI.16-19-06125.1996

Schludi, M. H., Becker, L., Garrett, L., Gendron, T. F., Zhou, Q., Schreiber, F., Popper, B., Dimou, L., Strom, T. M., Winkelmann, J., von Thaden, A., Rentzsch, K., May, S., Michaelsen, M., Schwenk, B. M., Tan, J., Schoser, B., Dieterich, M., Petrucelli, L., … Edbauer, D. (2017). Spinal poly-GA inclusions in a C9orf72 mouse model trigger motor deficits and inflammation without neuron loss. *Acta Neuropathologica*, 1–14. https://doi.org/10.1007/s00401-017-1711-0

Schludi, M. H., May, S., Grässer, F. A., Rentzsch, K., Kremmer, E., Küpper, C., Klopstock, T., Arzberger, T., Edbauer, D., Arzberger, T., & Edbauer, D. (2015). Distribution of dipeptide repeat proteins in cellular models and C9orf72 mutation cases suggests link to transcriptional silencing. *Acta Neuropathologica*, *130*(4), 537–555. https://doi.org/10.1007/s00401-015-1450-z

Sellier, C., Campanari, M.-L., Julie Corbier, C., Gaucherot, A., Kolb-Cheynel, I., Oulad-Abdelghani, M., Ruffenach, F., Page, A., Ciura, S., Kabashi, E., & Charlet-Berguerand, N. (2016). Loss of C9ORF72 impairs autophagy and synergizes with polyQ Ataxin-2 to induce motor neuron dysfunction and cell death. *The EMBO Journal*, e201593350. https://doi.org/10.15252/embj.201593350

Selvaraj, B. T., Livesey, M. R., Zhao, C., Gregory, J. M., James, O. T., Cleary, E. M., Chouhan, A. K., Gane, A. B., Perkins, E. M., Dando, O., Lillico, S. G., Lee, Y.-B., Nishimura, A. L., Poreci, U., Thankamony, S., Pray, M., Vasistha, N. A., Magnani, D., Borooah, S., … Chandran, S. (2018). C9ORF72 repeat expansion causes vulnerability of motor neurons to Ca2+-permeable AMPA receptor-mediated excitotoxicity. *Nature Communications*, *9*(1), 347. https://doi.org/10.1038/s41467-017-02729-0

Shefner, J. M., Al-Chalabi, A., Baker, M. R., Cui, L.-Y., de Carvalho, M., Eisen, A., Grosskreutz, J., Hardiman, O., Henderson, R., Matamala, J. M., Mitsumoto, H., Paulus, W., Simon, N., Swash, M., Talbot, K., Turner, M. R., Ugawa, Y., van den Berg, L. H., Verdugo, R., … Kiernan, M. C. (2020). A proposal for new diagnostic criteria for ALS. *Clinical Neurophysiology*, *131*(8), 1975–1978. https://doi.org/10.1016/J.CLINPH.2020.04.005

Shi, K. Y., Mori, E., Nizami, Z. F., Lin, Y., Kato, M., Xiang, S., Wu, L. C., Ding, M., Yu, Y., Gall, J. G., & McKnight, S. L. (2017). Toxic PRn poly-dipeptides encoded by the C9orf72 repeat expansion block nuclear import and export. *Proceedings of the National Academy of Sciences of the United States of America*, *114*(7). https://doi.org/10.1073/pnas.1620293114

Shi, Y., Lin, S., Staats, K. A., Li, Y., Chang, W.-H., Hung, S.-T., Hendricks, E., Linares, G. R., Wang, Y., Son, E. Y., Wen, X., Kisler, K., Wilkinson, B., Menendez, L., Sugawara, T., Woolwine, P., Huang, M., Cowan, M. J., Ge, B., … Ichida, J. K. (2018). Haploinsufficiency leads to neurodegeneration in C9ORF72 ALS/FTD human induced motor neurons. *Nature Medicine*, *24*(3), 313–325. https://doi.org/10.1038/nm.4490

Sivadasan, R., Hornburg, D., Drepper, C., Frank, N., Jablonka, S., Hansel, A., Lojewski, X., Sterneckert, J., Hermann, A., Shaw, P. J., Ince, P. G., Mann, M., Meissner, F., & Sendtner,

M. (2016). C9ORF72 interaction with cofilin modulates actin dynamics in motor neurons. *Nature Neuroscience*, *19*(12), 1610–1618. https://doi.org/10.1038/nn.4407

Smith, R. A., Miller, T. M., Yamanaka, K., Monia, B. P., Condon, T. P., Hung, G., Lobsiger, C. S., Ward, C. M., McAlonis-Downes, M., Wei, H., Wancewicz, E. V, Bennett, C. F., & Cleveland, D. W. (2006). Antisense oligonucleotide therapy for neurodegenerative disease. *The Journal of Clinical Investigation*, *116*(8), 2290–2296. https://doi.org/10.1172/JCI25424

Solomon, D. A., Stepto, A., Au, W. H., Adachi, Y., Diaper, D. C., Hall, R., Rekhi, A., Boudi, A., Tziortzouda, P., Lee, Y.-B., Smith, B., Bridi, J. C., Spinelli, G., Dearlove, J., Humphrey, D. M., Gallo, J.-M., Troakes, C., Fanto, M., Soller, M., … Hirth, F. (2018). A feedback loop between dipeptide-repeat protein, TDP-43 and karyopherin-α mediates C9orf72-related neurodegeneration. *Brain*, *141*(10), 2908–2924. https://doi.org/10.1093/brain/awy241

Spreux-Varoquaux, O., Bensimon, G., Lacomblez, L., Salachas, F., Pradat, P. F., Le Forestier, N., Marouan, A., Dib, M., & Meininger, V. (2002). Glutamate levels in cerebrospinal fluid in amyotrophic lateral sclerosis: a reappraisal using a new HPLC method with coulometric detection in a large cohort of patients. *Journal of the Neurological Sciences*, *193*(2), 73–78. https://doi.org/10.1016/S0022-510X(01)00661-X

Sreedharan, J., Blair, I. P., Tripathi, V. B., Hu, X., Vance, C., Rogelj, B., Ackerley, S., Durnall, J. C., Williams, K. L., Buratti, E., Baralle, F., de Belleroche, J., Mitchell, J. D., Leigh, P. N., Al-Chalabi, A., Miller, C. C., Nicholson, G., & Shaw, C. E. (2008). TDP-43 mutations in familial and sporadic amyotrophic lateral sclerosis. *Science (New York, N.Y.)*, *319*(5870), 1668–1672. https://doi.org/10.1126/science.1154584

Stewart, H., Rutherford, N. J., Briemberg, H., Krieger, C., Cashman, N., Fabros, M., Baker, M., Fok, A., DeJesus-Hernandez, M., Eisen, A., Rademakers, R., & Mackenzie, I. R. A. (2012). Clinical and pathological features of amyotrophic lateral sclerosis caused by mutation in the C9ORF72 gene on chromosome 9p. *Acta Neuropathologica*, *123*(3), 409–417. https://doi.org/10.1007/s00401-011-0937-5

Su, Z., Zhang, Y., Gendron, T. F., Bauer, P. O., Chew, J., Yang, W.-Y., Fostvedt, E., Jansen-West, K., Belzil, V. V., Desaro, P., Johnston, A., Overstreet, K., Oh, S.-Y., Todd, P. K., Berry, J. D., Cudkowicz, M. E., Boeve, B. F., Dickson, D., Floeter, M. K., … Disney, M. D. (2014). Discovery of a Biomarker and Lead Small Molecules to Target r(GGGGCC)-Associated Defects in c9FTD/ALS. *Neuron*, *83*(5), 1043–1050. https://doi.org/10.1016/J.NEURON.2014.07.041

Suh, E., Grando, K., & Van Deerlin, V. M. (2018). Validation of a Long-Read PCR Assay for Sensitive Detection and Sizing of C9orf72 Hexanucleotide Repeat Expansions. *The Journal of Molecular Diagnostics*, *20*(6), 871–882. https://doi.org/10.1016/J.JMOLDX.2018.07.001

Sullivan, P. M., Zhou, X., Robins, A. M., Paushter, D. H., Kim, D., Smolka, M. B., & Hu, F. (2016). The ALS/FTLD associated protein C9orf72 associates with SMCR8 and WDR41 to regulate the autophagy-lysosome pathway. *Acta Neuropathologica Communications*, *4*(1), 51. https://doi.org/10.1186/s40478-016-0324-5

Sutcliffe, J. S., Nelson, D. L., Zhang, F., Pieretti, M., Caskey, C. T., Saxe, D., & Warren, S. T. (1992). DNA methylation represses *FMR-1* transcription in fragile X syndrome. *Human Molecular Genetics*, *1*(6), 397–400. https://doi.org/10.1093/hmg/1.6.397

Suzuki, C. K., Bonifacino, J. S., Lin, A. Y., Davis, M. M., & Klausner, R. D. (1991). Regulating the retention of T-cell receptor alpha chain variants within the endoplasmic

reticulum: Ca(2+)-dependent association with BiP. *The Journal of Cell Biology*, *114*(2), 189–205. https://doi.org/10.1083/jcb.114.2.189

Swaminathan, A., Bouffard, M., Liao, M., Ryan, S., Bennion Callister, J., Pickering-Brown, S. M., Armstrong, G. A. B., & Drapeau, P. (2018). Expression of C9orf72-related dipeptides impairs motor function in a vertebrate model. *Human Molecular Genetics*. https://doi.org/10.1093/hmg/ddy083

Swinnen, B., & Robberecht, W. (2014). The phenotypic variability of amyotrophic lateral sclerosis. *Nature Reviews Neurology*, *10*(11), 661–670. https://doi.org/10.1038/nrneurol.2014.184

Tabet, R., Schaeffer, L., Freyermuth, F., Jambeau, M., Workman, M., Lee, C.-Z., Lin, C.-C., Jiang, J., Jansen-West, K., Abou-Hamdan, H., Désaubry, L., Gendron, T., Petrucelli, L., Martin, F., & Lagier-Tourenne, C. (2018). CUG initiation and frameshifting enable production of dipeptide repeat proteins from ALS/FTD C9ORF72 transcripts. *Nature Communications*, *9*(1), 152. https://doi.org/10.1038/s41467-017-02643-5

Talbot, K. (2011). Familial versus sporadic amyotrophic lateral sclerosis--a false dichotomy? *Brain*, *134*(12), 3429–3434. https://doi.org/10.1093/brain/awr296

Talbot, K. (2020). Amyotrophic Lateral Sclerosis: network vulnerability and monosynaptic connections. *Journal of Neurology, Neurosurgery & Psychiatry*. https://doi.org/10.1136/JNNP-2020-323331

Tamaki, Y., Shodai, A., Morimura, T., Hikiami, R., Minamiyama, S., Ayaki, T., Tooyama, I., Furukawa, Y., Takahashi, R., & Urushitani, M. (2018). Elimination of TDP-43 inclusions linked to amyotrophic lateral sclerosis by a misfolding-specific intrabody with dual proteolytic signals. *Scientific Reports*, *8*(1), 6030. https://doi.org/10.1038/s41598-018-24463-3

Tao, Z., Wang, H., Xia, Q., Li, K., Li, K., Jiang, X., Xu, G., Wang, G., & Ying, Z. (2015). Nucleolar stress and impaired stress granule formation contribute to C9orf72 RAN translation-induced cytotoxicity. *Human Molecular Genetics*, *24*(9), 2426–2441. https://doi.org/10.1093/hmg/ddv005

Therrien, M., Rouleau, G. A., Dion, P. A., & Parker, J. A. (2013). Deletion of C9ORF72 Results in Motor Neuron Degeneration and Stress Sensitivity in C. elegans. *PLoS ONE*, *8*(12), e83450. https://doi.org/10.1371/journal.pone.0083450

Thomson, E., Ferreira-Cerca, S., & Hurt, E. (2013). Eukaryotic ribosome biogenesis at a glance. *Journal of Cell Science*, *126*(Pt 21), 4815–4821. https://doi.org/10.1242/jcs.111948

Tran, H., Almeida, S., Moore, J., Gendron, T. F., Chalasani, U., Lu, Y., Du, X., Nickerson, J. A., Petrucelli, L., Weng, Z., & Gao, F.-B. (2015). Differential Toxicity of Nuclear RNA Foci versus Dipeptide Repeat Proteins in a Drosophila Model of C9ORF72 FTD/ALS. In *Neuron* (Vol. 87, Issue 6). https://doi.org/10.1016/j.neuron.2015.09.015

Troakes, C., Maekawa, S., Wijesekera, L., Rogelj, B., Siklós, L., Bell, C., Smith, B., Newhouse, S., Vance, C., Johnson, L., Hortobágyi, T., Shatunov, A., Al-Chalabi, A., Leigh, N., Shaw, C. E., King, A., & Al-Sarraj, S. (2012). An MND/ALS phenotype associated with C9orf72 repeat expansion: abundant p62-positive, TDP-43-negative inclusions in cerebral cortex, hippocampus and cerebellum but without associated cognitive decline. *Neuropathology : Official Journal of the Japanese Society of Neuropathology*, *32*(5), 505–514. https://doi.org/10.1111/j.1440-1789.2011.01286.x

Tsoi, H., Lau, T. C.-K., Tsang, S.-Y., Lau, K.-F., & Chan, H. Y. E. (2012). CAG expansion induces nucleolar stress in polyglutamine diseases. *Proceedings of the National Academy of Sciences of the United States of America*, *109*(33), 13428–13433. https://doi.org/10.1073/pnas.1204089109

Turner, B. J., & Talbot, K. (2008). Transgenics, toxicity and therapeutics in rodent models of mutant SOD1-mediated familial ALS. *Progress in Neurobiology*, *85*(1), 94–134. https://doi.org/10.1016/J.PNEUROBIO.2008.01.001

Ugolino, J., Ji, Y. J., Conchina, K., Chu, J., Nirujogi, R. S., Pandey, A., Brady, N. R., Hamacher-Brady, A., & Wang, J. (2016). Loss of C9orf72 Enhances Autophagic Activity via Deregulated mTOR and TFEB Signaling. *PLOS Genetics*, *12*(11), e1006443. https://doi.org/10.1371/journal.pgen.1006443

van Blitterswijk, M., DeJesus-Hernandez, M., Niemantsverdriet, E., Murray, M. E., Heckman, M. G., Diehl, N. N., Brown, P. H., Baker, M. C., Finch, N. A., Bauer, P. O., Serrano, G., Beach, T. G., Josephs, K. A., Knopman, D. S., Petersen, R. C., Boeve, B. F., Graff-Radford, N. R., Boylan, K. B., Petrucelli, L., … Rademakers, R. (2013). Association between repeat sizes and clinical and pathological characteristics in carriers of C9ORF72 repeat expansions (Xpansize-72): a cross-sectional cohort study. *The Lancet Neurology*, *12*(10), 978–988. https://doi.org/10.1016/S1474-4422(13)70210-2

van der Zee, J., Gijselinck, I., Dillen, L., Van Langenhove, T., Theuns, J., Engelborghs, S., Philtjens, S., Vandenbulcke, M., Sleegers, K., Sieben, A., Bäumer, V., Maes, G., Corsmit, E., Borroni, B., Padovani, A., Archetti, S., Perneczky, R., Diehl-Schmid, J., de Mendonça, A., … Cras, P. (2013). A Pan-European Study of the C9orf72 Repeat Associated with FTLD: Geographic Prevalence, Genomic Instability, and Intermediate Repeats. *Human Mutation*, *34*(2), 363–373. https://doi.org/10.1002/humu.22244

van Es, M. A., Hardiman, O., Chio, A., Al-Chalabi, A., Pasterkamp, R. J., Veldink, J. H., & van den Berg, L. H. (2017). Amyotrophic lateral sclerosis. *The Lancet*, *390*(10107), 2084–2098. https://doi.org/10.1016/S0140-6736(17)31287-4

van Es, M. A., Veldink, J. H., Saris, C. G. J., Blauw, H. M., van Vught, P. W. J., Birve, A., Lemmens, R., Schelhaas, H. J., Groen, E. J. N., Huisman, M. H. B., van der Kooi, A. J., de Visser, M., Dahlberg, C., Estrada, K., Rivadeneira, F., Hofman, A., Zwarts, M. J., van Doormaal, P. T. C., Rujescu, D., … van den Berg, L. H. (2009). Genome-wide association study identifies 19p13.3 (UNC13A) and 9p21.2 as susceptibility loci for sporadic amyotrophic lateral sclerosis. *Nature Genetics*, *41*(10), 1083–1087. https://doi.org/10.1038/ng.442

Van Mossevelde, S., van der Zee, J., Cruts, M., & Van Broeckhoven, C. (2017). Relationship between C9orf72 repeat size and clinical phenotype. *Current Opinion in Genetics & Development*, *44*, 117–124. https://doi.org/10.1016/j.gde.2017.02.008

Vance, C., Rogelj, B., Hortobágyi, T., De Vos, K. J., Nishimura, A. L., Sreedharan, J., Hu, X., Smith, B., Ruddy, D., Wright, P., Ganesalingam, J., Williams, K. L., Tripathi, V., Al-Saraj, S., Al-Chalabi, A., Leigh, P. N., Blair, I. P., Nicholson, G., de Belleroche, J., … Shaw, C. E. (2009). Mutations in FUS, an RNA processing protein, cause familial amyotrophic lateral sclerosis type 6. *Science (New York, N.Y.)*, *323*(5918), 1208–1211. https://doi.org/10.1126/science.1165942

Vasco Ferreira, J., Rosa Soares, A., Silva Ramalho, J., Pereira, P., & Girao, H. (2015). K63 linked ubiquitin chain formation is a signal for HIF1A degradation by Chaperone-Mediated Autophagy. *Scientific Reports*, *5*(1), 10210. https://doi.org/10.1038/srep10210

Vatsavayai, S. C., Yoon, S. J., Gardner, R. C., Gendron, T. F., Vargas, J. N. S., Trujillo, A., Pribadi, M., Phillips, J. J., Gaus, S. E., Hixson, J. D., Garcia, P. A., Rabinovici, G. D., Coppola, G., Geschwind, D. H., Petrucelli, L., Miller, B. L., & Seeley, W. W. (2016). Timing and significance of pathological features in *C9orf72* expansion-associated frontotemporal dementia. *Brain*, *139*(12), 3202–3216. https://doi.org/10.1093/brain/aww250

Viodé, A., Fournier, C., Camuzat, A., Fenaille, F., Latouche, M., Elahi, F., Ber, I. Le, Junot, C., Lamari, F., Anquetil, V., Becher, F., Becher, F., Letournel, F., Vital, A., Chapon, F., Godfraind, C., Maurage, C.-A., Deramecourt, V., Meyronnet, D., … Lannes, B. (2018). New Antibody-Free Mass Spectrometry-Based Quantification Reveals That C9ORF72 Long Protein Isoform Is Reduced in the Frontal Cortex of Hexanucleotide-Repeat Expansion Carriers. *Frontiers in Neuroscience*, *12*, 589. https://doi.org/10.3389/fnins.2018.00589

Vogel, J. P., Misra, L. M., & Rose, M. D. (1990). Loss of BiP/GRP78 function blocks translocation of secretory proteins in yeast. *The Journal of Cell Biology*, *110*(6), 1885–1895. https://doi.org/10.1083/jcb.110.6.1885

Vogiatzi, T., Xilouri, M., Vekrellis, K., & Stefanis, L. (2008). Wild type alpha-synuclein is degraded by chaperone-mediated autophagy and macroautophagy in neuronal cells. *The Journal of Biological Chemistry*, *283*(35), 23542–23556. https://doi.org/10.1074/jbc.M801992200

Vu, L. T., & Bowser, R. (2016). Fluid-Based Biomarkers for Amyotrophic Lateral Sclerosis. *Neurotherapeutics 2016 14:1*, *14*(1), 119–134. https://doi.org/10.1007/S13311-016-0503-X

Waite, A. J., Bäumer, D., East, S., Neal, J., Morris, H. R., Ansorge, O., & Blake, D. J. (2014). Reduced C9orf72 protein levels in frontal cortex of amyotrophic lateral sclerosis and frontotemporal degeneration brain with the C9ORF72 hexanucleotide repeat expansion. *Neurobiology of Aging*, *35*(7), 1779.e5-1779.e13. https://doi.org/10.1016/J.NEUROBIOLAGING.2014.01.016

Wang, B., Cai, Z., Tao, K., Zeng, W., Lu, F., Yang, R., Feng, D., Gao, G., & Yang, Q. (2016). Essential control of mitochondrial morphology and function by chaperone-mediated autophagy through degradation of PARK7. *Autophagy*, *12*(8), 1215–1228. https://doi.org/10.1080/15548627.2016.1179401

Wang, I., Guo, B., Liu, Y., Wu, C., Yang, C., Tsai, K., & Shen, C. J. (2012). Autophagy activators rescue and alleviate pathogenesis of a mouse model with proteinopathies of the TAR DNA-binding protein 43. *Proceedings of the National Academy of Sciences of the United States of America*, *109*(37), 15024–15029. https://doi.org/10.1073/pnas.1206362109

Wang, R., Xu, X., Hao, Z., Zhang, S., Wu, D., Sun, H., Mu, C., Ren, H., & Wang, G. (2019). Poly-PR in C9ORF72-Related Amyotrophic Lateral Sclerosis/Frontotemporal Dementia Causes Neurotoxicity by Clathrin-Dependent Endocytosis. *Neuroscience Bulletin*, *35*(5), 889–900. https://doi.org/10.1007/s12264-019-00395-4

Wang, Z., Ursu, A., Childs-Disney, J. L., Guertler, R., Yang, W., Bernat, V., Rzuczek, S. G., Fuerst, R., Zhang, Y., Gendron, T. F., Yildirim, I., Dwyer, B. G., Rice, J. E., Petrucelli, L., & Disney, M. D. (2019). The Hairpin Form of r(G4C2)exp in c9ALS/FTD Is Repeat-Associated Non-ATG Translated and a Target for Bioactive Small Molecules. *Cell Chemical Biology*, *26*(2), 179-190.e12. https://doi.org/10.1016/J.CHEMBIOL.2018.10.018

Wen, X., Tan, W., Westergard, T., Krishnamurthy, K., Markandaiah, S. S., Shi, Y., Lin, S., Shneider, N. A., Monaghan, J., Pandey, U. B., Pasinelli, P., Ichida, J. K., & Trotti, D. (2014). Antisense proline-arginine RAN dipeptides linked to C9ORF72-ALS/FTD form toxic

nuclear aggregates that initiate in vitro and in vivo neuronal death. *Neuron*, *84*(6), 1213–1225. https://doi.org/10.1016/j.neuron.2014.12.010

Werth, J., & Thayer, S. (1994). Mitochondria buffer physiological calcium loads in cultured rat dorsal root ganglion neurons. *Journal of Neuroscience*, *14*(1), 348–356. https://doi.org/10.1523/JNEUROSCI.14-01-00348.1994

Westergard, T., Jensen, B. K., Wen, X., Cai, J., Kropf, E., Iacovitti, L., Pasinelli, P., & Trotti, D. (2016). Cell-to-Cell Transmission of Dipeptide Repeat Proteins Linked to C9orf72-ALS/FTD. In *Cell Reports* (Vol. 17, Issue 3). https://doi.org/10.1016/j.celrep.2016.09.032

Westergard, T., McAvoy, K., Russell, K., Wen, X., Pang, Y., Morris, B., Pasinelli, P., Trotti, D., & Haeusler, A. (2019). Repeat-associated non- AUG translation in C9orf72- ALS / FTD is driven by neuronal excitation and stress. *EMBO Molecular Medicine*, *11*(2). https://doi.org/10.15252/emmm.201809423

White, C., & McGeown, J. G. (2002). Carbachol triggers RyR-dependent Ca^{2+} release via activation of IP_3 receptors in isolated rat gastric myocytes. *The Journal of Physiology*, *542*(3), 725–733. https://doi.org/10.1113/jphysiol.2002.020131

White, M. R., Mitrea, D. M., Zhang, P., Stanley, C. B., Cassidy, D. E., Nourse, A., Phillips, A. H., Tolbert, M., Taylor, J. P., & Kriwacki, R. W. (2019). C9orf72 Poly(PR) Dipeptide Repeats Disturb Biomolecular Phase Separation and Disrupt Nucleolar Function. *Molecular Cell*, *74*(4), 713-728.e6. https://doi.org/10.1016/J.MOLCEL.2019.03.019

Wilkinson, S. (2020). Emerging Principles of Selective ER Autophagy. *Journal of Molecular Biology*, *432*(1), 185–205. https://doi.org/10.1016/J.JMB.2019.05.012

Wing, S. S., Chiang, H. L., Goldberg, A. L., & Dice, J. F. (1991). Proteins containing peptide sequences related to Lys-Phe-Glu-Arg-Gln are selectively depleted in liver and heart, but not skeletal muscle, of fasted rats. *Biochemical Journal*, *275*(1), 165–169. https://doi.org/10.1042/bj2750165

Wittie, M., Nelson, L. M., Usher, S., Ward, K., & Benatar, M. (2013). Utility of Capture-Recapture Methodology to Assess Completeness of Amyotrophic Lateral Sclerosis Case Ascertainment. *Neuroepidemiology*, *40*(2), 133–141. https://doi.org/10.1159/000342156

Xiao, S., MacNair, L., McGoldrick, P., McKeever, P. M., McLean, J. R., Zhang, M., Keith, J., Zinman, L., Rogaeva, E., & Robertson, J. (2015). Isoform-specific antibodies reveal distinct subcellular localizations of C9orf72 in amyotrophic lateral sclerosis. *Annals of Neurology*, *78*(4), 568–583. https://doi.org/10.1002/ana.24469

Xiao, S., MacNair, L., McLean, J., McGoldrick, P., McKeever, P., Soleimani, S., Keith, J., Zinman, L., Rogaeva, E., & Robertson, J. (2016). C9orf72 isoforms in Amyotrophic Lateral Sclerosis and Frontotemporal Lobar Degeneration. *Brain Research*, *1647*, 43–49. https://www.sciencedirect.com/science/article/pii/S0006899316303110?via%3Dihub

Xu, W., Bao, P., Jiang, X., Wang, H., Qin, M., Wang, R., Wang, T., Yang, Y., Lorenzini, I., Liao, L., Sattler, R., & Xu, J. (2019). Reactivation of nonsense-mediated mRNA decay protects against C9orf72 dipeptide-repeat neurotoxicity. *Brain*, *142*(5), 1349–1364. https://doi.org/10.1093/brain/awz070

Xu, W., & Xu, J. (2018). C9orf72 Dipeptide Repeats Cause Selective Neurodegeneration and Cell-Autonomous Excitotoxicity in Drosophila Glutamatergic Neurons. *Journal of Neuroscience*, *38*(35), 7741–7752. https://doi.org/10.1523/JNEUROSCI.0908-18.2018

Xu, Z., Poidevin, M., Li, X., Li, Y., Shu, L., Nelson, D. L., Li, H., Hales, C. M., Gearing, M., Wingo, T. S., & Jin, P. (2013). Expanded GGGGCC repeat RNA associated with amyotrophic lateral sclerosis and frontotemporal dementia causes neurodegeneration. *Proceedings of the National Academy of Sciences of the United States of America*, *110*(19), 7778–7783. https://doi.org/10.1073/pnas.1219643110

Yamada, S. B., Gendron, T. F., Niccoli, T., Genuth, N. R., Grosely, R., Shi, Y., Glaria, I., Kramer, N. J., Nakayama, L., Fang, S., Dinger, T. J. I., Thoeng, A., Rocha, G., Barna, M., Puglisi, J. D., Partridge, L., Ichida, J. K., Isaacs, A. M., Petrucelli, L., & Gitler, A. D. (2019). RPS25 is required for efficient RAN translation of C9orf72 and other neurodegenerative disease-associated nucleotide repeats. *Nature Neuroscience*, *22*(9), 1383–1388. https://doi.org/10.1038/s41593-019-0455-7

Yamaguchi, A., & Takanashi, K. (2016). FUS interacts with nuclear matrix-associated protein SAFB1 as well as Matrin3 to regulate splicing and ligand-mediated transcription. *Scientific Reports*, *6*(1), 35195. https://doi.org/10.1038/srep35195

Yamakawa, M., Ito, D., Honda, T., Kubo, K., Noda, M., Nakajima, K., & Suzuki, N. (2015). Characterization of the dipeptide repeat protein in the molecular pathogenesis of c9FTD/ALS. *Human Molecular Genetics*, *24*(6), 1630–1645. https://doi.org/10.1093/hmg/ddu576

Yang, D., Abdallah, A., Li, Z., Lu, Y., Almeida, S., & Gao, F.-B. (2015). FTD/ALS-associated poly(GR) protein impairs the Notch pathway and is recruited by poly(GA) into cytoplasmic inclusions. *Acta Neuropathologica*, *130*(4), 525–535. https://doi.org/10.1007/s00401-015-1448-6

Yang, M., Liang, C., Swaminathan, K., Herrlinger, S., Lai, F., Shiekhattar, R., & Chen, J.-F. (2016). A C9ORF72/SMCR8-containing complex regulates ULK1 and plays a dual role in autophagy. *Science Advances*, *2*(9).

Yang, Q., She, H., Gearing, M., Colla, E., Lee, M., Shacka, J. J., & Mao, Z. (2009). Regulation of neuronal survival factor MEF2D by chaperone-mediated autophagy. *Science (New York, N.Y.)*, *323*(5910), 124–127. https://doi.org/10.1126/science.1166088

Yin, S., Lopez-Gonzalez, R., Kunz, R. C., Gangopadhyay, J., Borufka, C., Gygi, S. P., Gao, F.-B., & Reed, R. (2017). Evidence that C9ORF72 Dipeptide Repeat Proteins Associate with U2 snRNP to Cause Mis-splicing in ALS/FTD Patients. *Cell Reports*, *19*(11), 2244–2256. https://doi.org/10.1016/J.CELREP.2017.05.056

Yoshida, H. (2007). ER stress and diseases. *The FEBS Journal*, *274*(3), 630–658. https://doi.org/10.1111/j.1742-4658.2007.05639.x

Yoshino, H., & Kimura, A. (2006). Investigation of the therapeutic effects of edaravone, a free radical scavenger, on amyotrophic lateral sclerosis (Phase II study). *Amyotrophic Lateral Sclerosis*, *7*(4), 247–251. https://doi.org/10.1080/17482960600881870

Yu, P. B., Hong, C. C., Sachidanandan, C., Babitt, J. L., Deng, D. Y., Hoyng, S. A., Lin, H. Y., Bloch, K. D., & Peterson, R. T. (2008). Dorsomorphin inhibits BMP signals required for embryogenesis and iron metabolism. *Nature Chemical Biology*, *4*(1), 33–41. https://doi.org/10.1038/nchembio.2007.54

Zamiri, B., Reddy, K., Macgregor, R. B., & Pearson, C. E. (2014). TMPyP4 porphyrin distorts RNA G-quadruplex structures of the disease-associated r(GGGGCC)n repeat of the C9orf72 gene and blocks interaction of RNA-binding proteins. *The Journal of Biological Chemistry*, *289*(8), 4653–4659. https://doi.org/10.1074/jbc.C113.502336

Zhang, C., & Cuervo, A. M. (2008). Restoration of chaperone-mediated autophagy in aging liver improves cellular maintenance and hepatic function. *Nature Medicine*, *14*(9), 959–965. https://doi.org/10.1038/nm.1851

Zhang, K., Donnelly, C. J., Haeusler, A. R., Grima, J. C., Machamer, J. B., Steinwald, P., Daley, E. L., Miller, S. J., Cunningham, K. M., Vidensky, S., Gupta, S., Thomas, M. A., Hong, I., Chiu, S.-L., Huganir, R. L., Ostrow, L. W., Matunis, M. J., Wang, J., Sattler, R., … Rothstein, J. D. (2015). The C9orf72 repeat expansion disrupts nucleocytoplasmic transport. *Nature*, *525*(7567), 56–61. https://doi.org/10.1038/nature14973

Zhang, K. Y., Yang, S., Warraich, S. T., & Blair, I. P. (2014). Ubiquilin 2: A component of the ubiquitin–proteasome system with an emerging role in neurodegeneration. *The International Journal of Biochemistry & Cell Biology*, *50*, 123–126. https://doi.org/10.1016/J.BIOCEL.2014.02.018

Zhang, Q., An, Y., Chen, Z. S., Koon, A. C., Lau, K., Ngo, J. C. K., & Chan, H. Y. E. (2019). A Peptidylic Inhibitor for Neutralizing r(GGGGCC)exp-Associated Neurodegeneration in C9ALS-FTD. *Molecular Therapy - Nucleic Acids*, *16*, 172–185. https://doi.org/10.1016/J.OMTN.2019.02.015

Zhang, Q., Chen, Z. S., An, Y., Liu, H., Hou, Y., Li, W., Lau, K., Koon, A. C., Ngo, J. C. K., & Chan, H. Y. E. (2018). A peptidylic inhibitor for neutralizing expanded CAG RNA-induced nucleolar stress in polyglutamine diseases. *RNA (New York, N.Y.)*, *24*(4), 486–498. https://doi.org/10.1261/rna.062703.117

Zhang, X., Wang, F., Hu, Y., Chen, R., Meng, D., Guo, L., Lv, H., Guan, J., & Jia, Y. (2020). In vivo stress granule misprocessing evidenced in a FUS knock-in ALS mouse model. *Brain*, *143*(5), 1350–1367. https://doi.org/10.1093/brain/awaa076

Zhang, Y., Burberry, A., Wang, J., Sandoe, J., Ghosh, S., Udeshi, N. D., Svinkina, T., Mordes, D. A., Mok, J., Charlton, M., Li, Q., Carr, S. A., & Eggan, K. (2018). The C9orf72-interacting protein Smcr8 is a negative regulator of autoimmunity and lysosomal exocytosis. *Genes & Development*, *32*(13–14), 929–943. https://doi.org/10.1101/gad.313932.118

Zhang, Y. J., Gendron, T. F., Ebbert, M. T. W., O'Raw, A. D., Yue, M., Jansen-West, K., Zhang, X., Prudencio, M., Chew, J., Cook, C. N., Daughrity, L. M., Tong, J., Song, Y., Pickles, S. R., Castanedes-Casey, M., Kurti, A., Rademakers, R., Oskarsson, B., Dickson, D. W., … Petrucelli, L. (2018). Poly(GR) impairs protein translation and stress granule dynamics in C9orf72-associated frontotemporal dementia and amyotrophic lateral sclerosis. *Nature Medicine*, *24*(8), 1136–1142. https://doi.org/10.1038/s41591-018-0071-1

Zhang, Y. J., Gendron, T. F., Grima, J. C., Sasaguri, H., Jansen-West, K., Xu, Y. F., Katzman, R. B., Gass, J., Murray, M. E., Shinohara, M., Lin, W. L., Garrett, A., Stankowski, J. N., Daughrity, L., Tong, J., Perkerson, E. A., Yue, M., Chew, J., Castanedes-Casey, M., … Petrucelli, L. (2016). C9ORF72 poly(GA) aggregates sequester and impair HR23 and nucleocytoplasmic transport proteins. *Nature Neuroscience*, *19*(5), 668–677. https://doi.org/10.1038/nn.4272

Zhang, Y. J., Guo, L., Gonzales, P. K., Gendron, T. F., Wu, Y., Jansen-West, K., O'Raw, A. D., Pickles, S. R., Prudencio, M., Carlomagno, Y., Gachechiladze, M. A., Ludwig, C., Tian, R., Chew, J., DeTure, M., Lin, W.-L., Tong, J., Daughrity, L. M., Yue, M., … Petrucelli, L. (2019). Heterochromatin anomalies and double-stranded RNA accumulation underlie C9orf72 poly(PR) toxicity. *Science (New York, N.Y.)*, *363*(6428). https://doi.org/10.1126/science.aav2606

Zhang, Y. J., Jansen-West, K., Xu, Y.-F., Gendron, T. F., Bieniek, K. F., Lin, W.-L., Sasaguri, H., Caulfield, T., Hubbard, J., Daughrity, L., Chew, J., Belzil, V. V., Prudencio, M., Stankowski, J. N., Castanedes-Casey, M., Whitelaw, E., Ash, P. E. A., DeTure, M., Rademakers, R., … Petrucelli, L. (2014). Aggregation-prone c9FTD/ALS poly(GA) RAN-translated proteins cause neurotoxicity by inducing ER stress. *Acta Neuropathologica*, *128*(4), 505–524. https://doi.org/10.1007/s00401-014-1336-5

Zhou, Q., Lehmer, C., Michaelsen, M., Mori, K., Alterauge, D., Baumjohann, D., Schludi, M. H., Greiling, J., Farny, D., Flatley, A., Feederle, R., May, S., Schreiber, F., Arzberger, T., Kuhm, C., Klopstock, T., Hermann, A., Haass, C., & Edbauer, D. (2017). Antibodies inhibit transmission and aggregation of C9orf72 poly- GA dipeptide repeat proteins. *EMBO Molecular Medicine*, *9*(5), 687–702. https://doi.org/10.15252/emmm.201607054

Zhou, Q., Mareljic, N., Michaelsen, M., Parhizkar, S., Heindl, S., Nuscher, B., Farny, D., Czuppa, M., Schludi, C., Graf, A., Krebs, S., Blum, H., Feederle, R., Roth, S., Haass, C., Arzberger, T., Liesz, A., & Edbauer, D. (2020). Active poly-GA vaccination prevents microglia activation and motor deficits in a C9orf72 mouse model. *EMBO Molecular Medicine*, *12*(2). https://doi.org/10.15252/emmm.201910919

Zhu, Q., Jiang, J., Gendron, T. F., McAlonis-Downes, M., Jiang, L., Taylor, A., Diaz Garcia, S., Ghosh Dastidar, S., Rodriguez, M. J., King, P., Zhang, Y., La Spada, A. R., Xu, H., Petrucelli, L., Ravits, J., Da Cruz, S., Lagier-Tourenne, C., & Cleveland, D. W. (2020). Reduced C9ORF72 function exacerbates gain of toxicity from ALS/FTD-causing repeat expansion in C9orf72. *Nature Neuroscience*, *23*(5), 615–624. https://doi.org/10.1038/s41593-020-0619-5

Zou, Z., Zhou, Z., Che, C., Liu, C., He, R., & Huang, H. (2017). Genetic epidemiology of amyotrophic lateral sclerosis: a systematic review and meta-analysis. *Journal of Neurology, Neurosurgery & Psychiatry*, *88*(7), 540–549. https://doi.org/10.1136/JNNP-2016-315018

Zu, T., Gibbens, B., Doty, N. S., Gomes-Pereira, M., Huguet, A., Stone, M. D., Margolis, J., Peterson, M., Markowski, T. W., Ingram, M. A. C., Nan, Z., Forster, C., Low, W. C., Schoser, B., Somia, N. V, Clark, H. B., Schmechel, S., Bitterman, P. B., Gourdon, G., … Ranum, L. P. W. (2011). Non-ATG-initiated translation directed by microsatellite expansions. *Proceedings of the National Academy of Sciences of the United States of America*, *108*(1), 260–265. https://doi.org/10.1073/pnas.1013343108

Zu, T., Liu, Y., Bañez-Coronel, M., Reid, T., Pletnikova, O., Lewis, J., Miller, T. M., Harms, M. B., Falchook, A. E., Subramony, S. H., Ostrow, L. W., Rothstein, J. D., Troncoso, J. C., & Ranum, L. P. W. (2013). RAN proteins and RNA foci from antisense transcripts in C9ORF72 ALS and frontotemporal dementia. *Proceedings of the National Academy of Sciences of the United States of America*, *110*(51), E4968-77. https://doi.org/10.1073/pnas.1315438110